

University of Nebraska - Lincoln

DigitalCommons@University of Nebraska - Lincoln

---

Construction Systems -- Dissertations & Theses

Construction Systems

---

4-2014

# COMPARATIVE STUDY OF BASE-ISOLATED AND FIXED-BASE BUILDINGS USING A DAMAGE/COST APPROACH

Martin Lashgari

University of Nebraska-Lincoln, [mlashgari@unomaha.edu](mailto:mlashgari@unomaha.edu)

Follow this and additional works at: <http://digitalcommons.unl.edu/constructiondiss>



Part of the [Construction Engineering and Management Commons](#)

---

Lashgari, Martin, "COMPARATIVE STUDY OF BASE-ISOLATED AND FIXED-BASE BUILDINGS USING A DAMAGE/COST APPROACH" (2014). *Construction Systems -- Dissertations & Theses*. 16.

<http://digitalcommons.unl.edu/constructiondiss/16>

This Article is brought to you for free and open access by the Construction Systems at DigitalCommons@University of Nebraska - Lincoln. It has been accepted for inclusion in Construction Systems -- Dissertations & Theses by an authorized administrator of DigitalCommons@University of Nebraska - Lincoln.

COMPARATIVE STUDY OF BASE-ISOLATED AND FIXED-BASE BUILDINGS  
USING A DAMAGE/COST APPROACH

by

Martin Lashgari

A DISSERTATION

Presented to the Faculty of  
The College of Engineering at the University of Nebraska  
In Partial Fulfillment of Requirements  
For the Degree of Doctor of Philosophy

Major: Engineering  
(Construction)

Under the Supervision of Professor Terri R. Norton

Lincoln, Nebraska

April, 2014

COMPARATIVE STUDY OF BASE-ISOLATED AND FIXED-BASE BUILDINGS  
USING A DAMAGE/COST APPROACH

Martin Lashgari, Ph.D.

University of Nebraska, 2014

Adviser: Terri R. Norton

High performance base-isolated buildings are designed with a higher level of safety than the conventional fixed-base buildings under the current codes. As a sustainable development, these buildings have considerably lower social and economic impacts in a major event. The main factor limiting the extensive use of such systems is the higher initial construction costs. The cost estimations based on only initial investment may have concluded misleading results as the performance of those systems in earthquakes are different. Therefore, an evaluation considering initial costs and future repair costs due to damages from earthquakes gives a better scope for selection of an optimal design, among different alternatives.

There is an emerging trend in earthquake resistant design of buildings to consider both safety and cost factor using PEER probabilistic approach. This methodology is able to estimate to the probable losses including damages in building components, human injuries and associated costs in a fully probabilistic framework. This study is aimed at performing a cost-benefit comparative study of base-isolated and fixed-base buildings using PEER approach.

Performance of several multi-story concrete moment resisting frames was initially investigated using a cost-based response index or a simplified performance measure.

Calculated response indices of base-isolated models were up to 6 times lower than the fixed-base ones for the low-rise 3-story models at the highest hazard level. However, only a slight performance upgrade was achievable for rather high rise isolated building models.

As the main focus of this study, six benchmark office buildings were selected including five fixed-base and one base-isolated model for cost comparison purposes. Different seismic loads are used for the design of fixed-base buildings varying from one to three times the minimum seismic forces according to IBC-2012. The results of Time-Based Assessment shows that the lower long term costs of high performance buildings has the potential to justify their additional initial costs for most of the models. Isolated building performed superior to all fixed-base models in the cost-benefit analysis. Although the initial costs of the isolated model is over 6% higher than the fixed-base basic model, the total net present value of base-isolated building is 4.1% lower at an assumed interest rate of 7%.

## Acknowledgements

I would like to express my special appreciation and thanks to my advisor Professor Dr. Terri R. Norton for always being supportive to me and for encouraging my research. I would also like to thank my committee members, Professor Terence Foster, Professor George Morcoux, Professor Christopher Tuan, and Professor Ece Erdogmus for serving as my committee members and for your valuable comments and suggestions.

Finally, a special thanks to my family. I am unable to express my love and gratitude to my wife, my mother, and father for all of the sacrifices that you've made. Your support for me was what sustained me thus far. I wouldn't have made it without you. Thank you!

To:

Marjan Seyedirezvani

Shahzad Kamari

Ehsan Lashgari

## Table of Contents

Chapter 1 : Research Significance .....	1
1.1    Background.....	1
1.2    Problem Definition .....	4
1.3    Objectives .....	5
1.4    Scope.....	6
Chapter 2 : Preliminary Comparative Study.....	7
2.1    Introduction.....	7
2.2    Isolation Properties .....	9
2.3    Multi-Story Structural Model .....	11
2.4    Ground Motions.....	13
2.5    Force Reduction Factor.....	14
2.6    Response Index .....	21
2.7    Conclusion .....	33
Chapter 3 : Benchmark Buildings.....	35
3.1    Benchmark Buildings Description.....	35
3.2    Site Description.....	35
3.3    Building Layout .....	36
3.4    Gravity Loads .....	38
3.5    Structural Design .....	40

3.5.1	Reinforcement Ratio .....	40
3.5.2	Effective Stiffness .....	41
3.5.3	Strong-Column Weak Beam Principle.....	42
3.5.4	Non-Ductile Failure Modes .....	42
3.5.5	Fixed-Based Models .....	43
3.5.6	Seismically-Isolated Model .....	46
Chapter 4 : Performance Model.....		59
4.1	Introduction.....	59
4.2	Initial Costs .....	60
4.3	Occupancy and Population Model.....	67
4.4	Fragility Groups .....	70
4.5	Structural Component Fragility .....	71
4.6	Nonstructural Components Fragility .....	73
4.6.1	Exterior Closure .....	74
4.6.2	Interior Partitions .....	75
4.6.3	Steel Stairs .....	76
4.6.4	Acoustical Ceilings .....	77
4.6.5	Elevators .....	78
4.6.6	Plumbing.....	80
4.6.7	Sprinklers .....	81
4.6.8	HVAC System .....	82
4.6.9	Equipment and Furnishing.....	83
Chapter 5 : Response Analysis.....		84
5.1	Introduction.....	84
5.2	Earthquake Hazard Characterization .....	84
5.3	Structural Modeling .....	90

5.3.1	Fiber-Hinge Model.....	91
5.3.2	Lumped Plasticity Model.....	106
5.4	Collapse Capacity .....	114
5.5	Demand Drifts and Accelerations .....	125
Chapter 6 : Performance Assessment.....		141
6.1	Quality Assurance and Uncertainty Assumptions.....	141
6.2	Residual Drift.....	142
6.3	Collapse Modes.....	147
6.4	Consequence Functions .....	148
Chapter 7 : Loss Analysis and Decision Making.....		152
7.1	Realizations.....	152
7.2	Annualized Performance Measure.....	163
7.2.1	Repair Costs and Time.....	164
7.2.2	Casualties .....	173
7.2.3	Unsafe Placard .....	177
7.2.4	Collapse.....	178
7.3	Decision Making.....	179
Chapter 8 : Conclusion .....		187
References.....		191

## List of Tables

Table 2.1: Cost breakdown of a conventional 5-10 story office building.....	24
Table 2.2: Fragility curve properties of components .....	25
Table 2.3: Response index of fixed–base and isolated models in different hazard levels	31
Table 3.1: Dead load materials and objects .....	39
Table 3.2: Floors and roof live load .....	40
Table 3.3: Typical reinforcement ratio in column and beam components design.....	41
Table 3.4: Dead load materials and objects .....	41
Table 3.5: Design coefficients and factors for seismic design.....	44
Table 3.6: Vibration period of buildings .....	46
Table 3.7: Acceptable methods of analysis for base-isolated buildings.....	49
Table 3.8: Initial estimates of isolation design and maximum displacements .....	52
Table 3.9: Design parameters for isolation system .....	55
Table 3.10: Final estimates of isolation design and maximum displacement.....	55
Table 3.11: Maximum downward force for isolator units design .....	56
Table 3.12: Lead Rubber Bearings dimensions, Dis Inc. production .....	57
Table 4.1: Construction cost distribution of the building B1 .....	63
Table 4.2: Construction cost distribution of the building B2.....	63
Table 4.3: Construction cost distribution of the building B3.....	64
Table 4.4: Construction cost distribution of the building B4.....	64
Table 4.5: Construction cost distribution of the building B5.....	65
Table 4.6: Construction cost distribution of the building BI .....	65
Table 4.7: Structural components cost increase relative to B1 design.....	66

Table 4.8: Structural components cost breakdown .....	67
Table 4.9: Fragility groups in benchmark buildings .....	71
Table 4.10: Damage states for beam and column elements (joints) .....	72
Table 4.11: Damage states for the exterior curtain walls .....	74
Table 4.12: Damage states for the wallboard partitions.....	75
Table 4.13: Damage states for steel stairs.....	76
Table 4.14: Damage states for acoustical ceiling.....	78
Table 4.15: Damage states for hydraulic elevators .....	79
Table 4.16: Damage states for the piping system .....	80
Table 4.17: Damage states for sprinklers .....	81
Table 4.18: Damage states for HVAC system components .....	82
Table 4.19: Equipment and furnishing components .....	83
Table 5.1: Annual frequency of exceedance of different hazard levels .....	88
Table 5.2: Yield chord rotations predicted by Fardis equation (B1 model).....	103
Table 5.3: Yield chord rotations predicted by Fardis (2001) and Sezen (2002) (B1 model) .....	103
Table 5.4: Joint shear strength factor ( $\gamma$ ) according to ACI352-R02 .....	105
Table 5.5: yield chord rotation estimation using Fardis equation (model B1).....	110
Table 5.6: Capping and ultimate rotation capacity (B1 model).....	112
Table 5.7: Collapse capacity and 2% in 50 year demand spectral acceleration.....	125
Table 7.1: Median repair costs estimated for benchmark buildings .....	161
Table 7.2: Median repair costs per square foot and the reparability state.....	162
Table 7.3 Annualized fatality rate .....	173

Table 7.4: Annualized probability of unsafe placarding and reliability indices.....	177
Table 7.5: Annualized and 50-year probability of collapse and corresponding reliability indices .....	179
Table 7.6: Average revenues per employee (money.cnn, 2007).....	181
Table 7.7: Annual loss estimation during restoration period .....	181
Table 7.8: Average economic costs for unintentional human death and injuries (NSC, 2011) .....	182
Table 7.9: Average annual rate of return .....	183

## List of Figures

Figure 2.1: Bilinear force-deformation model of isolation.....	11
Figure 2.2: 5% Damped median linear response spectrum.....	14
Figure 2.3: Force reduction factor R for (a) fixed-base model (b) Isolated Tshift =2 s and $\eta=0.4$ (c) Isolated Tshift =2 s and $\eta=0.8$ (d) Isolated Tshift =4 s and $\eta=0.4$ (e) Isolated Tshift =4 s and $\eta=0.8$ .....	18
Figure 2.4: Isolation reduction factor R for (a) Isolated Tshift =2 s and $\eta=0.4$ (b) Isolated Tshift =2 s and $\eta=0.8$ (c) Isolated Tshift =4 s and $\eta=0.4$ (d) Isolated Tshift =4 s and $\eta=0.8$ .....	19
Figure 2.5: Modified isolation reduction factor R for.....	21
Figure 2.6: Cost percentage of components in buildings (Taghavi & Miranda, 2003) ....	23
Figure 2.7: Cost breakdown of non-structural components (Taghavi & Miranda, 2003).	23
Figure 2.8: Fragility curve for “Miscellaneous Fragile Objects” .....	26
Figure 2.9: Response index versus ductility .....	32
Figure 3.1: Location map for Los Angeles Bulk Mail site. ....	36
Figure 3.2: Plan Layout view of the 4-story building.....	37
Figure 3.3: Elevation view of building frames .....	38
Figure 3.4: Elevation view of the isolated building frames .....	47
Figure 3.5: Effective stiffness and damping of isolators .....	50
Figure 3.6: Effective stiffness and damping in the bilinear model .....	53
Figure 4.1: Normative quantities used for cost estimations.....	62
Figure 4.2: Variation in population by time of day during weekdays for office occupancy .....	68

Figure 4.3: Variation in population by time of day during weekends for office occupancy .....	69
Figure 4.4: Variation in population by month for office occupancy.....	70
Figure 4.5: Fragility curves for columns and beam elements (joints) .....	73
Figure 4.6: Fragility curves for curtain wall system.....	74
Figure 4.7: Fragility curves for wallboard partitions .....	76
Figure 4.8: Fragility curves for steel stairs .....	77
Figure 4.9: Fragility curves for acoustical ceiling .....	78
Figure 4.10: Fragility curves for hydraulic elevators.....	79
Figure 4.11: Fragility curves for sprinkler drops .....	81
Figure 5.1: Probabilistic seismic hazard curve .....	86
Figure 5.2: Uniform Hazard Curve (UHS) .....	87
Figure 5.3: Target spectrum and spectral acceleration of ground motions at each hazard level (continue) .....	90
Figure 5.4: Fiber element schematic drawing for a concrete column containing of 100 fibers for concrete and 9 fibers for steel bars.....	93
Figure 5.5: Stress-strain relationship using Mander et al. model .....	96
Figure 5.6: Stress-strain relationship for confined concrete (FEDEAS material) .....	97
Figure 5.7: Bond and bar stress distribution of reinforcing bars anchored joints (Lowes et al. model) .....	98
Figure 5.8: Bar stress versus slip using Lowes equation (reinforcing bars located at first story beams of B1 model).....	99

Figure 5.9: Normalized moment versus rotation (reinforcing bars located at first story beams of B1 model) .....	100
Figure 5.10: Bilinear idealization of bond-slip behavior .....	101
Figure 5.11: Shear deformation in the shear panel zone .....	104
Figure 5.12: Joint2D elements (Altoontash, 2004) .....	105
Figure 5.13: Shear stress-strain backbone curve for panel zones .....	106
Figure 5.14: Typical moment-rotation backbone diagram of plastic hinges .....	108
Figure 5.15: Modified moment-rotation backbone diagram for elements and plastic hinges .....	109
Figure 5.16: Collapse IDA for design B1 including all 40 ground motion components .	116
Figure 5.17: Collapse IDA for design B1 using critical ground motion components of each record .....	116
Figure 5.18: Collapse IDA for design B2 including all 40 ground motion components .	117
Figure 5.19: Collapse IDA for design B2 using critical ground motion components of each record .....	117
Figure 5.20: Collapse IDA for design B3 including all 40 ground motion components .	118
Figure 5.21: Collapse IDA for design B3 using critical ground motion components of each record .....	118
Figure 5.22: Collapse IDA for design B4 including all 40 ground motion components .	119
Figure 5.23: Collapse IDA for design B4 using critical ground motion components of each record .....	119
Figure 5.24: Collapse IDA for design B5 including all 40 ground motion components	120

Figure 5.25: Collapse IDA for design B5 using critical ground motion components of each record .....	120
Figure 5.26: Collapse IDA for design BI including all 40 ground motion components. .	121
Figure 5.27: Collapse IDA for design BI using critical ground motion components of each record .....	121
Figure 5.28: Collapse CDF for design B1 .....	122
Figure 5.29: Collapse CDF for design B2 .....	122
Figure 5.30: Collapse CDF for design B3 .....	123
Figure 5.31: Collapse CDF for design B4 .....	123
Figure 5.32: Collapse CDF for design B5 .....	124
Figure 5.33: Collapse CDF for design BI .....	124
Figure 5.34: Scatter of record by record peak floor acceleration and the medians for design B1 .....	127
Figure 5.35: Scatter of record by record peak floor acceleration and the medians for design B2 .....	128
Figure 5.36: Scatter of record by record peak floor acceleration and the medians for design B3 .....	129
Figure 5.37: Scatter of record by record peak floor acceleration and the medians for design B4 .....	130
Figure 5.38: Scatter of record by record peak floor acceleration and the medians for design B5 .....	131
Figure 5.39: Scatter of record by record peak floor acceleration and the medians for design BI .....	132

Figure 5.40: Scatter of record by record peak story drift and the medians for design B1 .....	133
Figure 5.41: Scatter of record by record peak story drift and the medians for design B2 .....	134
Figure 5.42: Scatter of record by record peak floor acceleration and the medians for design B3 .....	135
Figure 5.43: Scatter of record by record peak floor acceleration and the medians for design B4 .....	136
Figure 5.44: Scatter of record by record peak floor acceleration and the medians for design B5 .....	137
Figure 5.45: Scatter of record by record peak floor acceleration and the medians for design BI .....	138
Figure 5.46: Mean story drift ratio of all designs .....	139
Figure 5.47: Mean story acceleration of all designs .....	140
Figure 6.1: First story shear force-drift ratio diagram for B1 model .....	143
Figure 6.2: First story shear force-drift ratio diagram for B2 model .....	144
Figure 6.3: First story shear force-drift ratio diagram for B3 model .....	144
Figure 6.4: First story shear force-drift ratio diagram for B4 model .....	145
Figure 6.5: First story shear force-drift ratio diagram for B5 model .....	145
Figure 6.6: First story shear force-drift ratio diagram for BI model.....	146
Figure 6.7: Building repair fragility based on the residual drift .....	147
Figure 6.8: Repair cost versus repair quantity for suspended ceiling .....	150
Figure 6.9: Repair time versus repair quantity for suspended ceiling .....	151

Figure 7.1: Total repair cost vs realization number for B1 model .....	154
Figure 7.2: Total repair cost vs realization number for B2 model .....	155
Figure 7.3: Total repair cost vs realization number for B3 model .....	156
Figure 7.4: Total repair cost vs realization number for B4 model .....	157
Figure 7.5: Total repair cost vs realization number for B5 model .....	158
Figure 7.6: Total repair cost vs realization number for BI model.....	159
Figure 7.7: Repair cost distribution and the lognormal fitter curve for the 10% in 50 year earthquake intensity .....	160
Figure 7.8: Seismic hazard curve segments and the corresponding annual probabilities	164
Figure 7.9: Annualized repair costs for B1 model .....	166
Figure 7.10: Annualized repair costs for B2 model .....	166
Figure 7.11: Annualized repair costs for B3 model .....	167
Figure 7.12: Annualized repair costs for B4 model .....	167
Figure 7.13: Annualized repair costs for B5 model .....	168
Figure 7.14: Annualized repair costs for BI model.....	168
Figure 7.15: Annualized repair time for B1 model.....	170
Figure 7.16: Annualized repair time for B1 model.....	170
Figure 7.17: Annualized repair time for B3 model.....	171
Figure 7.18: Annualized repair time for B4 model.....	171
Figure 7.19: Annualized repair time for B5 model.....	172
Figure 7.20: Annualized repair time for BI model.....	172
Figure 7.21: Annualized injuries rate for B1 model .....	174
Figure 7.22: Annualized injuries rate for B2 model .....	174

Figure 7.23: Annualized injuries rate for B3 model .....	175
Figure 7.24: Annualized injuries rate for B4 model .....	175
Figure 7.25: Annualized injuries rate for B5 model .....	176
Figure 7.26: Annualized injuries rate for BI model .....	176
Figure 7.27: Total net present value (NPV) of benchmark buildings, 3% annual rate of return .....	183
Figure 7.28: Total net present value (NPV) of benchmark buildings, 5% annual rate of return .....	184
Figure 7.29: Total net present value (NPV) of benchmark buildings, 7% annual rate of return .....	184
Figure 7.30: Total net present value (NPV) of benchmark buildings, 9% annual rate of return .....	185
Figure 7.31: NPV of benchmark buildings to NPV of B1 design.....	186

## Chapter 1 : Research Significance

### 1.1 Background

Buildings behavior in earthquakes depends on various uncertainty factors. These uncertainties originate from different sources, earthquake nature, components behavior, and the analytical methods. Therefore, the response of the building is dependent on ground motions and an assembly of individual responses of structural and nonstructural components in a fully probabilistic framework. Despite a large number of reliability studies on individual components, recent studies have focused on the performance evaluation of structural system considering all major sources of uncertainties using Pacific Earthquake Engineering Research Center (PEER) performance-based design approach (Porter, Shaikhutdinov, & Beck, 2002; Krawinkler & Miranda, 2004). Lee and Mosalam (2006) identified and ranked significant sources of uncertainty with respect the engineering demand parameter (EDP); inter-story drift, roof acceleration, roof displacement. Haselton et al. (2008) conducted a research on performance assessment of four-story RC special moment resisting frames using PEER approach. They investigated eight structural design alternatives and conclusions were drawn on collapse safety, damage and repair costs, life safety risks and costs.

Base isolation systems have been used in earthquake prone areas to reduce the seismic forces rather than resisting it (Kelly, 1999; Komodromos, 2000). Although base isolation increases the structures level of safety, the cost of the isolation devices and other design and construction modifications, has limited its implementation (Mayes, 1990). Consequently, base isolation has been often employed only for the continued operation of

essential facilities. Base-isolated structures are designed with a higher level of safety than the fixed-base structures under current codes. Cost comparisons are difficult to make because the performance of code-designed fixed-base and base-isolated structures are not comparable. An evaluation based on the only construction costs without accounting for the differences in performance leads to a misleading inception of the system. While the common performance level is life safety for the conventional fixed-base buildings, the structural and non-structural damages substantially decrease as a result of base isolation application, often providing immediate occupancy performance objective according to first generation performance based design. The evaluations based only on initial investment costs without considering the future economic benefits have constrained a broad use of such a high performance system.

Performance-based design has been one of the major developments in structural engineering field since its introduction in the early 90's. The first generation was introduced in Vision 2000 (SEAOC, 1995) and were adapted and published by Seismic Evaluation and Retrofit of Concrete Buildings (ATC-40, 1996). It was a great step forward in design procedure as it allows for selection of different performance objective levels: Immediate Occupancy, Life Safety and Collapse Prevention. Although it has provided flexibility in design, the economic significance of design alternatives is not directly included in the methodology.

The structural Engineering community-Pacific Earthquake Engineering Research center-has been working on a new methodology in order to explicitly quantify and integrate the economic factor into design process. This procedure was first developed by PEER which introduced a new framework for performance-based earthquake engineering

(Krawinkler & Miranda, 2004). This allows integrating the uncertainties in ground motions and building component responses in a probabilistic framework. The performance assessment includes hazard determination, structural modeling and analysis, damage analysis and loss estimations. Their work has greatly contributed into the development of the future performance-based design methodology recently release by the Applied Technology Council (ATC-58, 2012)

The assessment type is based on quantifying the consequences of buildings response to earthquake. The performance measures must be meaningful and representative of parameters important to decision makers. In this methodology performance measures are probable future earthquake impacts expressed as follows (ATC-58, 2012)

- Casualties: the number of deaths and injuries of a severity requiring hospitalization;
- Repair cost: including the cost of repairing or replacing damaged buildings and their contents;
- Repair time: the period of time necessary to conduct repairs or replace damaged contents, building components or entire buildings; and
- Unsafe Placards: the probability that a building will be deemed unsafe for post-earthquake occupancy.

Performance assessment is a complicated procedure which requires considering all uncertainties involved. At this stage, using the information provided for each uncertain factor on the median, dispersion and types of distribution, a simulation is carried out by combining them using Monte Carlo technique. This simulation is repeated a large number

of times until an estimation of performance measures is obtained. Depending on computing power, this procedure may take a few hours to several days or to complete.

## **1.2 Problem Definition**

The primary goal of the engineering effort is to benefit the society in terms of human life safety in extreme events like an earthquake. Aside from the human safety, reducing the environmental and economic impact of a disaster like a big earthquake is desirable. The present seismic design principles do not provide any clear recommendations for the selection of an optimal structural system solution, among the various alternatives. Previous performance-based design methodologies provide guidance and recommendations for various structural systems to satisfy the requirements of a selected performance objective. Such recommendation are made independent of the fact that of how different structural designs are compared in terms of the costs. On the other hand, the general inception of the engineering community on the cost consequences of high performance structural systems including base isolation has limited their use. To address this problem, high performance base isolation systems require a complete reevaluation considering initial and long term seismic costs. PEER performance assessment methodology is able to provide a powerful means for estimation of long term consequences of different design alternatives. The methodology is a big step forward in the performance-base design evolution path; but the applicability is restricted to due to its high analysis costs and time.

### 1.3 Objectives

For the good of the society, the future consequences of today's decisions are required to be accounted for in a sustainable design. The effectiveness of base-isolation in reducing the impact due to large earthquake is evident. This fact serves both toward decreasing the social and environmental impact in a sustainable development. The main objective of this research is to compare the long term consequences of the high performance and the fixed-base structural systems in including repair costs, repair time, business interruption costs, fatalities and injuries. This research mainly focuses on:

- Clarifying the potential of base isolation systems in providing an economical yet reliable and safe design alternative. The focus is to assess performance of base isolated and non-isolated designs considering initial costs and future losses during the useful life span of the building to help owners and designers on making decisions.
- The effect of different design seismic loads, for example seismic demands associated with different risk categories in International Building Code (2012), on the total costs.

Some minor objectives include:

- Perform a comparative analysis on how the fixed-base nonlinearly-performing structural systems are compared with the corresponding linearly-performing isolated systems in terms of the seismic demand forces
- Compare the performance of fixed-based and isolated models based on a simplified response index.

## **1.4 Scope**

Chapter two of this dissertation focuses on the comparative study of seismic demand for isolated and non-isolated multi-story buildings. The performance of these systems is also compared using a simplified response index. A more realistic performance assessment is carried out by using benchmark building alternatives designed for this purposes as explained in chapter 3. The performance model including initial cost analysis and fragility specifications of components are discussed in chapter 4. Responses analysis and assumptions made for performance assessment is also discussed in detail in chapters 5 and 6. Repair costs and time, human injuries and fatalities, and collapse probabilities are estimated in chapter 7 for all benchmark buildings and conclusions are made based on the net present value of all costs involved.

## Chapter 2 : Preliminary Comparative Study

### 2.1 Introduction

The fundamental period of many structures falls within the frequency range at which an earthquake releases most of its energy, thus amplifying the seismic forces. Historically, base isolation systems have been used in earthquake prone areas to reduce seismic forces (Komodromos, 2000). Although base isolation helps to make structures safer, it is not often implemented due to the cost of the required devices and other design and construction modifications (Mayes, 1990). As a result, base isolation is currently utilized primarily for the continued operation of essential facilities or other types of buildings where a highly-effective and less intrusive property of the base-isolation is desirable such as in historical buildings.

Research has shown that the structural performance of base-isolated buildings is better than that of fixed-based buildings. At the same time, however, isolated structures tend to be more susceptible to damage if yielding occurs in the superstructure (Kikuchi & Black, 2008) Comparative studies that use a response measure have been useful for determining the relative performance of buildings in differing design configurations. Ryan et al. (2006), for example, proposed a Comparative Performance Measure (CPM) for single degree of freedom systems based on the relative amounts of maximum drift and acceleration obtained from a nonlinear time history analysis. Sayani and Ryan (2009) developed a response index (RI) and also used it to evaluate the performance of single degree of freedom systems. They considered maximum drift, peak floor acceleration, and system ductility in their response index. The authors concluded that the superstructure

design strength of a single story isolated building is less than that of a fixed-base building with identical ductility when evaluated for a consistent performance objective.

Cost comparisons are difficult to make because the performance of fixed-base and base-isolated structures are not comparable. An evaluation based only on construction costs that does not account for performance differences may be misleading. Most fixed-base buildings meet the requirements for the life safety seismic performance level while base isolated structures generally meet the requirements of the immediate occupancy performance level.

A new methodology for performing a seismic assessment is being proposed to improve performance based design (ATC-58, 2012). Unlike previous methods, this new assessment tool considers the structural components, nonstructural components, and the building contents to estimate future earthquake damage. The objective of this study is to measure and compare the performance of fixed-base and base-isolated multi-story buildings while applying the developing performance based evaluation concept. The force reduction factors in various superstructure ductility demands are determined and compared for both isolated and fixed-base systems. Finally, a new cost-based approach for the response index (RI) calculation is introduced. As an improvement over the previously suggested RI equations, this new index is able to show the performance of the analyzed buildings based on the probable amount of damage and costs associated with the structural components, non-structural components, and building contents of a building. The response index of multi-story models under seismic motion is investigated using nonlinear time history analyses. The effect that various isolation properties (the

characteristic strength, period shift, and natural vibration period of the superstructure) have on the proposed response index is also evaluated.

## 2.2 Isolation Properties

Since the effectiveness of the base-isolation originates mainly from the increased natural period of vibration, its effect should be accounted for in the analyses by a factor known as the period shift. A period shift is defined as the difference between the fixed-base and isolated buildings (Sayani & Ryan, 2009). The isolator performs mostly within its post yield phase due to its relatively low yield strength. Therefore, the building period can be calculated based on the post yield stiffness of the isolation device and the superstructure's linear stiffness. The larger the period shift, the greater the mitigating effect of isolation. The calculation for the period shift is given in Eq. (2-1).

$$T_{shift} = T_b - T_s \quad (2-1)$$

where  $T_{shift}$  is period shift and  $T_b$ ,  $T_s$  are the isolated and fixed-base models fundamental natural periods, respectively. Ryan and Chopra developed a characteristic strength parameter for selecting an appropriate isolation device (Ryan & Chopra, 2004). The strength parameter was shown to be effective for predicting the energy dissipation capacity of the isolator independent of its period. This parameter includes the intensity of ground motion. As such, the isolation characteristic strength can be calibrated with respect to earthquake intensity. The period range at which base-isolated structures perform is mainly within the velocity-sensitive region of the spectrum. Therefore, the PGV (peak ground velocity) was proposed as representative of the ground motion intensity. The characteristic strength,  $\eta$ , is defined as follows:

$$\eta = \frac{Q}{m\omega_b \dot{u}_{go}} \quad (2-2)$$

where  $Q$  is characteristic strength;  $m$  is sum of the masses at floors and isolation level;  $\omega_b$  is base isolation frequency;  $\dot{u}_{go}$  is peak ground velocity. The greater the PGV, the higher the yield strength,  $Q$ , needs to be to keep  $\eta$  constant. The characteristic strength is inversely proportional with the frequency. This means that lowering the isolation frequency (increasing the period) decreases the required yield strength for the same  $\eta$  value. The system mass is also given in the denominator of the equation. As such, any increase in mass must be met with a proportional increase in strength to adequately maintain the characteristic strength. The value for  $\eta$  ranges between 0.2 and 0.8 due to the practical design limitations of isolation devices. A lower response is expected in the lower bound of  $\eta$  since this enables greater isolation deformation and consequently reduced superstructure responses. Figure 2.1 shows the bilinear elasto-plastic model for the isolation used in this study, assuming the conventionally accepted ratio of plastic stiffness as 1/10<sup>th</sup> of the stiffness of the elastic one.

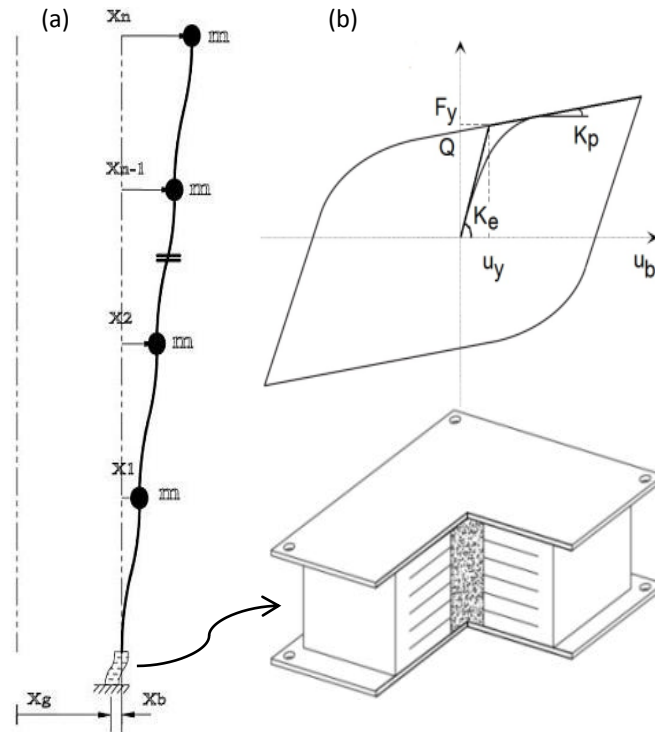


Figure 2.1: Bilinear force-deformation model of isolation

### 2.3 Multi-Story Structural Model

In the current study, a 3-story, 7-story, 11-story, 15-story model considered for performance evaluation with fundamental natural periods of vibration of 0.4s, 0.8s, 1.2s, 1.6s, respectively. The stiffness of models was then computed by trial and error such that those target periods of vibration were obtained using a linear dynamic modal analysis. In order to be in the practical range of periods in real structures, the target period values were selected based on the empirical equation for period of vibration of a steel moment resisting frame given in ASCE7-10 (2010). Story strength distribution over the height of the structure was considered proportional to earthquake lateral force profile. A good estimation of lateral force profile could be either mode shape one or a linear triangular

profile. Finally, a modified lateral force profile approximation which has been offered by several codes was used as following:

$$C_{vx} = \frac{w_x h_x^k}{\sum_{i=1}^n w_i h_i^k} \quad (2-3)$$

Based on this equation, the strength demand at each level is calculated and assigned to it as its yield strength. A stiffness distribution proportional to strength was also considered with values such that target fundamental period of vibration is achieved. The assumed stiffness and strength distribution delivers equal yield drift limits for all the stories resulting in a rather linear lateral deformation profile under presumed lateral load. This is close to condition where a combination of lateral shear-type deformations and lateral flexural-type deformations constitutes the final deformations. Masses were considered lumped at floors with equal amounts providing a uniform distribution. With assumed stiffness profile and mass values, story stiffness values are determined with some trial and error attempts performing linear dynamic analysis to reach the target periods. This modeling methodology enables repeating numerous analyses by continuously altering strength and stiffness over a wide range of values while tracking and recording the trend of results. The above mentioned methodology is very useful in rapid prototyping model buildings for research purposes where only the overall behavior of the structure is of concern.

After building the models with the first mode period of vibration equal to the target value, nonlinear dynamic analyses can be performed assuming an elastic-plastic behavior for each story with previously computed linear limit stiffness and yield strength values. Dynamic analyses were performed considering all effective modes of vibration. The

equation of motion of a multi-story structure on a base isolation system, as shown in Figure 2.1, can be expressed as:

$$[M]\{\ddot{u}\} + [C]\{\dot{u}\} + [K]\{u\} = -[M]\{I\}(\ddot{u}_g + \ddot{u}_b) \quad (2-4)$$

where  $\{\ddot{u}\}$ ,  $\{\dot{u}\}$  and  $\{u\}$  are acceleration; velocity and deformation vectors;  $\ddot{u}_g, \ddot{u}_b$  are ground and base isolation acceleration;  $[M]$  is mass matrix;  $[C]$  is damping matrix and  $[K]$  is stiffness matrix. This equation can also be written as the follows:

$$\begin{bmatrix} [M_s] & 0 \\ 0 & m_b \end{bmatrix} \begin{Bmatrix} \{\ddot{u}_s\} \\ \{\ddot{u}_b\} \end{Bmatrix} + \begin{bmatrix} [C_s] & 0 \\ 0 & C_b \end{bmatrix} \begin{Bmatrix} \{\dot{u}_s\} - \{I\}\dot{u}_b \\ \dot{u}_b \end{Bmatrix} + \begin{Bmatrix} \{f_s\} \\ f_b \end{Bmatrix} = - \begin{bmatrix} [M_s] & 0 \\ 0 & m_b \end{bmatrix} \{I\} (\ddot{u}_g + \ddot{u}_b) \quad (2-5)$$

where  $\{\ddot{u}_s\}$  and  $\{\dot{u}_s\}$  are superstructure acceleration and deformation vectors;  $[M_s]$  is superstructure mass matrix;  $[C_s]$  is superstructure damping matrix;  $C_b$  is isolation damping;  $\{f_s\}$  and  $f_b$  are superstructure force vector and isolation force.

## 2.4 Ground Motions

In an attempt to provide response spectra and time histories in investigations, different suites of ground motions have been provided as a part of SAC Steel Project at three probabilities of occurrence (2% in 50 years, 10% in 50 years and 50% in 50 years) for Boston, Seattle, and Los Angeles corresponding to seismic zones 2, 3 and 4 respectively. Each Suite contains 10 pairs of scaled motions provided for firm soil conditions and scaled to match to the target spectrum. For the current study, Los Angeles 2%, 10%, 50% in 50 years suites were selected, which correspond to 72 year, 475 year, and 2475 year return periods, respectively. The 2% in 50 year values are close to the maximum considered ground motions offered by Building Seismic Safety Council and the USGS with a less than 10% difference. Figure 2.2 compares 5% damped acceleration

spectra of the 10 pairs of scaled motions with 2%, 10% and 50% probability of occurrence in 50 years along with their median spectra for each hazard level.

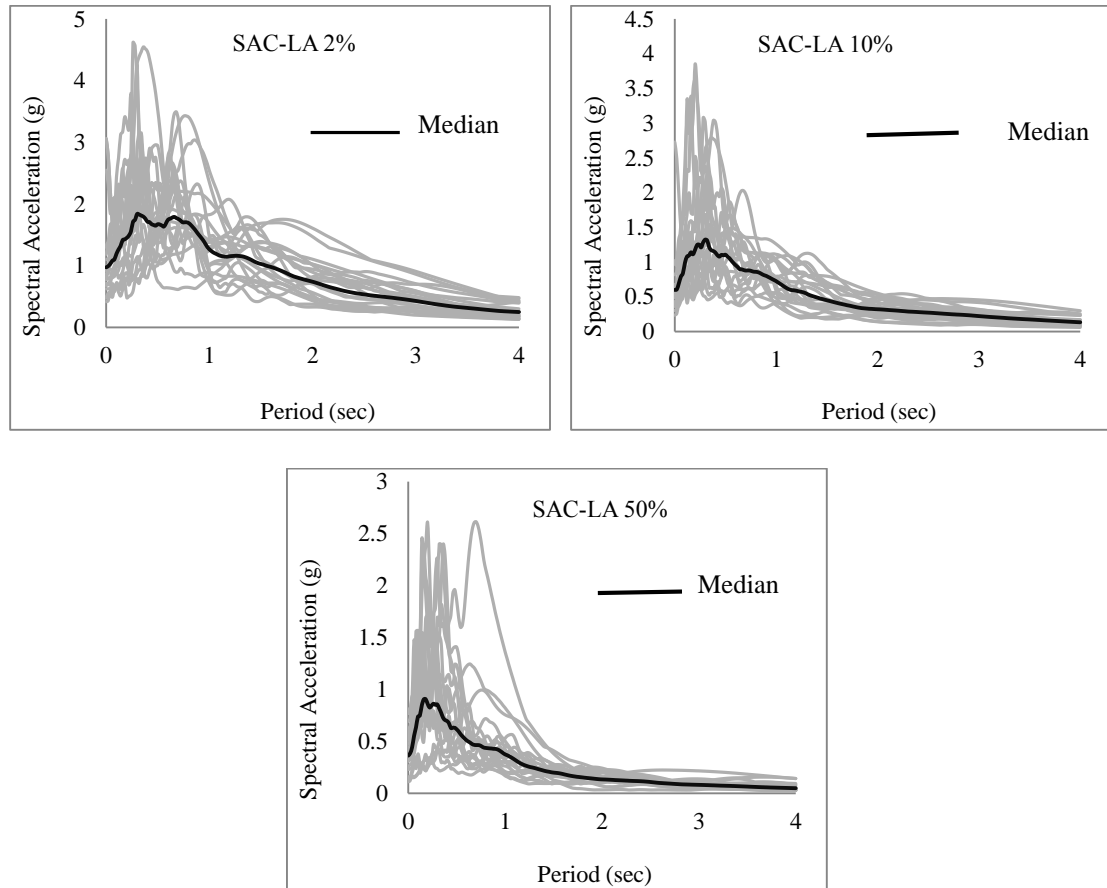


Figure 2.2: 5% Damped median linear response spectrum

## 2.5 Force Reduction Factor

Seismic resistance of fixed-based buildings usually uses the dissipating energy capacity of the structural members. This has led to introduction of response modification factors,  $R$ , which reduces the level of the lateral forces imposed by earthquake motions. With the application of the reduction factor, the elastic limit resistance demand decreases allowing for the nonlinear deformations to develop in the components. This calls for a

sufficient ductility capacity to be provided in structural design to satisfy the demand ductility. Ductility is the major contributing factor affecting the reduction factor. Due to high level of inelastic deformations of the base isolation device and consequently long periods of isolation vibration, this factor requires some modifications in these systems. Current codes suggest a reduction factor of less than 2 which is much smaller than the suggested values for fixed-base buildings. Therefore, the design forces of structural elements in a base-isolated structure may not be necessarily lower than those in corresponding elements in the fixed-based one.

In this study, methodology were directed such that to catch the effect of both base isolation and superstructure characteristics on the performance of base-isolated structures. Two different values for period shift  $T_{shift}$ , and normalized characteristic strength  $\eta$ , were considered. The median responses for the ground motions were used in the calculations and were obtained using the following equation:

$$\bar{X} = \exp \left[ \frac{\sum_{i=1}^n \ln x_i}{n} \right] \quad (2-6)$$

where  $x_i$  is the variable for which the median is calculated. Force reduction factor was defined as the ratio of base shear of the structure performing linearly to nonlinear one. Force reduction factor was then printed against ductility demand for different models. Ductility was defined as the maximum story nonlinear deformation divided by yield deformation. The largest ductility value of all stories was used in diagrams in the horizontal axis. The potential of previously mentioned modeling approach is revealed at this point where numerous analysis efforts are needed to be performed in a wide range of

ductility demands. Results can be generated in various ductility demands by changing the yield strength of the models consistently over a wide range of values.

Figure 2.2(a) illustrates the variation of force reduction factor against ductility demand in the fixed-based building for the four multi-story models. The reduction factor keeps increasing with ductility for all models. The period,  $T_s$ , has a significant influence in increasing this parameter. Reduction factors of up to nearly 3, 4, 4, and 4.3 at a ductility level of 8 were achieved for periods of 0.4s, 0.8s, 1.2s and 1.6s, respectively. This is consistent with the trend of constant ductility spectra curves or inelastic design spectrum usually drawn for single degree of freedom systems (Chopra, 2007)

Figures 2.3(b-e) also present the diagrams derived for base isolated models. Figure 2.3(b-c) correspond to conditions in which  $T_{\text{shift}}=2$  s and  $\eta$  is 0.4 and 0.8, respectively. Here again, an increase in ductility gives rise to reduction factor as expected. A rise in superstructure period increases the reduction factor similar to what was observed in non-isolated system, but the maximum achievable reduction factor for different ductility levels has dropped significantly. For example, in the case of  $T_s=0.8$ s and a ductility of 8, the fixed-base system is capable of reaching a reduction factor of 4 as compared to a value of around 1.6 in the base-isolated system which is almost a 2.5 times ratio. In the graphs with a higher period shift, Figures 2.3(d-e) with  $T_{\text{shift}}=4$ sec, base isolation only was able to deliver a reduction of about 1.5 at its maximum ductility. In spite of large superstructure ductility, there was no considerable advantage, in terms of reduction of lateral forces, in base-isolated models.

Although the reduction factor is much smaller in isolated systems, the design base shear for the same ductility demand can still be lower. Therefore, a good comparison of

the systems can be obtained by computing the ratio of the base shear of the non-isolated structure to that of isolated structure for the same superstructure ductility demand, called isolation reduction factor hereafter. This parameter represents the probable decrease in the design base shear demand of isolated buildings. Figure 2.4(a-d) illustrates the variation of base shear ratio against ductility given for different isolation properties and superstructure periods. The ratio is always greater than one showing that the use of base isolation decreases the base shear regardless of the properties of structure and isolation device. All diagrams show a decreasing trend with an increase in ductility. For example, in the case of  $T_s=1.6$  s,  $\eta=0.4$  and  $T_{\text{shift}}=2$ s in Figure 2.4(a), the ratio decreases from a value of 3 in ductility 1 to a value of 1.3 in ductility 8. For the higher isolation period shift,  $T_{\text{shift}}=4$ s in Figure 2.4(c), this parameter drops from 5 to 1.9 showing a better performance as predicted. In cases of lower superstructure periods,  $T_s=0.4$ s and  $T_s=0.8$ s, the calculated reduction factor are significantly higher in all amounts of ductility demonstrating the fact that isolation works better in low-rise buildings.

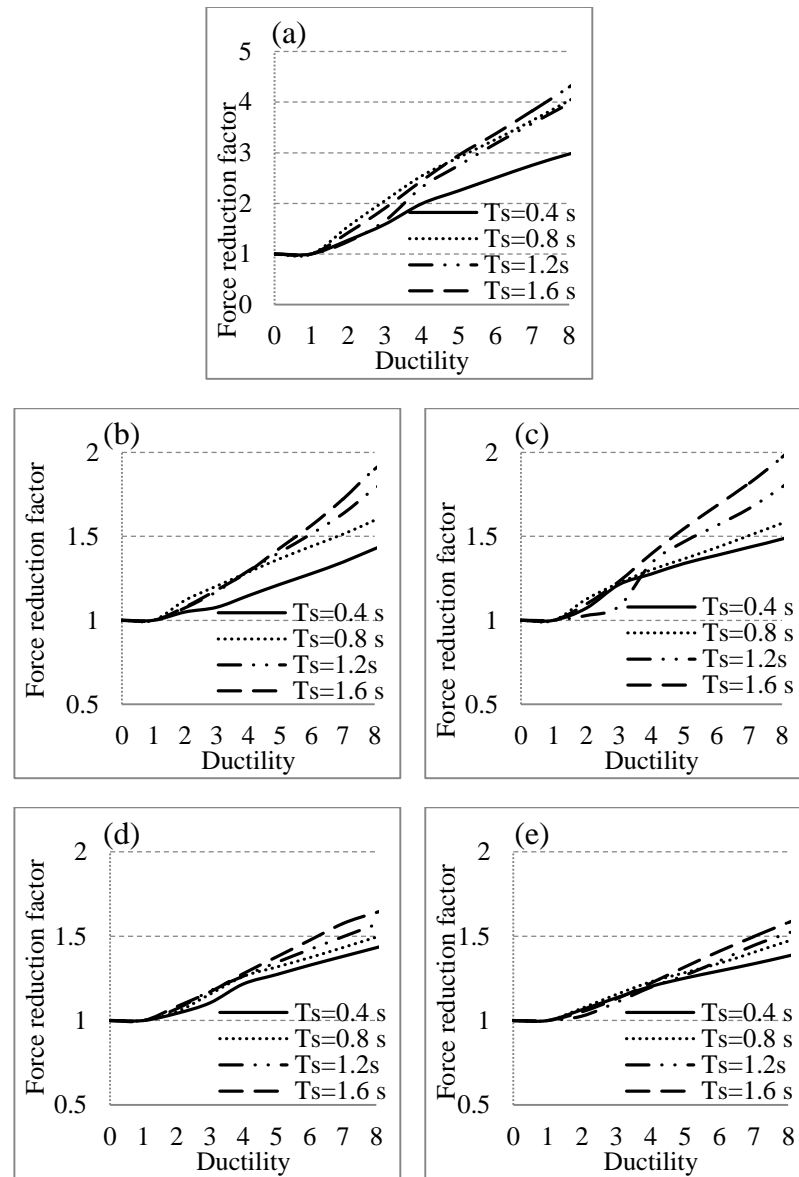


Figure 2.3: Force reduction factor  $R$  for (a) fixed-base model (b) Isolated  $T_{\text{shift}}=2$  s and  $\eta=0.4$  (c) Isolated  $T_{\text{shift}}=2$  s and  $\eta=0.8$  (d) Isolated  $T_{\text{shift}}=4$  s and  $\eta=0.4$  (e) Isolated  $T_{\text{shift}}=4$  s and  $\eta=0.8$

It is recommended to design the base-isolated structure in a way that no substantial nonlinear deformation occurs in the superstructure as it not only increases the damage

during an earthquake (lower performance level) but also delivers no substantial reduction in the design base shear demand of the studied models. This ensures a significant reduction in the design base shear of isolated system over its corresponding non-isolated system with identical ductility. Although a great reduction in forces is not accessible in this methodology, as the ductility reducing effect is intentionally eliminated from design procedure, a substantial performance increase is gained due to linear behavior of the superstructure during the earthquake.

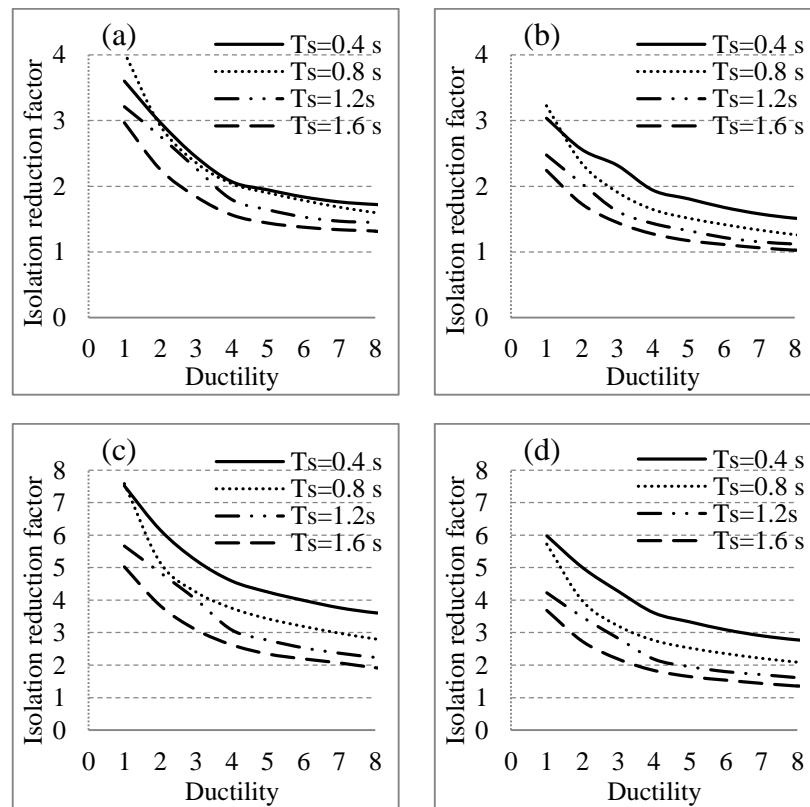


Figure 2.4: Isolation reduction factor  $R$  for (a) Isolated  $T_{shift}=2$  s and  $\eta=0.4$  (b) Isolated  $T_{shift}=2$  s and  $\eta=0.8$  (c) Isolated  $T_{shift}=4$  s and  $\eta=0.4$  (d) Isolated  $T_{shift}=4$  s and  $\eta=$

As a comparative study, it is worth to compare the base shear demand of an isolated model performing linearly with the ductility ratio equal to one to that of non-isolated model acting at different ductility amounts. This comparison may illustrate if any benefit in terms of the design base shear demand is obtainable when the isolated system is to behave linearly, during an extreme event. Therefore, a modified reduction factor is defined as the base shear of non-isolated system to that of isolated in the ductility of one. The results are represented in Figure 2.5(a-d) given for different isolation properties and superstructure periods. It is clear that increasing ductility will decrease modified reduction factor as the non-isolated building base shear demand is greatly reduced by increasing ductility. As a ductility of about 8 is achievable for a vast variety of ductile structures the comparison can be simply made at this point. In Figure 2.5(a) where  $\eta=0.4$  and  $T_{\text{shift}}=2\text{s}$  a reduction of 1.2, 1, 0.8, 0.7 is obtained for periods of 0.4s, 0.8s, 1.2s and 1.6s, respectively. While demonstrating a reduced design base shear for a rather rigid low-rise model ( $T_s=0.4\text{s}$ ), isolation delivers no reduction for the three latter mid-rise to high-rise models. Therefore, the isolated system has the potential to even be economical in stiff structures yet providing a better performance. In medium and rather high rise buildings,  $T_s=1.2\text{s}$  and  $T_s=1.6\text{s}$ , the isolated system experiences an increased base shear demand over the regular system at the rates of 0.8 and 0.7, respectively. In other diagrams where the period shift is very large,  $T_{\text{shift}}=4\text{s}$  in Figure 2.5(c-d), more force reduction occurs. Although this configuration leads to lower design forces, it may not be used as a basis for comparison as the design limitations in base isolation device does not often allow it.

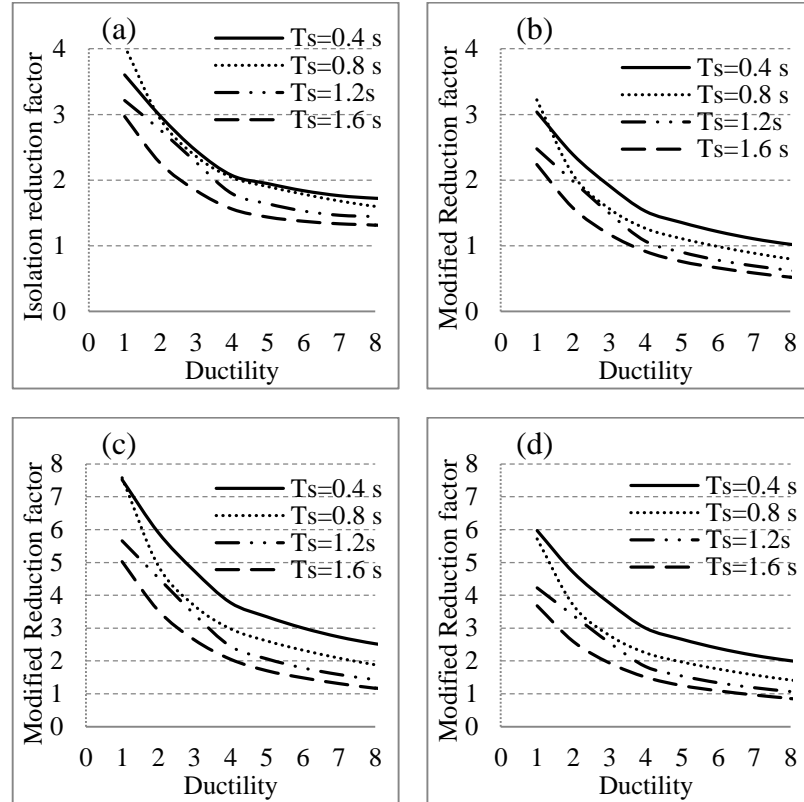


Figure 2.5: Modified isolation reduction factor R for

- (a) Isolated  $T_{shift} = 2s$  and  $\eta = 0.4$  (b) Isolated  $T_{shift} = 2s$  and  $\eta = 0.8$  (c) Isolated  $T_{shift} = 4s$  and  $\eta = 0.4$  (d) Isolated  $T_{shift} = 4s$  and  $\eta = 0.8$

## 2.6 Response Index

The new performance assessment methodology is released (ATC-58, 2012) which evaluates the performance through the loss estimation of building as a result of damage to structural, nonstructural and even contents of the building. Building components are classified into structural, nonstructural and contents. These elements are then categorized into acceleration sensitive, drift sensitive and both acceleration and drift sensitive. The methodology assesses the probability that a certain level of damage occurs in individual

buildings subjected to future earthquake shakings. This state of the art methodology considers the uncertainties both in earthquake shakings and response of individual components using their fragility curves.

It is necessary to estimate the cost percentage of the components contributing to total cost of the building toward a new response index formulation. Taghavi and Miranda (Taghavi & Miranda, 2003) studied the cost distribution of various components of buildings of different occupancy types including residential apartments, office buildings, hotels and hospitals using R.S. Means. The result of their investigation is presented in Figure 2.6. Structural costs can be as low as 18% of the total cost at its maximum value for office buildings. Contents costs exceed the structural cost in all buildings.

Nonstructural components compose the biggest portion in the total building cost at 62%, 70% and 48% corresponding to hotels, office and hospital buildings. Figure 1.7 indicates a cost distribution analysis over four studied buildings including a mid-rise apartment, hotel and office building and a high-rise hotel (Taghavi & Miranda, 2003). It is required to break the nonstructural component down into its composing elements as they can be different in terms of their sensitivity. Table 2.1 represents a more detailed cost break down of a conventional 5-10 story office building chosen for this study derived from the data provided by the same researchers.

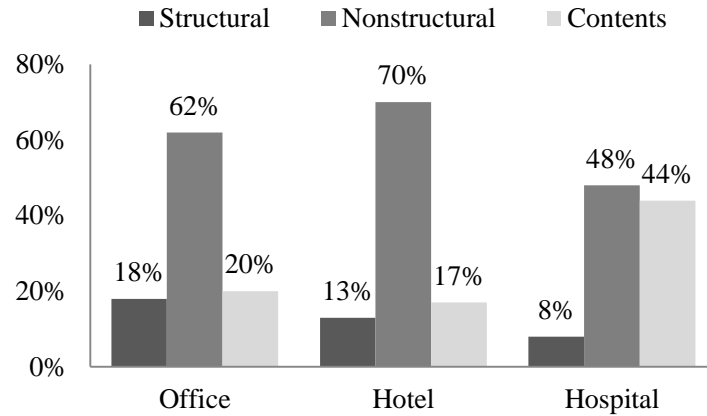


Figure 2.6: Cost percentage of components in buildings (Taghavi & Miranda, 2003)

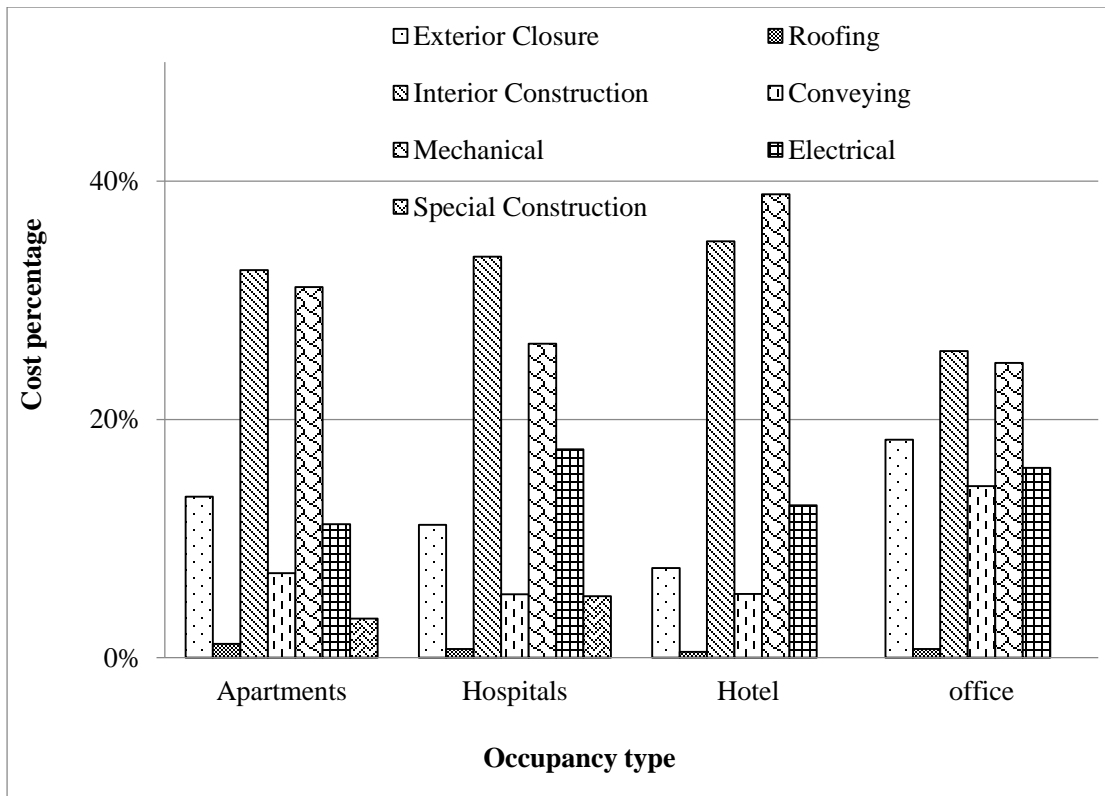


Figure 2.7: Cost breakdown of non-structural components (Taghavi & Miranda, 2003)

Table 2.1: Cost breakdown of a conventional 5-10 story office building

<b>Component Type</b>	<b>Cost percentage</b>
<b>Contents</b>	20.00%
<b>Structural</b>	18.00%
Exterior closure	11.20%
Roofing	1.04%
Interior	16.00%
<b>Nonstruc.</b> construction	
Conveying	9.20%
Mechanical	15.20%
Electrical	10.00%

The next step is to assess performance of each component according to its maximum acceleration or/and drift occurred during earthquake using its fragility curve. Fragility functions are statistical distributions representing the conditional probability of occurrence of a damage state for a demand value. A fragility curve characteristic is determined by its mean, dispersion and the type of distribution. A fragility curve library is prepared within in a software, PACT (ATC, 2012), made available as a part of ATC-58 project. The fragility functions are all assumed to be lognormally distributed variables provided in various damage states with different consequences. Hereby, it is of interest to employ this data for developing a cost-based index for comparison of different systems. Table 2.2 shows a list of components and their fragility curves properties and the sensitivity category assuming a steel moment resisting frame as the structural system.

A rational way is to include the cost percentage of components as weighting factors for final assessment of building performance. This gives each component an importance factor according to its cost. As a result, the proposed response index is as follow:

$$RI = \sum_{i=1}^n a_i \times p_i \quad (2-7)$$

where RI is response Index;  $a_i$  is importance factor equal to cost percentage; and  $p_i$  is the probability that the damage exceeds the predetermined damage state and is calculated using lognormal distribution equations as follows:

$$p_i = \Phi\left(\frac{\ln(x) - \mu_{\ln(x)}}{\beta_x}\right)$$

$$\beta_x^2 = \ln(V_x^2 + 1) \quad (2-8)$$

$$\mu_{\ln(x)} = \ln(\mu_x) - \frac{1}{2}\beta_x^2$$

where  $\mu_x$  and  $\beta_x$  are median and dispersion of lognormally distributed variable  $x$ ;  $V_x$  is coefficient of variation of variable  $x$  and  $\Phi$  is standard normal distribution function.

Table 2.2: Fragility curve properties of components

Component	Type	Cost percent	EDM	Fragility properties	
				Median	Dispersio
Post 1994 welded steel moment	Struct.	18.00%	Drift	0.050	0.350
Exterior Skin-Glass Curtainwall		11.20%	Drift	0.034	0.300
Exterior Roofing Concrete tile		1.04%	ACC.	1.900	0.400
Interior Walls GWB on Wood studs	Nonstruc	16.00%	Drift	0.030	0.400
Ceiling Systems Suspended		1.90%	ACC.	1.000	0.400
Conveying - Hydraulic elevator		9.20%	ACC.	0.400	0.300
Roof Mounted Equipment		15.20%	ACC.	1.600	0.500
Electrica		10.00%	ACC.	1.600	0.500
Miscellaneous housewares and art		3.00%	ACC.	0.200	0.500
Home Entertainment Equipment		3.00%	ACC.	0.200	0.500
Desktop Computers	Content	4.00%	ACC.	1.200	0.600
Servers and network Equipment		3.00%	ACC.	0.800	0.500
Tall File Cabinet		2.00%	ACC.	1.000	0.700
Unanchored Bookcase		2.00%	ACC.	0.400	0.300

For research purposes, the final damage state considered for all components refers to the most severe damage predictable in them. For example, the median drift value for the structural steel frame component is given as 0.05, indicating that there is a 50% probability of occurrence for the damage state if the drift in the story reaches a value of 0.05. These values are based on real observations of damage propagation and the failure of this particular structural system under various drift ratios. For example, Figure 2.8 illustrates the fragility curve for the “Miscellaneous Fragile Objects” component. The only damage state defined for this component is “fall off, objects break”. In the graph, the sensitivity parameter of the component (the peak floor acceleration) is shown on the horizontal axis. The probability that the damage in the component reaches the damage state, given the peak floor acceleration, is given on the vertical axis. There is a 50% probability that the damage state will occur when the acceleration reaches the median value, or 0.2g, and will keep increasing up to nearly 100% as it reaches 0.8g.

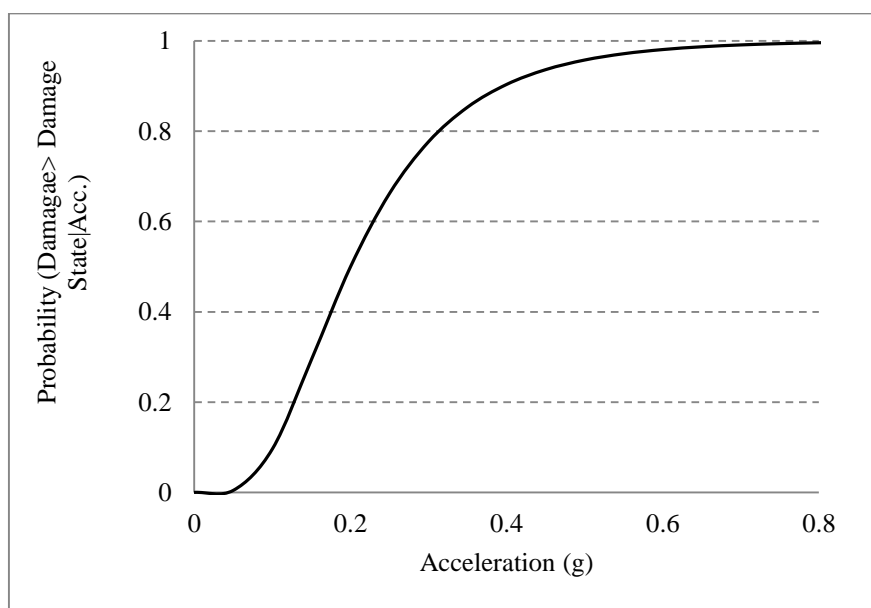


Figure 2.8: Fragility curve for “Miscellaneous Fragile Objects”

With the introduced equation, RI can be interpreted as probable damage costs as a fraction of total initial costs of the building during the earthquake. This definition delivers a meaningful tool through which the designer can decide on different alternatives of building designs. Again, taking the weighing factor  $a_i$  as the initial cost percentage implies that the repair cost percentage of a component is proportional to their initial cost percentage. A better evaluation based on the components final repair cost percentage delivers more accurate results. Until the complete set of fragility curves library are released, rough damage estimation is acceptable through this method.

The correlation of damages in different components largely adds to the complexity of the procedure of calculation of response index. The biggest correlation lies between the stability of structure and the functionality of all other components. In other words, if the building in this studies structurally collapses, none of the other components are able to continue their serviceability. Consequently, although the structural component does not compose a big portion of the total construction cost, its failure could cause a total loss of the assets. Therefore, a simple approach was taken by which the weighting factor of structural component increased to a unit value. This implies that structural severe damage or collapse is considered as a total loss.

Four previously discussed models were assessed and compared using the proposed response index. The mean story drifts and floor accelerations under the set of earthquakes used as inputs to the RI equation. Figure 2.9 indicates the variation of RI against ductility and superstructure period for different hazard levels. For LA 2% in 50 year suite in Figure 2.9(a-b), the non-isolated building RIs start at 0.43, 0.45, 0.40, 0.37 at a ductility of 1 and ends in 0.61, 0.6, 0.58, 0.56 at a ductility of 8 corresponding to superstructure

periods of 0.4s, 0.8s, 1.2s, 1.6s, respectively. For the isolated buildings, RI has decreased significantly to a value about 0.17 for all models at ductility equal to 1. This simply means a performance upgrade of 350% times over the fixed-based structure with the same ductility level. At the highest ductility,  $\mu=8$ , the isolated buildings performs at an RI of about 0.47 showing only a 25% improvement over the average fixed-base models performance.

For LA 10% in 50 year suite in Figure 2.9(c-d), a similar trend is observable with the difference that the RI indices are generally decreased with respect to LA 2% in 50 suite due to reduced hazard intensity. Response indices of 0.3, 0.28, 0.25 and 0.2 were observed at  $\mu=1$ , comparable to values 0.08, 0.11, 0.11, 0.10 for the isolated building performing at the same ductility corresponding to models with  $T_s=0.4s, 0.8s, 1.2s, 1.6s$ , respectively. A response improvement equal to 375%, 250%, 230% and 100% is achieved as a result of isolation application. However, at the higher bound of ductility,  $\mu=8$ , only performance upgrades of 30%, 21%, 12% and 10% were calculated showing that isolation is not able to maintain its advantage, especially in models with higher periods of vibration ( $T_s= 1.2s$  and  $1.6s$ ). An important result is that the lowest response index for fixed-base models was neither achieved in the linear structure (ductility=1) due to high floor accelerations nor in the highly deformed structure (ductility=8) where the inelastic drift ratios were high. The best response (less RI) was often achieved at a ductility of about 4 where fairly low levels of acceleration and drift ratio, combined together, resulted in a higher performance.

In general, the performance difference between the isolated and non-isolated high rise models decrease with respect to the lower rise ones. However, the performance can

still improve considerably for models with low ductility demands. This difference significantly decreases as the ductility at which the systems are compared is increased. Thus, in a high-rise model, the isolation model is not able to show a significant advantage over the fixed-based corresponding model when both performing with similar high ductility demands.

The response indices of the base isolated models at a ductility of 1 were also compared to those of the fixed-base models, performing at a higher ductility level. This is closer to real design conditions in which the goal is for the superstructure to perform rather linearly in a base-isolated building, while the structural ductility capacity is employed in the fixed-base design. An exact comparison point must be determined to avoid misleading conclusions since the base shear demand of the compared systems may not be identical. Referring back to Figure 2.5(a-b) where the  $T_s=0.4s, 0.8s, 1.2s, 1.6s$ , isolated model experiences a higher design base shear at  $\mu=1$  compared to a corresponding fixed-base building, performing at a higher ductility level. A comparison can reasonably be made at the point where the base shear demand of the isolated model is equal to that the fixed-base model. Therefore, a balance point ductility,  $\mu^*$ , is introduced at which the base shear of the fixed-base model is equal to that of the isolated one performing at a ductility equal to 1. This is the condition where the analysis procedure will lead to similar structural forces for both systems.

The results are summarized in Table 2.3 for different hazard levels. While the base isolated model RIs are measured equally at around 0.17 at the LA-2% hazard level, the corresponding fixed-base model values continue to decrease from 0.94 to 0.30 for 3-story to 15-story models, respectively. At the LA 10% hazard level, the RI is close to 0.10 in

base-isolated models while the corresponding fixed-base system RIs change between 0.66 to 0.16 for 3-story to 15-story models, respectively. The same procedure continues at the minimum hazard level for LA 50% in 50 year ground motion suites. In this case, the isolated model shows a response index of about 0.05 while the corresponding indices of the fixed-base models change from 0.11 to 0.05 for the low-rise 3-story to high-rise 15-story models, respectively.

The seismic isolation proves to be capable of protecting the structural, nonstructural, and building contents from severe damage as well as the related financial consequences of this damage). The isolated model was able to perform at nearly 6 and 3.5 times better than the fixed-base system in 3-story and 7-story models for the LA 2% suite. Since it can reduce the extremely high RI values, it is likely that the isolation devices would be useful for protecting buildings from extremely high levels of damage (with RIs of 94% and 60%, respectively). It should also be noted that considerable improvements were achieved at less intense hazard levels, such as for the LA 10% in 50 year suite and LA 50% in 50 year suite levels. The performance gap between the isolated and non-isolated models consistently shrinks in building models that have a greater number of floors. Thus, compared to low-rise fixed-base models, high-rise fixed-base models behaved much better with considerably lower response indices. They even performed rather similarly to the isolated models. The response index only decreases from 0.29 to 0.17 in the 15-story model for the LA 2% in 50 year suite when the base isolation model is used. This means that the base isolation model is not as effective in terms of improving building performance when there are medium to high periods of vibration. Since it is not

as effective, and the technical difficulties and costs associated with their use are high, isolation devices are not usually considered a design alternative for high-rise buildings.

Table 2.3: Response index of fixed–base and isolated models in different hazard levels

	SAC LA 2% in 50			SAC LA 10% in 50			SAC LA50% in 50		
	Fixed-base		Isolated	Fixed-base		Isolated	Fixed-base		Isolated
	$\mu^*$	RI	RI	$\mu^*$	RI	RI	$\mu^*$	RI	RI
3-story	11.	0.94	0.16	9.3	0.66	0.083	6.8	0.27	0.048
7-story	8	0.60	0.17	8.3	0.52	0.11	4.6	0.11	0.056
11-story	6.1	0.38	0.18	6.1	0.26	0.11	4.3	0.09	0.048
15-story	5.1	0.29	0.17	4.7	0.16	0.10	2.1	0.051	0.031

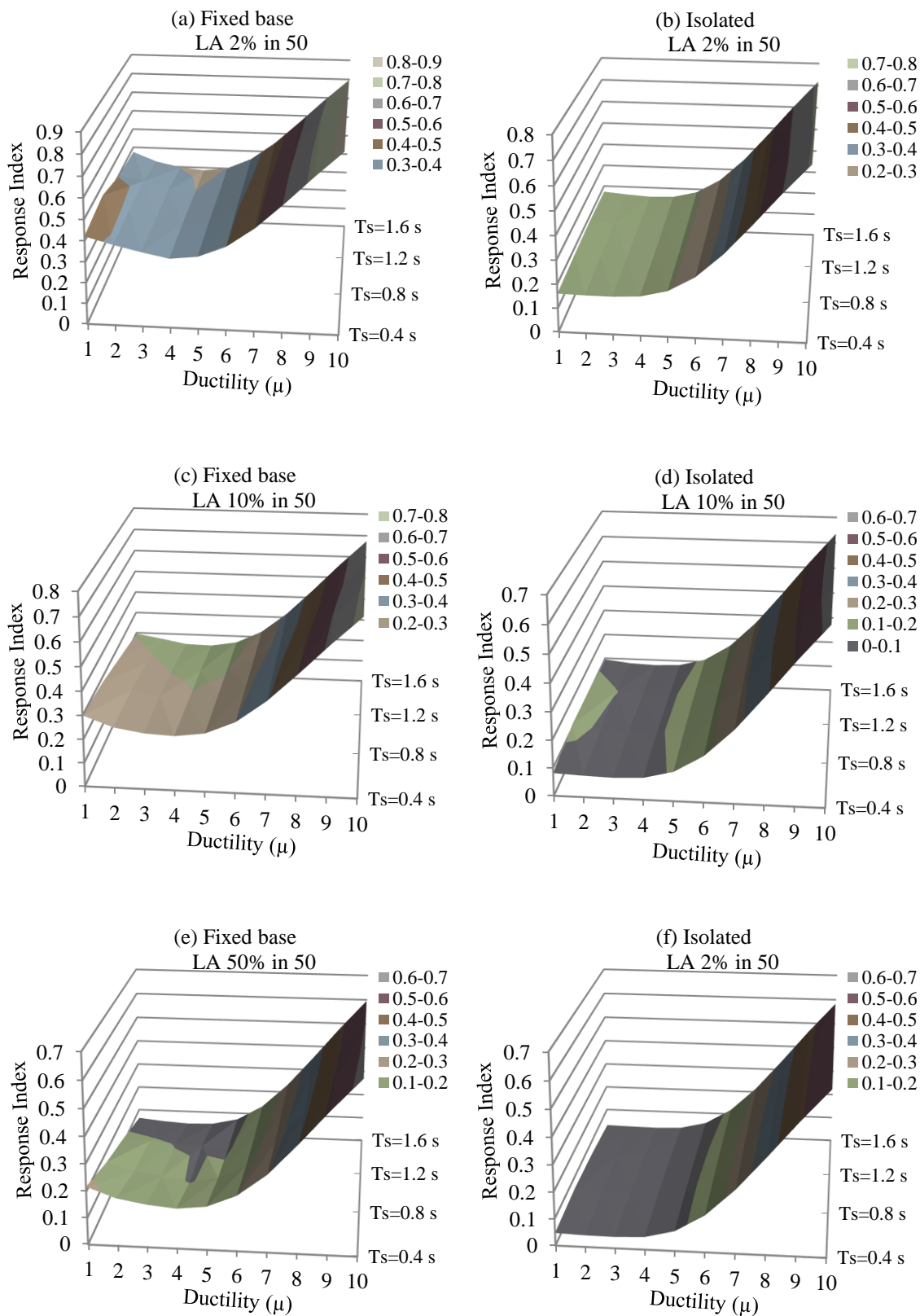


Figure 2.9: Response index versus ductility

## 2.7 Conclusion

This study presented a comparative study of isolated and fixed-base multi-story buildings using a cost-based response index. In the first part of the research, low-rise to high-rise fixed-base models were compared to corresponding isolated models and the base shear demands calculated. The analysis indicates that linearly performing isolated models are capable of reducing the base shear demands in low-rise to mid-rise buildings.

A new formulation for the RI was created based on the probable damages to the building components during seismic motion. For a typical office building with, the calculated RIs of isolated models were up to 6 times lower than the fixed-base ones for the low-rise 3-story model at the highest hazard level (LA 2%). Considerably lower improvements were achieved under less intense hazard levels, such as for the LA 10% in 50 year suite and 50% in 50 year suite. However, only a slight performance upgrade was achievable for rather high rise isolated building models (and especially for those located at low seismic hazard zones).

The potential of the proposed index formulation lies mostly in its simplicity and ease of application with respect to the detailed PEER methodology. Although it is an approximation based on the PEER approach, the formulation tool is very effective for making initial comparisons. Since it substantially reduces the analysis time and cost, the index may also serve as a tool for making cost comparisons among design alternatives for small building projects, a context in which such comparisons are typically not employed.

By improving the accuracy of the proposed RI, future research could be done by evaluating the response index of buildings in various states or locations in the United States. Future studies may want to consider different types of structural systems, the

number of stories, and the occupancy category as variables in the RI. These factors may be especially useful in rapid or initial performance comparisons between different design alternatives.

A limitation of this study is that the models did not recognize the different relationships between the lateral strength and stiffness. More work may thus need to be done to investigate how the trend observed in this work compares with that of other multi-story systems with different stiffness distributions. In order to get more accurate results, the relationship between the stiffness and strength for each story of a building can also be modeled with degrading properties. Further research is needed to determine the percent repair costs associated with the components. With the inclusion of these costs, the overall accuracy of the RI formulation can be improved. One shortcoming of the proposed RI is that it does not completely consider the correlation of the losses among all of the components. Future studies may thus want to look at integrating the effect of correlation into the response index equation.

## **Chapter 3 : Benchmark Buildings**

### **3.1 Benchmark Buildings Description**

This study investigates six four-story office buildings designed to comply with International Building Code (2012) and ACI 318-11 (2011). The buildings are located in the high seismic region of the Los Angeles urban area. The design variability is achieved by considering different levels of seismic design loads corresponding to different seismic risk category demand. Five fixed-based models are designed with design base shear ranging from 1 to 3 times the minimum values suggested by International Building Code provisions (IBC, 2012). A seismically isolated building is also designed according to aforementioned codes and ASCE7 guidelines (ASCE7, 2010). Buildings layout and details regarding the structural and nonstructural components contributing to damage and loss analysis is discussed in this chapter.

### **3.2 Site Description**

The buildings construction site are assumed in California urban area. The site is located south of downtown Los Angeles, 33.996N, 118.162 W. This is the same location used for a research study conducted by Haselton et al (Haselton, et al., 2008). Their site selection objective was to represent NEHRP site class D while avoiding local site amplification due to lens-shaped underlying sediment.

There is no need to consider near-fault directivity pulses and near-fault ground motions for this site as no single fault produces a strong motion capable of dominating the site hazard. The site selection criteria best suits the objectives of this study to

represent a typical earthquake hazard for the California urban Area. Figure 3.1 is the site map including faults shown by red black and white lines corresponding to strike-slip, reverse, and normal faults, respectively. The shear wave velocity indicated to have an average of 285m/s in the upper 30 m corresponding to site soil condition of D according to NCHRP classification.

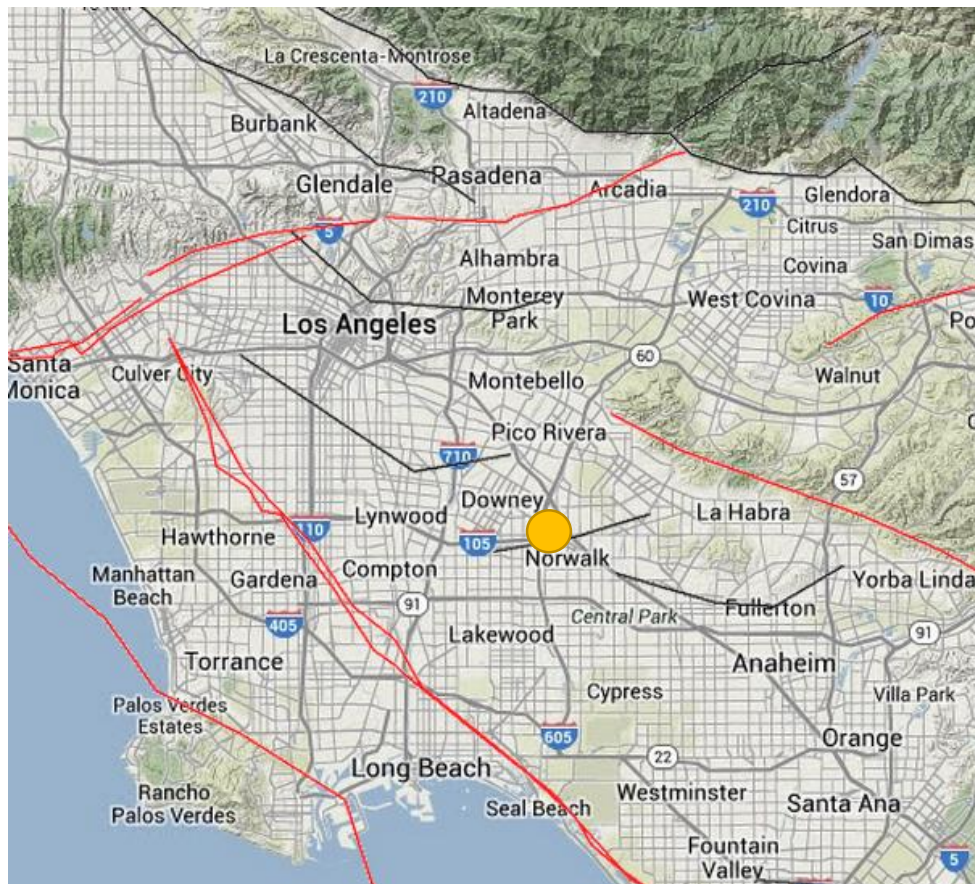


Figure 3.1: Location map for Los Angeles Bulk Mail site.

### 3.3 Building Layout

Common building bay sizes include rectangles of 20'×30', 20'×40' or similar dimensions like 18'×36'. Square bays of 20'×20', 24'×24', or 30'×30' are also used in

practice. The use of a square bays for research purpose has an advantage over the rectangle. It provides a fully symmetric plan layout where the frame can be identically designed in both directions. This is especially useful in avoiding unnecessary analysis and design effort as well as reducing the output volume. The benchmark building structural plan is shown in Figure 3.2 and the elevation plan is given in Figure 3.3. The bay dimension is 24-ft in all bays in both horizontal directions. The story height is 14-ft in all stories as a typical value for an office building. The complete symmetrical layout allows eliminating any unnecessary analytical and design variations in the two horizontal X and Y directions.

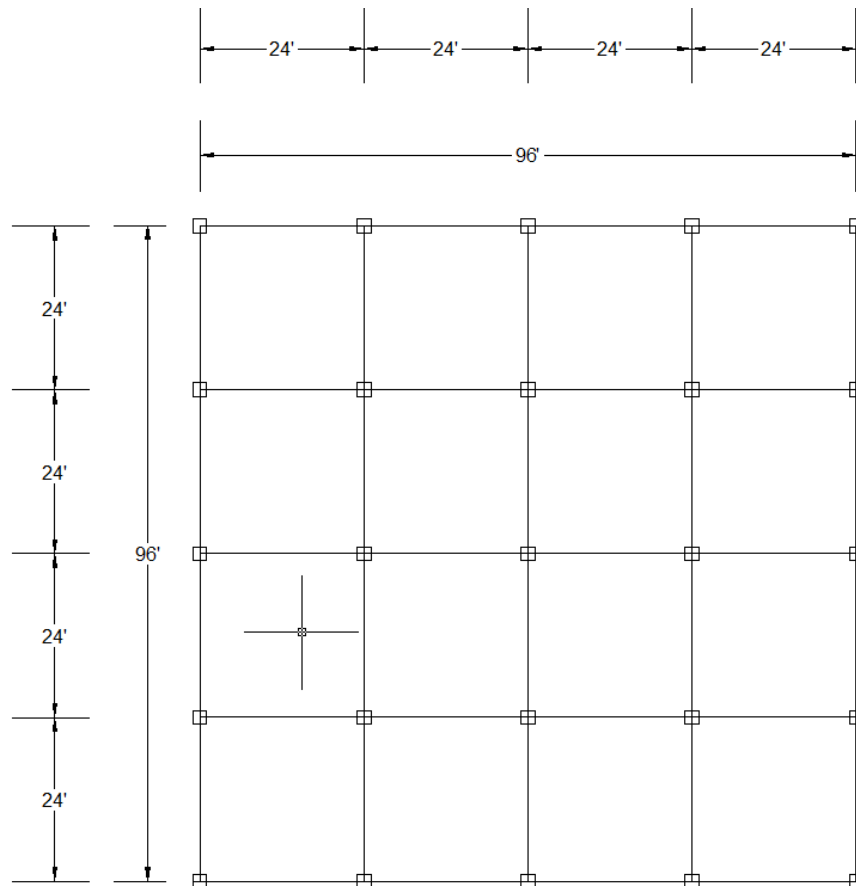


Figure 3.2: Plan Layout view of the 4-story building

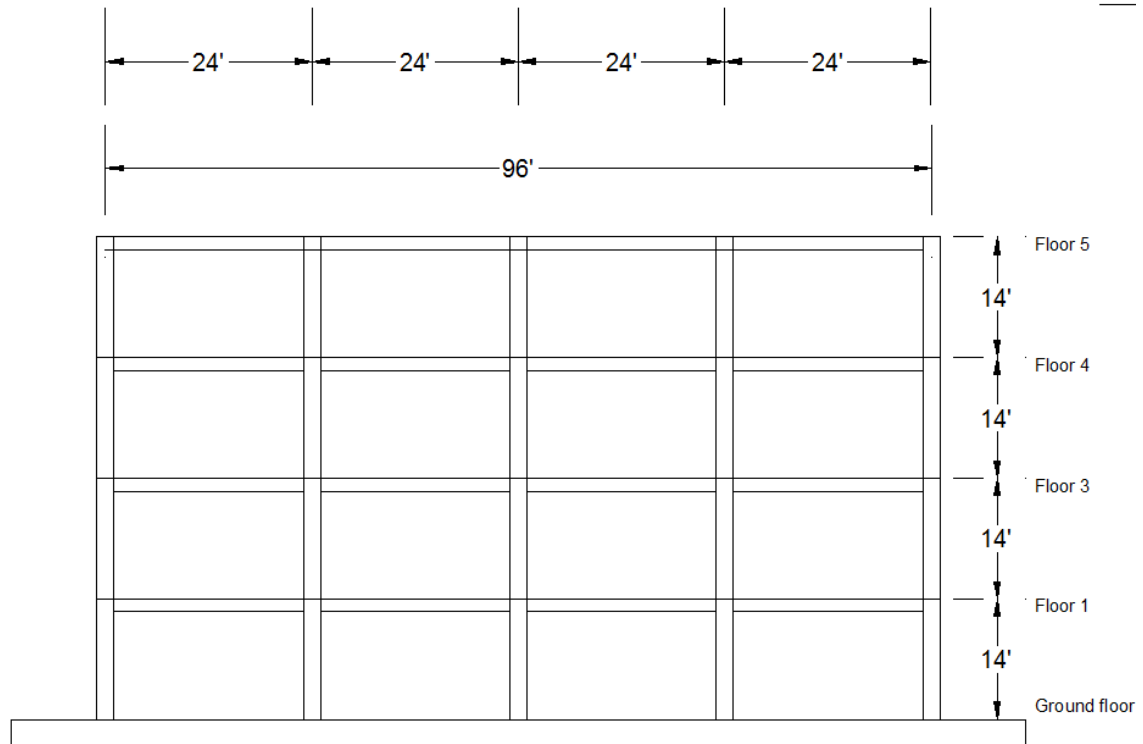


Figure 3.3: Elevation view of building frames

### 3.4 Gravity Loads

Dead loads known as permanent loads are the weight of non-movable material and structure. It includes the roof, floors, walls and claddings often presented on pounds per square foot basis. The assumed typical dead loads for the benchmark building is given in the Table 3.1. The construction material listed in the table is targeted at achieving a practical loading condition for a typical office building in the United States.

Table 3.1: Dead load materials and objects

Component and material	Dead Load (psf)
Flooring:	
Concrete, normal weight per 1" thickness 9"	112.5
Vinyl tile, 1/8"	1.5
Roofing	
Concrete, normal weight per 1" thickness 9"	135
EPDM	6.5
Ceilings:	
Channel suspended acoustical 1.5	1.5
Walls & Partitions:	
4" Metal Studs, 16" OC, 20 ga	1.8
½" GWB T & F (Level 4), both sides	4.2
Prime & Paint (2 Coats), both sides	1
Mechanical and Electrical	5

The total dead load of floors and roof is determined as follows:

9" concrete slab.....= 112.5 psf  
 Vinyl tile, 1/8" ..... = 1.5 psf  
 Acoustical hung ceiling..... = 1.5 psf  
 Mechanical/Electrical.....=5 psf

Sub-total = 120.5 psf

Live Loads include loads from human occupants, movable objects, furnishing, and storage. The assumed live loads are given in Table 3.2. Per IBC 1607.5, a uniformly distributed live load of 15 psf is applied on all floors. This is particularly introduced for places like office buildings where the portion locations are subject to change. Floor live loads are subject to reduction in any floor area in accordance with the IBC section 1607.10.

Table 3.2: Floors and roof live load

Location	Load (psf)
Floors	
Offices	50
Lobbies	100
Corridors	80
Partitions	15
Roof	
Flat roof	20

### 3.5 Structural Design

Building structure is the special moment resisting frame (SMRF) according to IBC (2012) and ACI 318-11 provisions (2011). Moment resisting frames allow much flexibility in architecture space planning. The moment concrete frames are assigned to seismic design category D, thus special detailing and proportioning of structural elements is required according to ACI 318-11 (2011) to ensure ductile behavior.

#### 3.5.1 Reinforcement Ratio

Reinforcement ratio in columns and beams is a design variants which was kept within a practical range for all designs. In order to maintain consistency in cost estimations, this is important as this parameter can affect the cost of structural elements. This criterion eliminates the unnecessary variants to affect and possibly deviate the cost comparisons. Table 3.3 shows reinforcement ratio ranges assumed for column and beams. These values were selected based on the practitioner designs to reflect the current practice in the design firms. A reinforcement ratio of at least 60% of the tension reinforcement is assumed for beams designs which exceeds the minimum 50% recommended. As a common engineering design practice, the maximum demand to

capacity ratio in any element is 0.8 as opposed to 1 indicating more conservative design philosophy.

Table 3.3: Typical reinforcement ratio in column and beam components design

Structural Component	Tension Reinforcement	Total Reinforcement
Columns	-	1.5%-2.5%
Beam	0.7%-1.4%	-

### 3.5.2 Effective Stiffness

Effective stiffness of cracked concrete members needs to be appropriately determined for the analysis. It can affect internal force distribution, base shear and building period. Effective stiffness is dependent on the amount of reinforcement and external forces. Thus, stiffness varies along the member length. Analytical programs often use simple effective stiffness equations given by design codes for beam and column elements. Table 3.4 represents ACI 318-11 (2011) recommendations for the ratio of effective stiffness to gross total stiffness of the section ( $I_e/I_g$ ).

Table 3.4: Dead load materials and objects

Element	$I_e/I_g$	
	ACI 318	ASCE 41
Beam	0.35-.50	0.3 if $P \leq 0.1 A_g f'_c$
Column	0.50-0.70	0.7 if $P \geq 0.5 A_g f'_c$

P is the axial compression force acting on the section;  $A_g$  is the gross cross sectional area and  $f'_c$  is the concrete 28 days compression strength

### **3.5.3 Strong-Column Weak Beam Principle**

Columns are the critical elements in the structural system in charge of supporting/transferring the building weight and lateral forces and transferring it to the foundation. The drift and consequently the damage tend to concentrate in one or few stories if the building has weak columns with respect to beams. Columns are required to be relatively stronger than connecting girders or beams for a more uniform distribution of lateral drift during an earthquake. Additionally, the probability of failure of these elements decreases significantly by strong column weak beam principle. Building codes have adopted this concept in their provisions often called as strong-column weak-beam principle to ensure the safe behavior of frames during strong earthquakes. This is reflected in codes by comparing the sum of column strengths to sum of beam strength at each joint in a moment resisting frame. In this study, all concrete frames were designed such that the strength ratio of columns to beams is at least 1.3 which exceeds the minimum, 1.2, recommended per ACI 318-11 (2011).

### **3.5.4 Non-Ductile Failure Modes**

Ductility is achieved when structural members yield in flexure rather than to fail in shear. Shear failure is considered brittle mode of collapse as the member experiences a sudden loss of capacity. The modern design codes do not allow non-ductile behavior of such members especially in high seismically active areas. For example, ACI 318-11 (2011) considers zero concrete shear strength when the member is subject to cyclic loads. Anchorage and lap splice failure are another brittle failure modes that significantly decrease the ductility capacity of the member. These failure modes are not expected to in

concrete frames designed according to modern building codes. Therefore, the benchmark buildings are designed to perform in a ductile manner where brittle modes of collapse are not predicted in the structural models.

### 3.5.5 Fixed-Based Models

The building site has a mapped short-period and 1-sec period ( $S_s$  and  $S_1$ ) spectral acceleration of 2.16g and 0.75g, respectively, according to IBC-2012 seismic hazard maps. The long-period transition period ( $T_L$ ) is also equal to 8s. Site coefficient factors,  $F_a$  and  $F_v$ , for site soil type D, are determined as 1.0 and 1.5, respectively. The 5%-damped design spectral response accelerations at short period and 1-sec period are:

$$\begin{aligned} S_{DS} &= 2/3 \times F_a \times S_s = 1.44 \\ S_{D1} &= 2/3 \times F_v \times S_1 = 0.75 \end{aligned} \quad (3-1)$$

The transition period  $T_s$  for the response spectrum is:

$$T_s = \frac{SD_1}{SDS} = \frac{0.75}{1.44} = 0.52 \quad (3-2)$$

According to IBC-2012 1604.5, office buildings are classified in risk category II. Seismic design category of E is applicable as the mapped spectral response acceleration at 1-second period is greater than 0.75. Occupancy importance factor  $I$ , equal to 1.0 is therefore applicable for seismic load calculations.

The seismic-force-resisting systems consists of moment resisting frames in the N-S. E-W directions. For the buildings, assigned to Seismic Design Category E, all moment-resisting frames are required to be designed and detailed as special moment frames. Table 3.5 gives the response modification coefficient ( $R$ ), the system over strength factor ( $\Omega_0$ ),

and the deflection amplification factor ( $C_d$ ) for the selected structural system according to ASCE7 (2010).

Table 3.5: Design coefficients and factors for seismic design

Response Direction	Frame Type	R	$\Omega_0$	Cd
N-S and E-W	Special moment frame	8	3	5.5

There is no type of plan or vertical irregularities present in buildings. The mass is distributed rather uniformly over the floors and the story stiffness varies smoothly along the height eliminating any potential causes of irregularities. According to ASCE7 (2010) for the simplified design procedure, the design base shear for the structure is:

$$V = C_s \times W \quad (3-3)$$

where  $W$  is the effective weight of the building and  $C_s$  is the seismic response coefficient calculated as follows :

$$C_s = \frac{S_{D1}}{T(R/I)} \quad (3-4)$$

where  $T$  is the fundamental period of vibration,  $I$  is importance factor, and all of the other terms have been previously defined in this chapter. An importance factor of 1 is applicable for an office building based on the design recommendations. The benchmark buildings are to be designed with different levels of base shear up to 3 times the minimum values. This is applied by using different importance factors in equation 3-4. This coefficient is used for adjusting minimum loads for the buildings associated with different seismic risk categories; for example 1.25 and 1.5 values are used for buildings in seismic risk category of III and IV.

B1 model is the building designed based on the minimum requirements for an office building. Seismic risk category II and an importance factor of 1 are used for this model. Design B2 is based on the seismic design forces 25% higher suggested for building in seismic risk category III. This category is used for buildings with substantial hazard do human life in the event of failure. Design B3 is based on forces 50% greater than B1 representing seismic demand forces used for analysis and design of essential facilities, categorized in seismic risk category III. The two latter models, B3 and B4, are designed for seismic loads 100% and 200% greater than the minimum requirement offered in B1. These design seismic loads are beyond the maximums suggested by IBC (2012) for the design of essential facilities ( $I=1.5$ ). B4 and B5 are only used to investigate the effect of extra safe building designs on the long term costs and consequences which will be explained in full details in the following chapters. In equivalent lateral load procedure, ELF, the fundamental period of vibration is determined in accordance with ASCE 7-10 section 12.8.1:

$$T_a = C_t h_n^x \quad (3-5)$$

where  $C_t$  and  $x$  coefficient are determined based on the structural system selected, and  $h_n$  is the height of the building. This equation is based on lower bound regression analysis for period of vibration of buildings measured in California. Thus, the results are conservative in predicting responses including base shear.

A modal dynamic analysis was carried out for the vibration period estimation. Flexibilities including flexural, shear, bond-slip, and joint shear panel is accounted for in the structural model built in Openness as explained in full detail in chapter 4. The periods obtained in OpenSees is considerably higher than those obtained in SAP2000

(Computeres and Structures Inc., 2012). The model built in does not consider all those flexibilities and gives lower estimates of vibration period.

Modal analysis does not account for the nonstructural components stiffness and gives a higher estimate of vibration periods. Therefore, an upper bound period of vibration is suggested by ASCE7 (2010) through the use of  $C_u$  factor. Table 3.6 gives vibration periods for all building designs obtained by modal dynamic analysis and ASCE7 (2010) empirical equation. The empirical Equation, Equation 3-5, gives the same period for all buildings having the same structural system and height regardless of their structural elements dimensions. The period of vibration equal to 0.84s is the basis for seismic calculation in B1, B2, and B3. Dynamic analysis periods of B4 and B5 designs are used for seismic calculations as they are smaller than upper bound of empirical equation.

Table 3.6: Vibration period of buildings

Building model	I (importance factor)	ELF procedure			$C_u^* \times T_a$ (sec)	$T_d$ (sec)
		$C_t$	$h_n$ (ft)	$x$		
B1	1.0	0.016	56	0.9	0.84	1.36
B2	1.25				0.84	1.14
B3	1.5				0.84	0.88
B4	1.75				0.84	0.78
B5	3.0				0.84	0.64

\* Coefficient for the upper limit on the period equal to 1.4 per ASCE 7-10

### 3.5.6 Seismically-Isolated Model

The seismically isolated building inherits the same layout as the fixed-based buildings. The structure has plan dimensions of 96 ft. by 96 ft. at all floors having the

columns spaced at 24 ft in both horizontal directions. Increasing the bay size and consequently increased gravity loads on columns enhance the performance of isolation system. The large gravity loads on columns allows for reaching higher periods of vibration and lower seismic forces. Additionally, this would be also beneficial in terms of design economy due to reduced number of isolators. Anyway, to keep the design configuration the same as fixed-base buildings, the bay size was decided to be the same as 24 ft.

Figure 3.4 show a typical elevation plan of the isolated frames. The isolation system is located below first floor columns supported by a slab-girder floor system. The added floor provides stability for isolators against gravity and earthquake loads. The proper function of such structural elements including girders and column segments are essentially important to maintain the stability of isolation system.

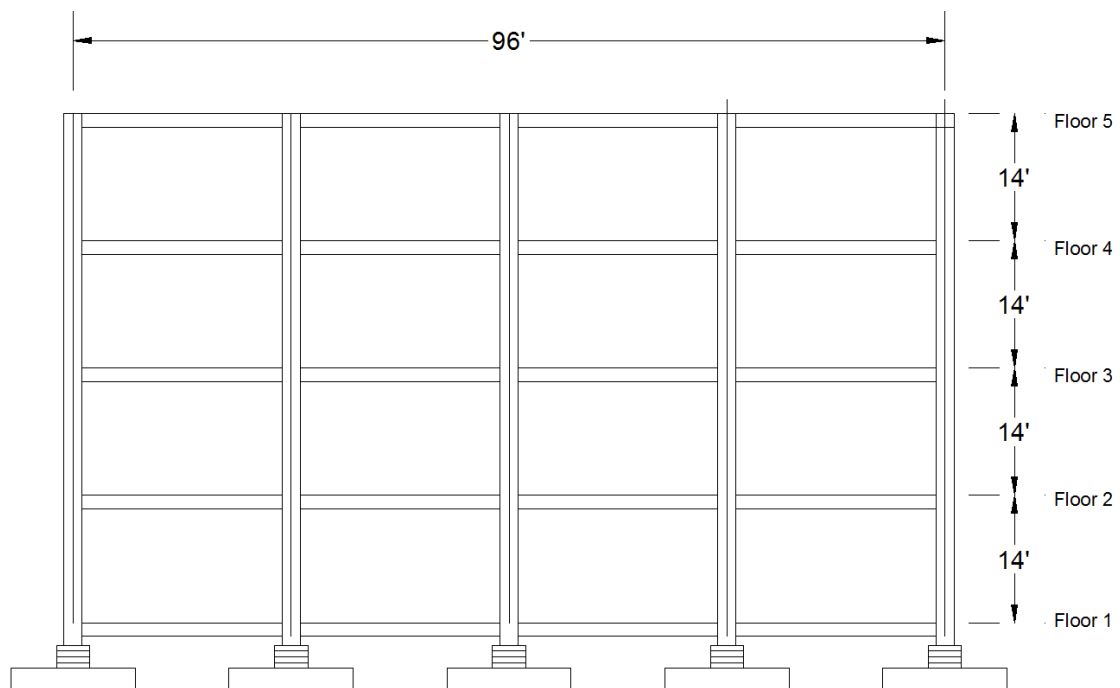


Figure 3.4: Elevation view of the isolated building frames

The design provisions of IBC (2012) requires the isolation system to sustain displacement and corresponding forces associated with the maximum considered earthquake. This ensures the stability and functionality of isolation devices even in a very big earthquake. Significant structural ductility demand is believed to produce large responses including drift demands resulting in excessive damage. Thus, the structure above the isolation interface is designed to sustain design forces while remaining elastic. Response modification factors is limited to 3/8 of those suggested for fixed-based buildings. Therefore, due to over strength factor in the design, isolated structures are expected to perform essentially elastic in the design level earthquake. For the benchmark isolated building, the response modification factor is:

$$R = \min \left\{ \begin{array}{l} 3/8 R_{fixed-based} = 3/8 * 8 = 3 \\ 2 \end{array} \right. \Rightarrow R = 2 \quad (3-6)$$

### 3.5.6.1 Analysis method

Three types of analysis are available, equivalent lateral force procedure (ELF), dynamic analysis using response spectrum, and nonlinear dynamic time history analysis. The period of vibration of most isolated building falls between 1s and  $T_L$ . The ELF analysis predicts the isolation displacement demand associated with the response spectrum shape in this period range. ELF analysis shall always be performed regardless of what type of analysis is selected because dynamics analysis responses must be revised based on ELF results. ELF and response spectrum analysis are less sophisticated methods

comparing to nonlinear dynamic analysis, therefore, there are limitations on these analyses applications.

Table 3.7 shows the acceptable methods of analysis in different site conditions. For the building of this study, the only condition which limits the use of the simple equivalent linear procedure is the  $S_1$  being greater than 0.6g. In this case, the two other methods including response spectrum analysis and time history analysis are acceptable methods. The more frequently used response spectrum analysis was selected to avoid more complicated design procedure of time history analysis.

Table 3.7: Acceptable methods of analysis for base-isolated buildings

Criteria	ELF	Response Spectrum Analysis	Time history analysis
$S_1 > 0.6g$	NP	P	P
Site class E, F	NP	NP	P
Height > 4 stories and 65 ft	NP	P	P
$T_M^* > 3.0$ s. and $T_D > 3T^*$			

$T_M^*$  the effective period of isolated structure at the maximum displacement

$T_D^*$  the effective period of isolated structure at the maximum displacement

### 3.5.6.2 Isolation system design displacement

Although the actual behavior of isolation system is nonlinear, the equivalent lateral force and modal dynamic response analysis use an effective stiffness and damping for modeling this components. Effective stiffness is the secant stiffness of the isolation device at the demand displacement shown in Figure 3.5. The effective viscous damping ( $\beta_D$ ) is based on the area of hysteresis loops measured by testing prototype of the isolator

device. Effective stiffness and effective damping are determined by the following equations according to ASCE7 (2010) Equation 17.8-1 and Eq. 17.8-2:

$$K_{eff} = \frac{|F^+| + |F^-|}{|\Delta^+| + |\Delta^-|}$$

$$\beta_{eff} = \frac{2}{\pi} \frac{E_{loop}}{(|\Delta^+| + |\Delta^-|)^2} \quad (3-7)$$

where the parameters are illustrated in Fig. 3.5

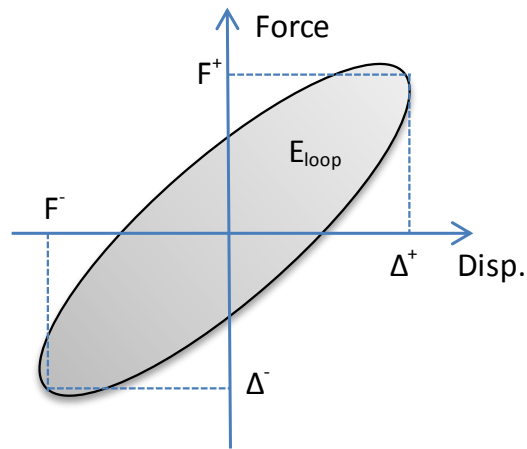


Figure 3.5: Effective stiffness and damping of isolators

The isolation system shall be designed to withstand a minimum design displacement determined according to ASCE 7-10 Eq. 17.5-1:

$$D_D = \frac{g}{4 \pi^2} \frac{S_{D1} T_D}{B_D} \quad (3-8)$$

where  $g$  is acceleration due to gravity,  $S_{D1}$  is the 5% damped spectral response at a period of 1 second,  $T_D$  is the system period and  $B_D$  is a coefficient related to effective damping of isolation system,  $\beta_D$ . This equation is identical to the equation for the maximum displacement of a single degree of freedom system having a period of  $T_D$  and

an effective damping of  $\beta D$ . When critical damping ratio is 5%,  $B_D$  is equal to 1.0 and increases as critical damping increases.  $B_D$  was initially estimated at 1.35 corresponding to a critical damping ratio of 15%. The minimum stiffness,  $K_{Dmin}$ , is determined using the deformational characteristics of the isolation system using ASCE7 (2010) Equation 17.5-2 which is based on single degree of freedom system dynamic characteristics:

$$T_D = 2\pi \sqrt{\frac{W}{K_{Dmin}g}} \rightarrow K_{Dmin} = \left(\frac{2\pi}{T_D}\right)^2 \frac{W}{g} = \left(\frac{2\pi}{2.5}\right)^2 \frac{7910}{386.4} = 129.2 \text{ kips/in} \quad (3-9)$$

where  $W$  is the effective weight of the building. Maximum displacement at the center of mass of the building,  $D_M$ , under the maximum considered earthquake is as follows:

$$D_M = \frac{g}{4\pi^2} \frac{S_{M1} T_M}{B_M} \quad (3-10)$$

where  $T_M$  is the effective period of vibration at maximum displacement, and  $B_M$  is defined similarly to  $B_D$  coefficient except that it is calculated at the maximum displacement,  $D_M$ . Stability of isolation system must also be checked for the total maximum displacement calculated based on the actual and accidental mass eccentricity in plan. Total maximum displacement shall include the most disadvantageous location of eccentric mass resulting in the largest isolators' displacement at the plan edges and corners. For a square building plan with rather uniformly distributed mass, the 5% accidental mass eccentricity imposes an extra 15% displacement to isolators at the corners.

Selection of an effective period of the isolated structure is the first step for the design of an isolated structure. A period of 2.5 to 3 times the fixed-base building period of

vibration is appropriate which can be used as a preliminary guess. Therefore, an effective period of 2.5 sec appears a good estimate as the period of vibration of fixed-base structures were determined to be around 1.01 sec. This is the period obtained in SAP2000 (Computeres and Structures Inc., 2012) comparing to 1.36s obtained in OpenSees (2002). Table 3.8 gives the design and maximum displacements for the structure.

Table 3.8: Initial estimates of isolation design and maximum displacements

Design displacement parameters			$D_D (in )$	Max. displacement parameters			$D_M (in )$	$D_{TM} (in )$
$S_{DI} (g)$	$T_D (sec)$	$B_D$		$S_{MI} (g)$	$T_D (sec)$	$B_D$		
0.75	2.5	1.35	13.6	1.125	2.5	1.35	20.4	23.5

A typical hysteresis loop for a Lead rubber bearing is presented in the Figure 3.6. The force intercept at zero displacement,  $Q_d$ , is known as characteristic strength. The characteristic strength is often dependent on the size of the lead core and often varies between 3 to 10 percent of the effective weight of the building. The high elastic stiffness provided by the lead core is important in limiting isolation displacement under wind loading or low intensities ground motions.

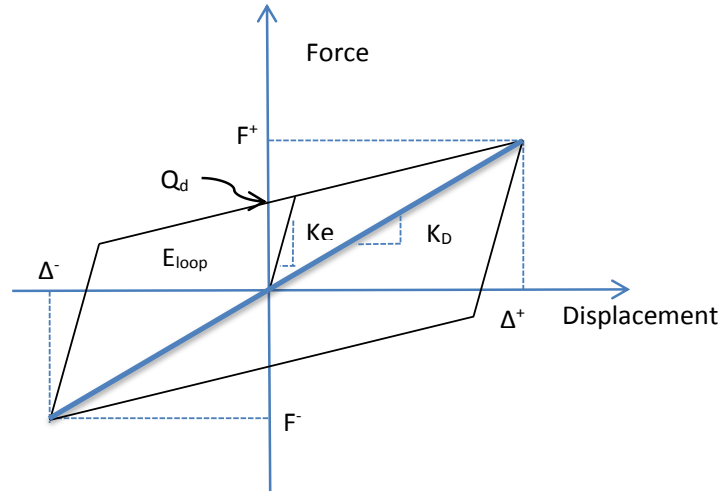


Figure 3.6: Effective stiffness and damping in the bilinear model

Assuming a characteristic strength equal to 5% of the building weight:

$$Q_d = 0.05 \times 7910 = 395.5 \text{ kips}$$

$$Q_{d,isolator} = \frac{Q_d}{25} = 15.8 \text{ kips} \quad (3-11)$$

The effective damping,  $\beta_D$ , at the design displacement,  $D_D$ , shall be based on the cyclic tests of isolator and can be estimated using ASCE7-10 Equation 17.8-7 as follows:

$$\beta_D = \frac{\sum E_D}{2\pi K_{D_{max}} D_D^2} \quad (3-12)$$

where  $\sum E_D$  the total energy dissipated in one cycle of hysteresis loading at a test displacement equal to design displacement;  $K_{D_{max}}$  is the maximum effective stiffness of the isolator at the design displacement. The effective damping,  $\beta_M$ , at the maximum displacement,  $D_M$ , shall also be based on the cyclic tests of the isolator and is calculated using ASCE7-10 Equation 17.8-8 as follows:

$$\beta_D = \frac{\sum E_M}{2\pi K_{M_{max}} D_M^2} \quad (3-13)$$

where  $\sum E_M$  is the total energy dissipated in one cycle of hysteresis loop at a test displacement equal to maximum displacement;  $K_{M \max}$  is the maximum effective stiffness of the isolator at the maximum displacement. Effective damping values,  $\beta_D$  and  $\beta_M$ , at the design displacement and maximum displacement must be calculated based on forces and deflections which produce the smallest effective damping. Therefore, the maximum effective stiffness values,  $K_{D \max}$  and  $K_{M \max}$  equal to 1.3 times the minimum stiffness are assumed based on the maximum permissible values given in ASCE7-10 resulting in conservative results.

Table 3.9 summarizes the calculations for effective damping at the design and maximum displacement. As the effective damping values are considerably lower than the primary assumptions, the ELF and dynamic analysis calculations must be repeated with the new damping values. Deformation demands are then revised according to Equations 17.6-1 and 17.6-2 of ASCE 7-10. Design and maximum displacements are allowed for a reduced but not less than 90% and 80%, respectively, if the dynamic analysis predicts lower values. Maximum demand displacement in response spectrum dynamic analysis is determined by simultaneous application of 100% MCE earthquake in one direction and 30% on the other direction. Total maximum displacement is then calculated as the vector sum of isolator displacement. Table 3.10 shows the final design and maximum displacement for isolation system which are slightly greater than initial estimations provided in the Table 3.8.

Table 3.9: Design parameters for isolation system

Parameter	Description	Calculation
$Q_d$	Characteristic strength	15.8 kips
$D_y$	Yield displacement	1 in
$D_D$	Initial Design displacement	13.6 in
$D_M$	Initial Max. displacement	20.4
$K_{Dmin}$	Minimum effective stiffness at design disp.	5.17 kips/in
$K_d$	Post yield stiffness	$(D_D * K_{Dmin} - Q_d) / (D_D - D_y) = 4.3$ kips/in
$K_{Dmax}$		1.3 $K_{Dmin} = 5.6$ kips/in
$K_{Mmin}$		$[Q_d + (D_M - D_y) * K_d] / D_M = 4.4$ kips/in
$K_{Mmax}$		1.3 $K_{Mmin} = 5.7$ kips/in
$\sum E_D$		$4Q_d(D_D - D_y) = 796$ kips.in
$\sum E_M$		$4Q_d(D_M - D_y) = 1226$ kips.in
$\beta_D$		0.12
$\beta_M$		0.082

Table 3.10: Final estimates of isolation design and maximum displacement

Design displacement parameters			$D'_D$ (in )	Max. displacement parameters			$D'_M$ (in )	$D'_{TM}$ (in )
$S_{DI}$ (g)	$T_D$ (sec)	$B_D$		$S_{MI}$ (g)	$T_D$ (sec)	$B_D$		
0.75	2.5	1.26	14.6	1.12	2.5	1.13	20.9	24.0

The axial force capacity of isolators must be checked against the allowable axial capacity often provided by the isolator producer. The uplift is not a possible phenomenon for a moment frame structural system, so only the axial compression capacity is of concern. Maximum downward axial force for the interior, edge, and corner isolators are presented in the Table 3.11.

Table 3.11: Maximum downward force for isolator units design

Location	Maximum downward force
Edge	222.7
Corner	318.4
Interior	597.6

Selection of base isolation units can be made using engineering properties provided by producers. This is useful for having a realistic design condition accurate engineering properties and cost estimations provided in the following sections. One of the isolation system suppliers, Dis Inc, offers a variety of Lead Rubber bearings. Table 3.12 presents the device dimensions including diameter and height and the number of rubber layers for an isolator with 37.5 in. diameters. Engineering properties of devices is also provided in this Table including the yielded stiffness, maximum allowed displacement, and axial load capacity. Maximum displacement is based on design limits of 250% rubber shear strain and 2/3 the isolator diameter. The rubber material availability with shear moduli from 55 psi to 100 psi along with possibility of having different number of layer gives the flexibility of generating a range of yielded stiffness properties as shown in the table. Characteristic strength is also dependent on the lead core area used in the isolator unit.

An isolation unit of 37.5 in. diameter with a maximum displacement capacity of 24 in. provides the closest properties to demand displacement. Available yielded stiffness,  $K_d$ , must be checked against  $K_{dmin}$  (4.3 kips/in). This value falls between 4 kips/in to 12 kips/in given for the selected isolator. It is worth of note that these criteria may impose serious limits on the selection of isolation systems with relatively low gravity loads. The

detail of the base isolation devices including number and thickness of layers, rubber shear moduli, and lead core diameter are determined based the required stiffens and strength.

Table 3.12: Lead Rubber Bearings dimensions, Dis Inc. production

Device size			Design properties		
Diameter (in)	Height (in)	Number of Layers	Yield stiffness (kip/in)	Design displacement (in)	Axial capacity (kip)
37.5	10-23	10-40	4-12	24	1500

### 3.5.6.3 Design Base Shear

Design provisions provide sufficient overstrength to avoid inelastic responses in the superstructure of isolated buildings. The structural elements shall be designed to sustain ground shakings as strong as maximum considered earthquake level without substantial inelastic response. For a conservative design base shear, design forces shall be based on the maximum stiffness of isolation system instead of minimum values which are used for displacement demand estimations.

Design forces of the elements above the isolation interface is permitted to be reduced by the response modification factor. Maximum forces in the superstructure are captured using the maximum effective stiffness of the isolation system. Maximum and minimum stiffness is often determined based on testing of isolator unit prototypes over three cycles of hysteresis test at design displacement,  $D_D$ . The maximum effective stiffness shall not exceed 130% of the minimum stiffness. Without further information about the isolator unit test results,  $K_{Dmax}$  is assumed as 1.3 times the minimum stiffness,  $K_{Dmin}$ , resulting in

conservative design forces. The design base shear of the elements below and above the isolation system,  $V_b$  and  $V_s$ , for the building is calculated as follows:

$$V_b = K_{D_{\max}} * D_D = 1.3 * 129.2 * 13.6 = 2284 \text{ Kip} / \text{ft} \quad (3-14)$$

$$V_s = \frac{V_b}{R_l} = \frac{K_{D_{\max}} * D_D}{R_l} = \frac{2284}{2} = 1142 \text{ Kip} / \text{ft}$$

The lateral force required for the design of isolation system and foundation and other elements below the isolation interface,  $V_b$ , is about 28% of the effective weight of the building. Superstructure design force,  $V_s$ , is around 14% of the effective weight of the building, 30 % greater than seismic demands required for the design of the fixed-base building, B1. Response spectrum analysis is also performed on the structure considering all effective modes of vibration. Response spectrum analysis resulted in a considerably lower shear force of 450kips, under the design level earthquake comparing to 1142 kips determined in ELF procedure. In this situation, design base shear,  $V_s$ , is permitted to be reduced by a factor of 0.8. Therefore, the minimum design shear force is:

$$V_s = \max \begin{cases} 0.8V_{s,ELF} = 914 \text{ kip} \\ V_{S,Dynamic} = 450 \text{ kip} \end{cases} \quad (3-15)$$

Response spectrum analysis must be scaled up. Therefore, the scale factor is determined as:

$$\text{Scale Factor} = \frac{914}{450} = 2.03 \quad (3-16)$$

This design force is slightly greater than the force required for the design of the corresponding fixed-based model, B1, which is 870 kips. Although the total forces are comparable between these buildings, the distributions of story shears considerably vary due to the dissimilar story stiffness distribution.

## Chapter 4 : Performance Model

### 4.1 Introduction

This chapter provides the performance model data required for the performance assessment of the benchmark buildings using the time-base assessment methodology. The performance model contains the type and estimated quantity of building components along with their fragility data. The performance model describes the necessary building information vulnerable to shaking of earthquake. According to ATC-58 (2012), this data must include:

- Replacement cost and time of the building
- Population estimation and its distribution over time and envelope of the building
- Structural components and assemblies which are vulnerable to earthquake motions; their demands including deformation and acceleration; and probable damage and consequences of such damages such as the collapse risk and repair costs.
- Nonstructural components and assemblies which are vulnerable to earthquake motions; and the maximum responses due to earthquake motions and the consequences including the probable casualties due to falling objects and debris generated, repair/replacement costs.

Performance Assessment Calculation Tool (PACT), developed as a part of ATC-58 (2012) project, provides valuable information concerning the fragility and consequence function

data for a wide variety of components in the building. PACT analytical tool it employed in the following sections of this chapter to assemble the building performance model.

## **4.2 Initial Costs**

Basic buildings data were presented in the previous chapter including the number of stories, story height, and floor areas. This provides basic information for the calculation of the initial or the replacement cost. Replacement costs are an essential part of the performance assessment methodology. Replacement costs and time affects the judgment for the reparability or irreparability status of the building. A threshold value is often assumed for the repair costs over which the building is deemed as irreparable.

Repair costs of 40% to 50% of the replacement costs is suggested by ATC-58 (2012) as the threshold. This value is definitely subject to change depending on the characteristics of the building under study. For example, in the case of historic or a landmark building, this threshold percentage can unlimitedly be increased to protect the existing building. In other cases of old building which does not carry the characteristic of the landmark buildings, the threshold value can be significantly reduced due to much lower present value of the asset.

The quantities of damageable components are based on both the actual quantities from the building layout and design and the normative quantities derived from the ATC-58 normative quantity tool. This tool provides an estimate of structural and non-structural components quantities given the occupancy category for the building. The values are given on a gross per square foot basis at 10<sup>th</sup>, 50<sup>th</sup>, and 90<sup>th</sup> percentile confidence level. These values are so useful for an approximate average takeoff and cost estimation of

typical buildings. This valuable data is the results of a survey on thousands of typical buildings in the nation. The quantity and cost estimation of most of nonstructural components of the benchmark buildings were evaluated based on this data. This method of cost estimation is most proper for this study as it represents the typical buildings in practice. Table 4.1 list the damageable components and the corresponding quantities for the benchmark buildings. It should also be added that the 50th percentile normative quantities were used for the estimation of the components.

RS Means (2013) cost per square foot estimator also provides list of typical components and corresponding costs used for office buildings. This helps to find each component's cost as the percentage of the whole. The estimation represents the average building cost for a 4-story concrete frame building with 14 feet story height, 400 feet perimeter, glass and metal curtain wall. Estimation are based on the Union prices which are customized for the specific site location, Los Angeles. Cost of structural elements including beams, columns, slabs, and foundation is then replaced by the actual estimated costs of these elements for each building. This is the main source of cost variation between buildings. The cost estimations of the damageable components are also revised based on the normative quantities to ensure consistency from construction cost to loss estimations process. It is also of note that the use of normative quantities did not significantly change the initial cost estimations obtained using RS Means. The cost estimation of the buildings of study is summarized in the Tables 4.1 to 4.6. The cost per square foot, total cost and cost percentage are provided in the tables. Cost estimations show 2%, 3%, 5.2%, 11.2%, and 6.4% increase for B2, B3, B4, B5, and BI models with respect to B1 model. More detailed estimation are provided in Appendix B.

Figure 4.1: Normative quantities used for cost estimations

<b>Component Type</b>	<b>Units of measurement</b>	<b>50<sup>th</sup> percentile quantity</b>	<b>Total quantity</b>
Gross area	SF	Based on layout	38400
Concrete beams	EA	Based on layout	144
Concrete columns	EA	Based on layout	100
Slab	SF	Based on layout	38250
Cladding (Curtain wall)	SF	Based on layout	21952
Interior partition length	100 LF per 1 gsf	1.0E-03	38.4
Ceramic tile floors	SF per 1 gsf	0.042	1613
Ceramic tile walls	100 LF per 1 gsf	7.6E-5	2.918
Ceiling - lay in tile	SF	Based on layout	38250
Stairs	EA	Based on layout	1
Elevators	EA	2.8E-5	1
<b>Plumbing</b>			
Plumbing fixtures	EA per 1 gsf	1.1E-3	42
Cold domestic water piping - 2 ½ inch diameter or smaller	1,000 LF per 1 gsf	4.2E-5	1.617
Cold domestic water piping – greater than 2 ½ diameter	1,000 LF per 1 gsf	1.5E-5	0.577
Hot domestic water piping - 2 ½ inch diameter or smaller	1,000 LF per 1 gsf	8.4E-5	3.234
Hot domestic waster piping – greater than 2 ½ diameter	1,000 LF per 1 gsf	3E-5	1.155
Sanitary waste piping	1,000 LF per 1 gsf	5.7E-5	2.194
<b>HVAC</b>			
Air handling units	CFM per 1 gsf	0.7	27000
Ducts – 6 sq. ft. or larger	1,000 LF per 1 gsf	2.0E-05	0.77
Ducts – less than 6 sq. ft.	1,000 LF per 1 gsf	7.5E-05	2.887
In-line drops and diffusers	EA per 1 gsf	9.0E-03	347
VAV boxes	EA per 1 gsf	2.0E-03	77
Heating water piping - 2 ½ inch diameter or smaller	1,000 LF per 1 gsf	5.0E-6	0.192
Heating water piping – greater than 2 ½ diameter	1,000 LF per 1 gsf	5.0E-6	0.192
<b>Electrical</b>			
Electrical distribution conduits	LF per 1 gsf	2.0E-01	8085
switchgear	EA per 1 gsf	1.5E-04	6
Lighting fixtures lay in fluorescent	EA per 1 gsf	1.5E-02	578
<b>Fire protection</b>			
Sprinkler piping	20 LF per 1 gsf	9.0E-03	346.5
Sprinkler drops	EA per 1 gsf	8.0E-03	308

Table 4.1: Construction cost distribution of the building B1

<b>Group</b>	<b>Description</b>	<b>% of Total</b>	<b>Cost Per S.F.</b>	<b>Cost</b>
A	Substructure	2.09%	\$4.27	\$164,530
B	Shell	30.23%	\$61.86	\$2,381,632
C	Interiors	17.52%	\$35.85	\$1,380,225
D	Services	30.16%	\$61.70	\$2,375,450
E	Equipment & Furnishings	20.00%	\$41.03	\$1,575,459
	Subtotal	100%	\$204.61	\$7,877,296
	Contractor Fees (GC, Overhead, Profit)	25.00%	\$51.15	\$1,969,324
	Architectural Fees	7.00%	\$17.90	\$689,263
	User Fees	0.00%	\$0.00	\$0.00
	Total Building Cost		\$273.66	\$10,535,883

Table 4.2: Construction cost distribution of the building B2

<b>Group</b>	<b>Description</b>	<b>% of Total</b>	<b>Cost Per S.F.</b>	<b>Cost</b>
A	Substructure	2.22%	\$4.64	\$178,350
B	Shell	31.42%	\$65.74	\$2,524,448
C	Interiors	17.18%	\$35.94	\$1,380,225
D	Services	29.57%	\$61.86	\$2,375,450
E	Equipment & Furnishings	19.61%	\$41.03	\$1,575,459
	Subtotal	100.00%	\$209.22	\$8,033,932
	Contractor Fees (GC, Overhead, Profit)	25.00%	\$52.30	\$2,008,483
	Architectural Fees	7.00%	\$18.31	\$702,969
	User Fees	0.00%	\$0.00	\$0
	Total Building Cost		\$279.83	\$10,745,38

Table 4.3: Construction cost distribution of the building B3

<b>Group</b>	<b>Description</b>	<b>% of Total</b>	<b>Cost Per S.F.</b>	<b>Cost</b>
A	Substructure	2.11%	\$4.42	\$202,371
B	Shell	31.53%	\$65.97	\$2,582,121
C	Interiors	17.18%	\$35.94	\$1,380,225
D	Services	29.57%	\$61.86	\$2,375,450
E	Equipment & Furnishings	19.61%	\$41.03	\$1,575,459
	Subtotal	100%	\$209.22	\$8,115,626
	Contractor Fees (GC, Overhead, Profit)	25.00%	\$52.30	\$2,028,907
	Architectural Fees	7.00%	\$18.31	\$710,117
	User Fees	0.00%	\$0.00	\$0
	Total Building Cost		\$279.83	\$10,854,65

Table 4.4: Construction cost distribution of the building B4

<b>Group</b>	<b>Description</b>	<b>% of Total</b>	<b>Cost Per S.F.</b>	<b>Cost</b>
A	Substructure	3.00%	\$6.49	\$249,400
B	Shell	32.77%	\$70.84	\$2,720,183
C	Interiors	16.63%	\$35.94	\$1,380,225
D	Services	28.62%	\$61.86	\$2,375,450
E	Equipment & Furnishings	18.98%	\$41.03	\$1,575,459
	Subtotal	100.00%	\$216.16	\$8,300,717
	Contractor Fees (GC, Overhead, Profit)	25.00%	\$54.04	\$2,075,179
	Architectural Fees	7.00%	\$18.91	\$726,313
	User Fees	0.00%	\$0.00	\$0
	Total Building Cost		\$289.12	\$11,102,20

Table 4.5: Construction cost distribution of the building B5

Group	Description	% of Total	Cost Per S.F.	Cost
A	Substructure	3.55%	\$8.11	\$311,256
B	Shell	35.61%	\$81.27	\$3,120,726
C	Interiors	15.75%	\$35.94	\$1,380,225
D	Services	27.11%	\$61.86	\$2,375,450
E	Equipment & Furnishings	17.98%	\$41.03	\$1,575,459
	Subtotal	100.00%	\$228.21	\$8,763,116
	Contractor Fees (GC, Overhead, Profit)	25.00%	\$57.05	\$2,190,779
	Architectural Fees	7.00%	\$19.97	\$766,773
	User Fees	0.00%	\$0.00	\$0
	Total Building Cost		\$305.23	\$11,720,66

Table 4.6: Construction cost distribution of the building BI

Group	Description	% of Total	Cost Per S.F.	Costs
A	Substructure	2.71%	\$5.91	\$226,753
B	Shell	33.69%	\$73.53	\$2,823,578
C	Interiors	16.47%	\$35.94	\$1,380,225
D	Services	28.34%	\$61.86	\$2,375,450
E	Equipment & Furnishings	18.80%	\$41.03	\$1,575,459
	Subtotal	100.00%	\$218.27	\$8,381,465
	Contractor Fees (GC, Overhead, Profit)	25.00%	\$54.57	\$2,095,366
	Architectural Fees	7.00%	\$19.10	\$733,378
	User Fees	0.00%	\$0.00	\$0
	Total Building Cost		\$291.93	\$11,210,209

Table 4.7 summarizes the cost increases of all the buildings relative to the building model B1. Although the structural components cost considerably increases with the increase in the design forces, the total cost increase is not substantial. The total cost in the B2 and B3 models show 2% and 3% increase over the base model, B1. These are the models corresponds to design forces in the risk category III and IV according to IBC (2012). For the most conservatively designed buildings, B4, B5, the increase is about 5.4% and 11.2%, respectively.

Table 4.7: Structural components cost increase relative to B1 design

<b>Model</b>	<b>Structural components Cost increase %</b>	<b>Total Cost increase %</b>
<b>B1</b>	0.0	0.0
<b>B2</b>	14.1	2.0
<b>B3</b>	22.1	3.0
<b>B4</b>	39.3	5.4
<b>B5</b>	82.3	11.2
<b>BI</b>	46.8	6.4

Table 4.8 summarizes the cost breakdown of the structural components including slabs, beams/columns, and foundations. For the basic design B1, the slab cost percentage is almost half of the total structural cost. The cost percentage of the slab keeps decreasing from models B1 to B5 as the slab design and cost associated with it remains essentially the same in all models. In building B5, beams and columns group end up comprising over 60% of the cost of structural components comparing to slabs with 23% cost percentage.

For the seismically isolated building, the cost of the beams, columns and foundation are slightly less than B3 model due to lower design seismic forces. When accounting for

isolator unit and the additional slab-girder system, base-isolated model costs exceeds B3's.

Table 4.8: Structural components cost breakdown

<b>Building Model</b>	<b>Cost percentage %</b>		
	Beams/columns	Slabs	foundation
<b>B1</b>	45.6	41.3	13.1
<b>B2</b>	49.5	36.9	13.6
<b>B3</b>	51.8	33.9	14.3
<b>B4</b>	54.8	29.8	15.4
<b>B5</b>	60.7	22.8	16.5
<b>BI</b>	52.8	35.0	12.2

### 4.3 Occupancy and Population Model

Occupancy type affects the number and distribution of the people in the building over time. For a residential building, the most populated time is the night time while for a commercial or office building, a minimum number of occupants are expected to be present in the building at this time. This also is true for the buildings of education occupancy category where almost no people are present at nights.

The same concept runs for the days of the week and months of the year. Variation by days of the week represents the effect of the weekends while the variation by month considers the effect of holidays. The variation in population is plotted against time of the day in Figure 4.1 for a commercial office building suggested by ATC-58 (2012). The vertical axis represents the peak number of occupants per 1000 square feet of the building area. The peak number of occupants is expected to occur during weekdays between 10AM to 11AM and 2PM to 3PM.

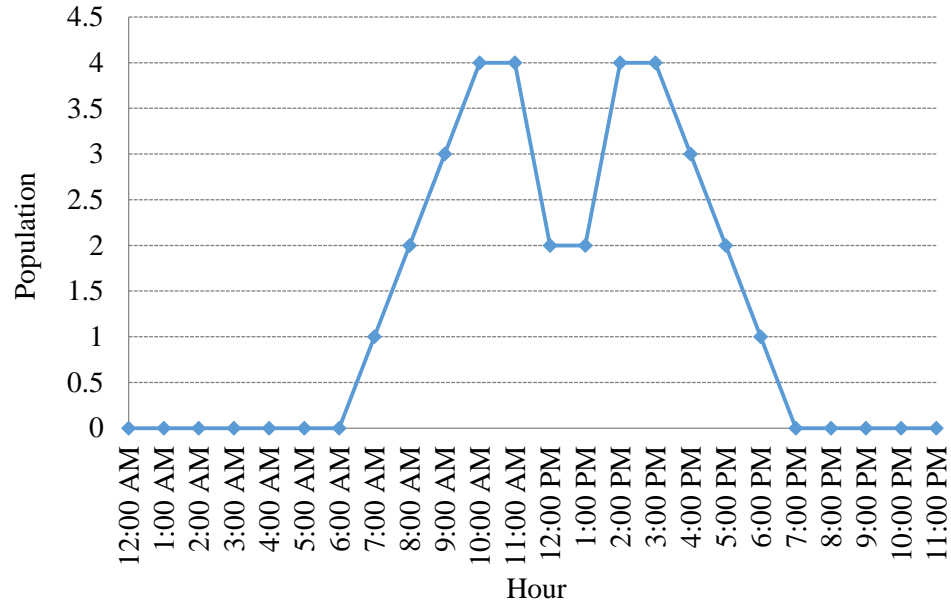


Figure 4.2: Variation in population by time of day during weekdays for office occupancy

The expected number of occupants during work hours in the weekends is assumed to be 5% of the peak numbers in the weekdays, equivalent to 0.2 occupants per square feet per ATC-58 (2012).

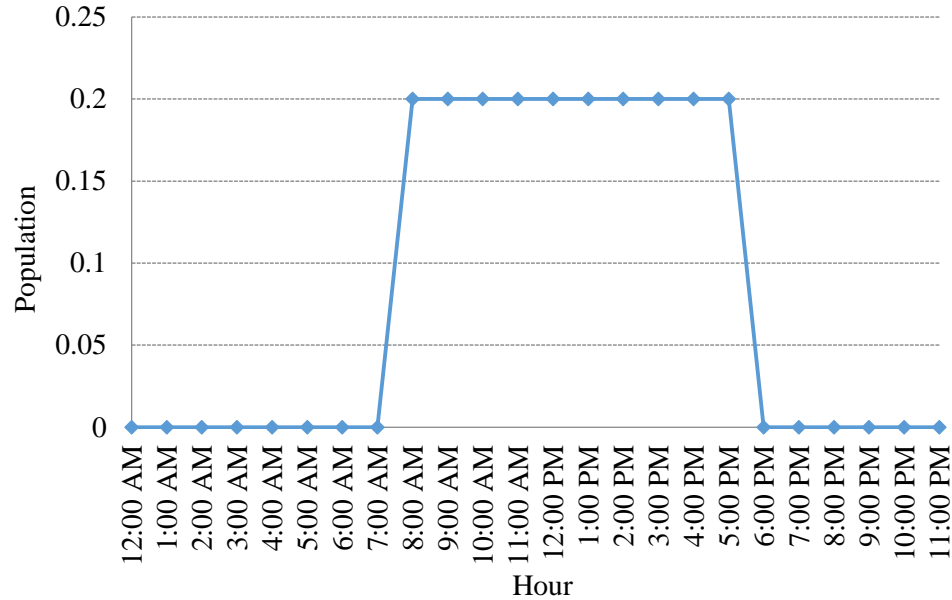


Figure 4.3: Variation in population by time of day during weekends for office occupancy

Figures 4.2 and 4.3 show the population distribution for the peak months of the year. To account for the month to month variability, the graph in Figure 4.4 is used which gives the population at each month as the percentage of the peak month population. The minimum population occurs during January due to holidays in which 91 percent of peak month population is present. Considering the random nature of the event, the earthquake can happen at any time of the day and the day of the year. Depending on the time and date of earthquake occurrence, different number of casualties is expected. The population models can help estimate the number of casualties in buildings simulating the earthquake random occurrence in time. The maximum and minimum number of casualties can also be estimated by assuming the upper and lower bound values in the population models.

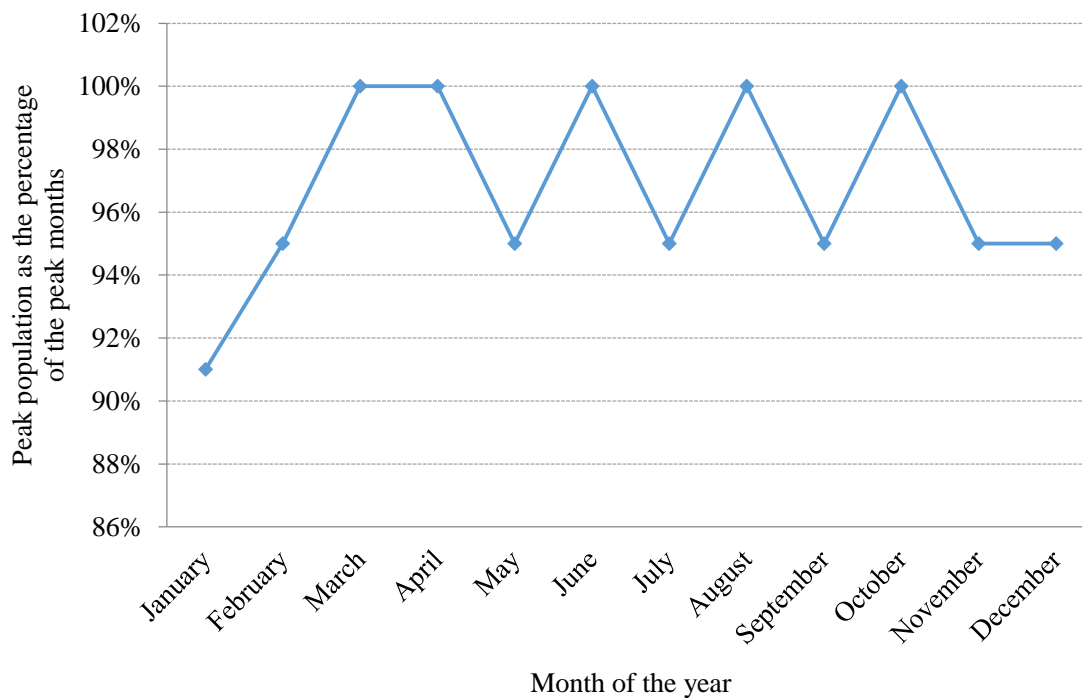


Figure 4.4: Variation in population by month for office occupancy

#### 4.4 Fragility Groups

Each component including structural, nonstructural, or content of the building is categorized into fragility groups. Fragility groups represent a set of components with the same material, construction and installation characteristics. The components of the same group are expected to experience similar damage and failure mode. Fragility groups are identified by a classification number based on the UNIFORMATE II.

Table 4.9 lists a set of fragility groups for the benchmark buildings which are used to construct the performance model. This table also contains information about the unique classification number and the demand parameter of each component for the purpose of damage assessment.

Table 4.9: Fragility groups in benchmark buildings

<b>Fragility group</b>	<b>Description</b>	<b>Demand parameter</b>
A10	Foundation	Assumed rugged
B1041	Concrete columns ACI-318-	Drift
B1061	Cold form steel structural	Drift
B2011	Exterior wall construction	Drift
B2022	Curtain walls	Drift
C1011	Fixed interior wall partitions	Drift
D1014	Hydraulic elevators	Acceleration
D20	Plumbing	Acceleration
D30	HVAC	Acceleration
D40	Fire protection	Acceleration
E	Equipment and furnishing	Acceleration

#### 4.5 Structural Component Fragility

Building component damage are expected to increase as the demand, either displacement or acceleration, increases. The function relating this two parameters is the fragility function. For the structural components, the demand parameter is the story drift ratio. Depending on the component type and detail, various fragility curves has been developed by researchers in the past several years which is gathered in the ATC-58 fragility library.

The slab and foundation is considered rug for the purpose of this study as the less damageable components comparing to beams and columns. Table 4.10 provides the fragility function parameters for beams and columns derived from the fragility library. The fragility curves are also shown in the Figure 4.5 for all damage states. The cost

consequence of the damage to such components is on a per joint basis including the beam, and column and the joint itself. Damage states 3-1 and 3-2 are mutually exclusive with probabilities of occurrence of 80 and 20 percent in a way that the occurrence of one damage state precludes the occurrence of the other.

Table 4.10: Damage states for beam and column elements (joints)

Damage state type	Description	Fragility parameters	
		Median (rad)	Dispersion
Damage state 1	Beams or joints exhibit residual crack widths > 0.06 in. No significant spalling. No fracture or buckling of reinforcing.	.02	0.4
Damage state 2	Beams or joints exhibit residual crack widths > 0.06 in. Spalling of cover concrete exposes beam and joint transverse reinforcement but not longitudinal reinforcement. No fracture or buckling of reinforcing.	.0071	0.45
Damage state 3-1 (fraction 0.8)	Beams or joints exhibit residual crack widths > 0.06 in. Spalling of cover concrete exposes a significant length of beam longitudinal reinforcement. Crushing of core concrete may occur. Fracture or buckling of reinforcement requiring replacement may occur.	0.05	0.3
Damage state 3-2 (fraction 0.2)	Beams or joints exhibit residual crack widths > 0.06 in. Spalling of cover concrete exposes beam and joint transverse reinforcement but not longitudinal reinforcement. No fracture or buckling of reinforcing.	0.05	0.3

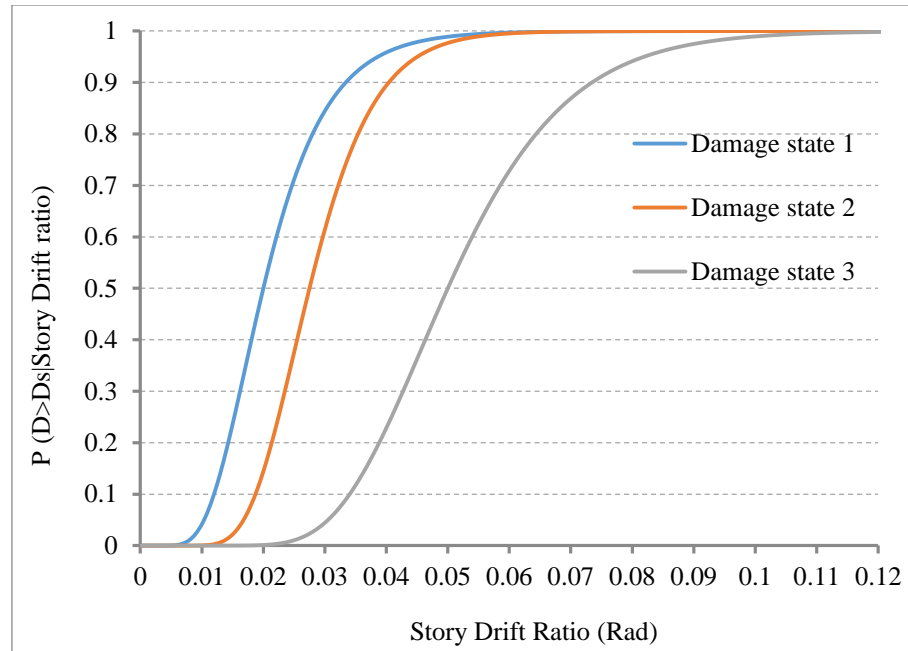


Figure 4.5: Fragility curves for columns and beam elements (joints)

#### 4.6 Nonstructural Components Fragility

Nonstructural components comprise a big portion of the building costs. A considerable number of these components are damageable to either drift, velocity or acceleration in an earthquake. The buildings of this study are aimed to represent a typical office building design in the U.S. Most of nonstructural components selected for the performance model and their fragility properties are given in the following sections. It includes the interior design, exterior closure, mechanical, electrical, and plumbing features mostly susceptible to ground motion shakings. These are the components that their fragility properties are already studied by the researchers as a part of the performance based assessment methodology. There are still many components, though less vulnerable to shakings, that can be incorporated into loss analyses in the future investigations when their fragility properties are known.

#### 4.6.1 Exterior Closure

A curtain wall consisting of glazing and aluminum frame is used for the exterior closure. The selected curtain wall is the stick built system in which the glass panels are installed at site. The glazing is dual pane also referred to as insulating glass with a considerably higher thermal resistance comparing to single pane glazing. Two damage states are predicted for this component as given in the table 4.11. Fig 4.6 also shows the fragility curves for all the damage states.

Table 4.11: Damage states for the exterior curtain walls

Damage state type	Description	Fragility parameters	
		Median (rad)	Dispersion
Damage state 1	Glass cracking	0.021	0.45
Damage state 2	Glass falls from frame	0.024	0.45

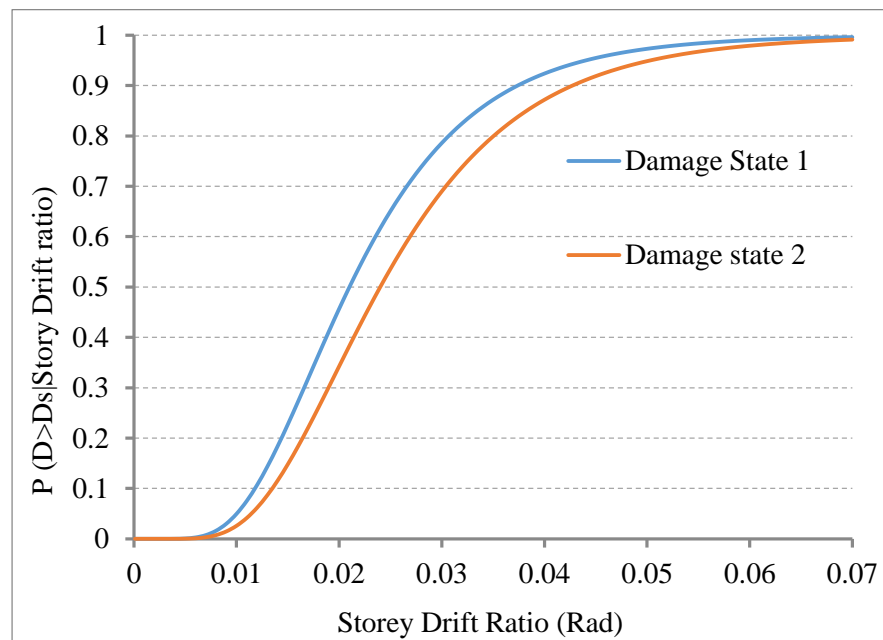


Figure 4.6: Fragility curves for curtain wall system

#### 4.6.2 Interior Partitions

Gypsum board partitions with the thickness of 5/8" and 1/2" are considered for the wallboards which are installed on 3-5/8" metal studs spaced at 24" OC using screw fasteners. The boards are fire rated (Type x) providing a minimum fire rating for the assembly of 1 hour. This type of boards often contains additives including glass fiber reinforcement formulated in the gypsum to increase fire resistance.

The peak transient drift ratio is the EDP for the wallboard partitions. It is also of note that the fragility curves are based on the lognormal distribution function. The fragility curve for this component predicts three different damage states for this component. Table 4.12 describes damage states and associate fragility parameters. Figure 4.2 shows the fragility curves for all damage states. For damage state 1, the repairs may include partial retape of joints and repainting of the wall board. Partial or full replacement of the wall boards including taping and repainting are required if damage state 2 or 3 occurs. Damage state 3 has a greater possibility of full component replacement comparing to damage state 2.

Table 4.12: Damage states for the wallboard partitions

Damage state	Description	Fragility parameters	
		Median (rad)	Dispersion
Damage state 1	Screws pop-out, minor cracking of wall board, warping or cracking of tape.	.0021	0.6
Damage state 2	Moderate cracking or crushing of gypsum wall boards (typically in corners and in corners of openings).	.0071	0.45
Damage state 3	Significant cracking and/or crushing of gypsum wall boards- buckling of studs and tearing of tracks.	0.012	0.45

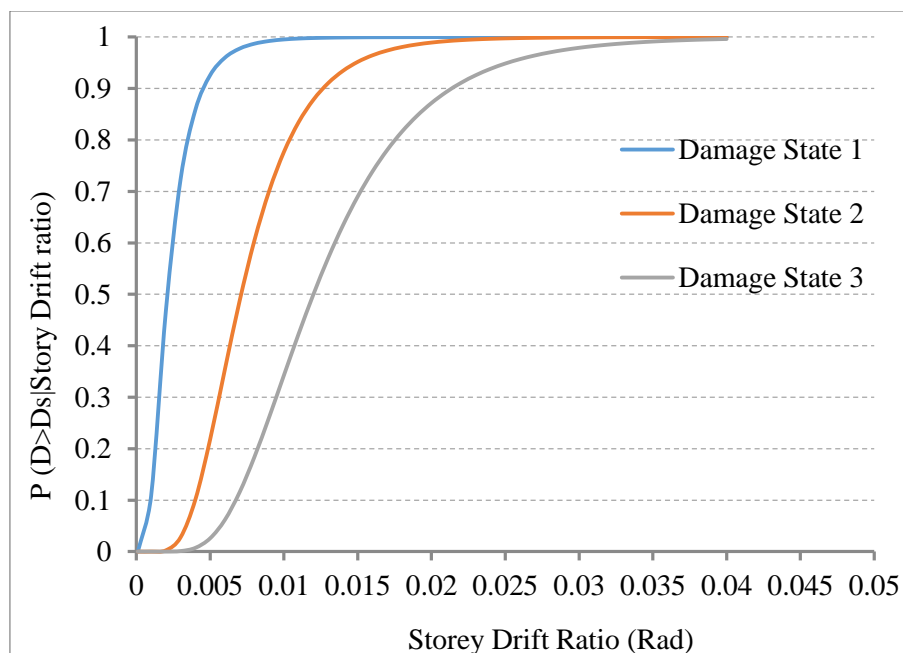


Figure 4.7: Fragility curves for wallboard partitions

### 4.6.3 Steel Stairs

Stairs performance in earthquake and their ability to adapt the lateral drifts are important in achieving the objectives of performance base-design. Prefabricated steel stairs joints with steel treads and landing are considered with no seismic joints provided. Three damage states are provided for this component which are described in Table 4.13 and illustrated in the Figure 4.8.

Table 4.13: Damage states for steel stairs

Damage state	Description	Fragility parameters	
		Median (rad)	Dispersion
Damage state 1	Non structural damage, local steel yielding.	0.005	0.6
Damage state 2	Buckling of steel, weld cracking.	0.017	0.6
Damage state 3	Loss of live load capacity. Connection and or weld fracture.	0.028	0.45

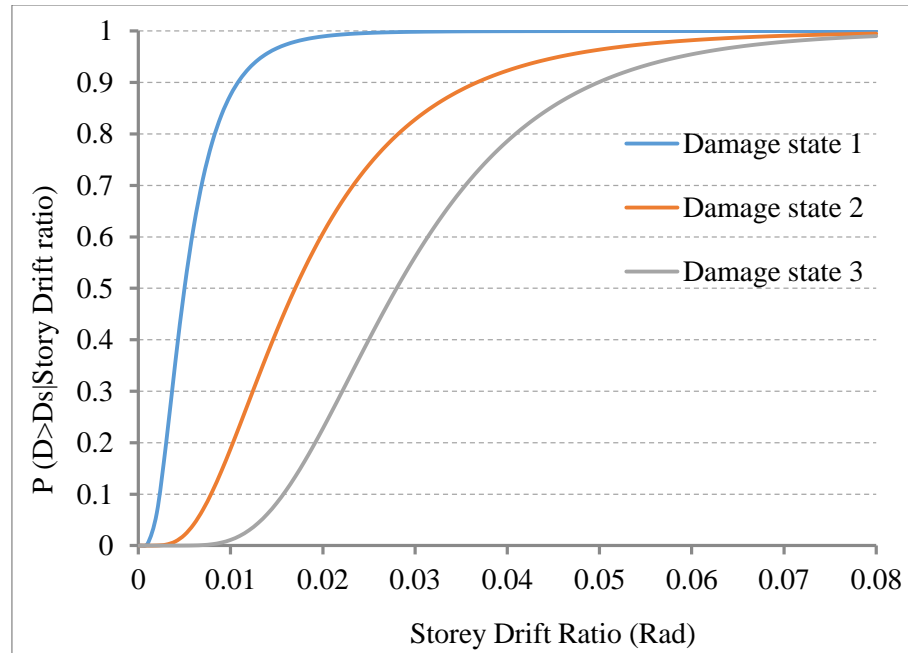


Figure 4.8: Fragility curves for steel stairs

#### 4.6.4 Acoustical Ceilings

Engineering demand parameter for the acoustical ceilings is the peak floor acceleration in either horizontal direction. The ceiling plan dimensions affect the fragility curve properties of this component. For the ceiling modules of smaller plan dimensions, a considerably lower damage or collapse probability is predicted by the fragility curves. For example, a plan area of between 1000 S.F. to 2500 S.F. of ceiling modules results in fragility properties and damage states provided in Table 4.14 with fragility curves given in Figure 4.9. Each damage state associates with a certain percentage of the total ceiling area that falls during the earthquake. It starts with 5% fall off area in damage state 1 and ends with the total collapse in damage state 3.

Table 4.14: Damage states for acoustical ceiling

Damage state type	Description	Fragility parameters	
		Median (g)	Dispersion
Damage state 1	5 % of tiles dislodge and fall.	0.45	0.40
Damage state 2	30% of tiles dislodge and fall and t-bar grid damaged.	0.7	0.40
Damage state 3	Total ceiling and grid collapse.	1.0	0.40

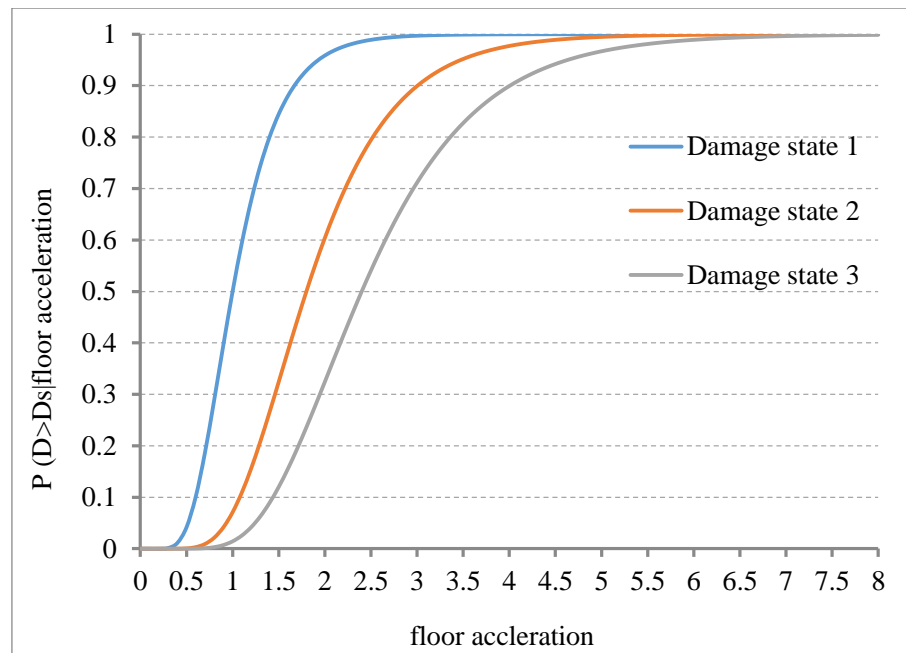


Figure 4.9: Fragility curves for acoustical ceiling

#### 4.6.5 Elevators

The engineering demand parameter for the elevator is peak floor acceleration. Porter (2006) developed a fragility function for hydraulic elevators based on the observation of their behavior in Loma Prieta and Northridge earthquakes. Only one damage state was introduced as the result of that study by the integration of various damage states in a sole damage state. The data provided by ATC-58 (2012) for the fragility functions of the

hydraulic elevators follows the same procedure. It lumps several damage states to multiple parts of the elevator into a single component fragility function. Each of the parts within the elevator component requires different repair action as the result of the damage. Table 4.15 provides damage to different parts of the elevator that can occur simultaneously. The Figure 4.10 also shows the fragility curve for the whole component. The median and dispersion are equal to 0.5g and 0.3, respectively.

Table 4.15: Damage states for hydraulic elevators

Damaged component	Fraction of the component damaged
Damaged controls.	0.3
Damaged vane and hoist-way switches, and or bent cab stabilizers, and or damaged car guide shoes.	0.49
Damaged entrance and car door, and or flooring damage.	0.44
Oil leak in hydraulic line, and or hydraulic tank failure.	0.37

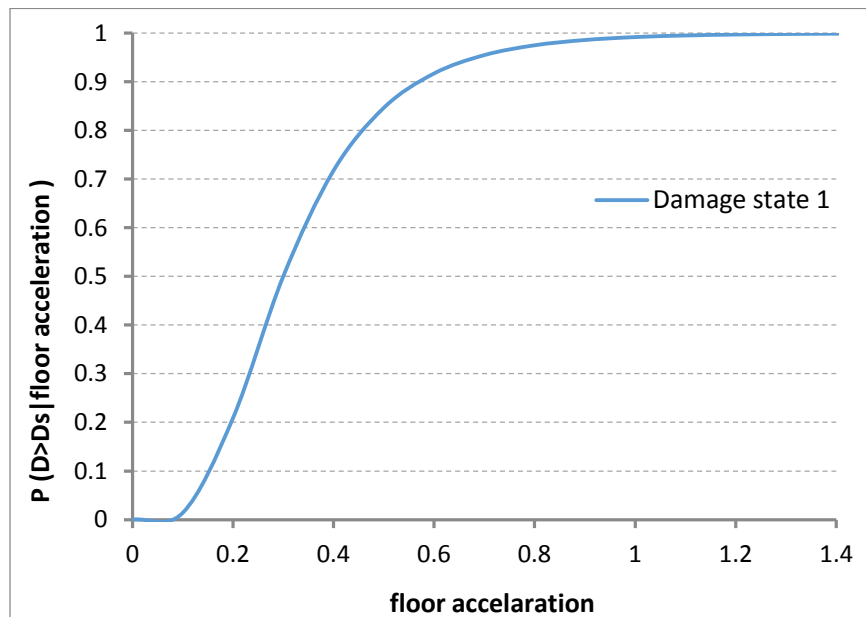


Figure 4.10: Fragility curves for hydraulic elevators

#### 4.6.6 Plumbing

Domestic water distribution system, and sanitary system are sensitive to peak ground acceleration as the sensitivity parameter. Cold, hot, steam, chilled, and sanitary waste piping are provided with different fragility functions in ATC-58 (2012). Fragility functions are also provided for the bracing elements. Table 4.16 provide the data for the fragility functions of the piping and bracing components used for the loss evaluation study.

Table 4.16: Damage states for the piping system

Component	Damage state type	Description	Fragility parameters	
			Median (g)	Dispersion
Cold and hot water (pipe diam.>2.5")	Damage state 1	Minor leakage at flange connections - 1 leak per 1000 feet of pipe	2.25	0.5
	Damage state 2	Pipe Break - 1 break per 1000 feet of pipe	4.1	0.5
Bracing (pipe diam.>2.5")	Damage state 1	Lateral Brace Failure - 1 failure per 1000 feet of pipe	1.5	0.5
	Damage state 2	Vertical Brace Failure - 1 failure per 1000 feet of pipe	2.25	0.5
Cold and hot water (pipe diam.<2.5")	Damage state 1	Small Leakage at joints - 1 leak per 1000 feet of pipe	0.55	0.5
	Damage state 2	Large Leakage w/ major repair - 1 leak per 1000 feet of pipe	1.1	0.5
Bracing (pipe diam.>2.5")	Damage state 1	Isolated support failure w/o leakage - 0.5 supports fail per 1000 feet of pipe (assuming supports every 20 feet)	2.25	0.5
Sanitary water	Damage state 1	Joints break - 1 break per 1000 feet of pipe	3	0.5
Sanitary water Bracing	Damage state 1	Isolated support failure w/o leakage - 0.5 supports fail per 1000 feet of pipe (assuming supports every 20 feet)	2.25	0.5

#### 4.6.7 Sprinklers

Automatic sprinkler provides fire protection for the buildings. The wet sprinkler system has threaded steel which drops into soft ceiling tiles. Two damage states are described for both drops and piping system as shown in Table 4.17. Fragility curves for sprinkler drops also shown in Figure 4.7.

Table 4.17: Damage states for sprinklers

	Damage state type	Description	Fragility parameters	
			Median (g)	Dispersion
Fire Sprinkler Drop	Damage state 1	Spraying & Dripping Leakage at drop joints - 0.01 leaks per drop	1.5	0.40
	Damage state 2	Drop Joints Break - Major Leakage - 0.01 breaks per drop	2.25	0.4
Fire Sprinkler Water Piping	Damage state 1	Spraying & Dripping Leakage at joints - 0.02 leaks per 20 ft section of pipe	1.9	0.4
	Damage state 2	Joints Break - Major Leakage - 0.02 breaks per 20 ft section of pipe	3.4	0.4

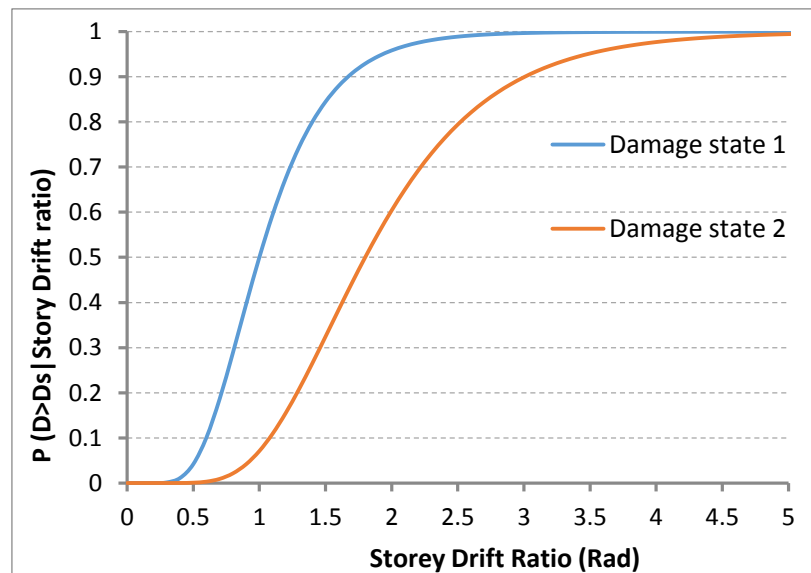


Figure 4.11: Fragility curves for sprinkler drops

#### 4.6.8 HVAC System

HVAC system includes package air handling unit installed on the roof and some other distribution components. The fragility parameters of these component are given in the table for 4.8 for different damage states. Two damage states for the AHUs are mutually exclusive with the probabilities of occurrence of 67% and 33%. Their relationship is such that the occurrence of one damage states precludes the occurrence of the other.

Table 4.18: Damage states for HVAC system components

Component	Damage state type	Description	Fragility parameters	
			Median (g)	Dispersion
Air Handling units - Capacity 5000 to < 10000CFM	Damage state 1 (0.67 fraction)	Equipment does not function. Damage to attached ducting or piping.	1.54	0.6
	Damage state 2 (0.33 fraction)	Equipment does not function Equipment damaged beyond repair.	1.54	0.4
Galvanized Sheet Metal Ducting, cross section area less than 6 sq. ft.	Damage state 1	Individual supports fail and duct sags - 1 failed support per 1000 feet of ducting	1.5	0.4
	Damage state 2	Several adjacent supports fail and sections of ducting fall - 60 feet of ducting fail and fall per 1000 foot of ducting	2.25	0.4
Galvanized Sheet Metal Ducting, cross section area greater than 6 sq. ft.	Damage state 1	Individual supports fail and duct sags - 1 failed support per 1000 feet of ducting	3.75	0.4
	Damage state 2	Several adjacent supports fail and sections of ducting fall - 60 feet of ducting fail and fall per 1000 foot of ducting	4.5	0.4
HVAC drops/diffusers	Damage state 1	HVAC drops or diffusers dislodges and falls	1.5	0.4
Variable Air Volume in line	Damage state 1	Coil damages connection to plumbing. Leakage of hot water	1.9	1.4

#### 4.6.9 Equipment and Furnishing

Damageable contents are given in Table 4.19 including office work stations, electronic equipment installed on walls, and desktop electronic.

Table 4.19: Equipment and furnishing components

Component	Damage state type	Description	Fragility parameters	
			Median (g)	Dispersion
Modular office work stations.	Damage state 1	Wall units need to be adjusted and straightened. Some elements are bent / damaged and need to be replaced	1	0.4
Electronic equipment on wall mount brackets	Damage state 1	Falls, does not function.	2.5	0.5
Desktop electronics including computers, monitors, stereos, etc, smooth surface	Damage state 1	Falls, does not function.	0.4	0.5

## **Chapter 5 : Response Analysis**

### **5.1 Introduction**

This chapter presents the procedure to analyze the benchmark buildings and estimation of demand parameters required for the loss analysis. Different analysis types including static or dynamic (linear or nonlinear) can be employed for the performance assessment procedure. Nonlinear time history analysis method was used for the analysis of benchmark buildings for the best accuracy. The following sections describe steps for capturing the median responses under ground motion shakings. Section 5.2 presents ground motion characterization and section 5.3 describes the details used to model the structural elements. The median responses including floor drifts and accelerations will be used as the inputs for the loss estimation analysis in chapter 6.

### **5.2 Earthquake Hazard Characterization**

Three types of analysis including, intensity-based assessment, scenario-based assessment, and time-based assessment are predicted by ATC-58 (2012). In scenario-based assessment, the performance of the building is evaluated at a particular level of earthquake intensity represented by a target response spectrum. Structural and nonstructural responses is then calculated for a suite of ground motions, scaled to match the target spectrum. If the performance of a building is to be evaluated under a particular historical earthquake, scenario-based assessment is the best choice.

Time-based assessment is a holistic performance assessment tool. It evaluates the performance of the building in a time frame often taken as the useful life span of the

building. This time can vary based of the needs of owner or decision makers. It takes into account all earthquake intensities which could occur within that period of time. Hazard analysis is a key step toward performing loss estimation analysis. Hazard analysis determines the hazard curve for the specific site where the building is located. Hazard curve is a function relating the probability of occurrence of the ground motions to corresponding intensities. The intensity measure is the spectral acceleration at the first mode period of the structure and the probability of occurrence is often expressed by annual probability of exceedance.

The first step in time-based assessment is to obtain the site specific hazard curve for the benchmark building. This hazard curve is supposed to provide a 5% damped spectral acceleration at the first mode period of the building response against the annual frequency of exceedance. An effective, quick way of conducting a probabilistic seismic hazard analysis (PSHA) is to use PSHA tool and the data provided by U.S. Geological Survey's National Seismic Hazard Mapping project. This reduces much time and effort needed for the PSHA analysis required for such projects.

Figure 5.1 shows the hazard curve for the site location of the benchmark buildings. The soil type is D with shear wave velocity of 259 m/s in the upper 30m of depth. The hazard curve is provide for peak ground acceleration and response spectrum acceleration at different period values ranging from 0.1sec to 5.0 sec.

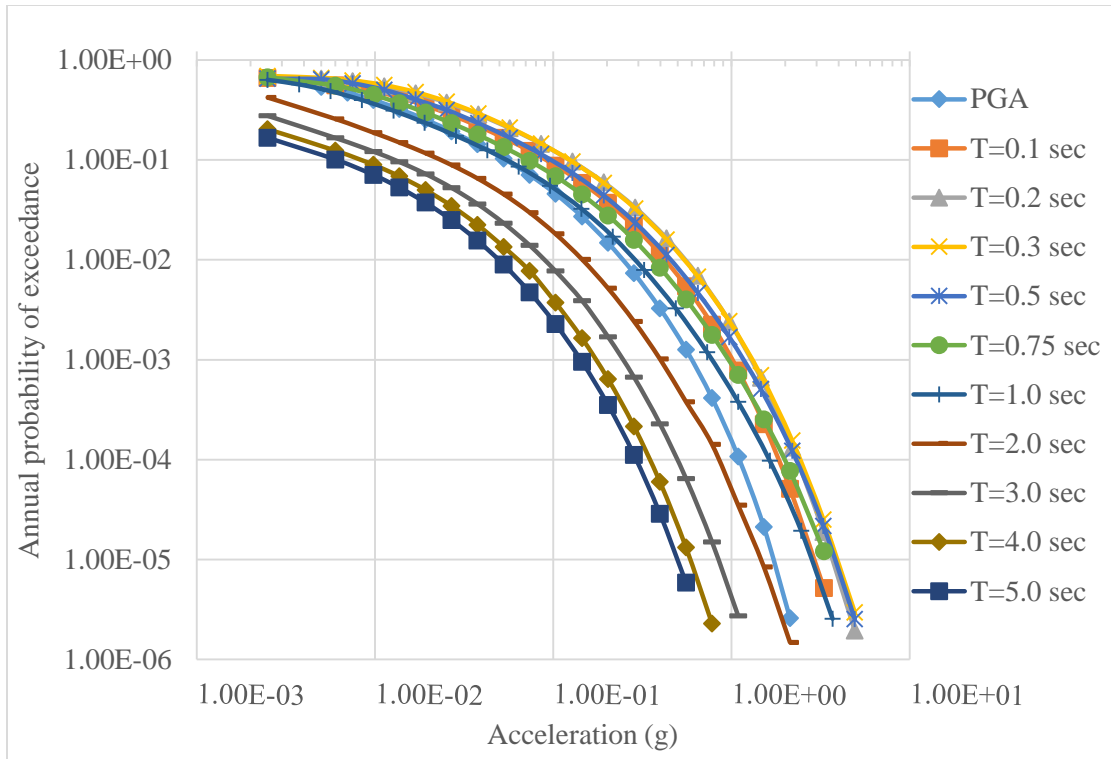


Figure 5.1: Probabilistic seismic hazard curve

The hazard curve is used to produce the target acceleration response spectra. Target spectra can be either Conditional Mean Spectra (CMS) or Uniform Hazard Spectra (UHS). For rare events with low annual probabilities of occurrence, the use of UHS leads to more conservative results than CMS.

Conditional Mean Spectra gives more realistic values by reducing the spectral values at periods other than the structure period of vibration due to less likelihood of simultaneous occurrence of maximum spectral values at different periods. In other words, the CMS is conditioned to the structural period of vibration,  $T$ , taken as the average building period of vibration at two main horizontal directions. CMS is derived by disaggregation of seismic hazard curves based on the risk from all possible sources around the building site. This process involves recognizing all possible combination of

earthquake source, magnitude and distance around the building site which contribute to the hazard.

For each benchmark buildings, a different target spectra and suites of ground motion will be required if CMS is used. This would considerably add to effort to generate such spectra and; therefore, UHS target spectrum was used for this study. Figure 5.2 shows the Uniform Hazard Curve Spectra for shaking intensities corresponding to 10-year to 5000-year return periods.

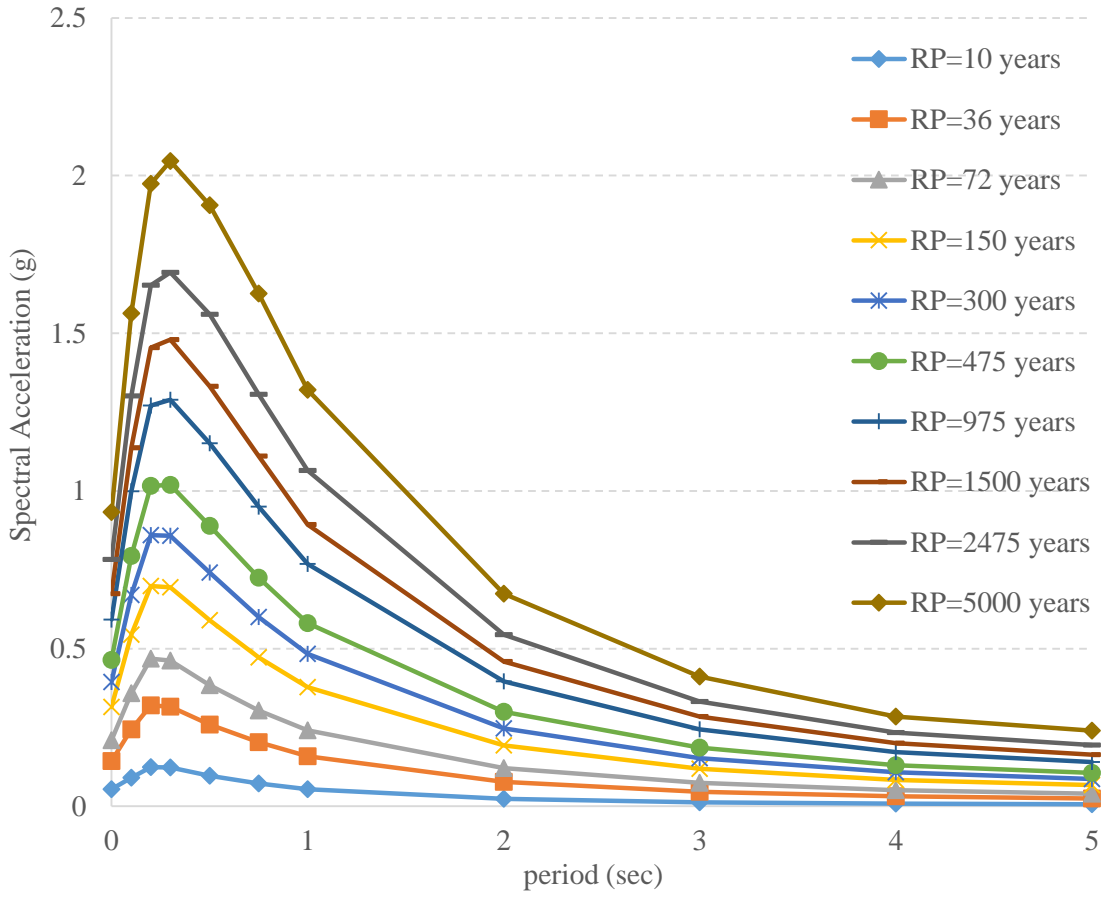


Figure 5.2: Uniform Hazard Curve (UHS)

The lowest intensity is a 10-year earthquake with a 99.3% probability of occurrence in a 50-year period. The highest intensity is an earthquake with 5000 years return period, corresponding to a 1 percent probability of occurrence in 50 years. Table 5.1 summarizes the annual frequency of exceedance associated with each hazard level.

Table 5.1: Annual frequency of exceedance of different hazard levels

<b>Return period (years)</b>	<b>Annual frequency of exceedance</b>
10	1.00E-1
36	2.77E-2
72	1.388E-2
175	5.714E-3
300	3.333E-3
475	2.105E-3
975	1.025E-3
1500	6.666E-4
2475	4.040E-4
5000	2.000E-4

For each hazard level, a suite of ground motions is selected and scaled to match the target spectrum determined by Uniform Hazard Spectra. A period range from 0.1 sec to 5 sec is used to match the target spectrum. This covers the minimum range of  $0.2T$  and  $2T$  suggested by ATC-58 (2012). The selected ground motions have been recorded on the soil type *D* matching the site soil condition of benchmark buildings. The range of shear wave velocity of 200 m/s to 360 m/s was used as the criteria to select ground motions. PEER ground motion database tool was used for this purpose. This online application is so useful for a quick selection and filtration of ground motions base on various criteria

including target spectral shape and shear wave velocity. Ground motions characteristics and the scaling factors are provided in appendix B for each hazard level.

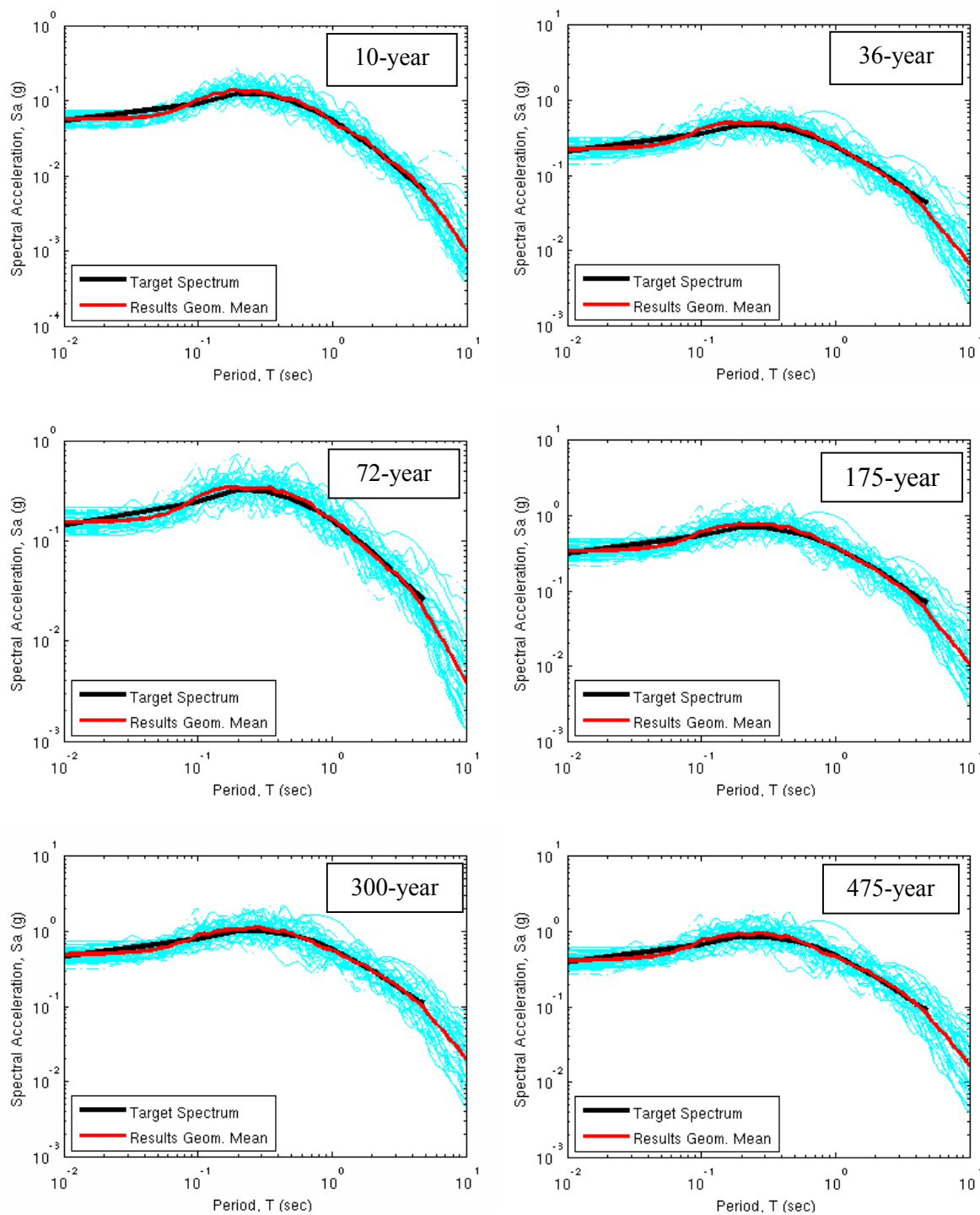


Figure 5.3: Target spectrum and spectral acceleration of ground motions at each hazard

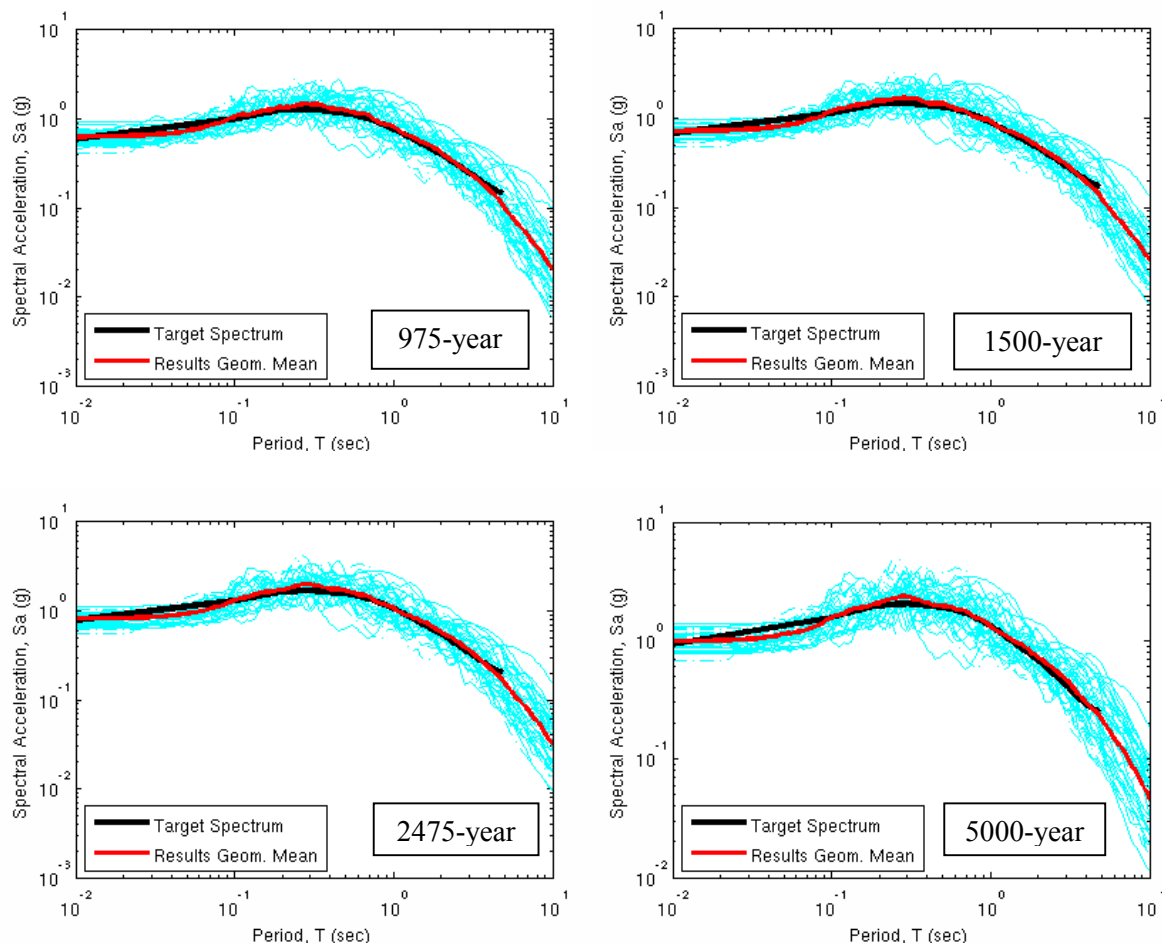


Figure 5.3: Target spectrum and spectral acceleration of ground motions at each hazard level (continue)

### 5.3 Structural Modeling

Loss estimations due to ground motion shakings depend on the calculated responses obtained in structural analysis. The uncertainty factors concerning the engineering demand parameters (EDP), accounted for by modeling uncertainty in ATC-58 (2012), depends on the accuracy of the structural component models used in the analysis. A more robust analytical procedure is associated with a lower dispersion in the EDPs and results in more reliable loss estimations.

This section discusses the details of structural modeling, elements used, and decisions relating to development of the model buildings. There are two general methods of modeling which are widely used for the nonlinear analyses, fiber-hinge and lumped plasticity model. Each approach has advantages for specific purposes which will be explained later. The current fiber models are not capable of estimating collapse fragility of the structures. Therefore, it is only used for pre-collapse analysis while the collapse evaluations uses the lumped plasticity model for which the collapse capacity of various elements are studied in the past.

### **5.3.1 Fiber-Hinge Model**

Fiber sections are used to estimate the response of the whole section by dividing it into fibers. Each fiber is assigned a material with a specific stress-strain relationship. The whole section response is computed by integrating the response of all fibers within the section using the principle of strain compatibility. A section response accuracy is dependent on the number of fibers and stress-strain relationships. Fiber elements are comprised of fiber sections along the length of element at which different properties can be assigned. Beams and columns of the benchmark buildings are modeled by fiber elements with five integration points along the lengths at which the responses are captured. Each section includes 200 fibers including concrete core and cover. Figure 5.4 shows a schematic fiber beam-column element comprised of 5 integration points along the length.

The assumptions used to build structural model with fiber-hinge elements are summarized as follows:

- Two dimensional frames
- Geometric nonlinearity with P-Delta effects
- Force-based elements for beams and columns with fiber sections
  - Giuffre-Menegotto-Pinto model for steel bars
  - Concrete material that captures tension softening
- Joint elements with the ability to model shear deformation in panel zones
- Lumped-plasticity end element springs capable of simulating the following phenomena
  - Bond-slip behavior
  - Shear deformation

These modeling assumptions are explained in further details in the following sections. The model was built in OpenSees (2002) as one of the most sophisticated programs for the structural analysis.

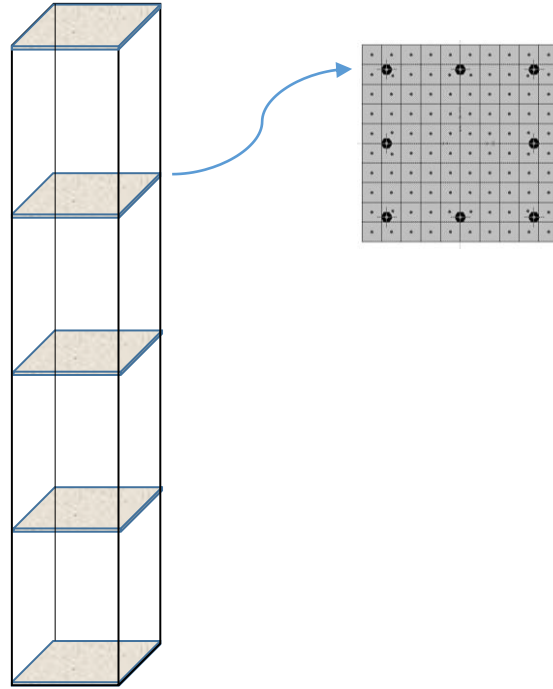


Figure 5.4: Fiber element schematic drawing for a concrete column containing of 100 fibers for concrete and 9 fibers for steel bars

### 5.3.1.1 Steel material

Several material models have been developed to simulate the cyclic response of steel material in reinforced concrete components. This study uses Giuffre-Menegotto-Pinto model for steel material (Taucer & Spacone, 1991). This model offers a bilinear backbone curve capable of capturing both isotropic and kinematic strain hardening. This material is accessible through steel02 material which was implemented in OpenSees by Filippou (2005). The expected yield strength of A615 Grade 60 steel bars is assumed 69 ksi according to Nowak and Szerszen (Nowak & Szerszen, 2003) and modulus of elasticity is also considered 29000 ksi.

For post yield elastic stiffness, we followed the work by Haselton et al. (Haselton, Liel, Taylor Lange, & Deierlein, 2006/2007). They proposed to reduce the strain-

hardening modules of steel material to account for the flexibility due to bond-slip behavior and shear deformation in the post yield range. They concluded that 50% of the post-yield flexibility comes from the bond-slip behavior and shear. So, they proposed to use a strain hardening of  $0.01 \cdot E_s$  instead of 0.018 proposed by Wang (1978). In the elastic range, element end springs are used to model the additional flexibility due to bond-slip and shear according to section 5.6.

### 5.3.1.2 Concrete material Model

Fillipou (2005) implemented the Concrete02 material in OpenSees. This model captures the response of the concrete both in compression and tension with the ability to simulate the tension-stiffening effect. Mander et al. (1988) proposed a uniaxial stress-strain relationship to model for confined concrete based on axial compressive tests of concrete specimens. They constructed their model based on the equations proposed by Popovics (1973) as follows:

$$\sigma = \frac{f_{cc} \times x \times r}{r - 1 + x^r} \quad (5-1)$$

Where  $\sigma$  is axial compressive stress and  $f_{cc}$  is peak strength of confined concrete;  $x$  and  $r$  are given by the following equations:

$$\begin{aligned} x &= \frac{\varepsilon}{\varepsilon_{cc}} \\ r &= \frac{E_c}{E_c - E_{sec}} \end{aligned} \quad (5-2)$$

where  $\varepsilon$  is compressive concrete strain;  $E_c$  is modulus of elasticity of concrete;  $E_{sec}$  is secant modulus of elasticity of confined concrete at peak stress;  $\varepsilon_{cc}$  is strain at the maximum stress  $f_{cc}$  given by:

$$\varepsilon_{cc} = \varepsilon_{co} \left[ 1 + 5 \left( \frac{f_{cc}}{f_{co}} - 1 \right) \right] \quad (5-3)$$

where  $f_{co}$  is the compressive strength of unconfined concrete. The confined concrete peak strength  $f_{cc}$  is given by:

$$f_{cc} = f_c \left[ 2.254 \sqrt{1 + 7.94 \frac{f_l}{f_c}} - 2 \frac{f_l}{f_c} - 1.254 \right] \quad (5-4)$$

where  $f_l$  is the effective confining pressure which is calculated for x and y directions of rectangular section as follows:

$$\begin{aligned} f_{lx} &= K_e \frac{A_{sx}}{s \cdot d_c} \times f_{yt} \\ f_{ly} &= K_e \frac{A_{sy}}{s \cdot b_c} \times f_{yt} \end{aligned} \quad (5-5)$$

where  $A_{sx}$  and  $A_{sy}$  are cross section area of transverse reinforcement;  $s$  is clear spacing between hoop bars or spirals;  $d_c$  and  $b_c$  are concrete core dimension measured center to center line of hoop bars;  $K_e$  is given by the following equation for rectangular hoops:

$$K_e = \frac{\left( 1 - \sum_{i=1}^n \frac{(w'_i)^2}{6b_c d_c} \right) \left( 1 - \frac{s}{2b_c} \right) \left( 1 - \frac{s}{2d_c} \right)}{(1 - 2\rho_{cc})} \quad (5-6)$$

where  $w'_i$  is the  $i^{\text{th}}$  clear distance between adjacent longitudinal bars and  $\rho_{cc}$  is the ratio of longitudinal reinforcement area to core area. Figure 5.5 shows concrete stress-strain curve using Mander et al. equation for confined and unconfined concrete (cover) of the first floor columns of B1 model.

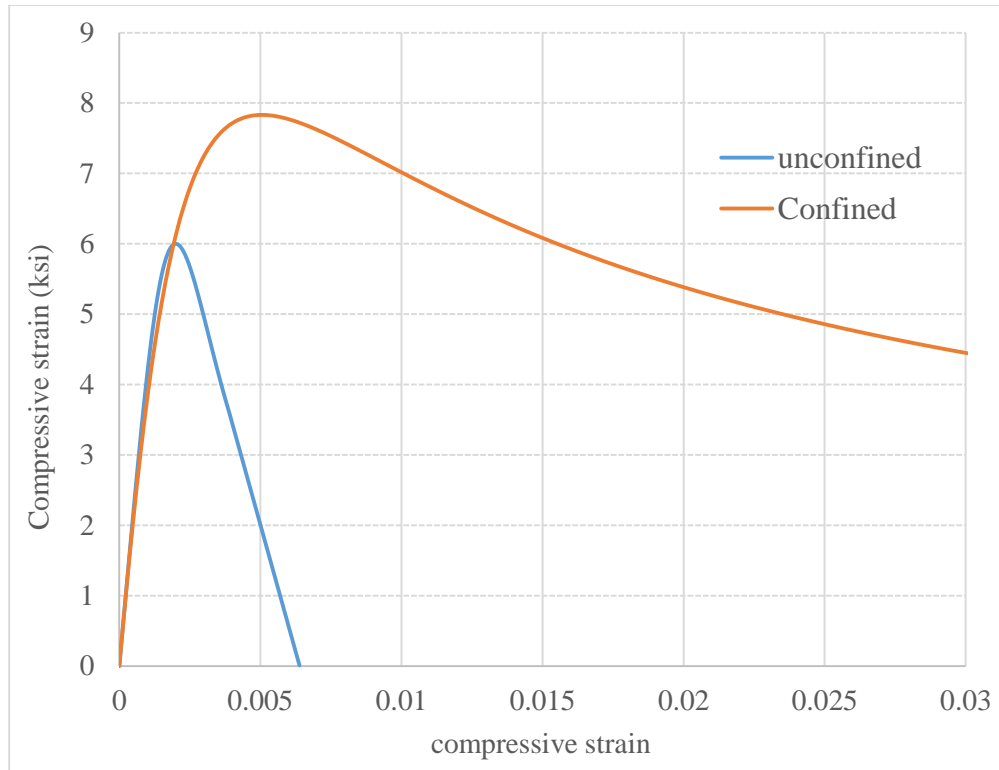


Figure 5.5: Stress-strain relationship using Mander et al. model

Peak compressive strength and strain obtained from Mander equation was used as an input to Concrete02 model in OpenSees which is based on the FEDEAS material library. This model assumes the initial stiffness as twice the secant stiffness through peak strength point (capping point). The post capping negative stiffness is also constant through crushing point. Linear tension-softening with the ability of considering the tensile strength is implemented into the model. Figure 5.6 shows the backbone stress-strain curve constructed based on this material for confined concrete.

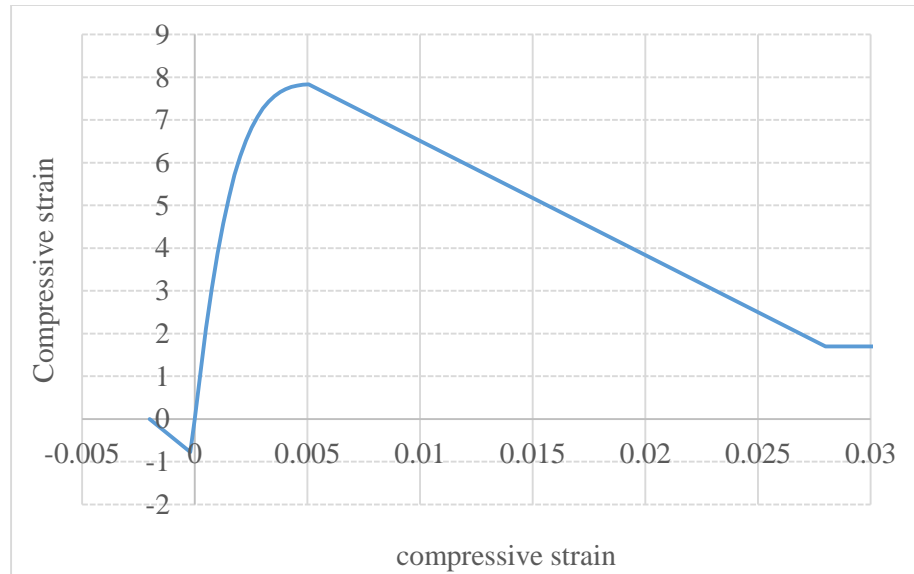


Figure 5.6: Stress-strain relationship for confined concrete (FEDEAS material)

### 5.3.1.3 Bond-slip model

The seismic response of entire structure depends on the completeness of the model developed for this purpose. Bond-slip of reinforcing bars anchored in joints is a substantial source of deformations in concrete structures. Experimental tests show the global response of beam-column connections is affected to by the local bond response (Sritharan, Ingham, Priestley, & Seible, 1998). Bond-slip of reinforcing bars increases fixed-end rotation at joints and thus considerably gives rise to global deformations.

This study follows the work developed by Lows et al (2003) for bond-slip modeling. They divided the anchorage length into pre-yield and post-yield zones as shown in Figure 5.7. By integrating strains over the bond length, slip values are given separately for post and pre-yield zone:

$$\begin{aligned} slip(pre-yield) &= \frac{1}{8} \frac{f_s^2}{\tau_E \times E} d_b & f_s < f_y \\ slip(post-yield) &= \frac{f_y^2}{8\tau_E E} d_b + \frac{(f_s - f_y)f_y}{4\tau_y E} d_b + \frac{(f_s - f_y)^2}{8\tau_y E_h} d_b & f_s \geq f_y \end{aligned} \quad (5-7)$$

where  $f_y$  is the steel yield strength,  $E$  is the steel modulus of elasticity,  $E_h$  is the steel hardening modulus, and  $d_b$  is the nominal bar diameter. Lowes et al (2004) suggested the average bond strength for elastic and yielded steel,  $\tau_E$  and  $\tau_y$ , based on the experimental data by Shima et al. (1987) as follows:

$$\begin{aligned} \tau_y &= 4.8\sqrt{f'_c} \text{ psi} \\ \tau_E &= 21\sqrt{f'_c} \text{ psi} \end{aligned} \quad (5-8)$$

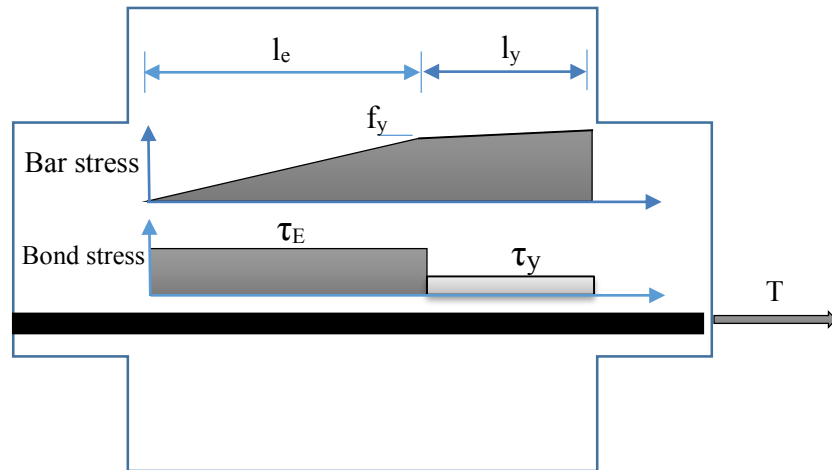


Figure 5.7: Bond and bar stress distribution of reinforcing bars anchored joints  
(Lowes et al. model)

Figure 5.8 shows the stress-slip diagram of the reinforcement bars for B1 model first story beams (#5 bar,  $f_y=60$ ksi,  $f_c=6$ ksi) using Lowes model. The equivalent moment normalized to yield moment versus rotation is also given in Figure 5.9. A lever arm equal

to  $(d-d')$  is assumed for rotation calculations based on Fardis (2003) suggestion where  $(d-d')$  is the distance between tension and compression reinforcement.

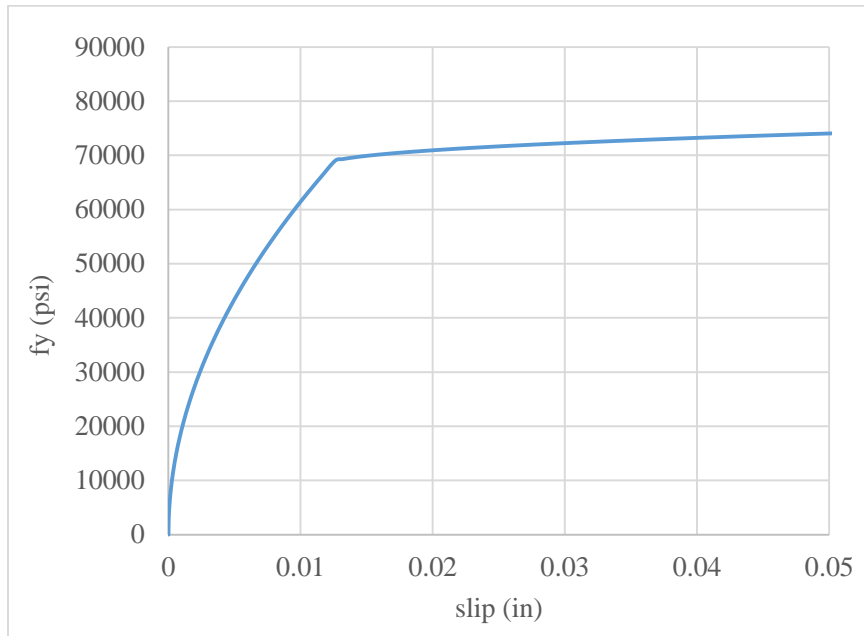


Figure 5.8: Bar stress versus slip using Lowes equation (reinforcing bars located at first story beams of B1 model)

Cyclic behavior of the bond-slip model is suggested by Mitra and Lowes (2004) which considers the pinching behavior. The pinching point stiffness and strength is similarly set at 25 percent initial stiffness and yield strength, respectively.

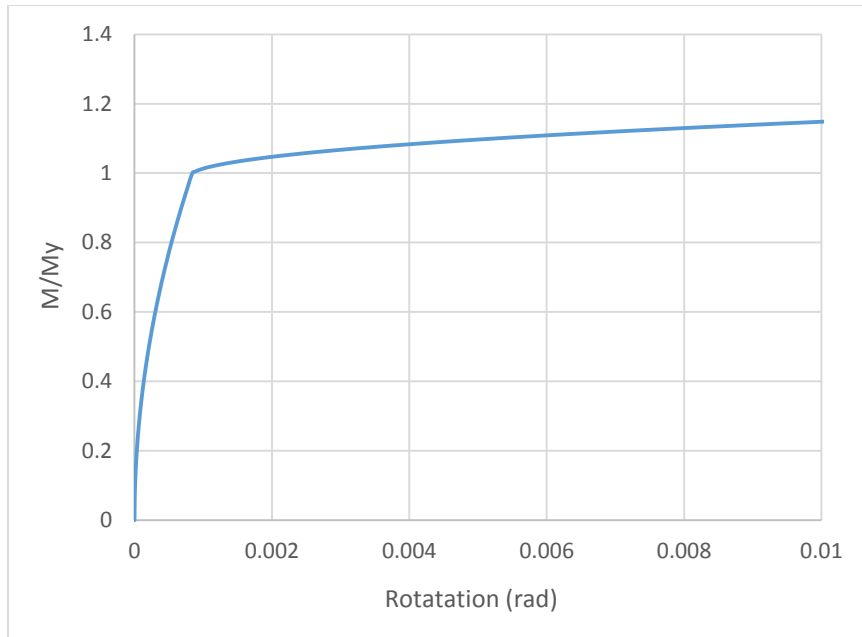


Figure 5.9: Normalized moment versus rotation (reinforcing bars located at first story beams of B1 model)

We followed Haselton (2007) modeling technique by using end element springs capable of simulating the bond-slip response prior to reinforcement yielding. A bilinear idealization of bond-slip behavior is assumed with a secondary stiffness  $K_2$  equal to 25% of the initial stiffness  $K_1$  as shown in the Figure 5.10 with the point of stiffness change set at 40% of flexural yield strength. This model is only useful for pre-yield bond-slip behavior and therefore does not account for the extra flexibility in the post-yield range. They suggested to decrease the steel hardening ratio by 50% to account for the extra flexibility originating from shear and bond-slip.

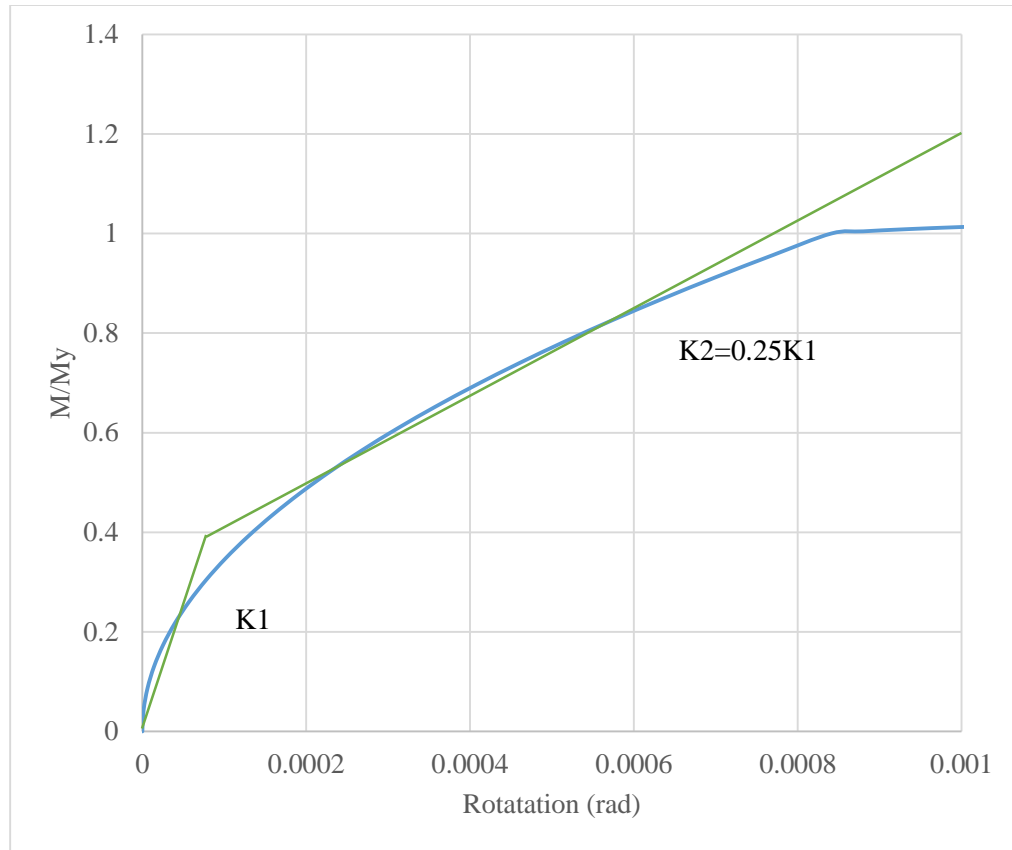


Figure 5.10: Bilinear idealization of bond-slip behavior

#### 5.3.1.4 Shear Model

Although shear strength capacity is not a possible failure mode for recently designed reinforced concrete frames, shear deformations comprise a considerable portion of total deformations. Considering shear flexibility results in the structure to adapt larger lateral displacements and disregarding it leads to a conservative prediction of lateral deformation capacity of the structures.

Current fiber elements are not capable of incorporating the shear response in the analysis, but end springs can be used to capture the shear behavior (Haselton et al. 2007). The stiffness of such springs must be accordingly calibrated for this purpose. Fardis and

Panagiotakos (2001) equations can be used for this purpose, but they predicted extremely large shear flexibilities (Haselton, Liel, Taylor Lange, & Deierlein, 2006/2007)

Table 5.2 shows the predicted chord yield rotations using Fardis equation for B1 model elements including flexural, shear, and bond-slip portions. Shear deformations are on the same order of flexural for these elements. We conclude these predictions are very large and corresponds to a very low effective shear stiffness. As Fardis model is based on the total regression analysis over the results of thousands of tests, their proposed model is more accurate when used for total deformation prediction. On the other hand, their model is most appropriate to be used for a lumped plasticity model where the flexibility due to flexural, shear and bond slip behavior is combined in the plastic hinge.

Among several models that have been developed to predict shear deformations at yield Sezen (2002) model has shown to have a good match with experimental results while the other models usually over predict the shear deformations (Chaturvedi et al. 2005). Equation 5-9 gives their proposed equation that estimates the displacement at yield:

$$\delta_{y, shear} = \left( \frac{3}{0.2 + 0.4 \times P_r} \right) \frac{V_y L}{E_c A_g} \quad (5-9)$$

where  $P_r$  is axial load ratio defined as ratio of applied axial load to nominal axial load carrying capacity of columns,  $L$  is the length of element,  $E_c$  is the concrete modulus of elasticity,  $A_g$  is the gross cross sectional area,  $V_y$  is the shear force acting on the section when plastic moments forms at the ends of the elements. Assuming a double curvature element,  $V_y$  is given by:

$$V_y = \frac{2M_y}{L} \quad (5-10)$$

Table 5.2: Yield chord rotations predicted by Fardis equation (B1 model)

Structural element	$\theta_y$ (rad)			
	flexure	shear	bond-slip	total
Corner column – 1 <sup>st</sup> Story	0.002454	0.00275	0.000686	0.005890
Edge column – 1 <sup>st</sup> Story	0.002730	0.00275	0.000686	0.006166
Interior column – 1 <sup>st</sup> Story	0.002954	0.00275	0.000686	0.006390
Corner column – 2 <sup>nd</sup> Story	0.003364	0.00275	0.000686	0.006800
Edge column – 2 <sup>nd</sup> Story	0.003598	0.00275	0.000686	0.007034
Interior column – 2 <sup>nd</sup> Story	0.003948	0.00275	0.000686	0.007384
Beam -1 <sup>st</sup> Story	0.003672	0.00275	0.000514	0.006936
Beam - 2 <sup>nd</sup> Story	0.005712	0.00275	0.000429	0.008891

Table 5.3 compares contribution of shear in the total yield rotation. As mentioned before, Fardis model overestimates the shear flexibility of the elements. Thus, for the fiber-hinge model, we decided to employ the Sezen model for shear deformations prior to yield. For post-yield behavior, the hardening ratio of steel reinforcement is reduced by 50 percent to account for the shear and bond-slip flexibility.

Table 5.3: Yield chord rotations predicted by Fardis (2001) and Sezen (2002) (B1 model)

Structural element	$\theta_y$ (rad)	
	Fardis (2001)	Sezen (2002)
Corner column – 1 <sup>st</sup> Story	0.00275	0.000301
Edge column – 1 <sup>st</sup> Story	0.00275	0.000341
Interior column – 1 <sup>st</sup> Story	0.00275	0.000393
Corner column – 2 <sup>nd</sup> Story	0.00275	0.000323
Edge column – 2 <sup>nd</sup> Story	0.00275	0.000341
Interior column – 2 <sup>nd</sup> Story	0.00275	0.000365
Beam -1 <sup>st</sup> Story	0.00275	0.000206
Beam - 2 <sup>nd</sup> Story	0.00275	0.000138

### 5.3.1.5 Joint panel shear

Current design provisions prevent any shear failure in joint-panels but the shear deformations arising from these zones are significant. Figure 5.11 shows a schematic illustration of the shear deformation of a concrete joint. The inelastic deformations in the panel zones are essentially important for simulating the shear cracking and the additional flexibility coming from it.

Altoonash (2004) developed a model to predict the shear deformation in concrete joints and implemented it into the OpenSees program. The joint model is named Joint2D and it is capable of modeling both end element plastic hinges and shear panel zone behavior. The rotational springs at the center of the joint are used to model the shear behavior of the panel zone. The rotational stiffness of this spring is calculated using the shear equivalent moment concept. The rotational stiffness of the spring is calibrated to produce the same shear stress on the sides of the parallelograms given the shear distortion at the joint. The shear equivalent moment is calculated by multiplying the joint average shear stress by the joint volume.

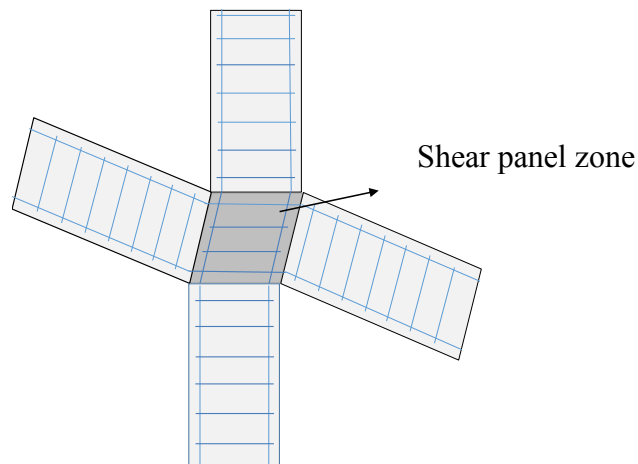


Figure 5.11: Shear deformation in the shear panel zone

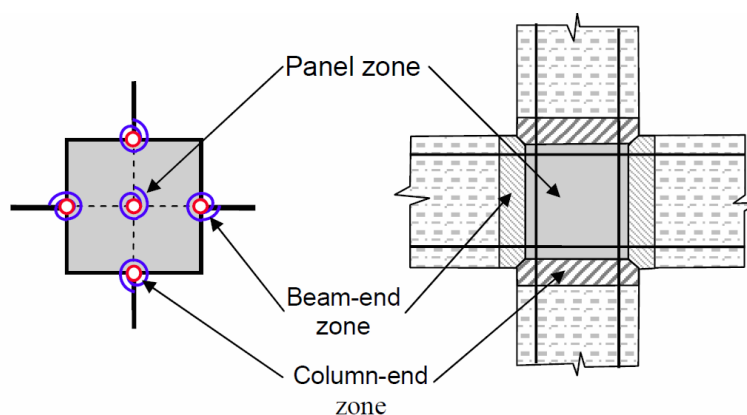


Figure 5.12: Joint2D elements (Altoontash, 2004)

Shear stress-strain relationship for panel zones has been the subject of several research studies (Umemura & Aoyama, 1969; Meinheit & Jirsa, 1981). ACI352-R02 (2002) provides the nominal average shear strength of concrete joints based on the number of joint faces confined:

$$v_j = \gamma \sqrt{f_c} \text{ (psi)} \quad (5-11)$$

Where  $\gamma$  is the joint shear strength factor given in Table 5.4. The number of vertical faces around the joint providing confinement is the effective factor for determining the shear strength.

Table 5.4: Joint shear strength factor ( $\gamma$ ) according to ACI352-R02

Joint type	Interior	Exterior	Corner
Continuous Column	20	15	12
Roof column	15	12	8

Haselton et al (2008) suggested a shear stress-strain backbone curve as shown in Figure 5.13. The uncracked shear strength is approximately 25% of the peak strength with a shear strain of 0.0002. The strain corresponding to peak strength is set equal to 0.004. They suggested to use a post capping stiffness of -7% of the cracked stiffness. The cyclic behavior can also be modeled by the pinching material with the unloading stiffness equal to the uncracked stiffness (Altoontash, 2004). The pinching point occurs at a shear strain of 25% the maximum historic shear strain and shear stress.

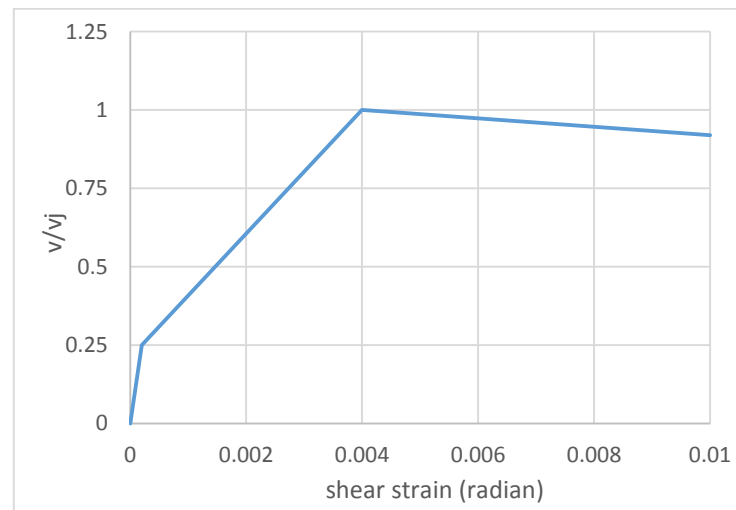


Figure 5.13: Shear stress-strain backbone curve for panel zones

### 5.3.2 Lumped Plasticity Model

Although fiber-hinge model is a very good method of simulating pre-collapse behavior, it is not capable of properly predicting the collapse capacity. For this reason, lumped plasticity model is used for collapse analysis. The key assumptions for this model is summarized as follows:

- Two dimensional frame built in OpenSees

- Geometric nonlinearity with P-Delta effects
- Force-based elements for elastic beams and columns with nonlinear rotational spring to model end plastic hinges that is able to capture:
  - Bond-slip behavior (modeled using joint2D element end spring in OpenSees)
  - Shear deformation (modeled using joint2D element end spring in OpenSees)
- Joint elements simulating of modeling shear deformation in panel zones (Joint2D element center spring)

Joint panel zone is modeled the same as explained for fiber-hinge model. The plastic hinge properties including the initial stiffness, yield/ultimate moment and rotations, and the plastic rotation capacity are discussed in the following sections.

### 5.3.2.1 Element-hinge Model

Lumped-plasticity model consists of elastic beam and column elements with end plastic hinges to represent the behavior in the post-yield phase. The period of vibration and demand seismic forces are dependent on the effective stiffness of the components. Therefore, the initial stiffness of the elements and plastic hinges must be calibrated to properly represent the effective stiffness of the component. Figure 5.14 represents a typical trilinear moment-rotation diagram for a plastic hinge. The elastic stiffness ( $K_e$ ), yield and ultimate moment ( $M_y$  &  $M_u$ ), the chord rotation at the at yield and ultimate moment often referred to as yield and capping rotation ( $\theta_y, \theta_p$ ), post capping negative

stiffness ( $K_c$ ), and residual strength moment ( $M_r$ ) are the parameters to define the backbone curve.

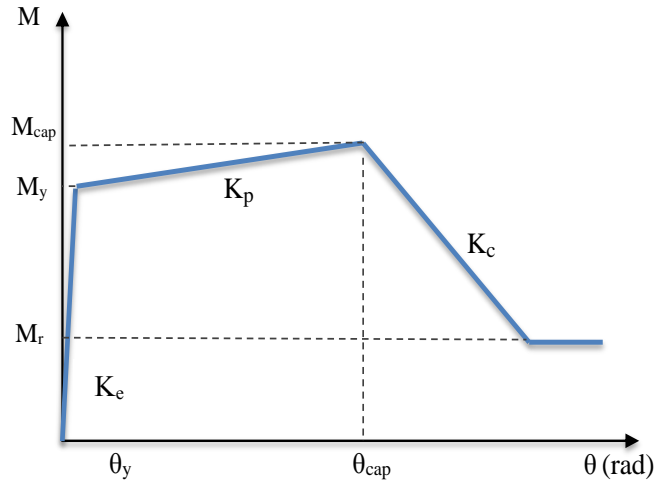


Figure 5.14: Typical moment-rotation backbone diagram of plastic hinges

The initial stiffness of the elements and plastic hinges work in series. Ibarra and Krawinkler (Ibarra, Medina, & Krawinkler, 2005) suggested a method to calibrate the stiffness for the element and the end plastic hinges that results in the same stiffness of the original member. Assuming a double curvature for beam and column elements and stiffness multiplier of 10 ( $n=10$ ), the initial stiffness of the beam and column elements ( $K_e$ ) and end plastic hinges increases to  $1.1K_e$  and  $11 K_e$  according to the following equation:

$$K_{beam.column} = \frac{n+1}{n} K_e \quad (5-12)$$

$$K_{spring} = (n+1)K_e$$

Damping is only assigned to elastic beam-columns elements. When a large value of multiplier factor is used ( $n=10$ ). In addition, cyclic behavior of the beam and column elements is only represented by the end plastic hinges.

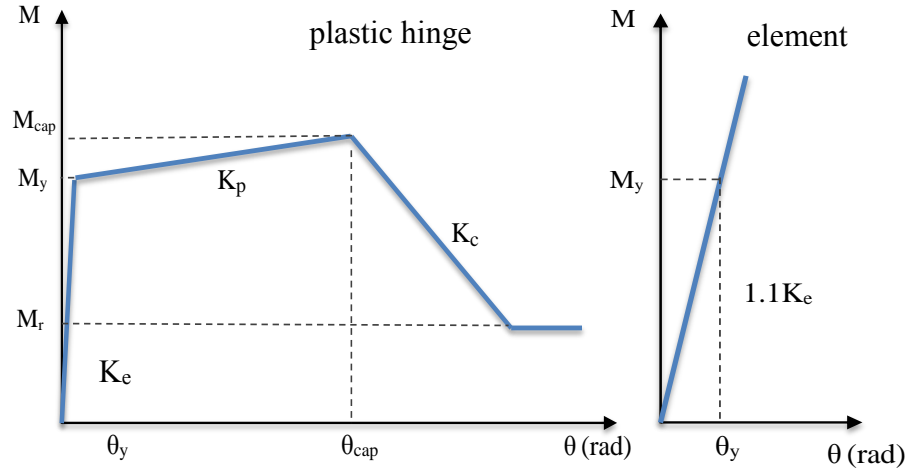


Figure 5.15: Modified moment-rotation backbone diagram for elements and plastic hinges

### 5.3.2.2 Hinge yield rotation and effective stiffness

Fardis (2003) proposed an empirical equation that estimates the chord rotation of beam-columns concrete elements at the onset of flexural yielding. They used a database of past experimental studies for their regression analysis. The equation predicts the yield chord rotation of elements incorporating flexural, shear and bond slip deformations:

$$\theta_y = \theta_{y,flexural} + \theta_{y, shear} + \theta_{y, bond-slip} \quad (5-13)$$

$$\theta_{y,flexural} = \phi_y \frac{L_s}{3}$$

$$\theta_{y, shear} = 0.00275 \quad (5-14)$$

$$\theta_{y, bond-slip} = a_{sl} \frac{\varepsilon_y}{(d-d')} \times \frac{0.2d_b f_y}{\sqrt{f'_c}}$$

where  $\theta_y$  is the chord rotation at yield,  $\phi_y$  is the yield curvature,  $L_s$  is the shear span,  $a_{sl}$  is the bond-slip indicator,  $\varepsilon_y$  is longitudinal steel yield strain,  $(d-d')$  is the distance from

top to bottom longitudinal steel,  $d_b$  is bar diameter,  $f_y$  is longitudinal steel yield strength, and  $f_c'$  is concrete compressive strength. As they performed the regression analysis to predict the total deformation, we conclude that this equation best suits for the use in a lumped plasticity model where the combined effect of three components of the deformations is desired. Fadis et al. (2003) also provided equations to predict the yield curvature  $\phi_y$ . The moment curvature diagram of the section can also be determined using fiber section and proper material models which is used in this study.

Estimations of yield rotation was presented in Table 5.2 for several beams and column elements of model B1. The effective stiffness of beams and columns is obtainable by dividing the yield moment by the yield rotation. The ratio of effective stiffness to uncracked stiffness is provided in Table 5.5. Depending on the column axial force, the effective stiffness varies between 0.26 to 0.46 which is considerably lower than the FEMA 356 (2000) suggested value of 0.7. Beams effective stiffness ratio is estimated at 0.2 far less than 0.35 suggested in FEMA 356.

Table 5.5: yield chord rotation estimation using Fardis equation (model B1)

Structural element	$EI_{eff}/EI$
Corner column – 1 <sup>st</sup> Story	0.26
Edge column – 1 <sup>st</sup> Story	0.30
Interior column – 1 <sup>st</sup> Story	0.39
Corner column – 2 <sup>nd</sup> Story	0.37
Edge column – 2 <sup>nd</sup> Story	0.40
Interior column – 2 <sup>nd</sup> Story	0.46
Beam -1 <sup>st</sup> Story	0.20
Beam - 2 <sup>nd</sup> Story	0.20

### 5.3.2.3 Ultimate plastic rotation capacity

Fardis (2003) and Panagoitakos (2001) proposed an empirical equation to predict the ultimate rotation capacity of reinforced concrete elements using a large database of results of cyclic tests over rectangular columns with conforming reinforcement which failed in flexural mode. They defined the ultimate rotation capacity at the point beyond the capping point where 20% decrease in load carrying capacity has occurred:

$$\theta_{u,mono}^{pl} = a_{st}^{pl} (1 + 0.55a_{sl})(1 - 0.4a_{wall})(0.2)^v \left( \frac{\max(0.01, \omega')}{\max(0.01, \omega)} \right)^{0.225} \left( \frac{L_s}{h} \right)^{0.375} 25^{\left( \frac{\alpha f_{yw}}{f_c} \right)} 1.3^{100\rho_d} \quad (5-15)$$

where :

$\theta_{u,mono}^{pl}$  : Plastic rotation at the point of 20% strength loss relative to capping point

$a_{st}$  : coefficient relating to type of steel

$a_{sl}$  : bond-slip indicator

$a_{wall}$  : a coefficient equal to zero for non-wall members

$v$  : axial load ratio ( $P/A_g f_c$ )

$\omega$  and  $\omega'$  : tension and compression steel ratio

$L_s$  : shear span length

$h$  : height of the section

$\alpha$  : confinement effectiveness factor

$\rho_s$  : transverse reinforcement ratio

$\rho_d$  : ratio of diagonal reinforcement steel

$f_{yw}$  : is the yield strength of longitudinal reinforcement (MPa)

$f'_c$  : concrete compressive strength (MPa)

Zareian (2006) suggested to use 1.1 for the ratio of  $M_c/M_y$  based on the database of tests on reinforced concrete columns with axial load ratio of less than 0.2. Haselton et al.

(2006) also suggested a post capping stiffness of -7% of the elastic stiffness. They used this stiffness and Fardis ultimate rotation capacity  $\theta_{u,mono}^{pl}$  to back calculate the capping rotation  $\theta_{cap}^{pl}$  using the following equation:

$$\theta_{cap}^{pl} = \theta_{u,mono}^{pl} - 0.2M_y / K_c \quad (5-16)$$

Where all parameters have been previously defined. Table 5.5 shows the estimated capping and ultimate rotation capacity for several beam and column elements of model B1. The capping ratio varies between 0.047 to 0.063 depending on element reinforcement detail and axial load. These prediction are considerably higher than those proposed in FEMA series. The confinement effect of transverse reinforcement in special moment resisting frame considerably contributes in increasing the rotation capacity.

Table 5.6: Capping and ultimate rotation capacity (B1 model)

Structural element	$\theta_{cap}^{pl}$ (rad)	$\theta_{u,mono}^{pl}$ (rad)
Corner column – 1 <sup>st</sup> Story	0.047	0.063
Edge column – 1 <sup>st</sup> Story	0.055	0.071
Interior column – 1 <sup>st</sup> Story	0.058	0.075
Corner column – 2 <sup>nd</sup> Story	0.054	0.072
Edge column – 2 <sup>nd</sup> Story	0.060	0.079
Interior column – 2 <sup>nd</sup> Story	0.061	0.081
Beam -1 <sup>st</sup> Story	0.062	0.080
Beam - 2 <sup>nd</sup> Story	0.063	0.087

#### 5.3.2.4 Cyclic deterioration

Hysteresis models with degrading stiffness, strength and pinching behavior best estimate the sideway collapse capacity. Ibarra and Krawinkler (2003) formulated an energy based cyclic deterioration model including basic strength, post-capping strength,

unloading stiffness, and reloading stiffness. The deterioration at each cycle is represented by a parameter  $\beta_i$ , ranging between 0 and 1, defined as follows:

$$\beta_i = \left( \frac{E_i}{E_t - \sum_{j=1}^i E_j} \right)^c \quad (5-17)$$

Where

$E_i$  : hysteresis energy dissipated at cycle  $i$

$\sum_{j=1}^i E_j$  : total dissipated energy in all previous cycles

$E_t$  : hysteresis energy capacity equal to  $\gamma F_y \delta_y$

$c$  : a parameter defining the rate of deterioration

This model was implemented in OpenSees by the name “Modified Ibarra-Medina-Krawinkler” deterioration model. It uses four parameters to individually calibrate each of the aforementioned properties. Four other parameters are also used to specify the rate of deterioration. These parameters must be calibrated based on experimental results on reinforced concrete components. Energy dissipation capacity is defined by factor  $\gamma$  used in  $E_t$  term which is greatly dependent on the confinement effect provided by transverse reinforcement. Haselton et al. (2008) suggested a mean value of  $\gamma$  equal to 110 with  $c$  equal to 1.0 based on the experimental data of reinforced concrete elements with conforming details. This study also uses the same values for modeling hysteresis behavior in concrete beam and column elements.

## 5.4 Collapse Capacity

Incremental dynamic analysis (IDA) is currently the most reliable method of estimating the global dynamic stability capacity of reinforced concrete frames. In this procedure, nonlinear dynamic analysis is performed on the structure multiple times for a ground motion record with various intensity levels. The ground motion intensity is scaled up to the intensity level where the dynamic analysis leads to failure.

The Spectral acceleration at the first mode period of the building is often considered as the intensity measure. Intensity measure is then plotted against an engineering demand parameter (EDM) often taken as the maximum inter-story drift of all stories.

The inability of the building to sustain gravity load while seismic loads acts on the building is the cause of the collapse. An important cause of collapse is P-Delta effect due to large story deformations. It results in an incremental collapse where the deteriorated component are not capable of resisting the secondary moments and shear. Local collapse in a deficient beam or column also results in excessive forces in adjacent elements. The failure is then propagated to other elements until the global collapse occurs. This study does not consider non-ductile failure modes like shear which are unlikely to occur in code conforming beam and column elements. The global side collapse is usually incepted as the phenomena where the increase in dynamic loads is not followed by an increase in the resistance. IDA analysis assumptions used in this research are summarized as follows:

- The 2% in 50 year suite consist of 40 ground motion components at both horizontal directions (20 records) is used to predict the collapse evaluations. This is the largest intensity level which is available often called maximum credible earthquake.

- Maximum inter-story drift and spectral acceleration at the first mode period of the building are used as the EDM and intensity measure (IM).
- Nonlinear time history analysis (NLTH) is employed assuming lumped-plasticity model with P-Delta effect.
- Two dimensional models are used for all incremental dynamic analysis. Benchmark buildings have symmetric layouts which minimizes the need to construct 3d models. Three dimensional analysis are computationally intensive and considerably adds to the complexity of the problem.
- Collapse state concluded where either the convergence has not reached due to numerical model instability or a large EDM occurs with a load increment.

Figures 5.16 to 5.27 show the collapse IDAs for all benchmark building structures. IDA collapse is given for either 40 or 20 ground motions for each model. The collapse IDA consisting of 20 diagrams is obtained using the critical ground motion component of each record. The collapse capacity for each model is conservatively obtained based on this diagram. Figures 5.28 to 5.33 show the cumulative distribution function of collapse predicted by various ground motions and the fitted lognormal CDF.

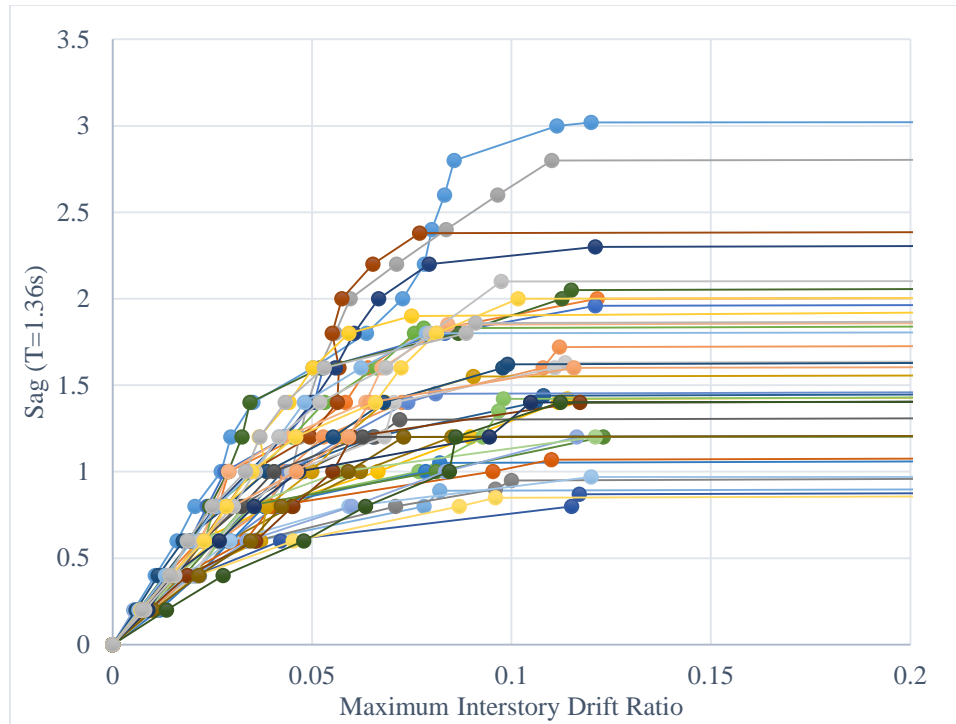


Figure 5.16: Collapse IDA for design B1 including all 40 ground motion components

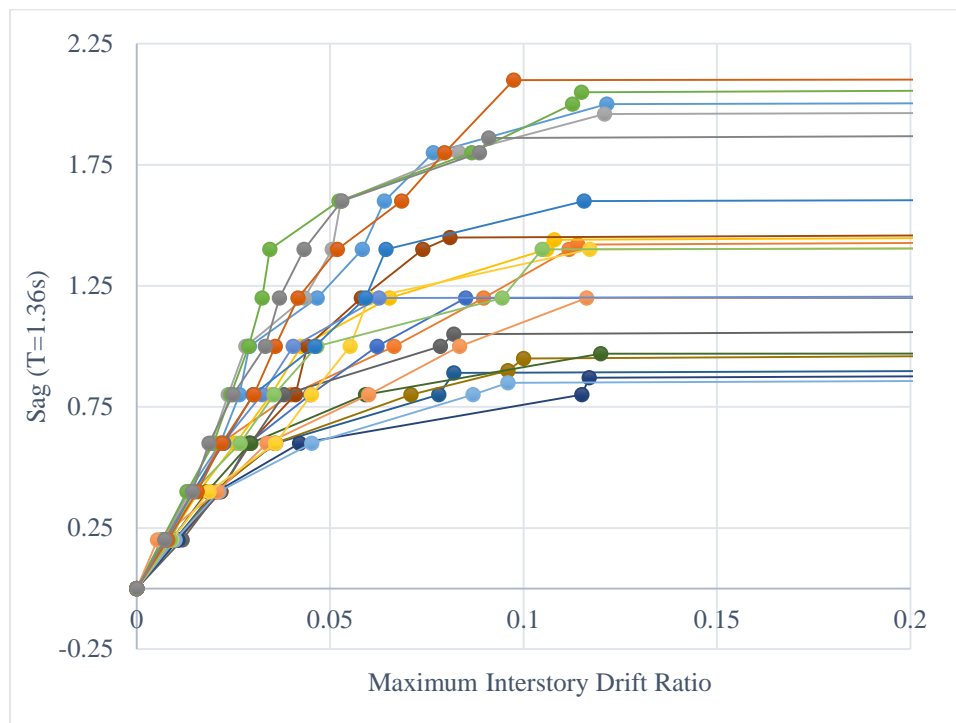


Figure 5.17: Collapse IDA for design B1 using critical ground motion components of each record

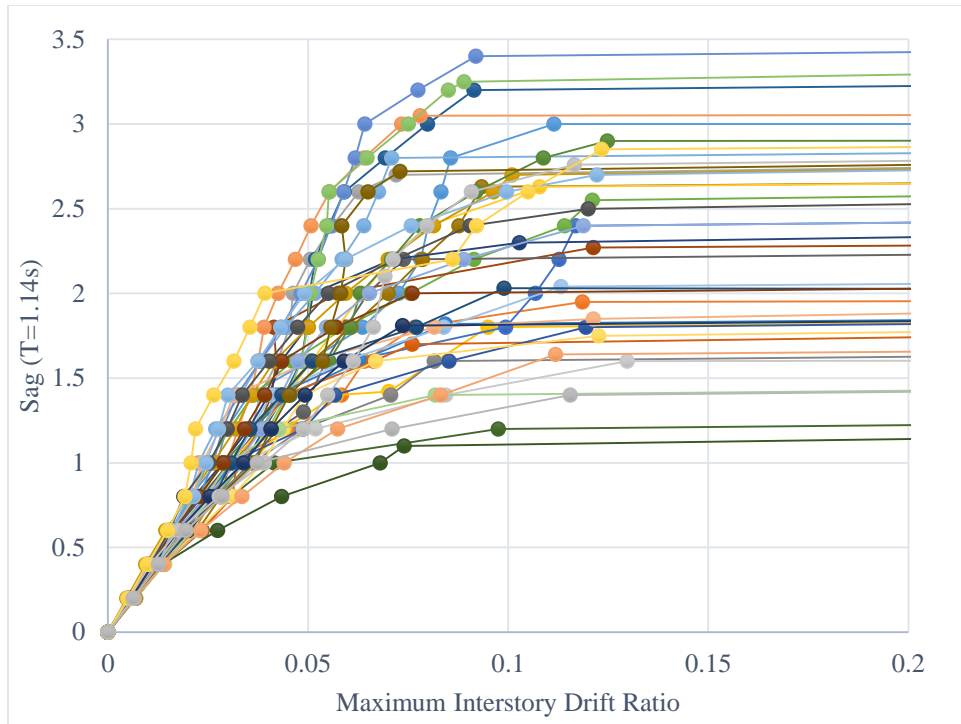


Figure 5.18: Collapse IDA for design B2 including all 40 ground motion components

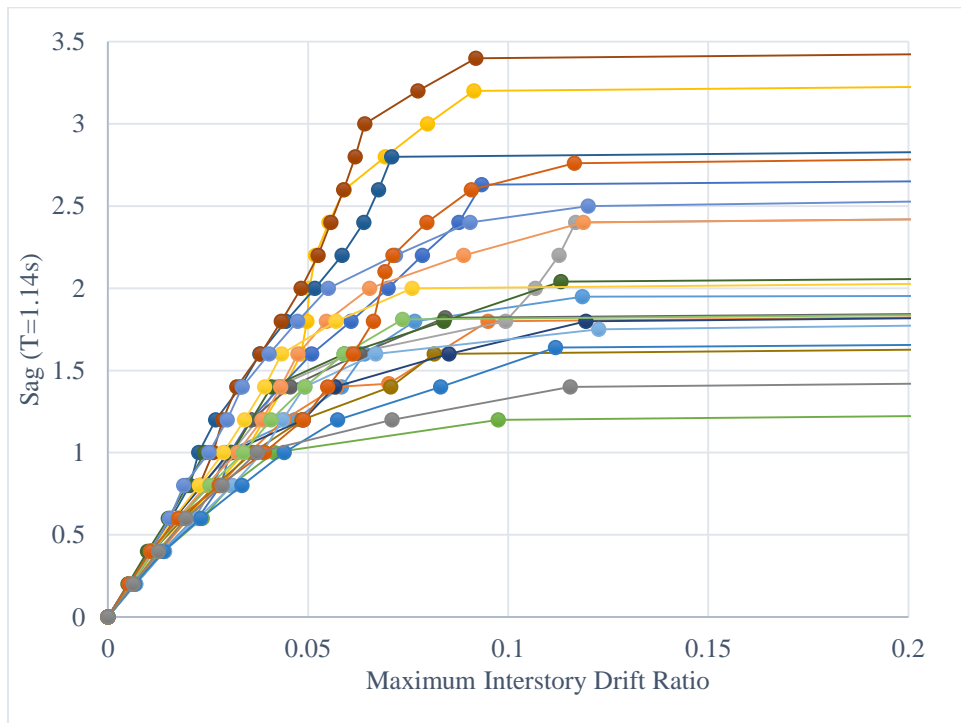


Figure 5.19: Collapse IDA for design B2 using critical ground motion components of each record

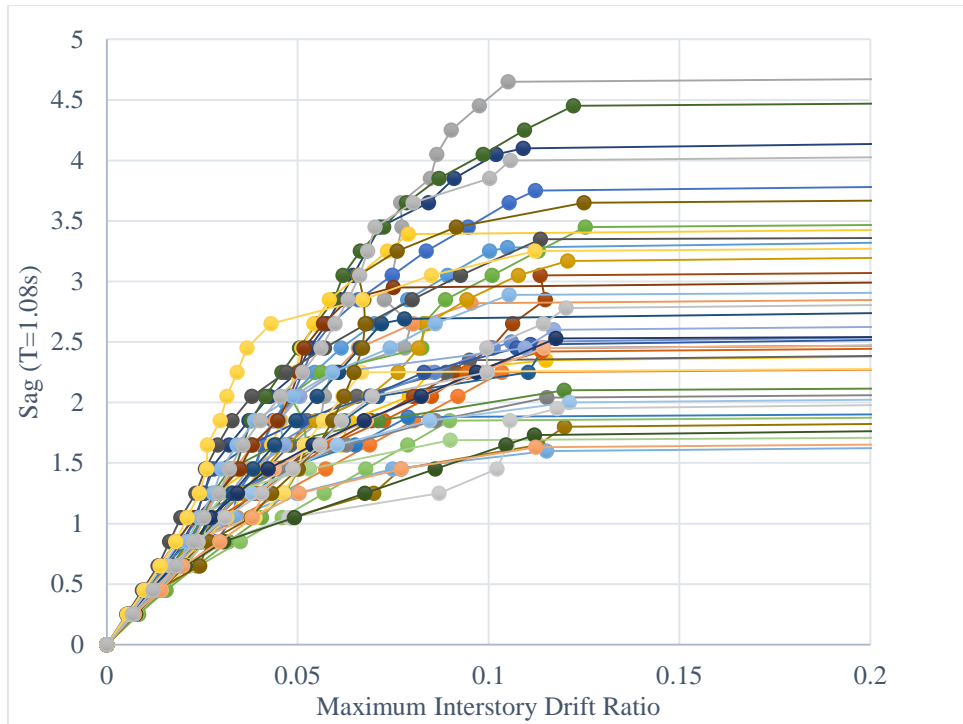


Figure 5.20: Collapse IDA for design B3 including all 40 ground motion components

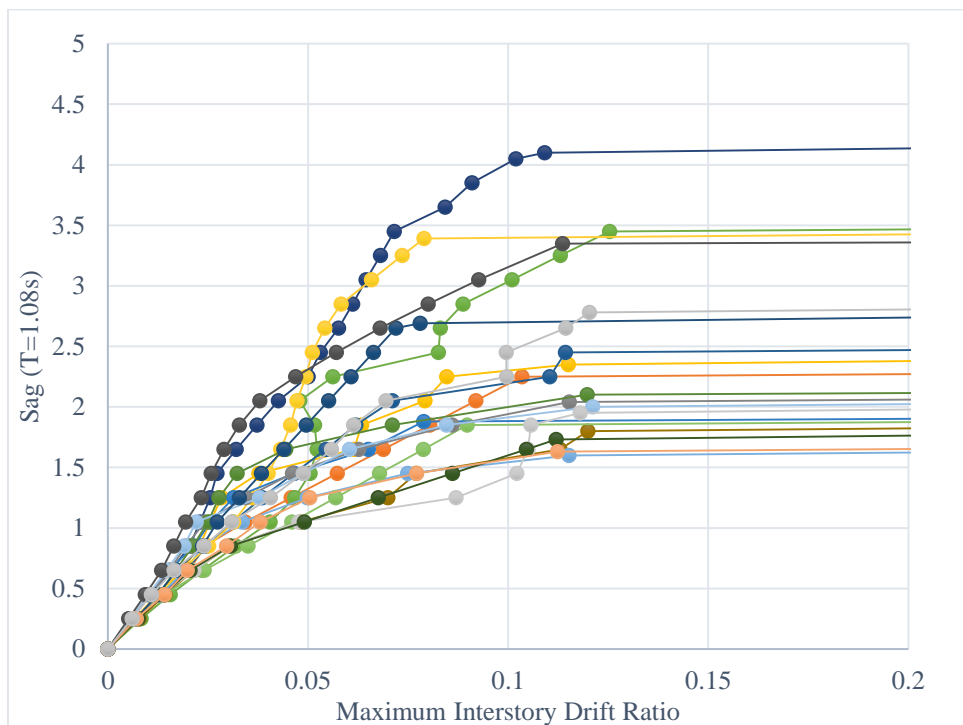


Figure 5.21: Collapse IDA for design B3 using critical ground motion components of each record

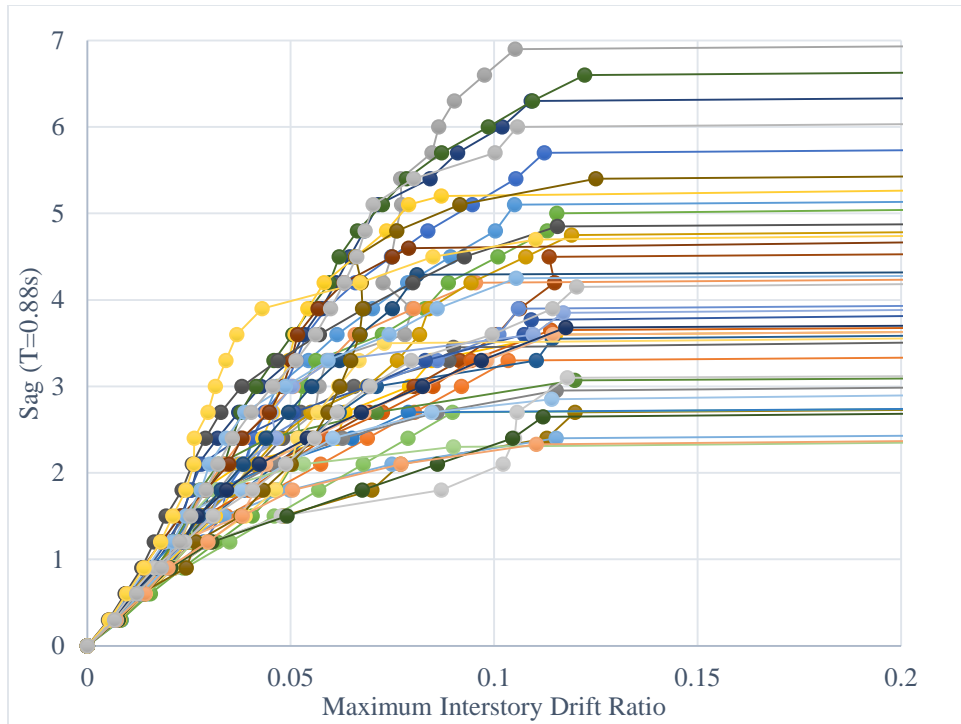


Figure 5.22: Collapse IDA for design B4 including all 40 ground motion components

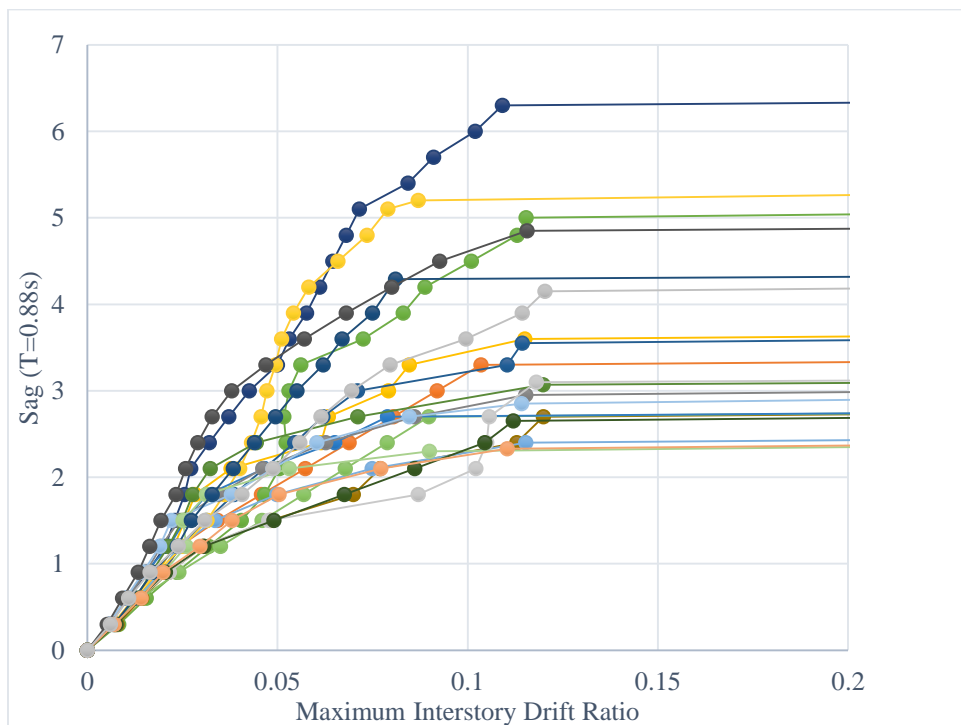


Figure 5.23: Collapse IDA for design B4 using critical ground motion components of each record

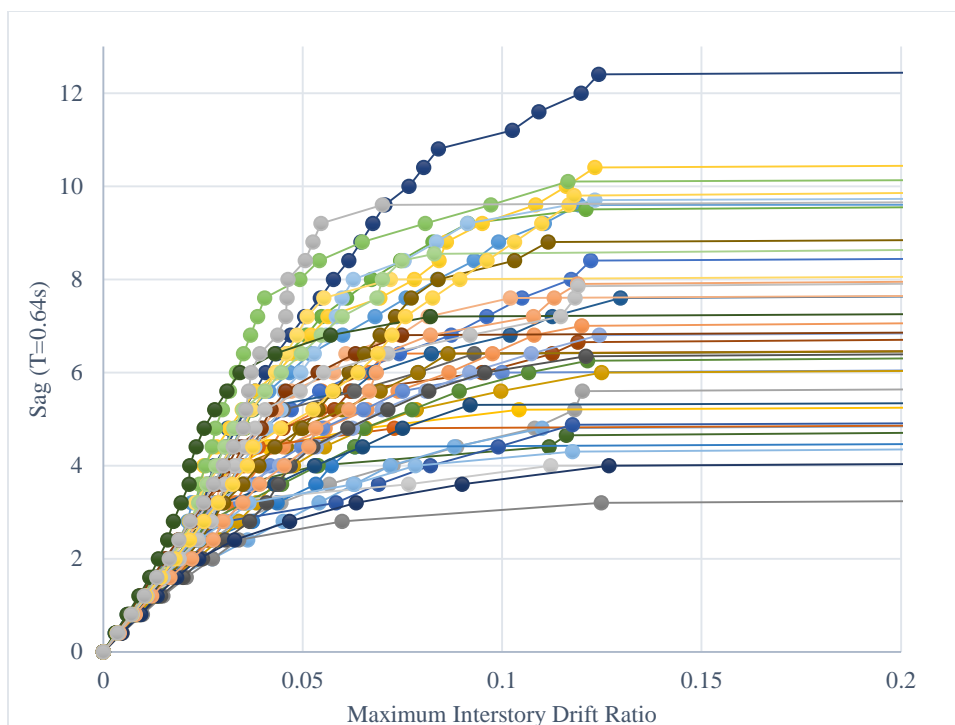


Figure 5.24: Collapse IDA for design B5 including all 40 ground motion components

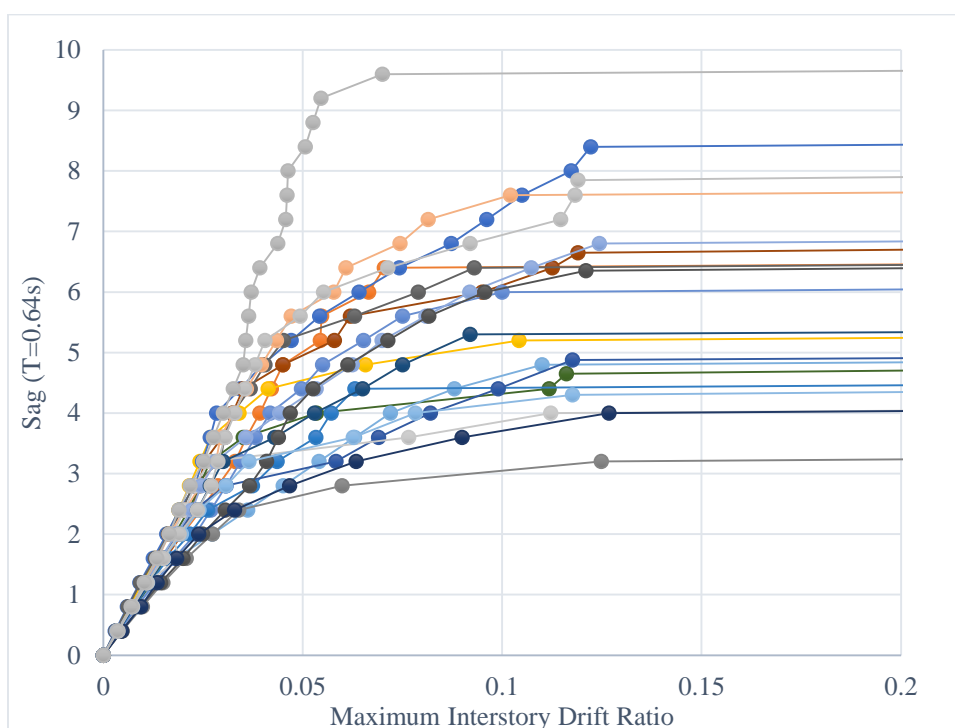


Figure 5.25: Collapse IDA for design B5 using critical ground motion components of each record

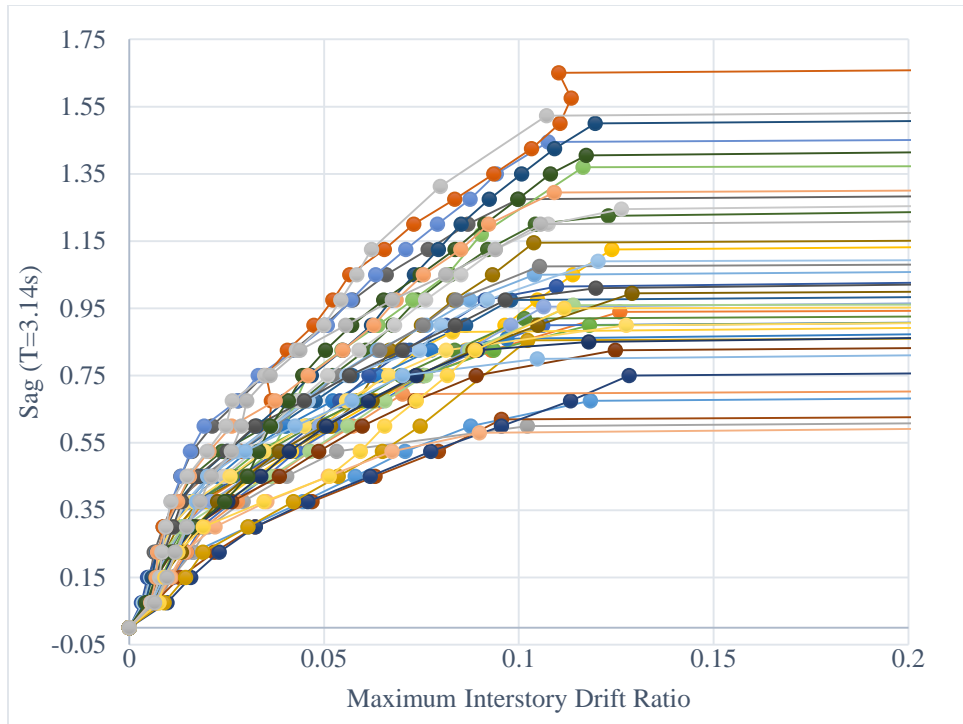


Figure 5.26: Collapse IDA for design BI including all 40 ground motion components

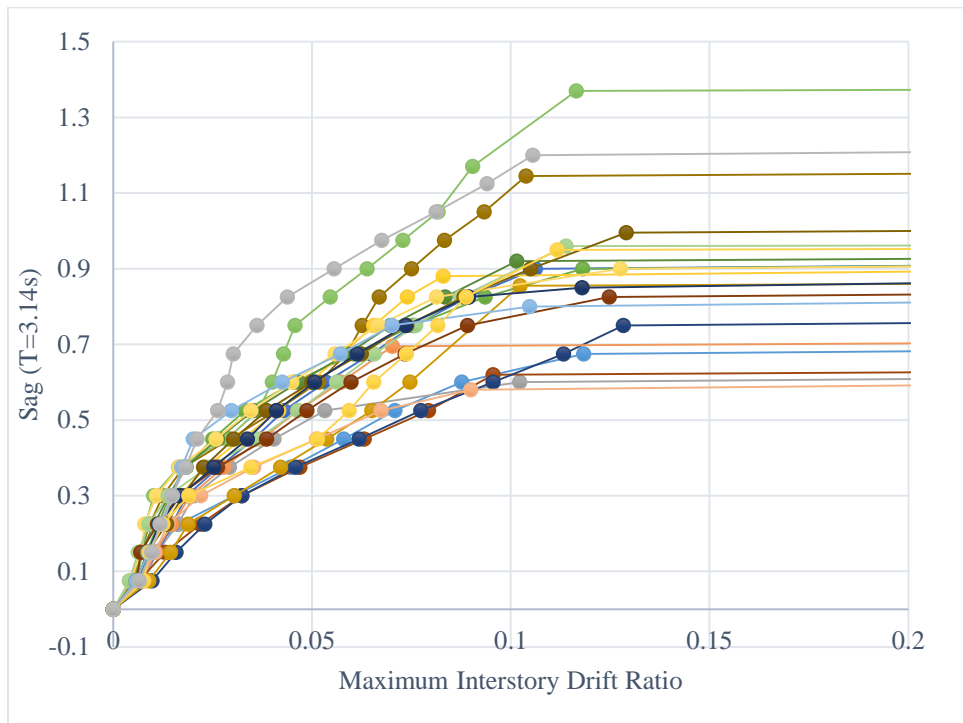


Figure 5.27: Collapse IDA for design BI using critical ground motion components of each  
record

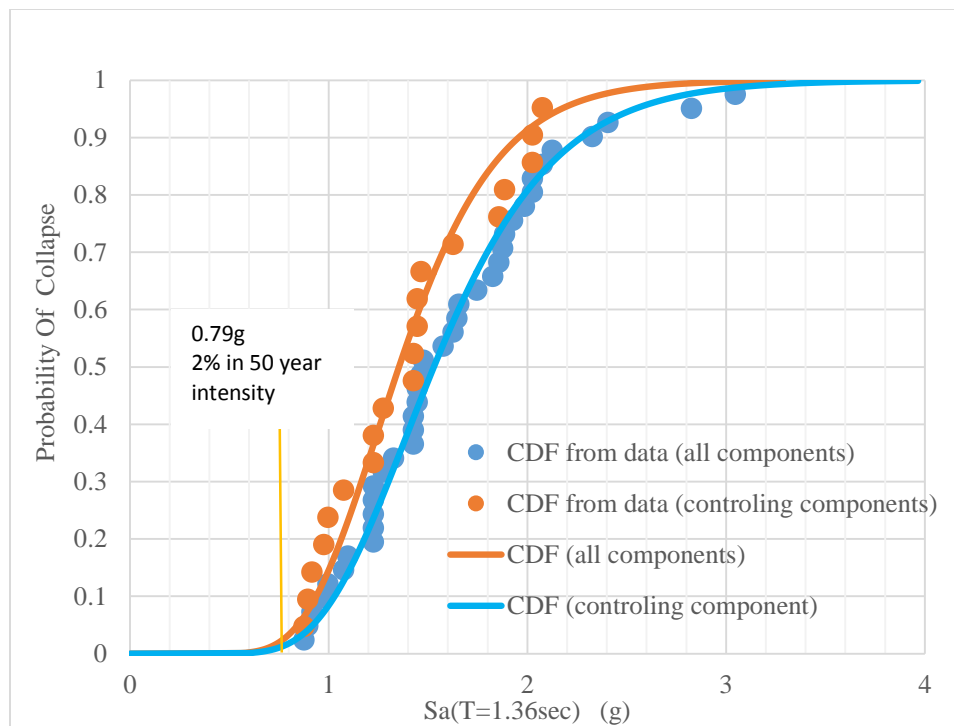


Figure 5.28: Collapse CDF for design B1

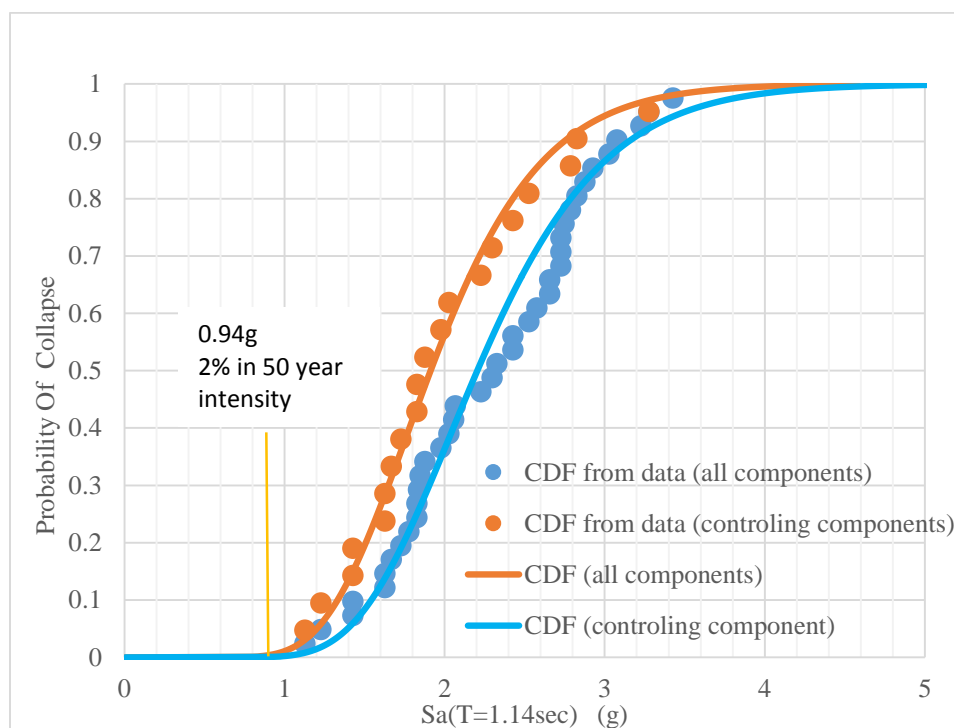


Figure 5.29: Collapse CDF for design B2

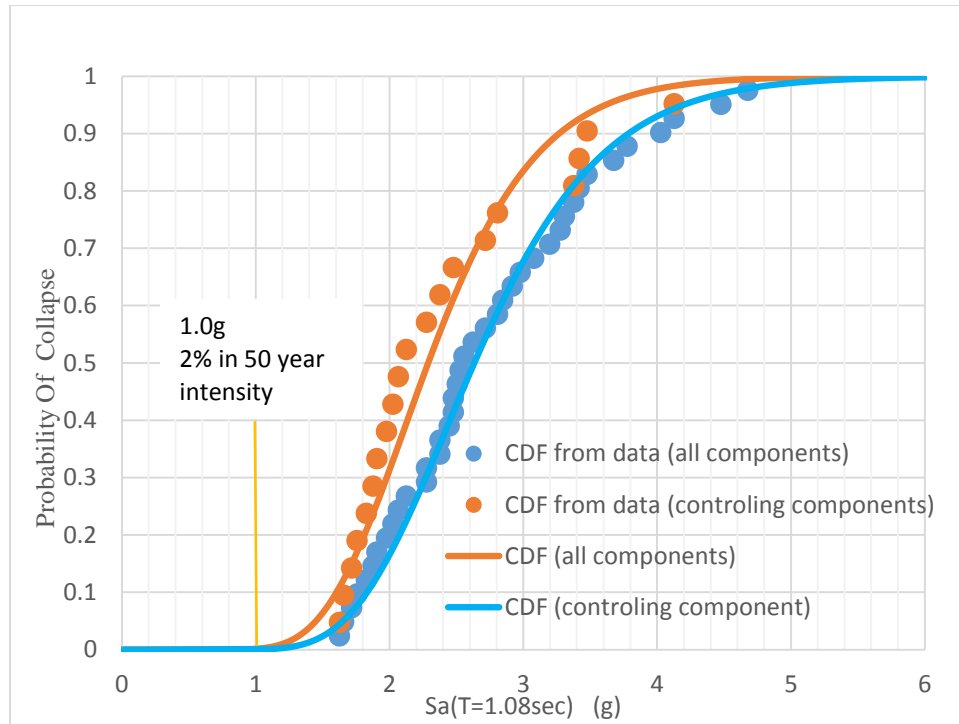


Figure 5.30: Collapse CDF for design B3

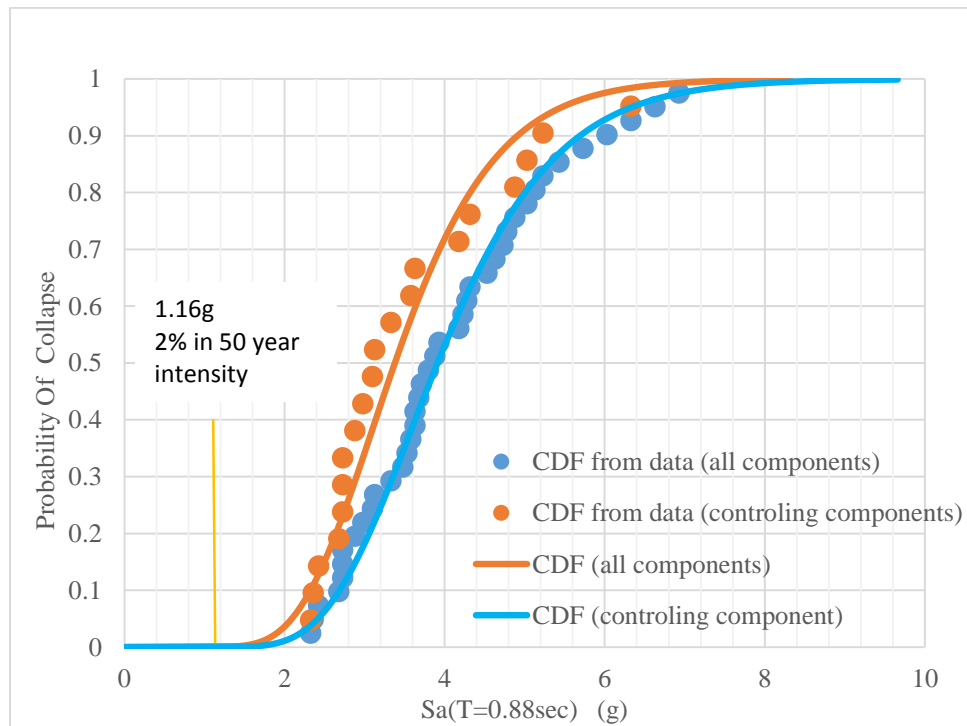


Figure 5.31: Collapse CDF for design B4

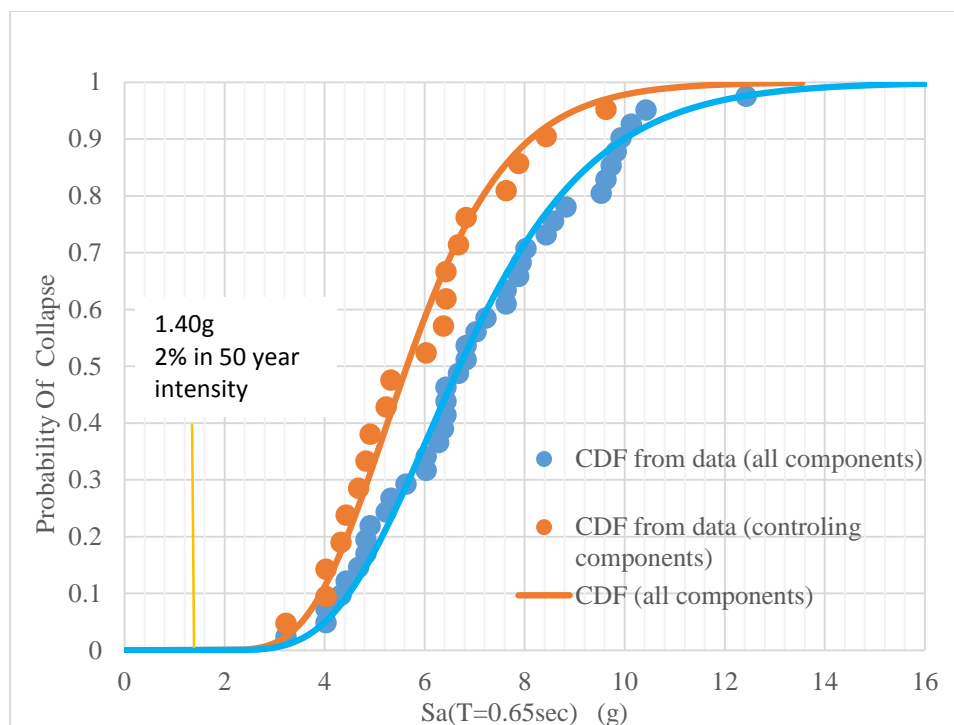


Figure 5.32: Collapse CDF for design B5

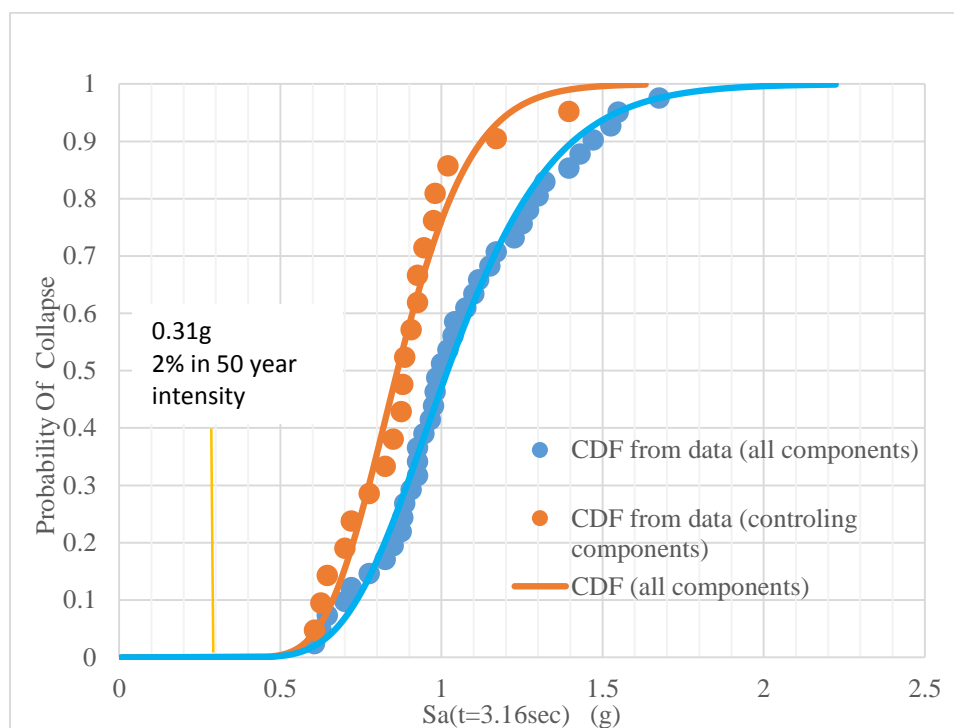


Figure 5.33: Collapse CDF for design BI

Table 5.7 gives the mean spectral acceleration  $S_a(T)$  at the verge of collapse and the dispersion for all designs including isolated model. Demand spectral acceleration for the 2% in 50 year earthquake along with the ratio of capacity to demand is also provided.

Table 5.7: Collapse capacity and 2% in 50 year demand spectral acceleration

<b>Design</b>	<b>collapse capacity</b> <b><math>S_{ac}(T)</math> [g]</b>	<b>2% in 50 year</b> <b>demand <math>S_{ad}(T)</math> [g]</b>	<b><math>S_{ac}(T)/ S_{ad}(T)</math></b>
<b>B1</b>	1.42	0.79	1.80
<b>B2</b>	1.85	0.94	1.97
<b>B3</b>	2.10	1.0	2.10
<b>B4</b>	3.11	1.16	2.68
<b>B5</b>	5.67	1.41	4.02
<b>BI</b>	0.89	0.30	2.97

B1 model has the smallest capacity to demand ratio while the B5 model has the highest ratio among all models. The ratio of capacity to demand in B1 to B5 models does not exactly follow the importance factors used for the design. For example, B5 model is supposed to be three times stronger than the B1 model while the results offers it only can be 2.25 time stronger. This inconsistency partially originates from the inherent inaccuracy in the simple nature of equivalent static analysis procedure comparing to nonlinear dynamic analysis. The design earthquake spectrum offered by ASCE7-10 and the period of vibration used for earthquake load calculations are different from those obtained by dynamic models.

### 5.5 Demand Drifts and Accelerations

Nonlinear time history analysis must be carried out for 10 suites of ground motions as explained in section 5.2. The spread plasticity model (fiber-hinge) was used for this

purpose and the median story responses including drifts and accelerations were plotted for each intensity level represented by return period in Figure 5.34 and Figure 5.45. Fixed-base design show constantly decreasing drift ratios and increasing story accelerations in higher capacity models.

Mean story drift for all models is plotted for different shaking intensities in Figure 5.46. A side by side comparison between different models in this diagram shows that model BI, offers no clear advantage over designs like B1 model for very low shaking intensities (10 and 50- year return periods) as the isolation devices remain in the elastic range for such small intensities. For higher intensities, BI model show considerably lower drift ratios with respect to B1 to B4 models. Drift ratios are comparable between BI and B5 models with slightly lower drifts recorded for B5 model for high intensity shakings.

Mean story accelerations is also plotted for different shaking intensities in Figure 5.47. As opposed to drift results, recorded accelerations for high capacity fixed-base models are considerably greater than the other models. These models although provide a higher capacity and safety against collapse with the low drift ratios, they are not able to keep the accelerations low when it comes to acceleration.

At very low shaking intensities (10-year and 50-year return period earthquakes), recorded acceleration for BI model is close to those of fixed-base models as the isolation system performs in the elastic range. For higher intensities, recorded accelerations are substantially small relative to B1 to B5 models. In contrary, the ability to reduce both demand parameters, drift and accelerations, gives the isolation system an edge.

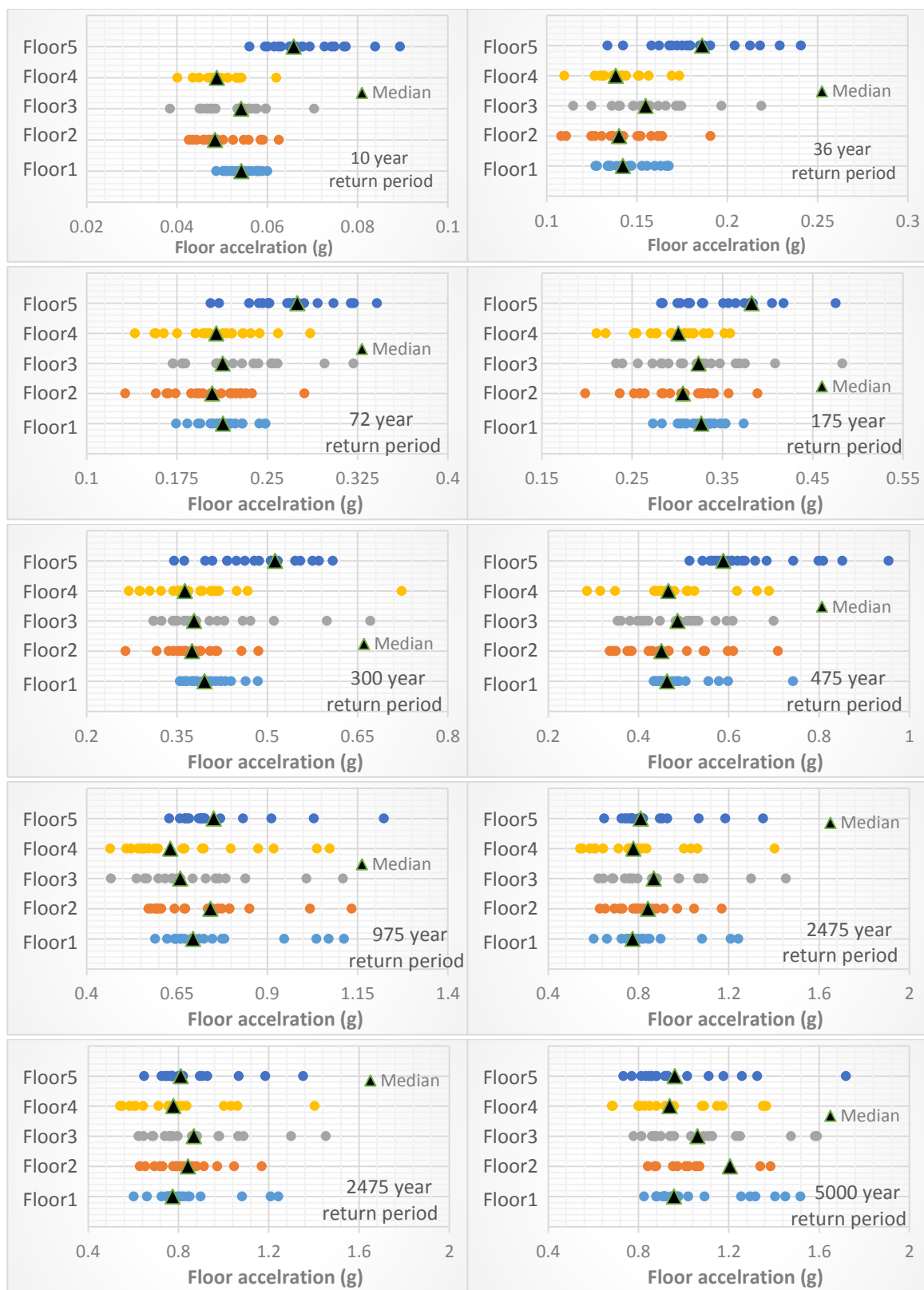


Figure 5.34: Scatter of record by record peak floor acceleration and the medians for

design B1

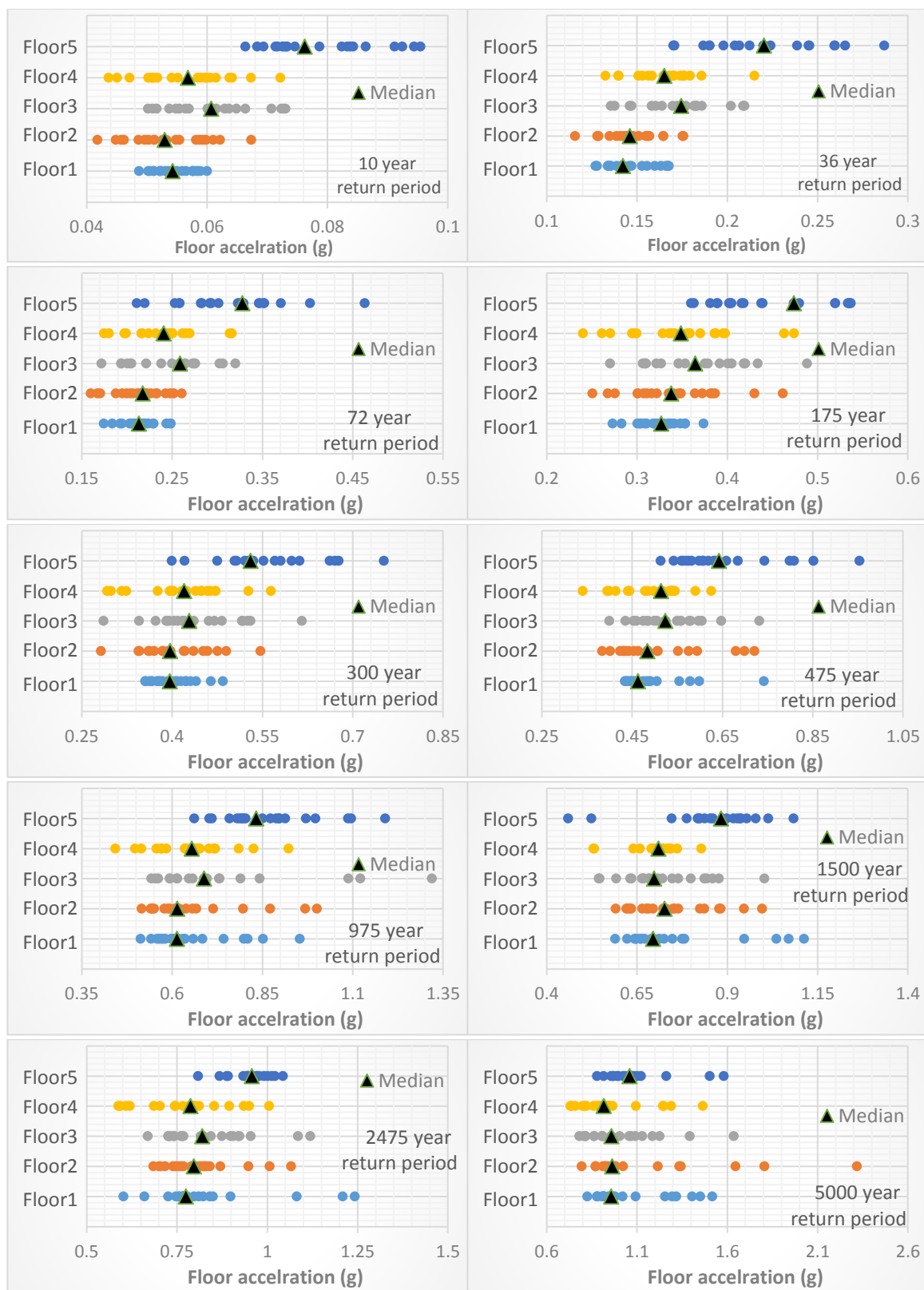


Figure 5.35: Scatter of record by record peak floor acceleration and the medians for

design B2

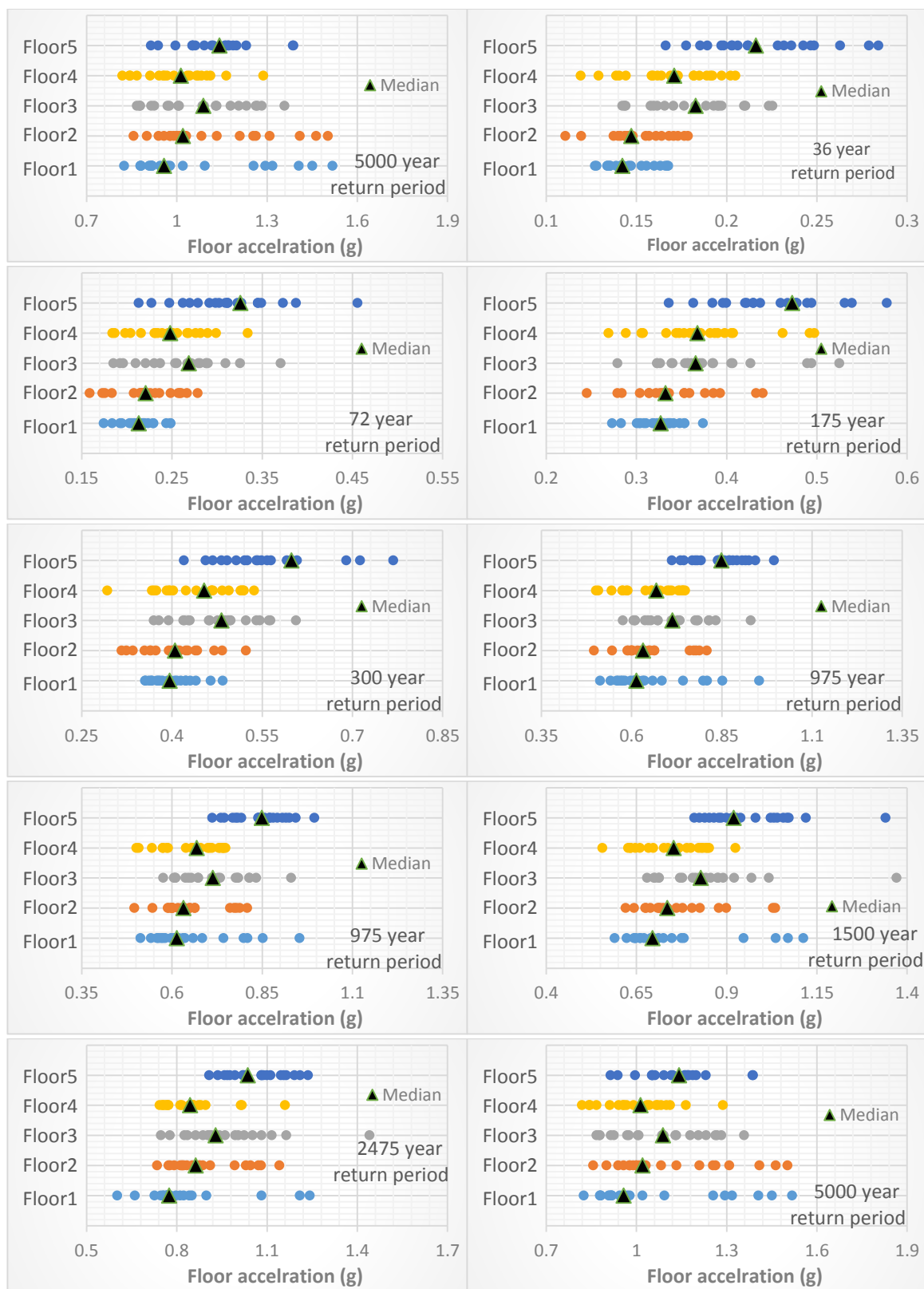


Figure 5.36: Scatter of record by record peak floor acceleration and the medians for

design B3

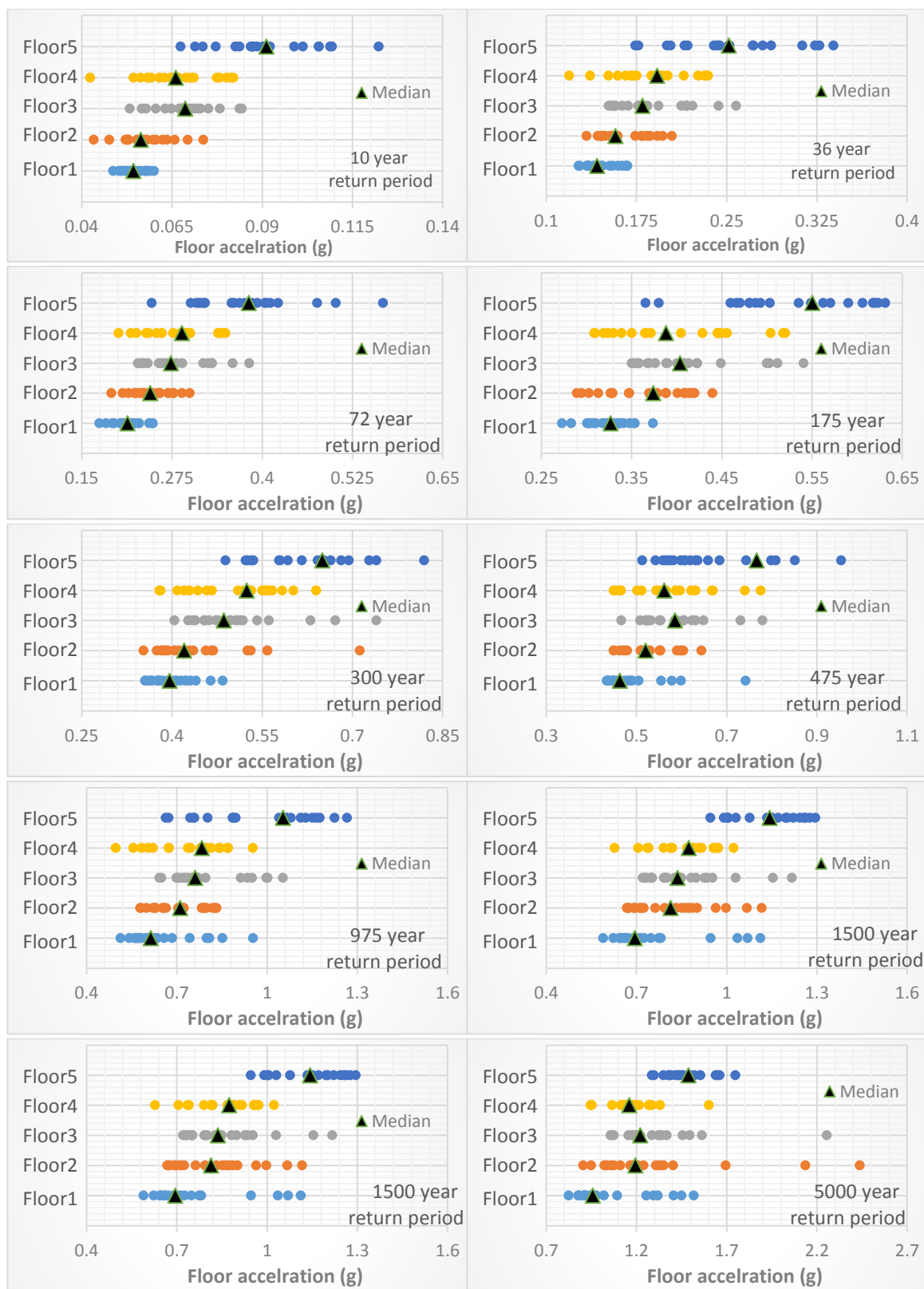


Figure 5.37: Scatter of record by record peak floor acceleration and the medians for

design B4



Figure 5.38: Scatter of record by record peak floor acceleration and the medians for

design B5

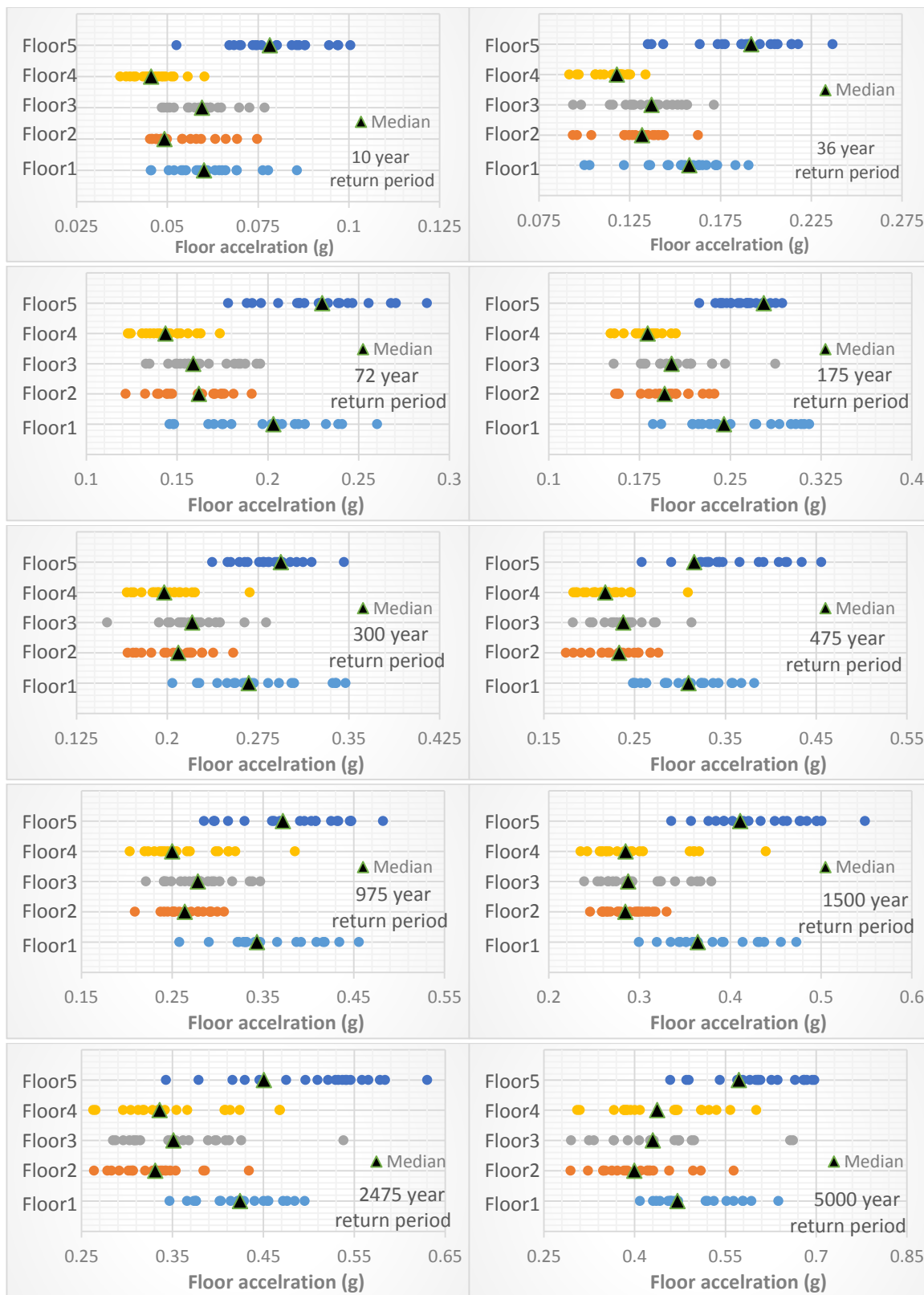


Figure 5.39: Scatter of record by record peak floor acceleration and the medians for

design BI

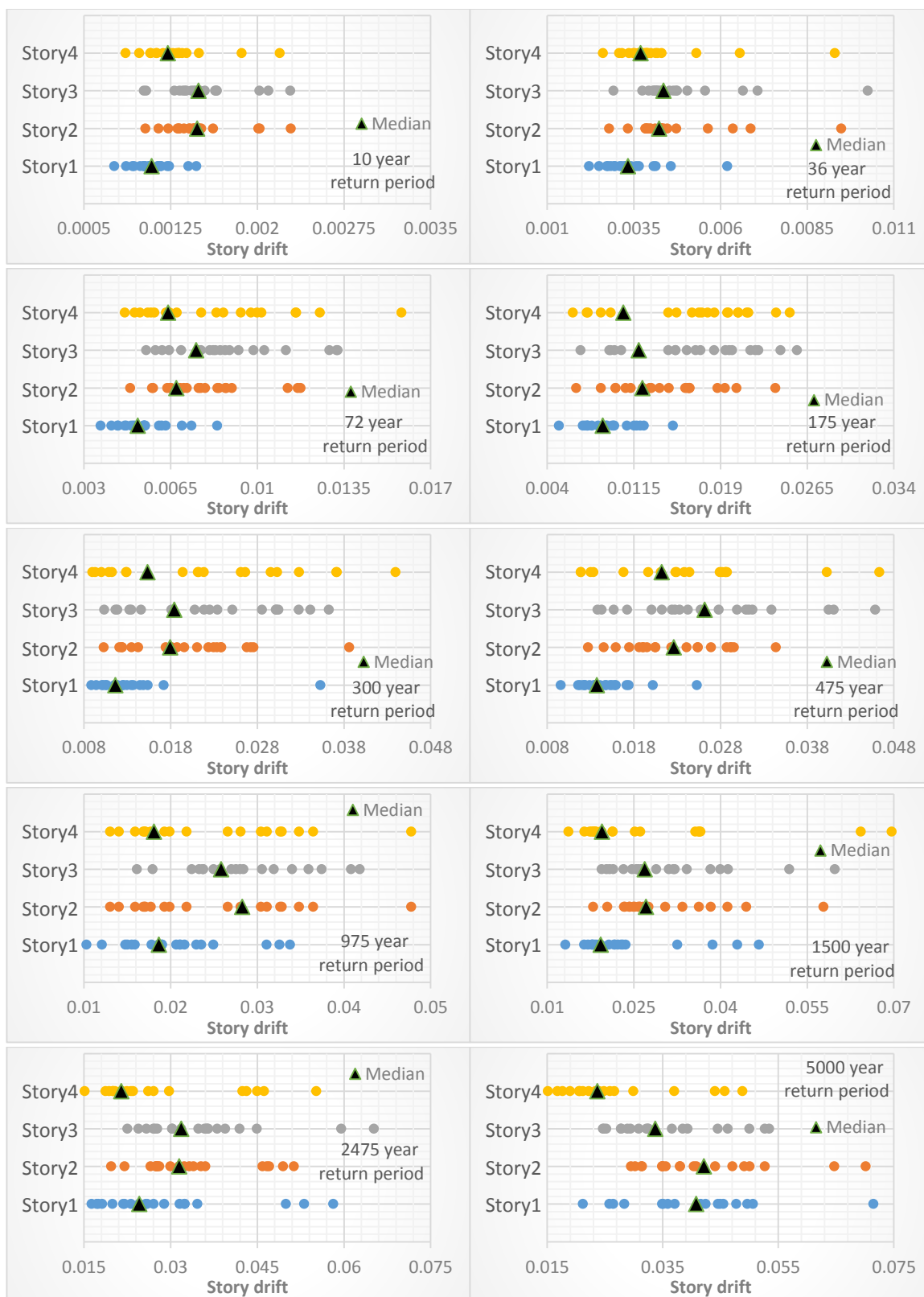


Figure 5.40: Scatter of record by record peak story drift and the medians for design B1

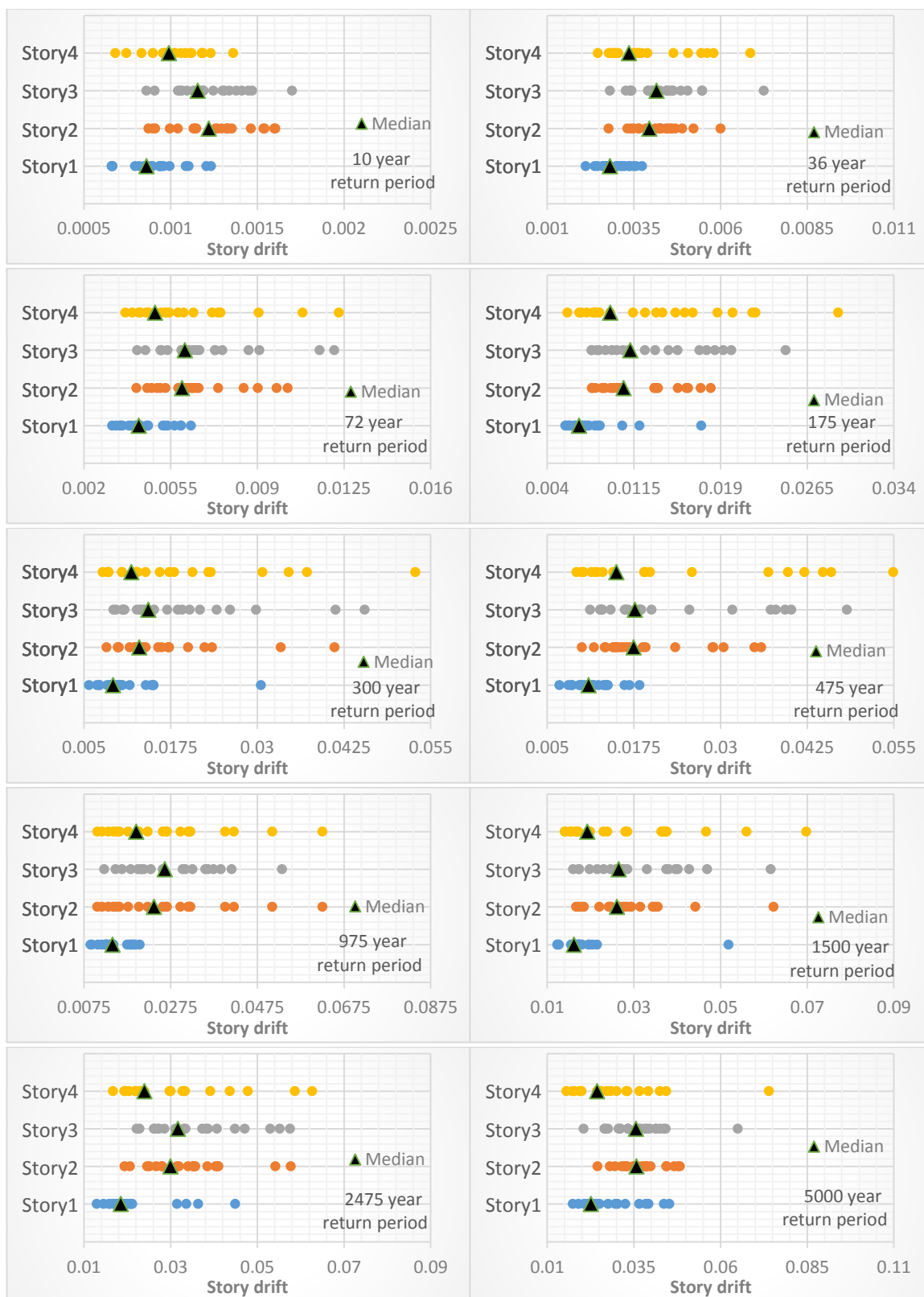


Figure 5.41: Scatter of record by record peak story drift and the medians for design B2

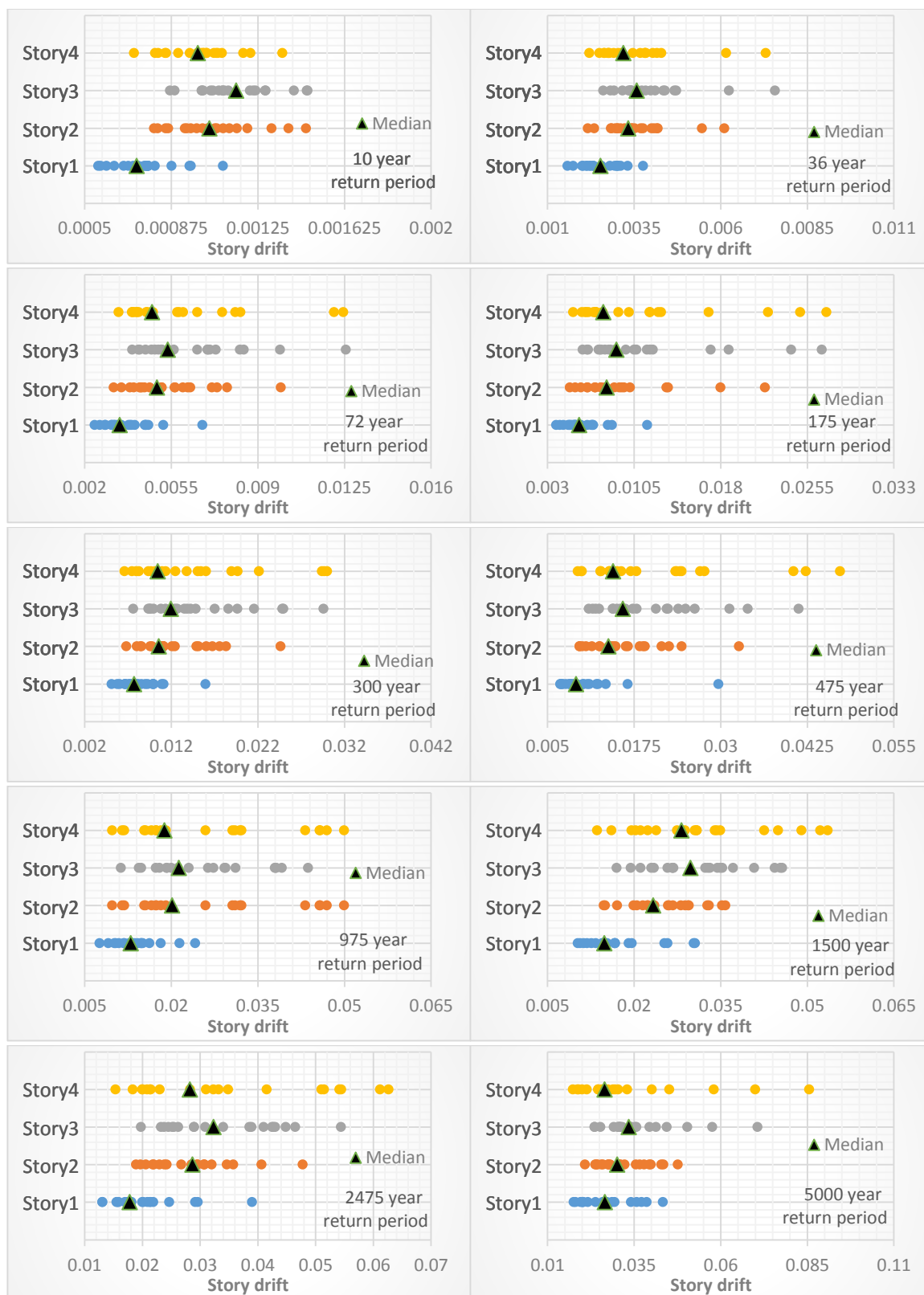


Figure 5.42: Scatter of record by record peak floor acceleration and the medians for design B3

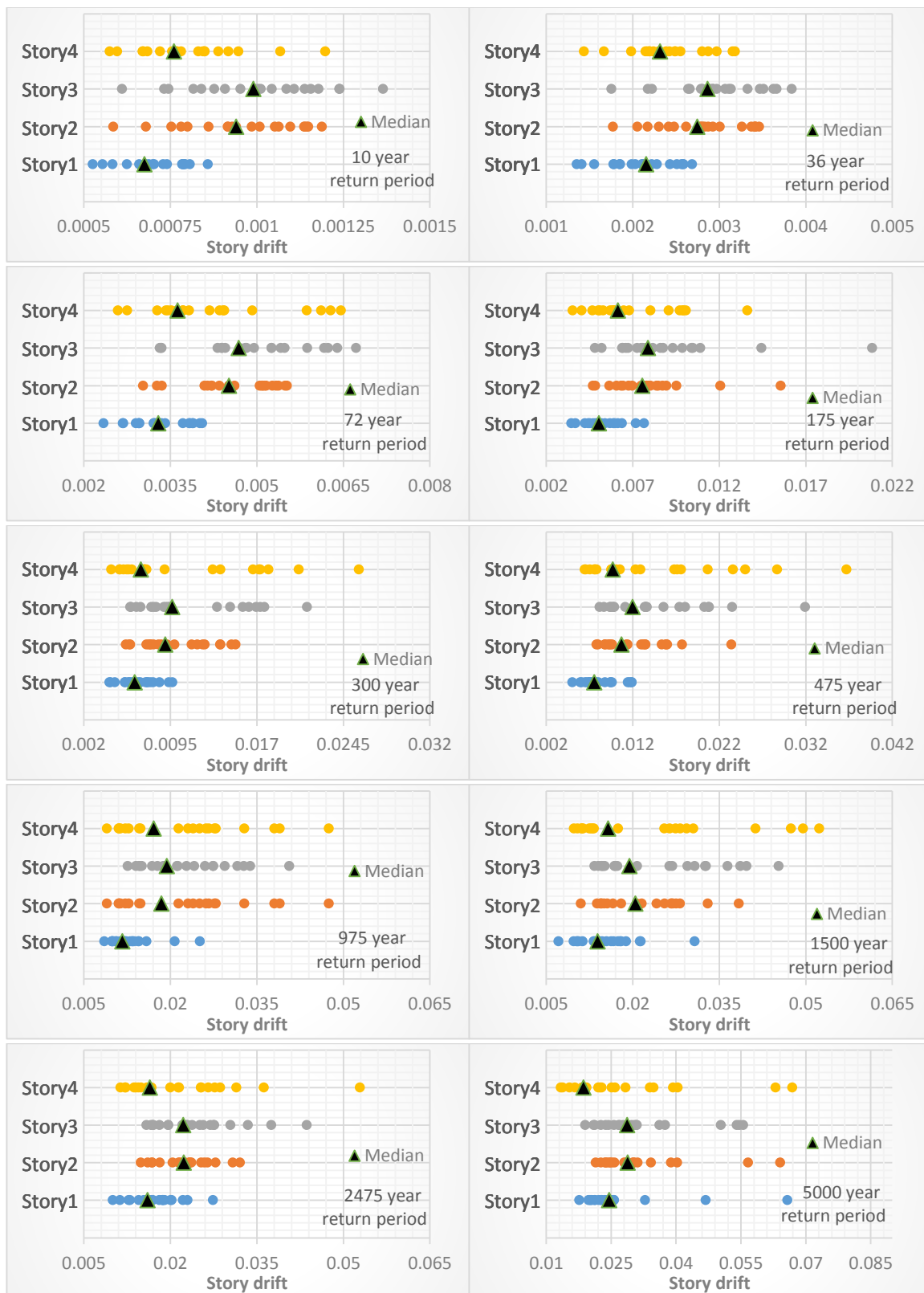


Figure 5.43: Scatter of record by record peak floor acceleration and the medians for design B4

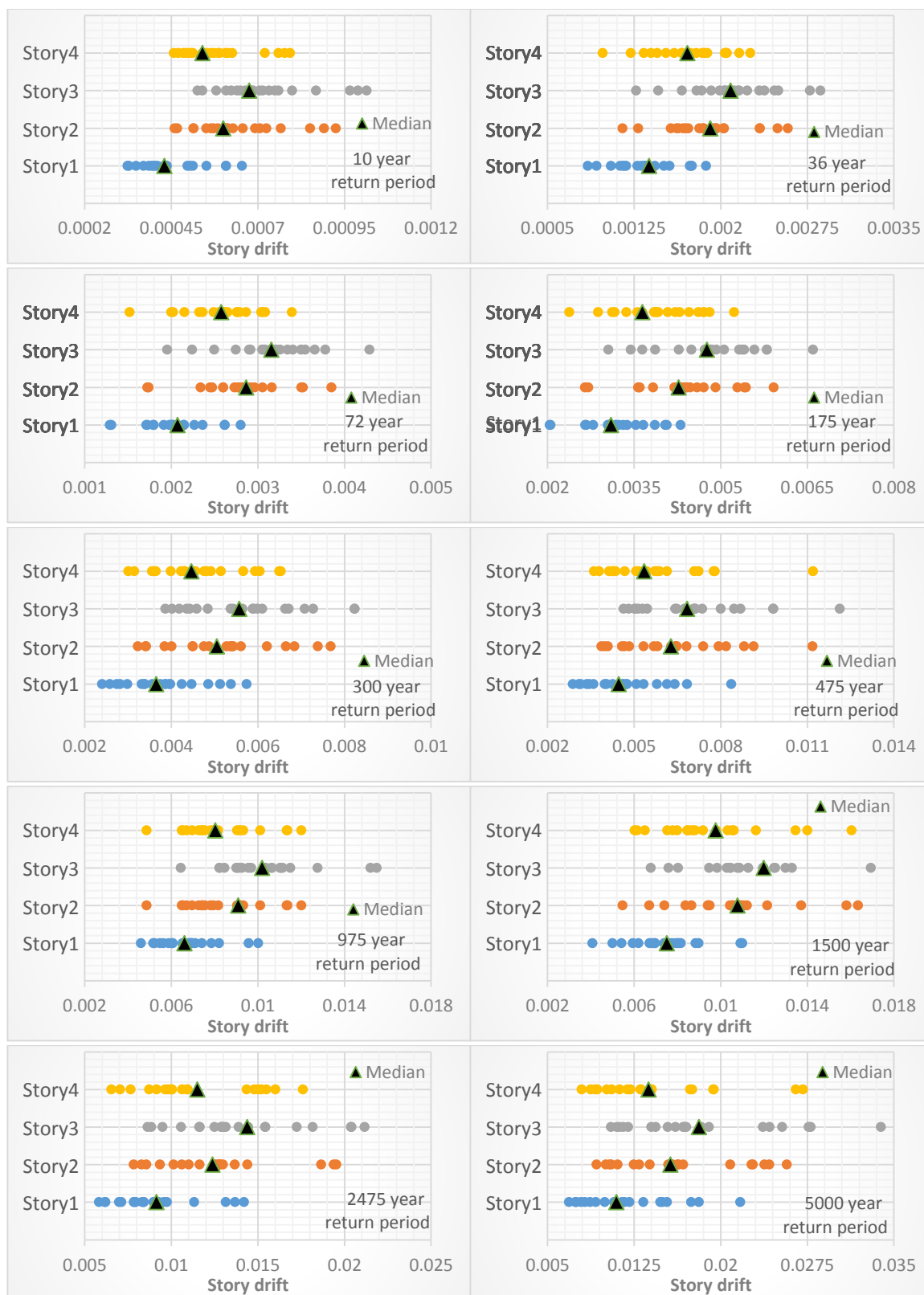


Figure 5.44: Scatter of record by record peak floor acceleration and the medians for

design B5

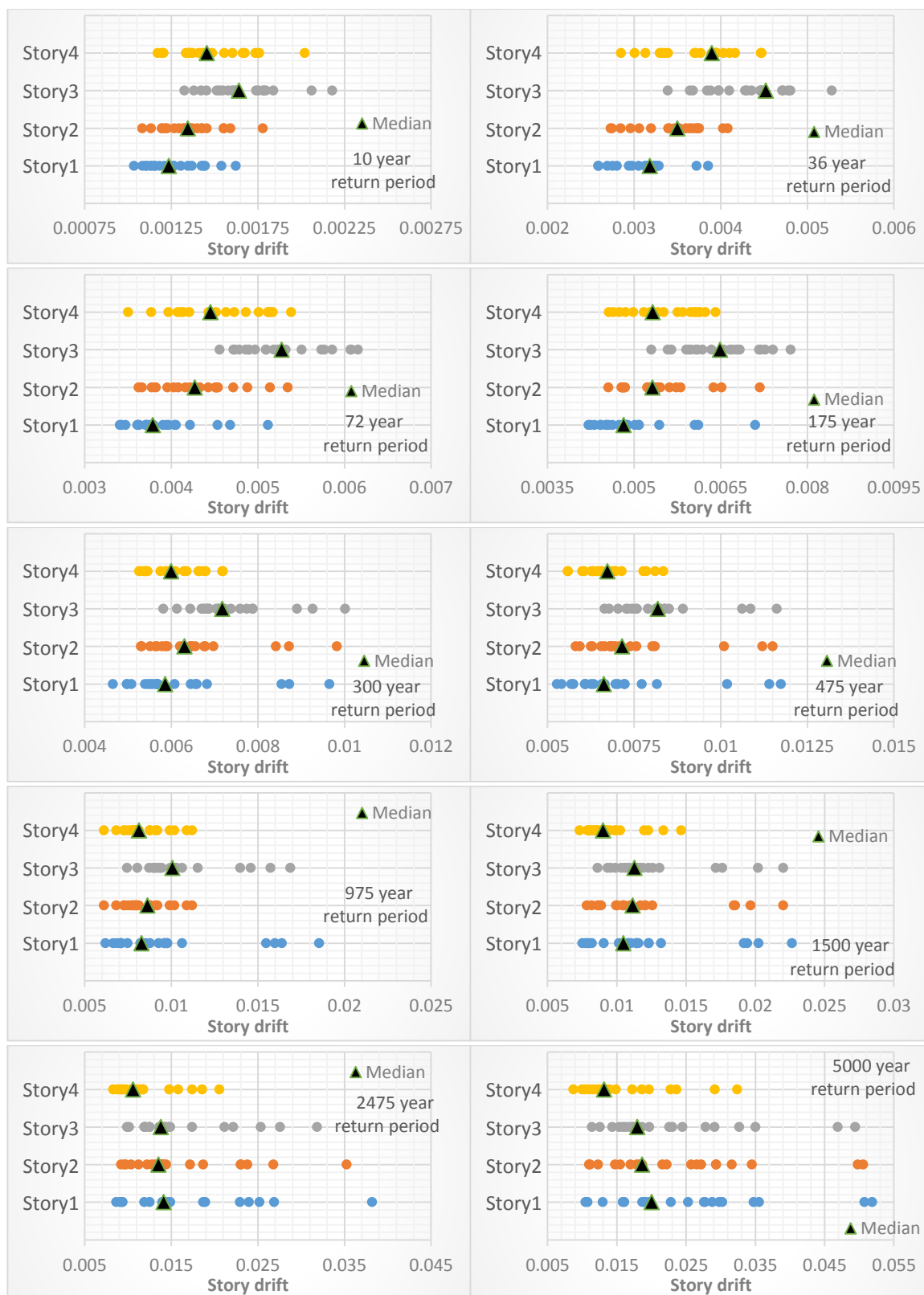


Figure 5.45: Scatter of record by record peak floor acceleration and the medians for

design BI

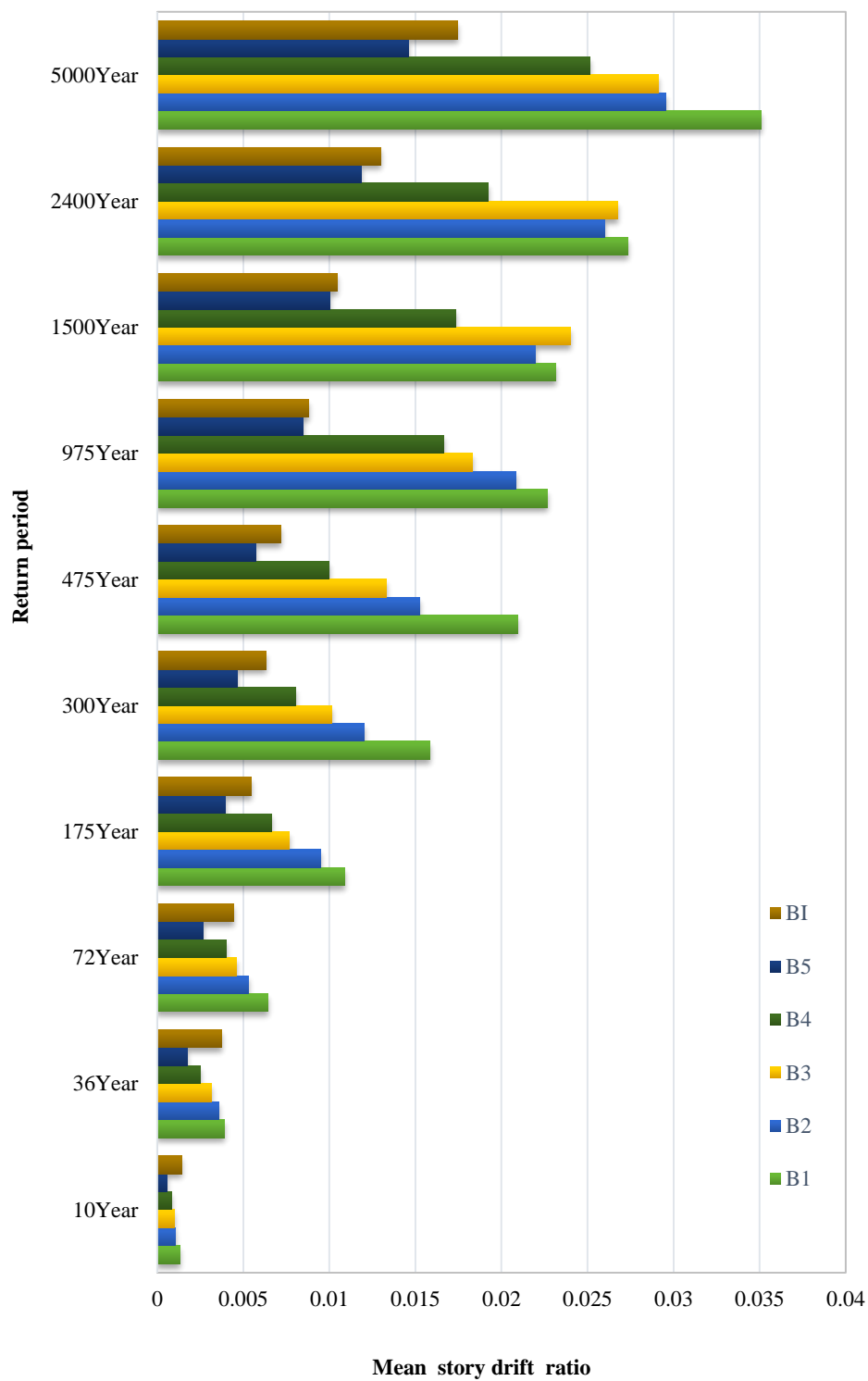


Figure 5.46: Mean story drift ratio of all designs

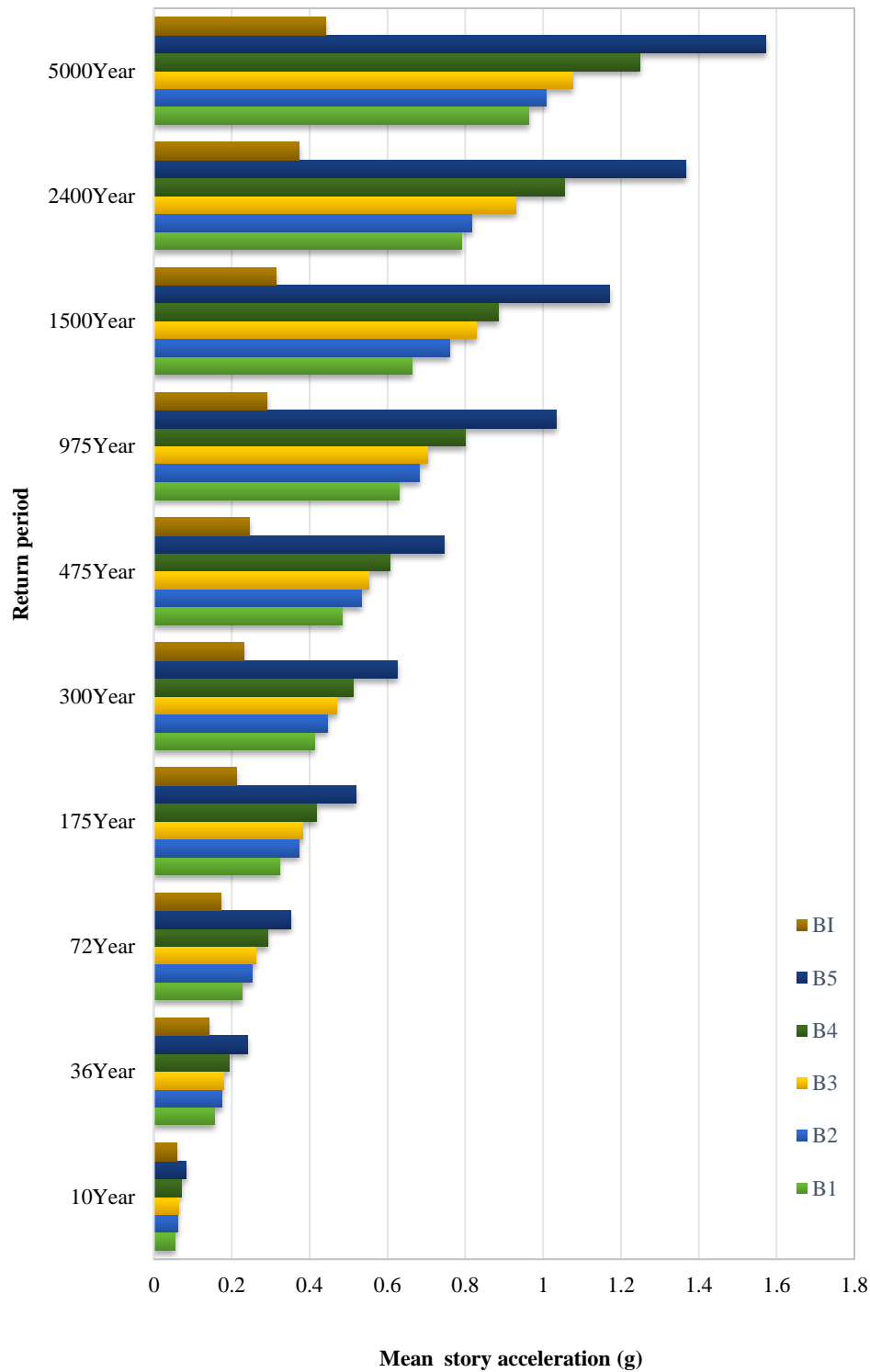


Figure 5.47: Mean story acceleration of all designs

## Chapter 6 : Performance Assessment

### 6.1 Quality Assurance and Uncertainty Assumptions

Uncertainties involved in the performance assessment procedure considerably affect the building performance. The uncertainties comes from the fact that the assumed values for each factor effective in the performance assessment procedure might be different from those initially presumed. Uncertainty in each parameter consists of the distribution function type and the corresponding mean and dispersion. A large dispersion value for a parameter reflects a higher uncertainty while a small dispersion shows a lower uncertainty and better prediction accuracy for that parameter.

Material property is uncertain as the actual and nominal strength are different. While graded steel material possess the lowest dispersion among the common structural material, wood has the highest dispersion. Construction quality is another source of uncertainty. Depending on the level of construction quality control, a dispersion value  $\beta_c$  of 0.1, 0.25, and 0.4 is suggested by ATC-58 (2012) for superior, average, and limited quality assurance, respectively. This dispersion includes both the effect of material and construction quality. The benchmark building is assumed to have an average construction quality assurance, so that a quality assurance dispersion of 0.25 is assumed.

Analytical tools and simplified methods for demand calculations are another source of uncertainty. The completeness and accuracy of mathematical models including stiffness, strength, hysteretic and deterioration models used to model the building components is called the analytical model uncertainty  $\beta_q$  (Quality and completeness of the analytical model).  $\beta_q$  values of 0.1, 0.25, and 0.4 is also suggested for superior,

average, and low quality similar to construction quality assurance dispersions. The definition of average quality of the analytical model is deemed a better match for the numerical modeling quality used in this study, thus a dispersion value of 0.25 is used.

A combination of both construction and analytical model quality is called Modeling Uncertainty  $\beta_m$  and is calculated as follows:

$$\beta_m = \sqrt{\beta_c + \beta_q} = \sqrt{0.25^2 + 0.25^2} = 0.35 \quad (6-1)$$

Each earthquake record used in performance assessment produces a different demand often peak acceleration or deformation. This uncertainty is named Record-to-Record variability which considers the response variability. Due to relatively large number of records used for the performance assessment in this study, the inherent variability in the response is deemed to sufficiently represent the dispersion.

## 6.2 Residual Drift

Residual drift ratio in each orthogonal direction of the building along with the peak story drift, peak floor velocity and acceleration are the demands typically used in the performance assessment. Residual drift ratio is directly related to the reparability of the building after the earthquake. Large residual drift ratios can cause an irreparable flag and consequently total loss. Current nonlinear time history analysis procedure provides an inaccurate estimate of the residual drift ratio which is sensitive to model assumptions including component hysteresis response and slopes for hardening and softening behavior. Thus, the residual drift ratio at each story level must be calculated based on the maximum drift ratio obtained for each nonlinear time history analysis. The following equation is suggested in ATC-58:

$$\begin{aligned}
 \Delta_r &= 0 & \Delta < \Delta_y \\
 \Delta_r &= 0.3(\Delta - \Delta_y) & \Delta_y < \Delta < 4\Delta_y \\
 \Delta_r &= (\Delta - 3\Delta_y) & \Delta > 4\Delta_y
 \end{aligned}
 \tag{6-2}$$

Where  $\Delta$  is the median story drift ratio and  $\Delta_y$  is the yield drift ratio at the point where significant yielding has initiated in the story. For the moment resisting frame used for this study, the yield story drift ratio is estimated at the point where beams and columns have reached their yield moment capacity. Yield drift calculations is estimated using pushover analysis with an equivalent lateral force. The lateral load pattern was assumed similar to first mode shape of the structure. Figures 6-1 to 6-6 give the first story shear force versus story drift ratio for all models. The yield story drift ratio ranges between 1.28% to 1.54% with the stiffer models (B4 and B5) in the lower bound of the range.

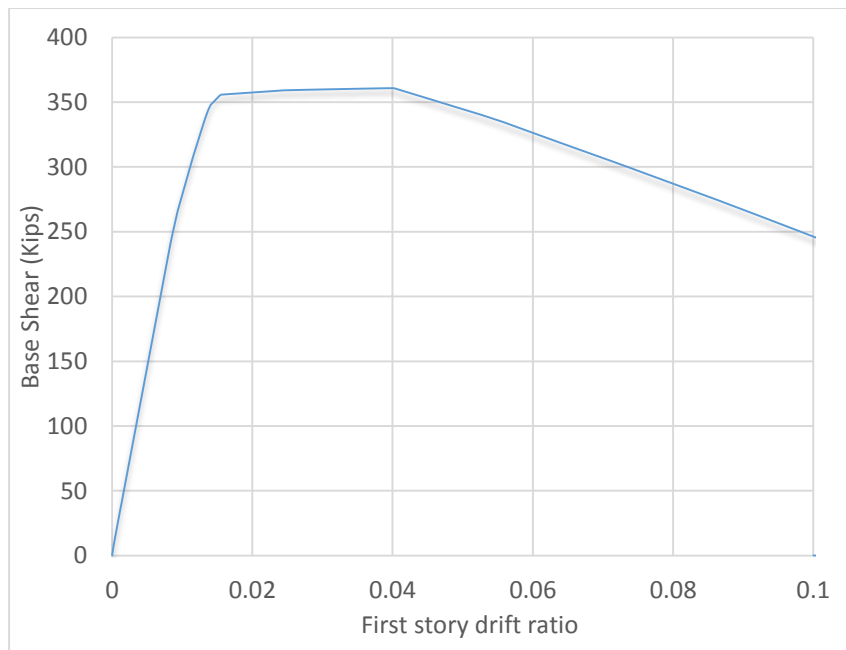


Figure 6.1: First story shear force-drift ratio diagram for B1 model

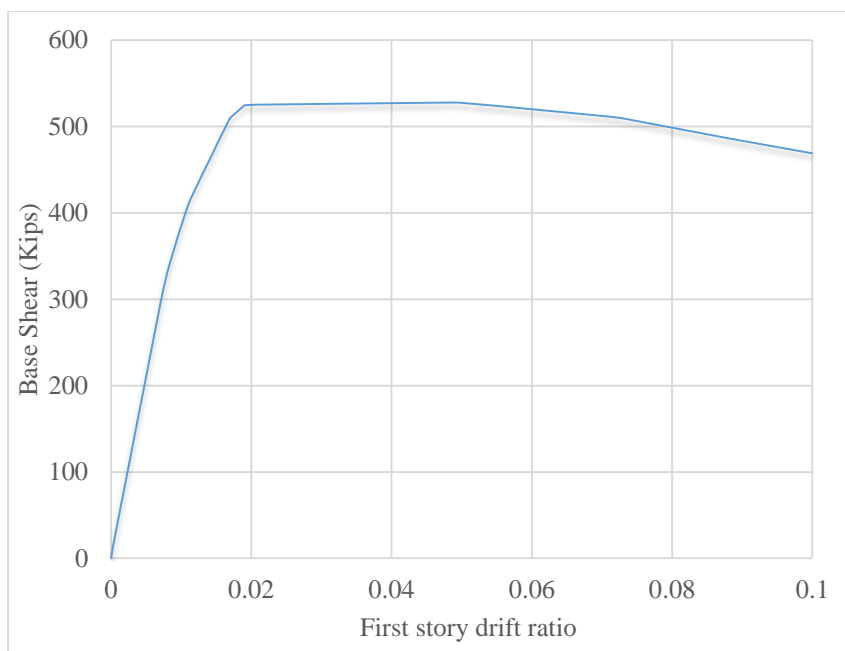


Figure 6.2: First story shear force-drift ratio diagram for B2 model

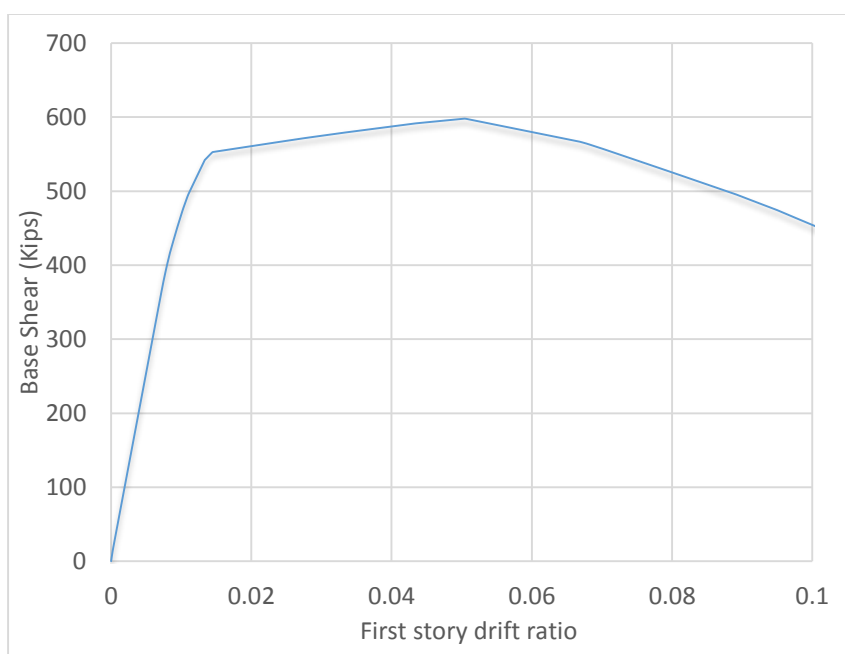


Figure 6.3: First story shear force-drift ratio diagram for B3 model

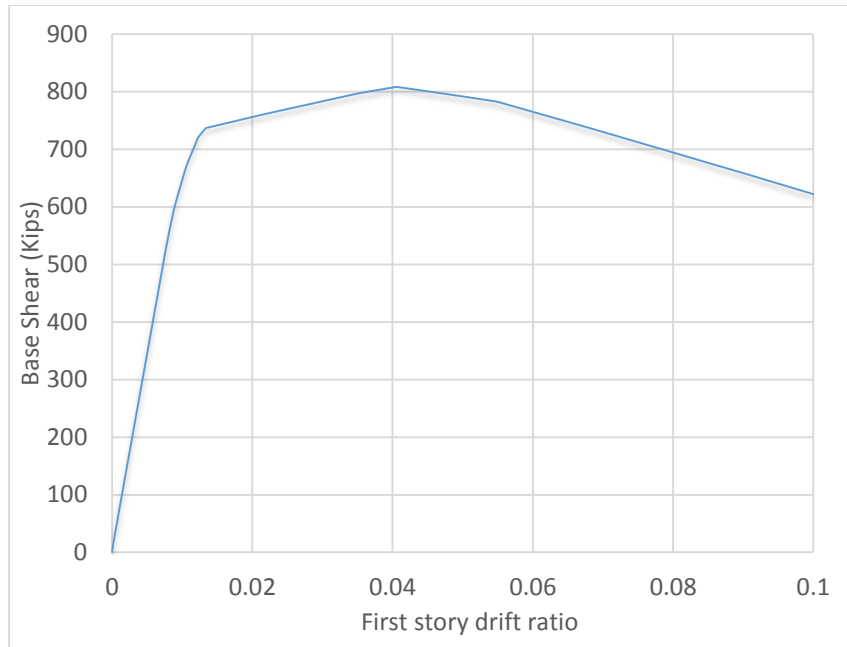


Figure 6.4: First story shear force-drift ratio diagram for B4 model

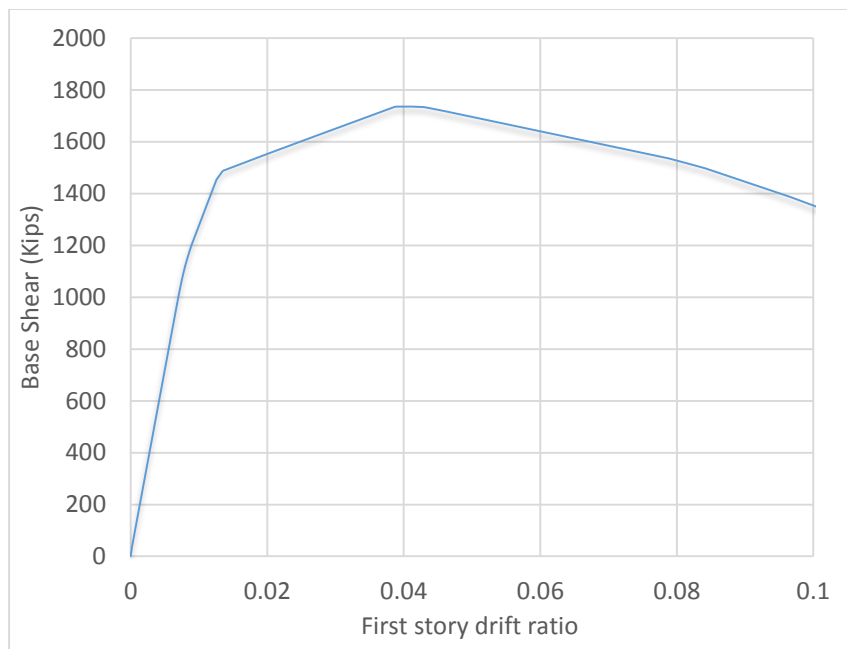


Figure 6.5: First story shear force-drift ratio diagram for B5 model

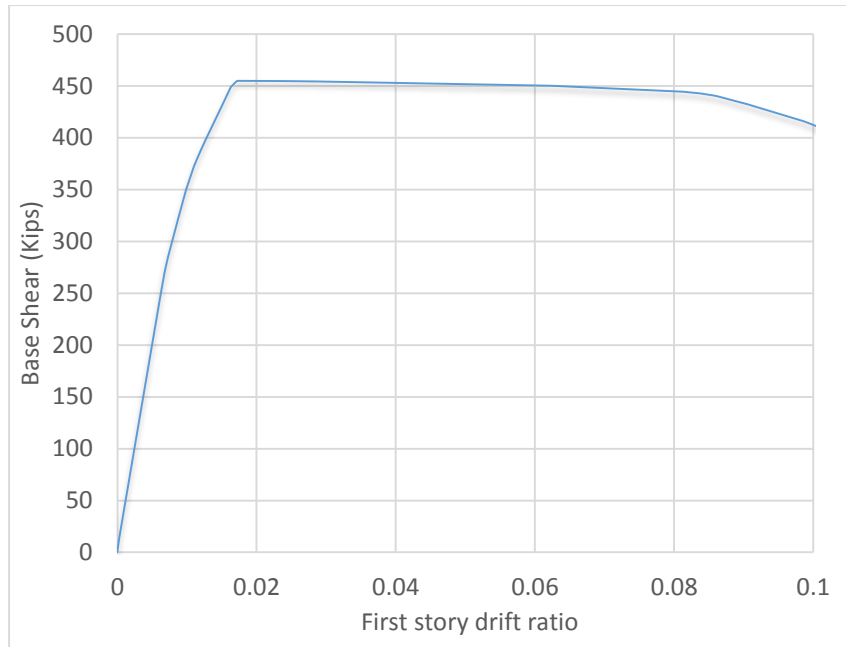


Figure 6.6: First story shear force-drift ratio diagram for BI model

The irreparability flag status is determined using building repair fragility assuming a median residual drift at which the building is deemed as impractical to repair. A lognormal distribution function with a typical median residual drift of 0.01 and dispersion of 0.3 is assumed for repair fragility and shown in Figure 6.7.

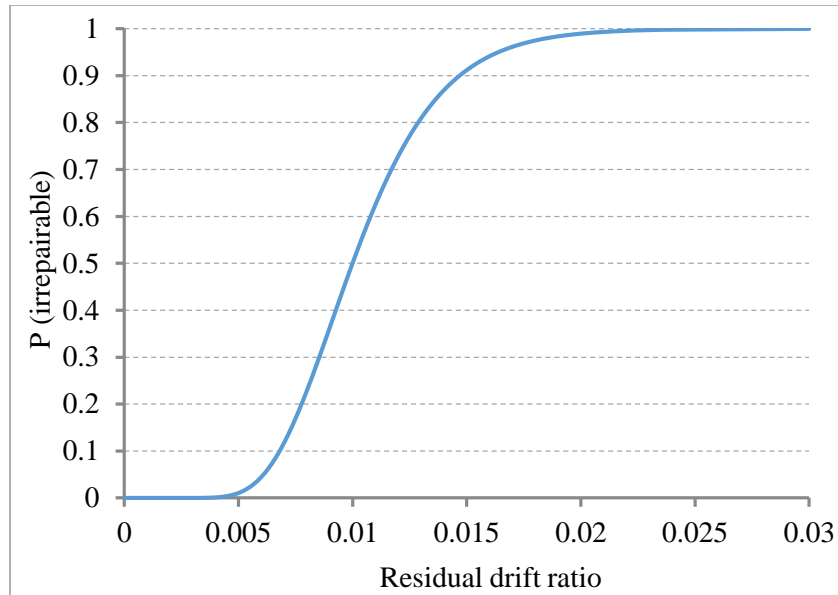


Figure 6.7: Building repair fragility based on the residual drift

### 6.3 Collapse Modes

Collapse modes are the possible ways in which the building is likely to collapse. For example, for the buildings of study at least five modes of collapse is likely to occur; Total collapse in all stories, collapse of floor 2 onto floor 1, collapse of floor 3 onto floor 2, collapse of floor 4 onto floor 3, and collapse of roof onto floor 4. Each of these collapse modes is associated with different potential injuries and fatalities. For the total collapse of all stories, the maximum number of injuries or fatalities will occur while in the partial collapse modes less casualties and injuries are likely. The probability of occurrence of each mode must be determined based on engineering judgment and calculations. The sum of the probability of occurrence of all modes must equal 1. The probability of occurrence of the total collapse mode for a multi-story building seems considerably greater as the initiation of other modes of collapse is likely to trigger a progressive collapse. Based on the FEMA P-58/BD-3.7.8 recommendations and

engineering judgment using the collapse modes occurred in the structures during collapse fragility determination process, the following collapse modes given in Table 6.1 and 6.2 are assumed.

Table 6.1 Probabilities of collapse mode, fatalities and serious Injuries

	Mode 1	Mode2	Mode 3	Mode 4	Mode 5
Probability of the Collapse	0.6	0.1	0.1	0.1	0.1
Probability of Fatality	0.9	0.9	0.9	0.9	0.9
Probability of Injury	0.1	0.1	0.1	0.1	0.1

Table 6.2 Collapse floor area ratios for the collapse modes

Floor	Collapse floor area ratio				
	Mode	Mode2	Mode3	Mode4	Mode5
Floor 1	1.0	0	0	0	0
Floor 2	1.0	1.0	0	0	0
Floor 3	1.0	0	1.0	0	0
Floor 4	1.0	0	0	1.0	0
Roof	1.0	0	0	0	1.0

#### 6.4 Consequence Functions

Consequence function consist of repair costs, time, fatalities, injuries, and unsafe placarding. Each component damage state has a series of fragility functions concerning repair costs, repair time, potential life hazard and the affected area per unit quantity of component, and the extent at which the damage could result in an unsafe placard.

According to ATC-58 (2012), repair costs and time includes cleaning the affected area where damage has occurred along with removal of mechanical, electrical or

plumbing systems to gain access for the repair. The rest of procedure includes procurement of material and equipment, implementing repairs, replacement of systems removed for access, and cleanup.

Repair cost and time is dependent on the quantity of repair actions. A lower bound quantity below which there is no discount for economies of scale is associated with a maximum unit cost. An upper quantity is also introduced above which no further economies of scale is obtainable. Repair action greater than the upper quantity are performed using the minimum unit costs. The cost of repair actions varies linearly for the quantities between the upper and lower quantity.

Repair time consequence function is dependent on several uncertain factors. It is calculated using similar calculations used for estimating repair costs. To facilitate the calculations, each damage state is associated with a number of labor hours required for repair action assuming a maximum number of workers per square foot. Values between one workers per 2000sf to one worker per 250sf is suggested as a practical range. This factor determines whether the building will be occupied during repair process. Large workers density requires an unoccupied building. This factor is considered 0.002 (500 workers per square foot) which is greater than the default value of 0.001 used in PACT resulting in lower repair time.

As an example, the suspended ceiling used for the buildings of the study has three damage states, each related to a set of consequence functions. The variation of average repair time and costs for damage state 3 is illustrated in Figures 6.8 and 6.9 using parameters given in the Table 6.3. The unit repair quantity for this component is equal to

600 square feet. At each quantity along horizontal axis, there is a distribution of repair cost and time with the average shown in diagram and a dispersion obtained in Table 6.3.

Table 6.3 Lower and upper quantity parameters for repair cost and time of suspended ceiling component (C3032.003, ATC-58 fragility library)

Parameter	Repair cost	Repair cost
Distribution Type	Lognormal	Lognormal
Dispersion	0.20	0.21
Lower quantity	0.3846 (230sf)	0.3846 (230sf)
Average repair cost/time for lower quantity	19756 (\$32.9 per sf)	61.75 days
Upper quantity	3.846 (230sf)	0.3846 (230sf)
Average repair cost/time for upper quantity	13677 (\$22.8\$ per sf)	42.68 days

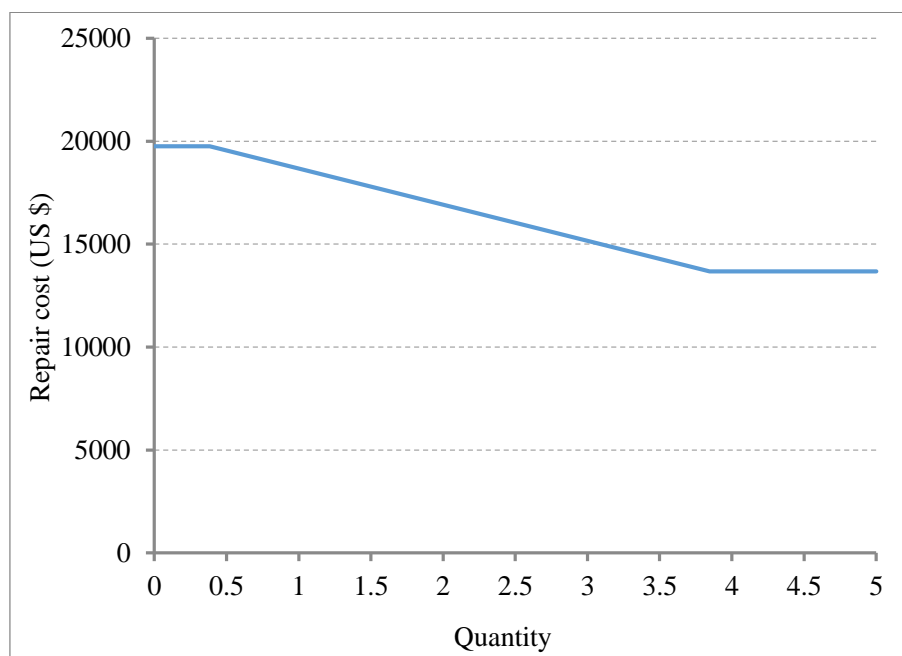


Figure 6.8: Repair cost versus repair quantity for suspended ceiling

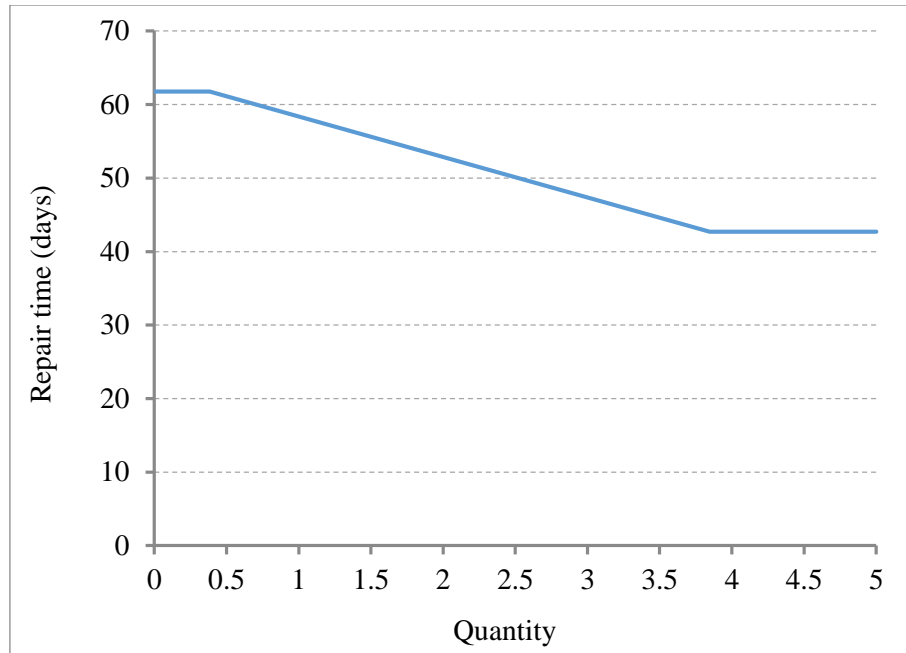


Figure 6.9: Repair time versus repair quantity for suspended ceiling

## Chapter 7 : Loss Analysis and Decision Making

### 7.1 Realizations

Different uncertain factors are involved in performance assessment procedure. Earthquake records variability produces a set of demands including acceleration, velocity, story drifts and residual story drifts. Damage state occurred in each component for each set of demands is also determined by the components fragility functions. Damage consequences including repair costs and time is estimated using consequence fragility functions. The rate of injuries, casualties, and collapse and irreparability flag is also determined in the same manner.

Monte Carlo simulation is the most reliable approach for performance assessment of this multivariable probabilistic problem. A set of random variables is produced in this technique each associated with an uncertain factor. The consequences for each component is determined based on the random number generated as a random event. The sum of all consequences comprise an outcome called realization. Performance assessment requires many realizations to calculate the median consequence quantity. The total number of 500 realizations used for the current study which is deemed to provide sufficient accuracy. Monte Carlo simulation can be time and memory intensive depending on the number of realizations, and the number and quantity of components. In components with uncorrelated fragility, for each unit quantity of the component an independent random generation is produced leading to a large amount of calculation in each realization. As the most components is assumed with uncorrelated fragility the simulation duration is noticeably long.

The results of realizations for the design-base earthquake level corresponding to a probability of occurrence of 10% in 50-year is shown in Figures 7.1 to 7.6 for all buildings. In these Figures, repair costs of different components and the total repair costs is given for all 500 realizations. Realization number is given in the horizontal axis sorted in a way that larger numbers correspond to a larger total repair costs. The results of realizations for 10-year, 72 year, and 2475-year return period earthquakes corresponding to probability of occurrence of 99.4%, 50%, 10%, and 2% in 50-year is also provided in appendix B.

Repair costs changes from hundreds of thousands of dollars to total loss for B1 model as shown in Figure 7.1. Total loss is due do irreparable residual drift predicted by a considerable number of realizations at the right end of the diagram. Generally, lower repair costs is predicted for B2 to B5 and BI model with the B2 and BI showing the lowest and highest improvements. Total number of realizations predicting total loss due to irreparable residual drift decreases when model changes from B1 to B5 and then BI. No collapse occurred in any model and no total loss due to residual drift is predicted by both B5 and BI models which has led to their superior performance comparing to other models.

Total repair cost distribution and the lognormal fitted curve is given in Figures 7.7 for 10% in 50 year intensity. Repair costs distribution diagrams for the rest of intensities is provided in Appendix B. In some models like B1, total replacement costs is predicted by a considerable number of realizations. Therefore, repair cost distribution is flat at right top showing irreparable residual drift or collapse has occurred in a number of realizations

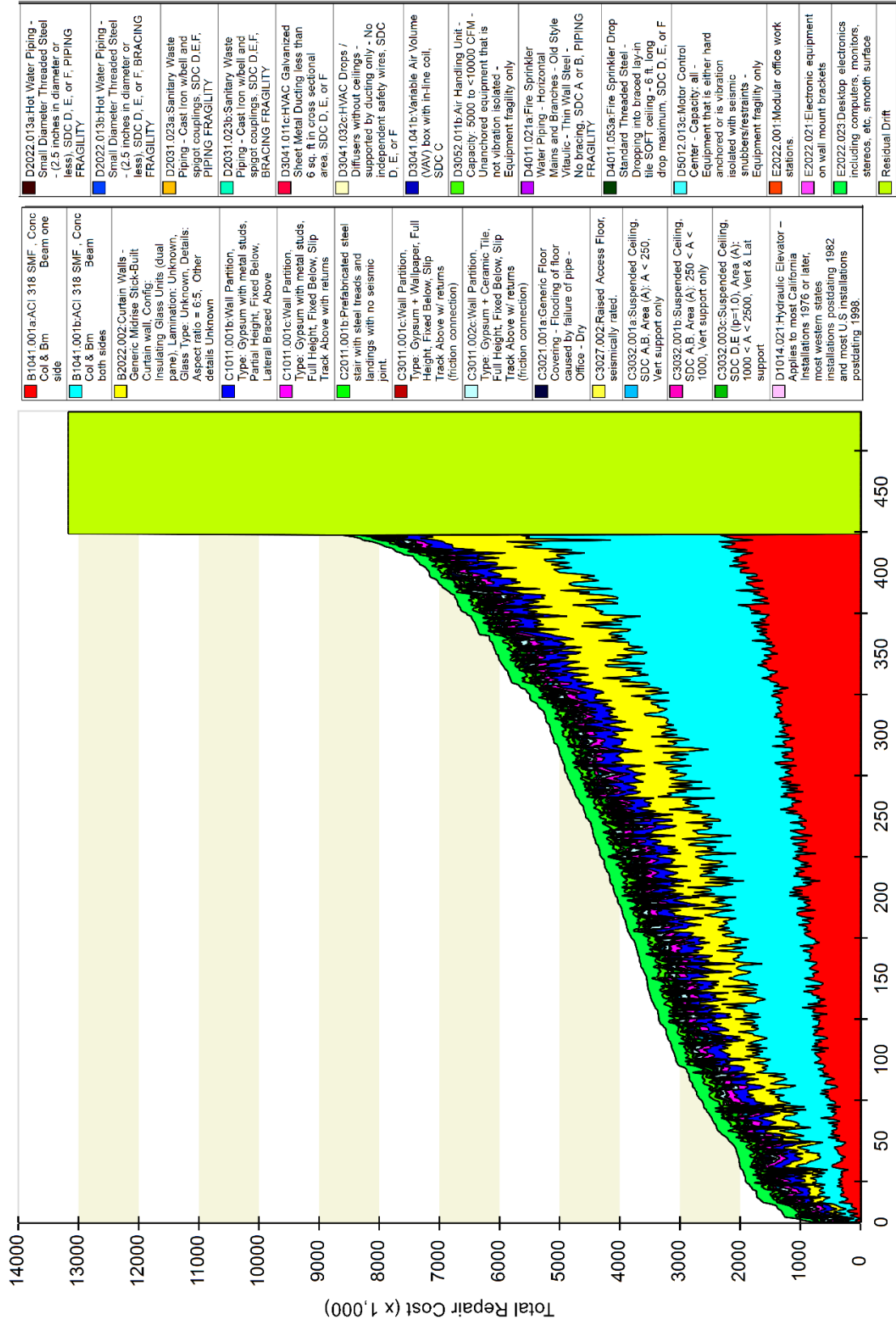


Figure 7.1: Total repair cost vs realization number for B1 model

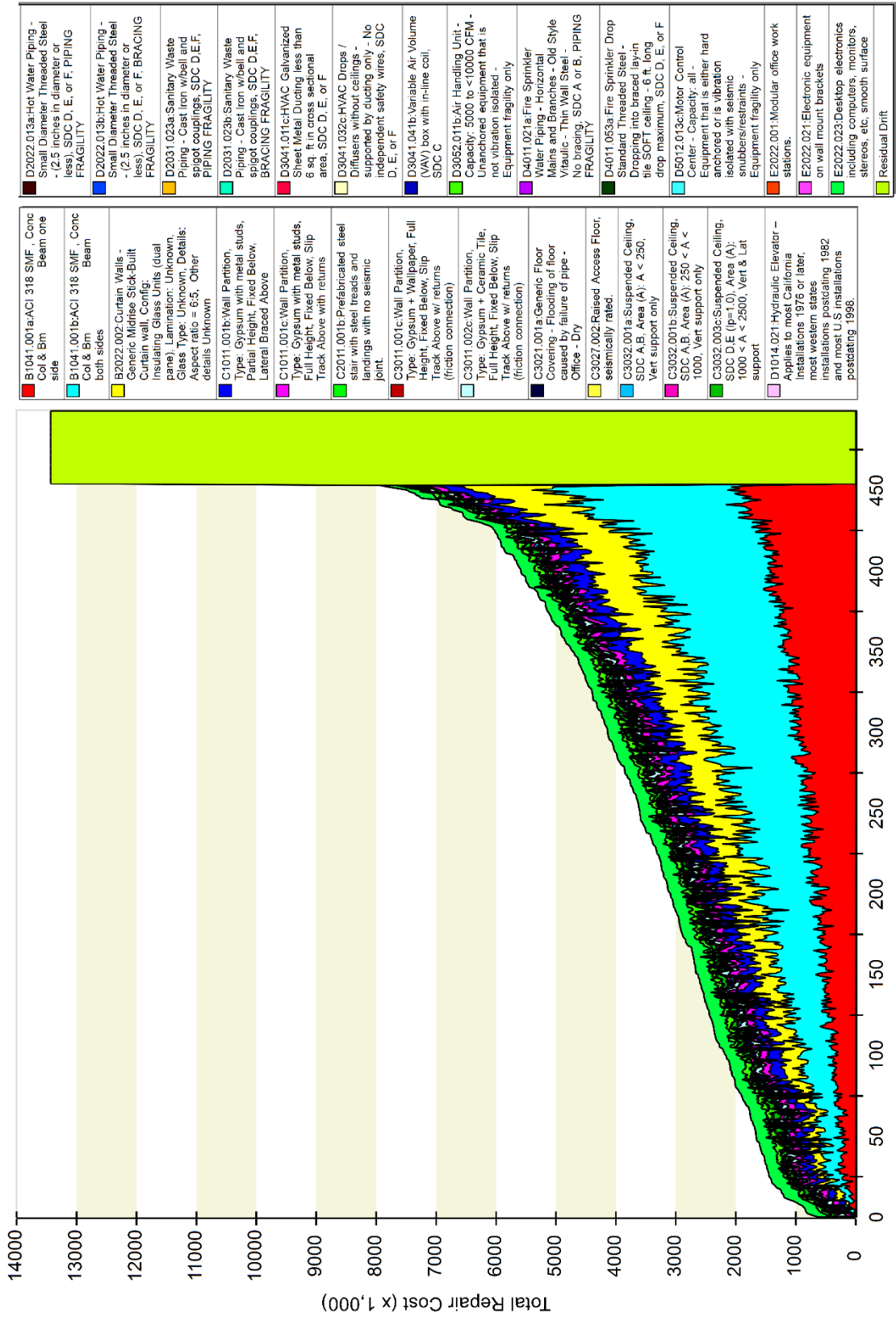


Figure 7.2: Total repair cost vs realization number for B2 model

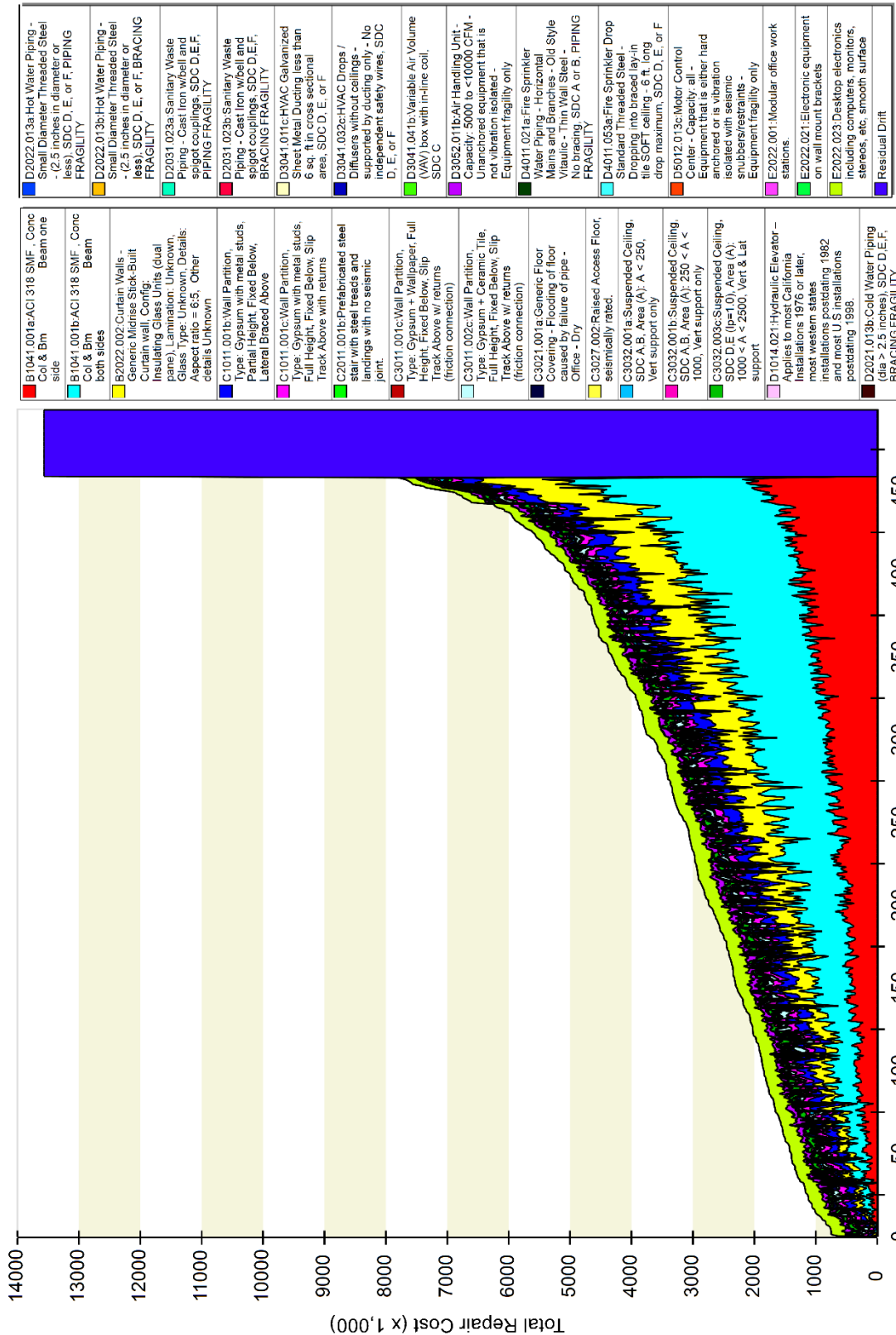


Figure 7.3: Total repair cost vs realization number for B3 model

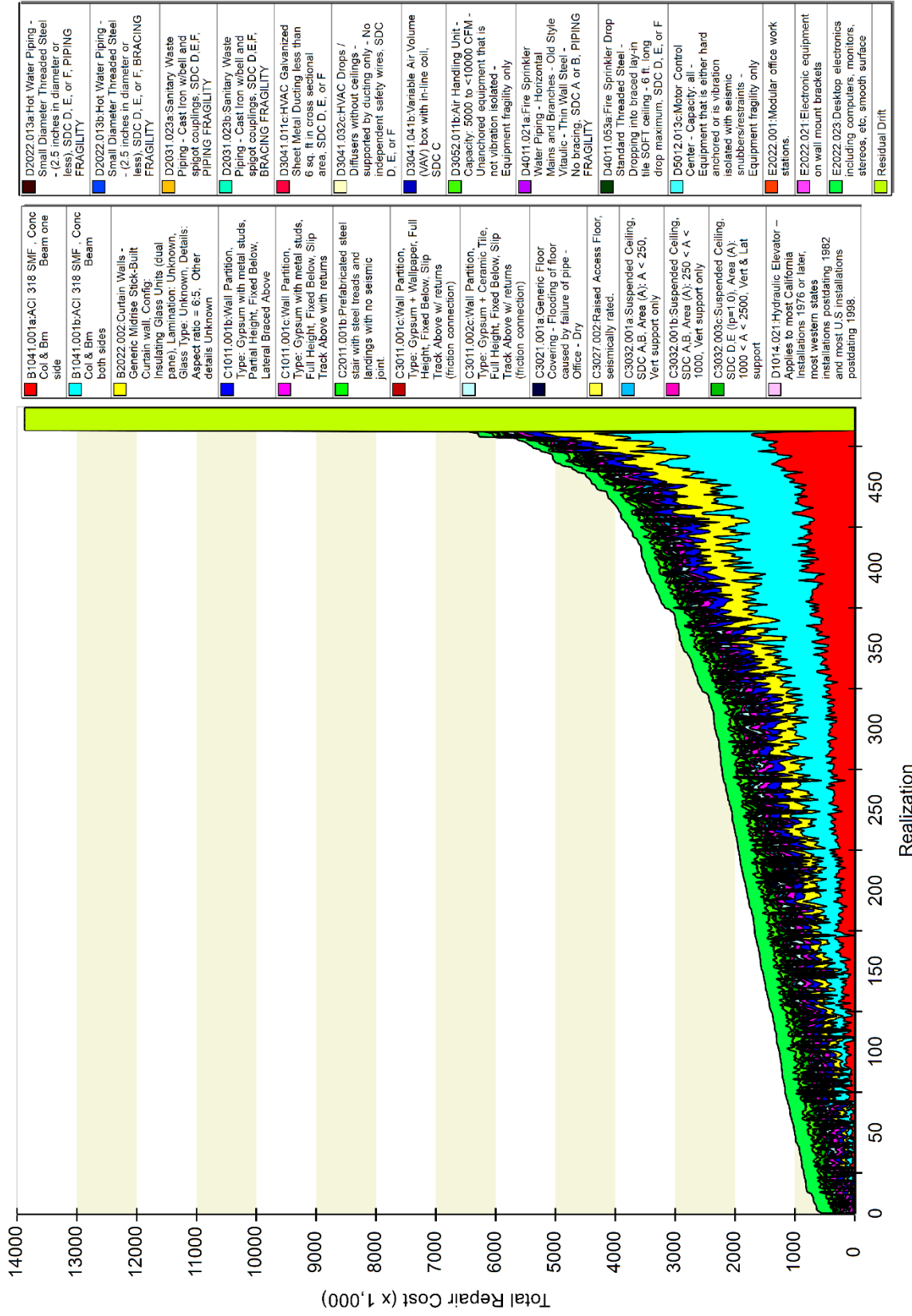


Figure 7.4: Total repair cost vs realization number for B4 model

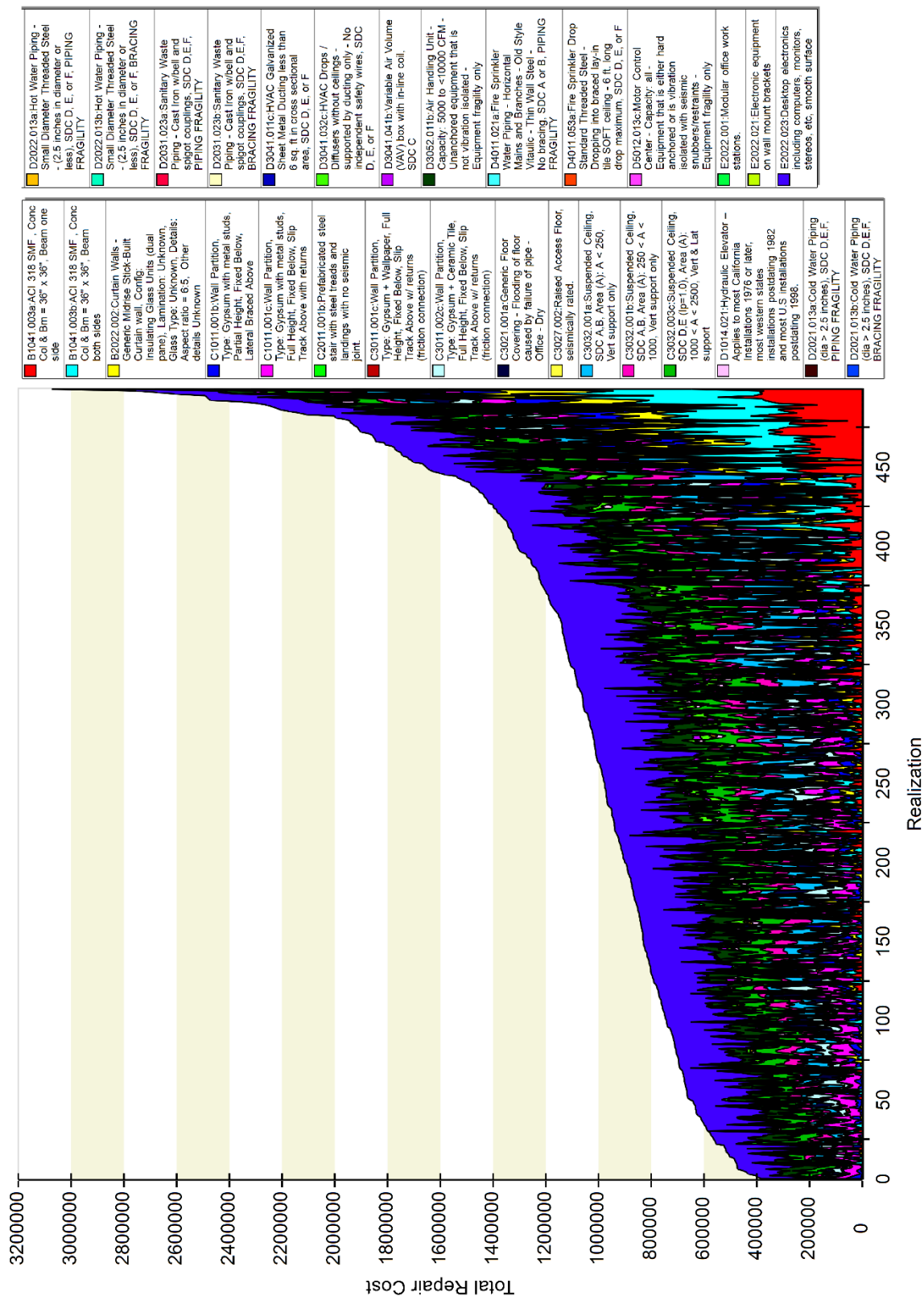


Figure 7.5: Total repair cost vs realization number for B5 model

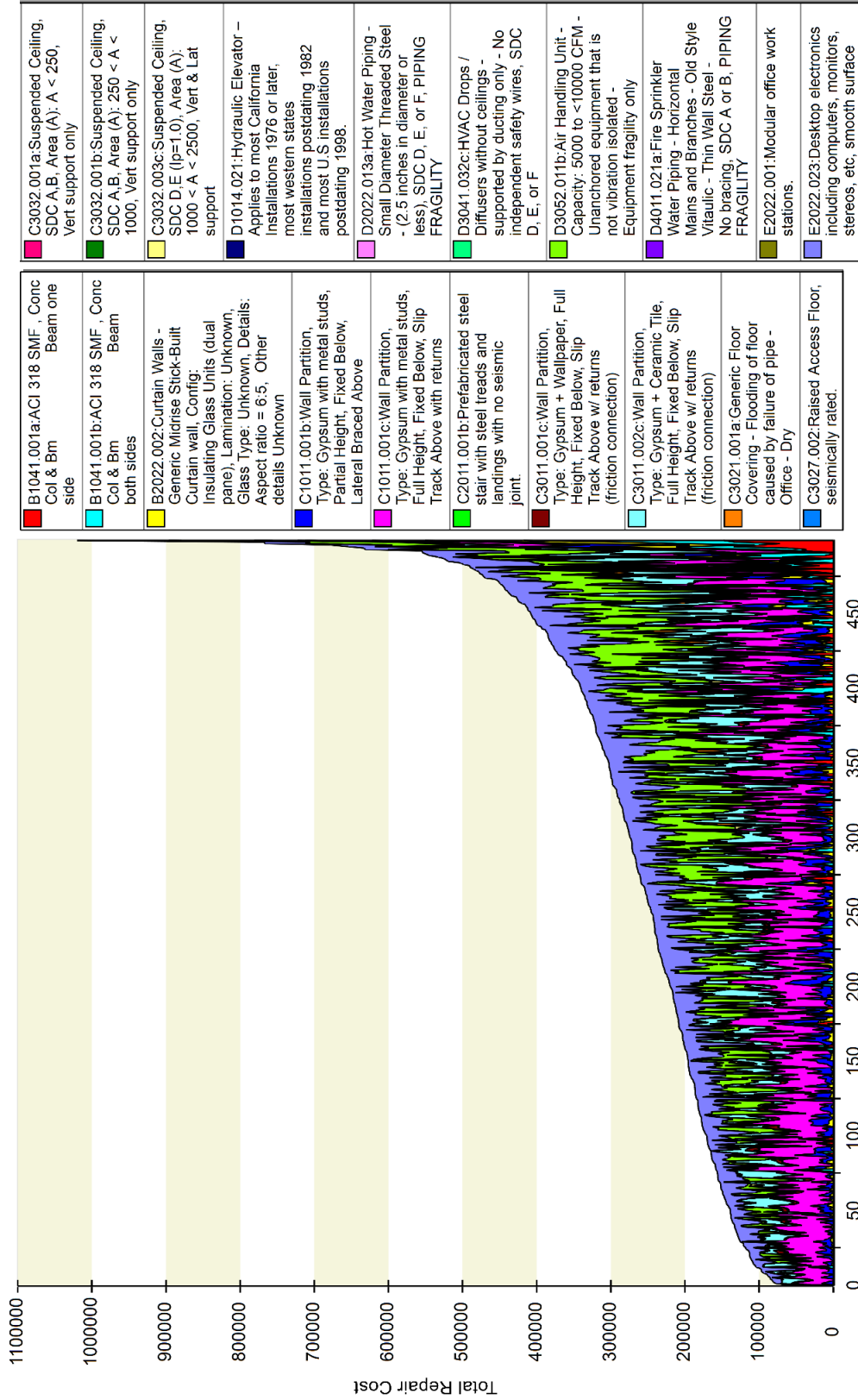


Figure 7.6: Total repair cost vs realization number for BI model

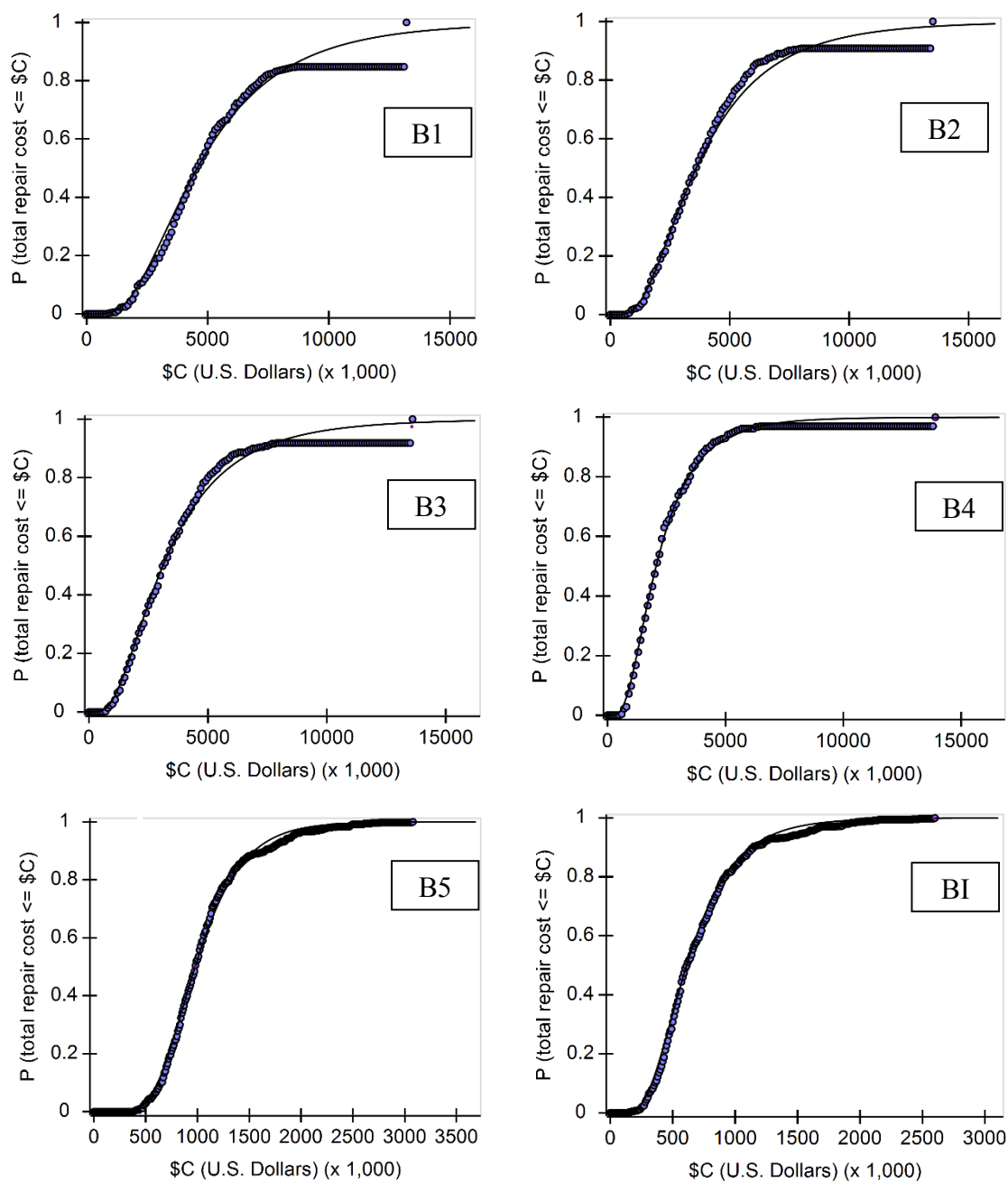


Figure 7.7: Repair cost distribution and the lognormal fitter curve for the 10% in 50 year earthquake intensity

Table 7.1 gives the median repair costs with given shaking intensities with 50%, 10%, and 2% in 50-year return period. For the lowest earthquake intensity (50% in 50 year), estimated repair costs reduces from \$752,000 in model B1 to \$388,000, in model B4. Model B5 does not show any further substantial decrease in repair costs due to large accelerations recorded in this model. In contrary, Base-isolated model shows a considerable reduction in repair costs due to considerably smaller recorded floor accelerations. Repair cost reduction of 67% is obtained for this model with respect to B1 model.

For the design based earthquake (10% in 50 year), a constant repair cost decrease is recorded for stronger models as expected due to decreased drift ratios. Base isolation devices are more effective in reducing drifts and accelerations as they perform fully nonlinear at this intensity level. A cost reduction percentage of 87% with respect to B1 model is obtained when base isolation system is used. B5 model is able to offer 78% cost increase relative to B1 model. At the very high shaking intensity, 2% in 50 year, a similar trend of decreasing repair costs occurs, but B5 model outperforms the BI in terms of repair costs. B5 is able to reduce costs by 67% while the BI model offers a 61% reduction. A larger cost decrease greater than B5 model is attainable for BI the through selection of more effective isolation devices.

Table 7.1: Median repair costs estimated for benchmark buildings

Earthquake Intensity	Average repair cost (US Dollars *1000)					
	B1	B2	B3	B4	B5	BI
<b>50% in 50 year</b>	752	505	441	388	370	246
<b>10% in 50 year</b>	4520	3590	3160	2068	978	611
<b>2% in 50 year</b>	7190	6466	5750	4920	2343	2809

Table 7.2 gives the repair costs per square feet of the building area by dividing the total costs by the total floor areas. The decision about whether a damaged building should be repaired or replaced is usually determined by using a threshold. The threshold is a cap over which the building is likely to be replaced than repaired. FEMA suggests a 50% of the total replacement cost of the building for the threshold while some researchers have suggested a 40% value based the owner's decisions made in the past (ATC-58, 2012). This threshold can considerably fluctuate depending on the age and historical importance of the building. The accessibility to the building site for demolishing and replacement can also affect the threshold selection. Table 7.2 repair costs are accompanied by a color showing their reparability based on suggested thresholds. Green color shows repair costs of less than 40% representing a repairable damage. Repair costs of more than 50% is shown by the red color representing an irreparable damage. Any repair costs between 40% to 50% is represented by yellow color implying that the damage state can be deemed as either repairable or irreparable depending on building and conditions described earlier.

Table 7.2: Median repair costs per square foot and the reparability state

Earthquake Intensity	Median repair cost (US dollars per square feet)					
	B1	B2	B3	B4	B5	BI
50% in 50 year	19.5	13.1	11.5	10.1	9.6	6.4
10% in 50 year	117.4	93.2	82.1	53.7	25.4	15.9
2% in 50 year	186.8	167.9	149.4	127.8	60.9	73.0

The damages experienced for 50% and 10% in 50-year earthquakes are repairable in all building designs. For the largest intensity, 2% in 50 year, B1 design shows irreparable damage while the two fixed-base designs, B2 and B3, might be repairable depending on the other effective factors. The other fixed-base designs with capacities beyond the minimum code requirements (B4 and B5) have experienced repairable damage. The base-isolated design is also fully repairable with repair costs less than 20% of the total replacement costs.

## **7.2 Annualized Performance Measure**

Annualized performance measure is defined as the mean value of performance measure per year over a period equal to useful life of the building. This parameter is only computable when time-based assessment is employed.

Each ground motion intensity with a particular annual probability of occurrence is associated with a series of performance measures such as repair costs, time, unsafe placard, fatalities and serious injuries. The annual probability of occurrence of each shaking intensity multiplied by that performance measure or impact quantity results in the annual mean value of the performance measure for the given intensity. Annualized total value for the performance measure is calculated by summing these values for all shaking intensities.

Figure 7.8 illustrates the seismic hazard curve for B1 model in which the annual frequency of exceedance of shaking is plotted against spectral acceleration at the first mode period of the building. It is divided into 10 segments at which midpoints are the shaking intensities previously used for performing time-history analysis. The difference

between the end points annual frequency of exceedance is also shown for each segment. This is the annual probability that shaking intensity falls in that segment.

The annual value of a performance measure is obtained by multiplying performance measure at each segment intensity by the corresponding annual probability as shown in the Figure 7.8, and then summing over all segments.

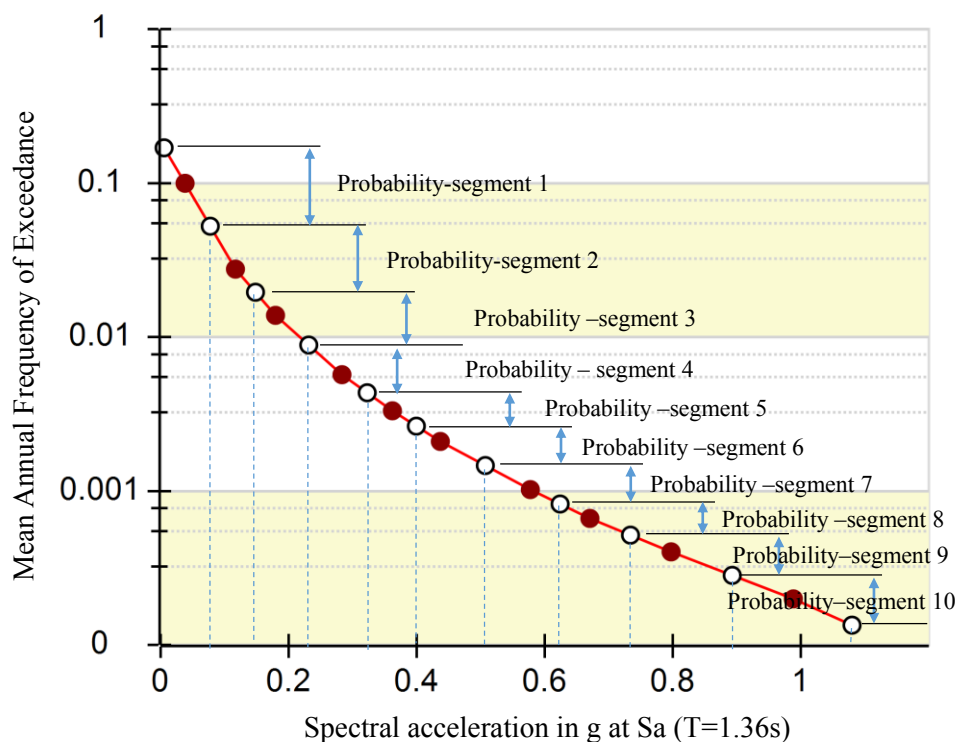


Figure 7.8: Seismic hazard curve segments and the corresponding annual probabilities

### 7.2.1 Repair Costs and Time

Figures 7.9 to 7.14 show the repair costs versus annual probability of exceedance for all designs. Each shaking intensity contribution to total costs is plotted with a different color. The total area under the envelope diagram is the total annualized repair costs which

is printed at the top of diagrams. Total repair costs is the sum of areas associated with each shaking intensity. A larger area implies larger contribution of that intensity to the total costs. Low shaking intensities have high probabilities of occurrence, but their corresponding repair costs are little. On the other hand, high shaking intensities features low probabilities of occurrence and high repair cost consequences. From the figures, it seems that to some extent very low and especially very high earthquake intensities are less important in terms of their impact on total repair costs. Three medium intensity earthquakes, intensity 2, 3, and 4 with 32, 72, 150 years return periods have most contributed into total costs.

Annualized repair costs starts with \$67403 (\$1.75/S.F.) for B1 model and decreases gradually for higher capacity models. Model B5 recorded a value \$25034 (\$0.65/S.F.) which shows nearly 63% reduction with respect to model B1. Base-isolated model offers the lowest repair costs of all models equal to \$22572 (\$0.59/S.F.) which shows a 67% reduction relative to model B1.

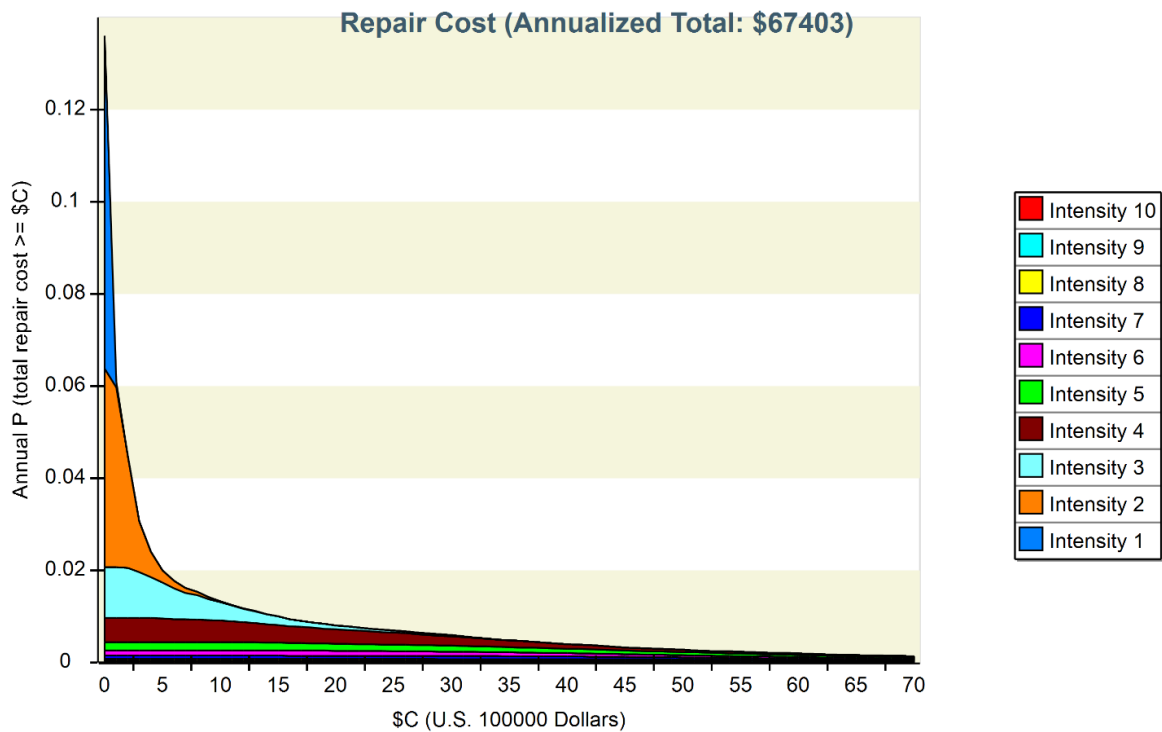


Figure 7.9: Annualized repair costs for B1 model

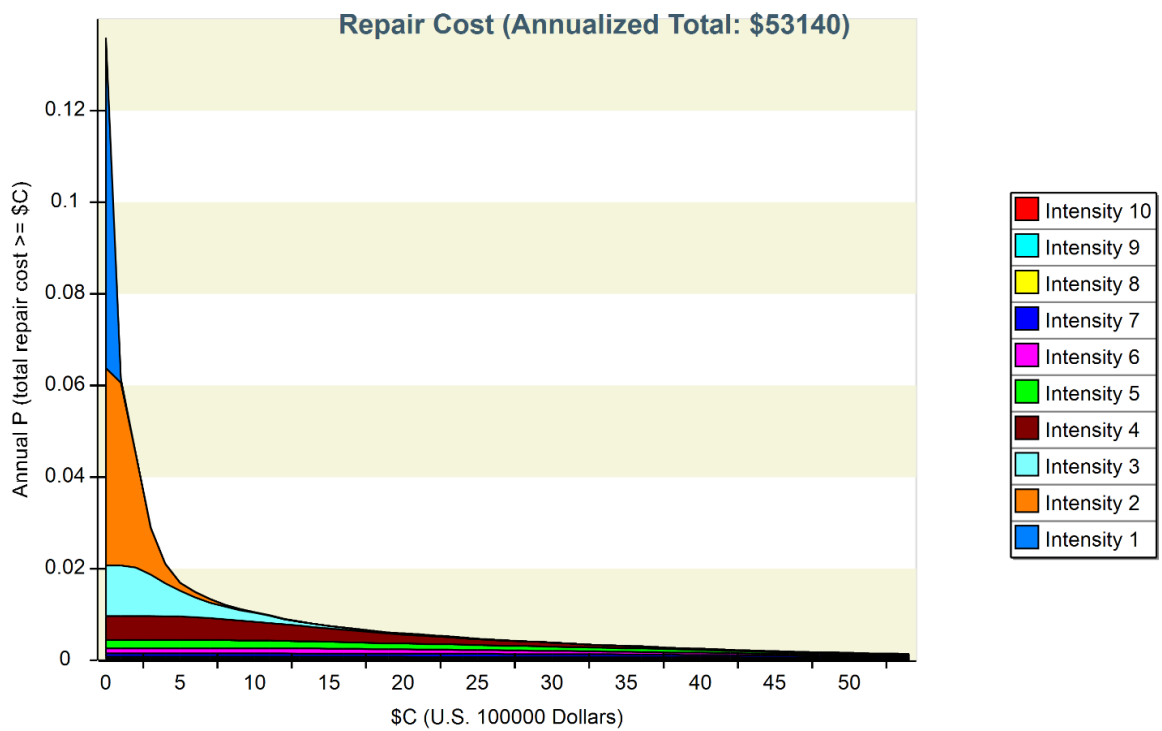


Figure 7.10: Annualized repair costs for B2 model

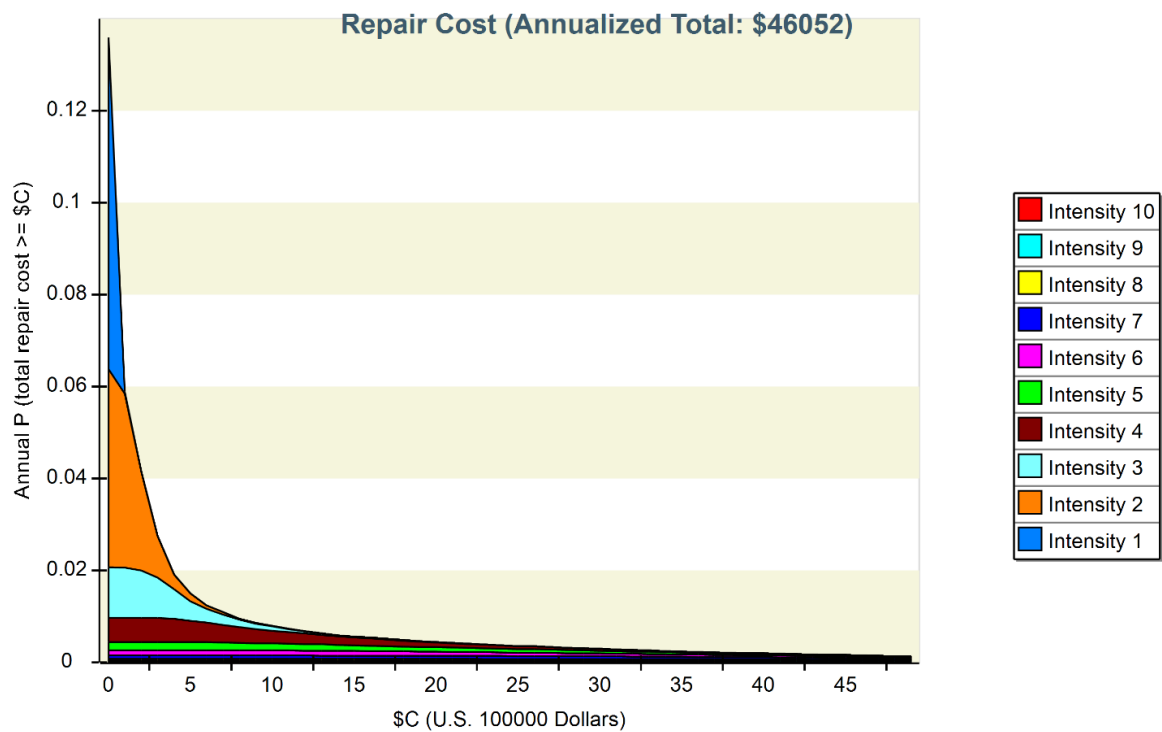


Figure 7.11: Annualized repair costs for B3 model

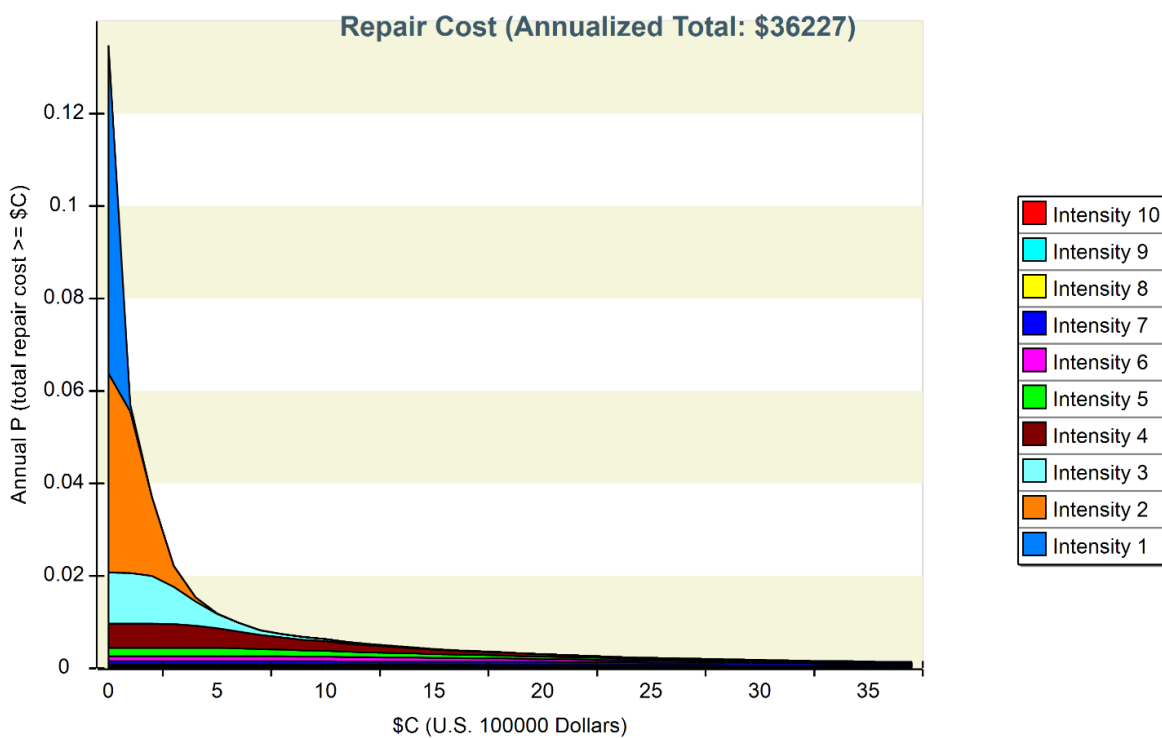


Figure 7.12: Annualized repair costs for B4 model

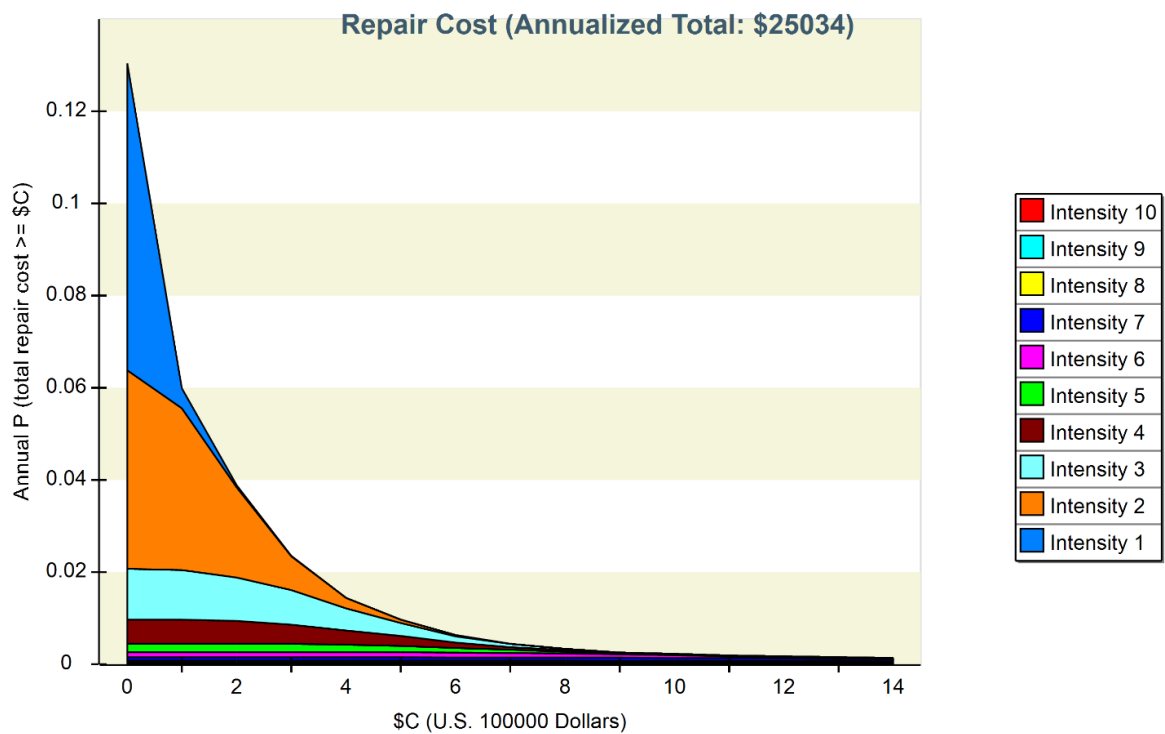


Figure 7.13: Annualized repair costs for B5 model

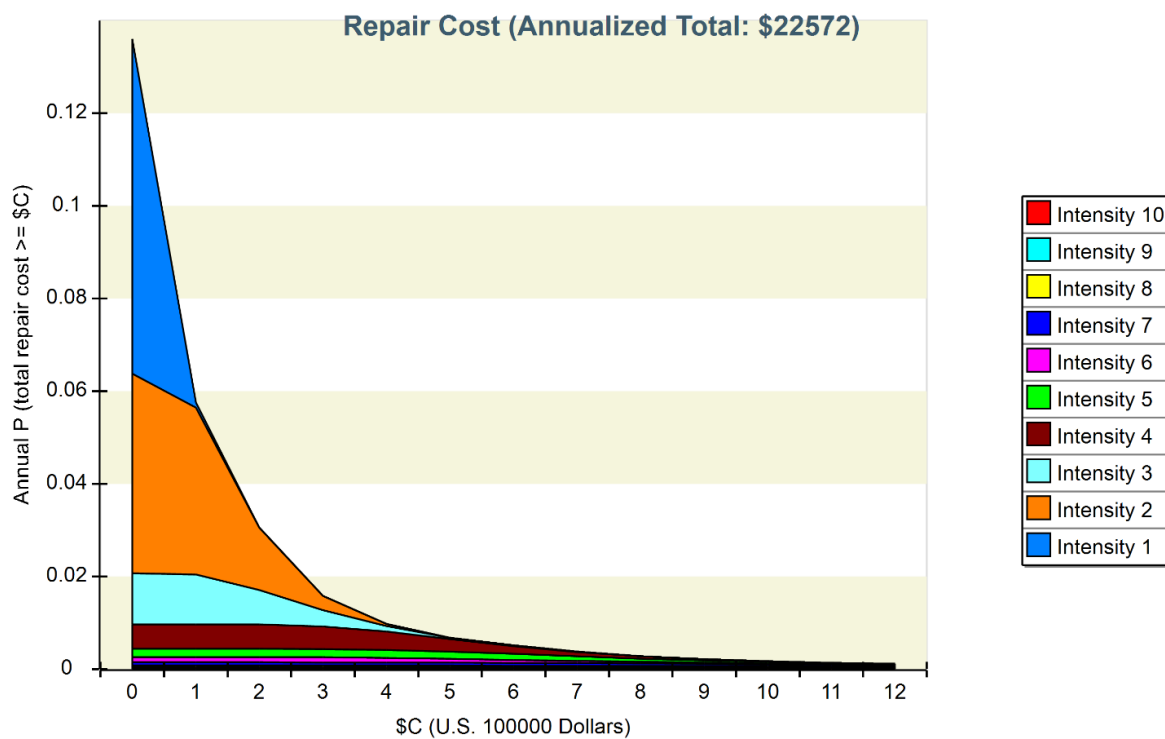


Figure 7.14: Annualized repair costs for BI model

Annualized repair time can be more important as repair costs as it can pose downtime in the operability of the building resulting in considerable revenue loss. Repair time estimation is carried out similar to for repair cost estimation procedure. Two options are available for this performance measure, serial and parallel activity. In parallel option, all floors can be repaired simultaneously by deferent crews resulting in lower repair time. The actual schedule for the building repair is between these two extremes. For conservative conclusions, the parallel option is selected for this study which leads to less repair time difference between high performance model and low performance ones (For example, B5 compared to B1). Figures 7.15 to 7.20 gives the annualized total repair time for all models. Annualized repair time varies from 2.94 days for B1 to 0.85 days for B5 which shows a 71% reduction. BI model annualized repair time is 0.93, slightly greater than B5 model with 68% decrease over the B1 model.

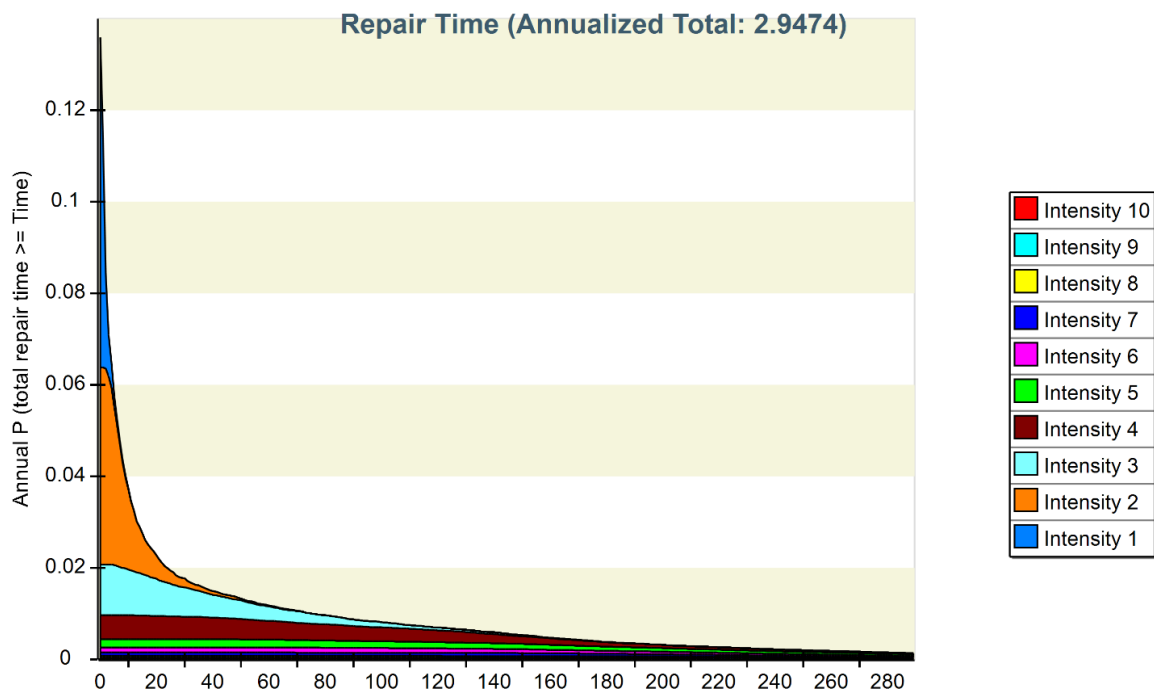


Figure 7.15: Annualized repair time for B1 model

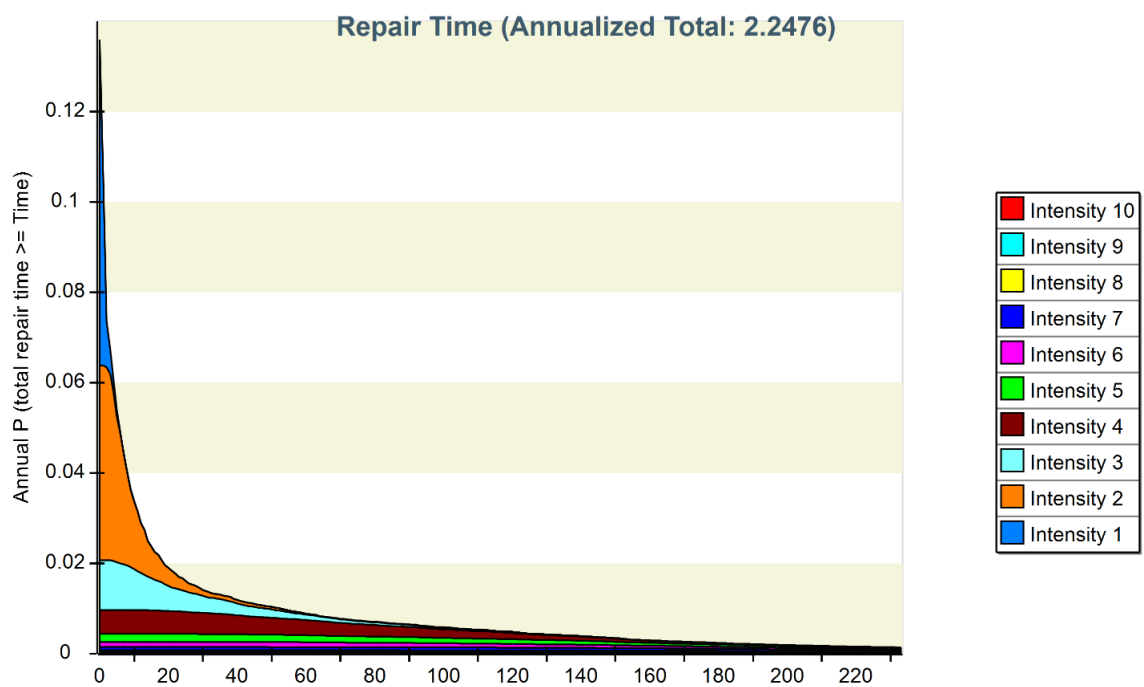


Figure 7.16: Annualized repair time for B1 model

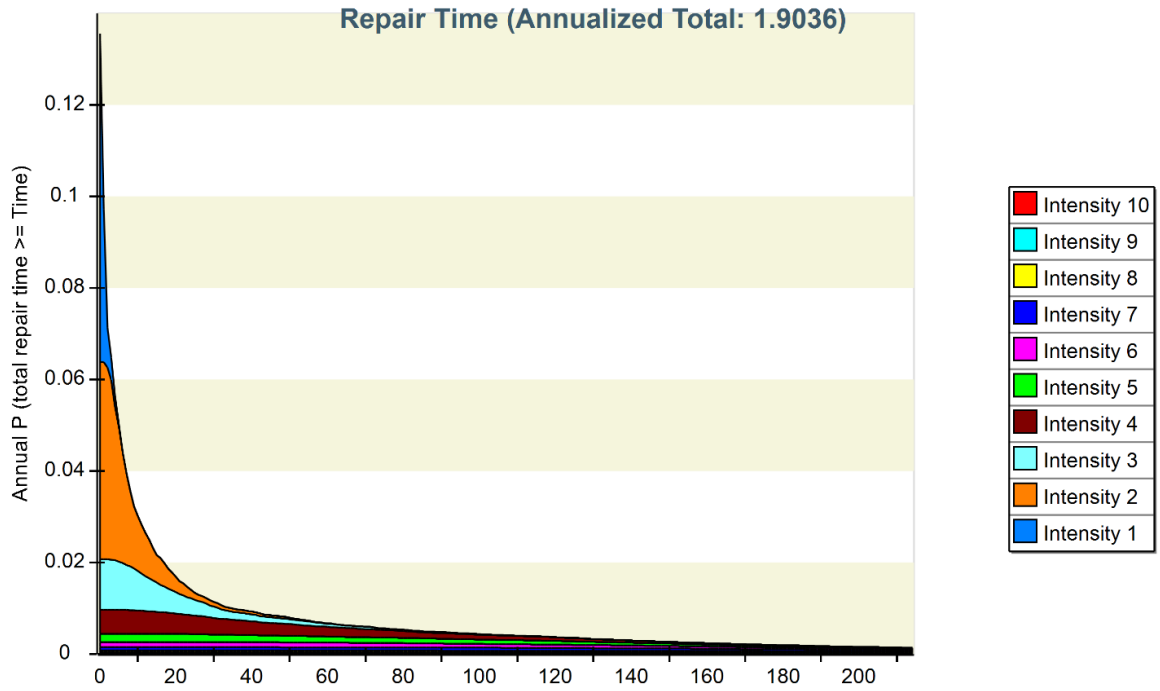


Figure 7.17: Annualized repair time for B3 model

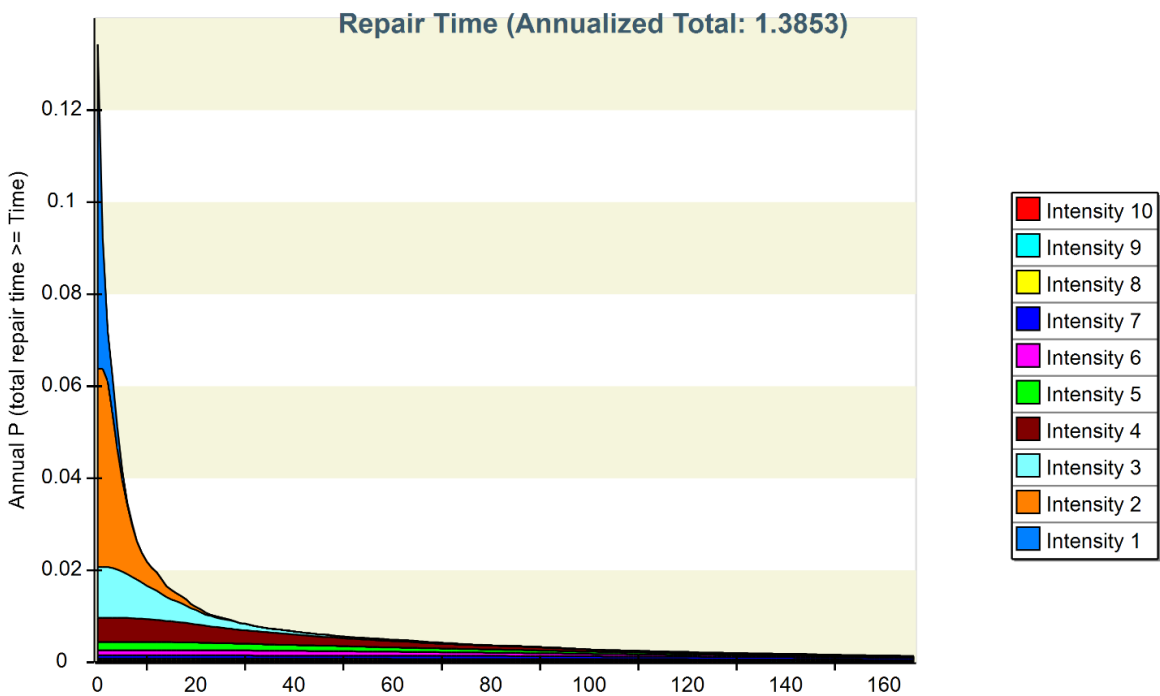


Figure 7.18: Annualized repair time for B4 model

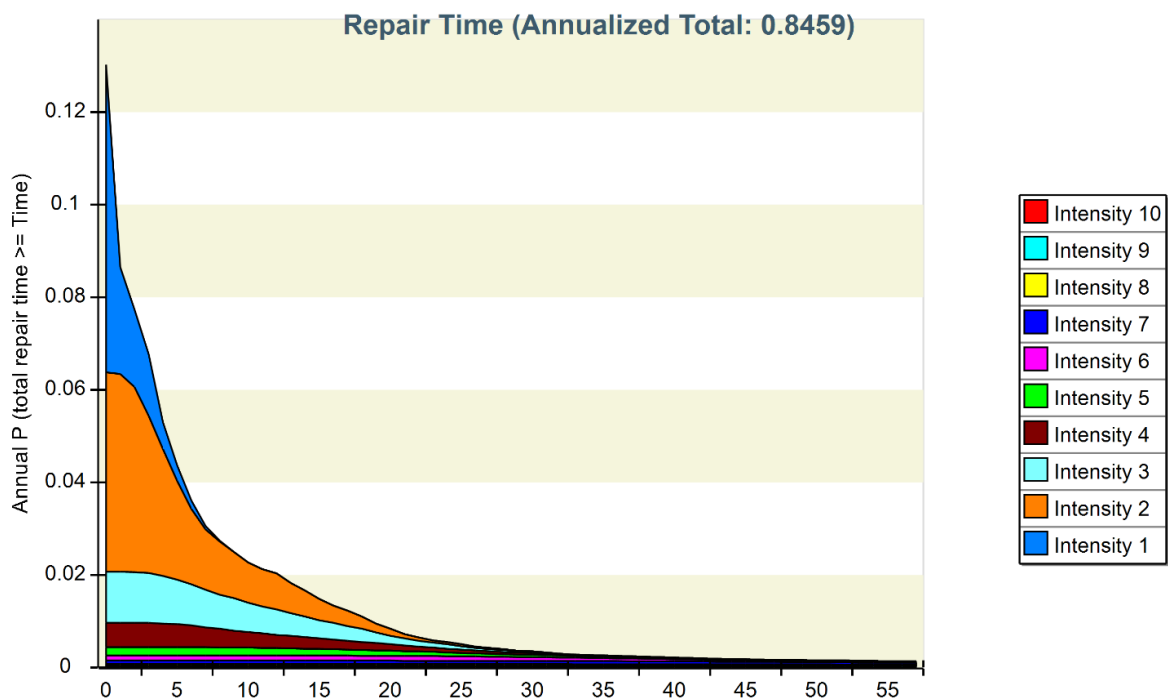


Figure 7.19: Annualized repair time for B5 model

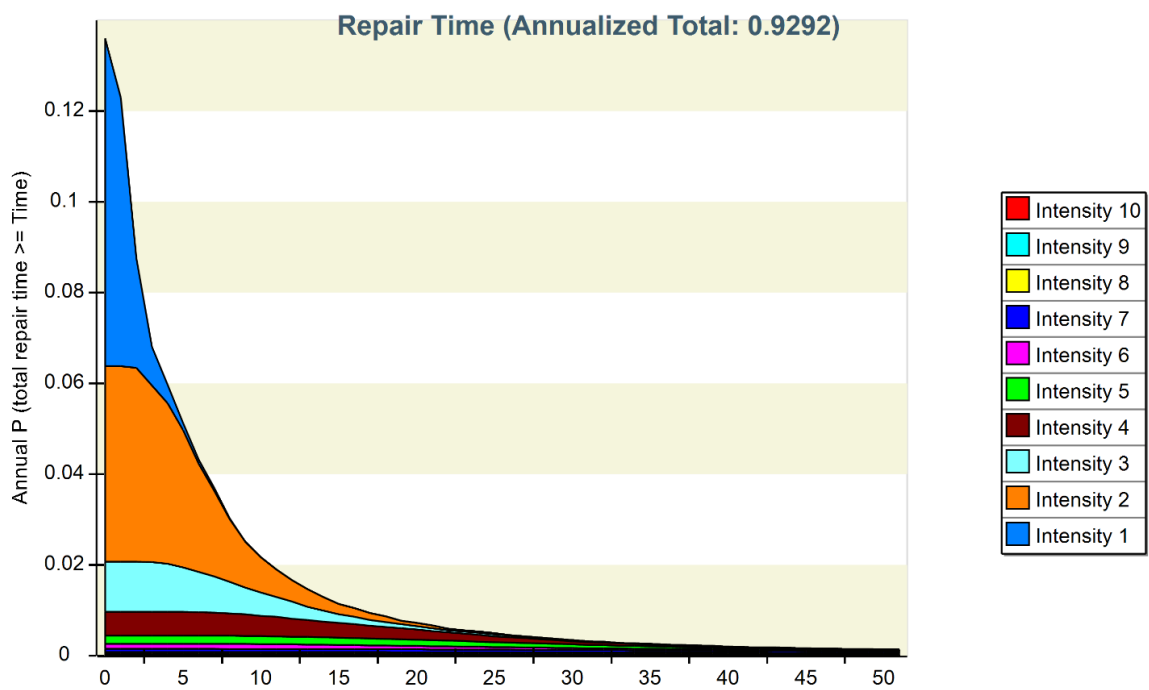


Figure 7.20: Annualized repair time for BI model

### 7.2.2 Casualties

Human losses including fatalities and serious injuries are integral parts of any performance assessment conducted on buildings. Annualized fatalities and serious injuries can be estimated in the same way as total repair costs estimation. Annualized serious injuries are presented in Figures 7.21 to 7.26 for all models. The highest rate of annual injuries is estimated at 0.0426 for B1 model and reduces to 0.0169 in B5 (60% reduction) model with all other fixed-base models varying in this range. The lowest rate of annualized injuries estimated at 0.0084 occurs for BI model with over 80% decrease with respect to B1 model.

Our analysis resulted in negligible annual rate of fatalities with values presented in Table 7.3. The fatality rate for B1, B2 and B3 are estimated as 0.0012, 0.00052, and 0.00044, respectively. Fatality rates are equal to 0.06, 0.026 and 0.022 for B1, B2 and B3 models in a 50-year period which are negligible for these code conforming designs.

Table 7.3 Annualized fatality rate

<b>B1</b>	<b>B2</b>	<b>B3</b>	<b>B4</b>	<b>B5</b>	<b>BI</b>
0.0012	0.00052	0.00044	0.00030	<0.0001	<0.0001

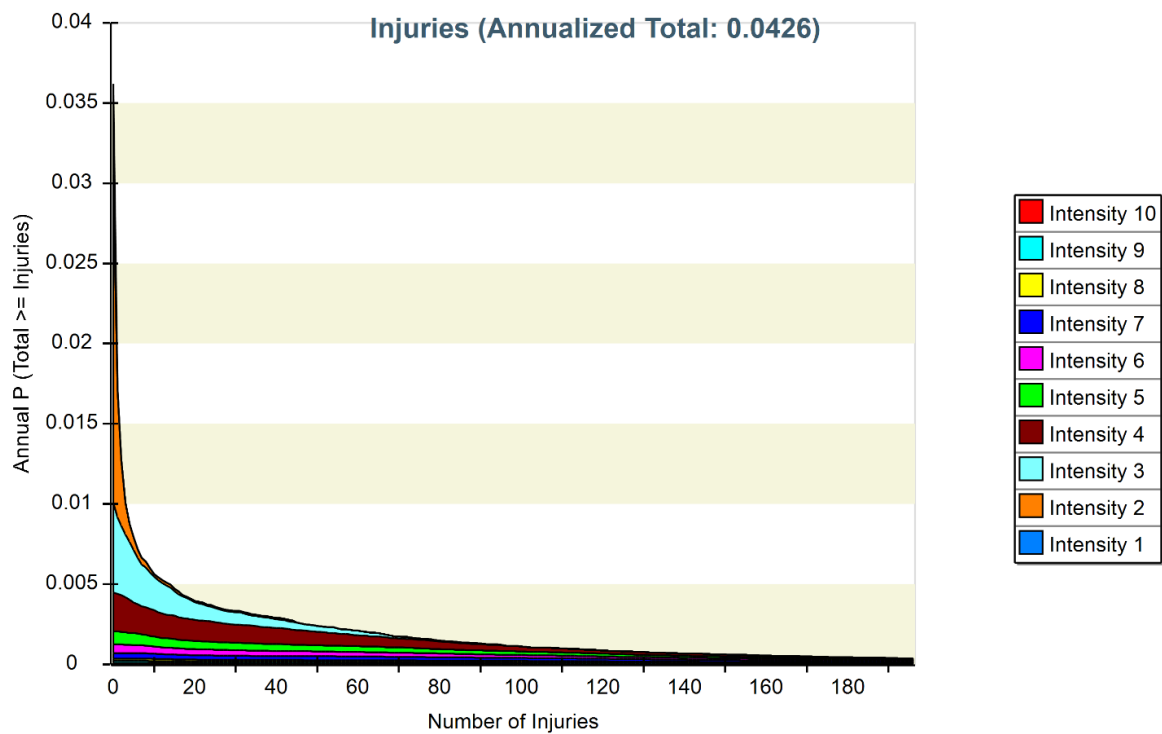


Figure 7.21: Annualized injuries rate for B1 model

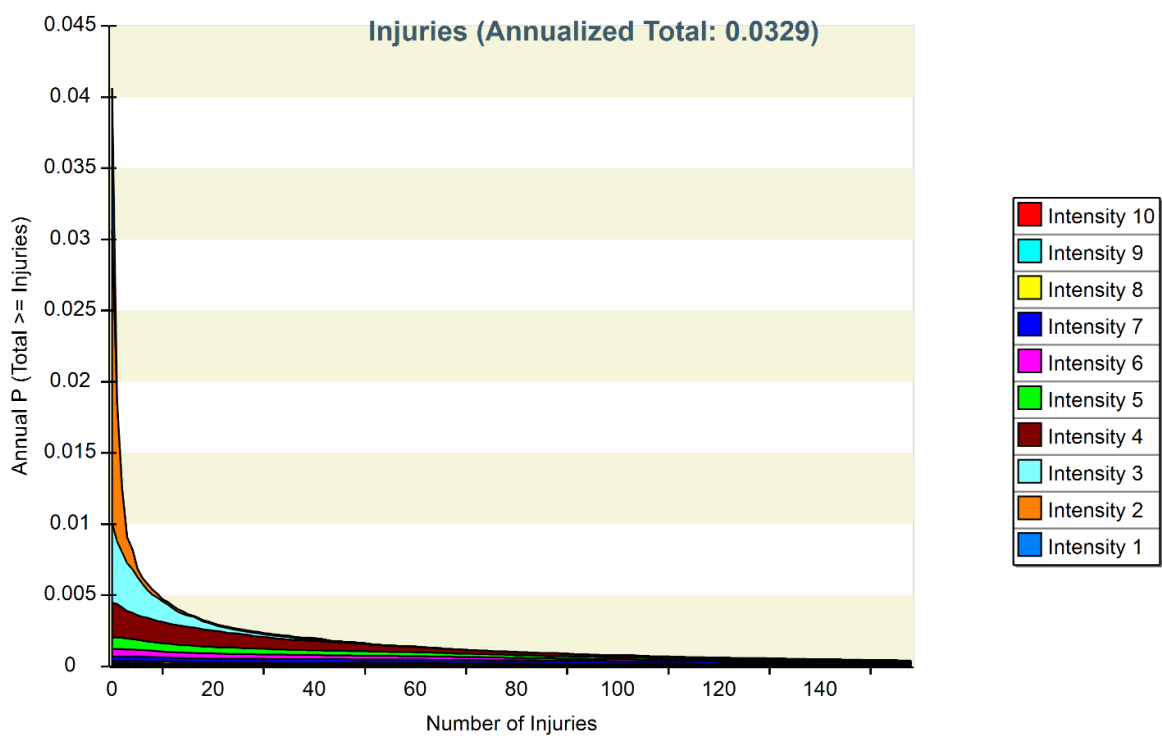


Figure 7.22: Annualized injuries rate for B2 model

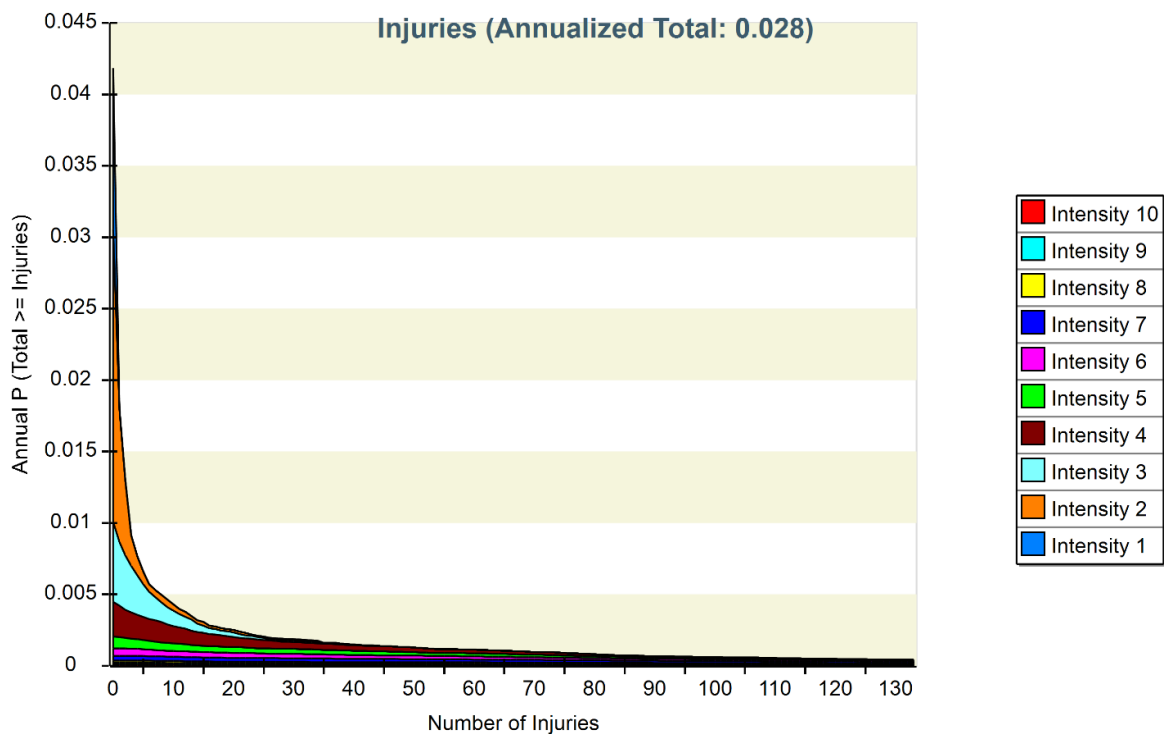


Figure 7.23: Annualized injuries rate for B3 model

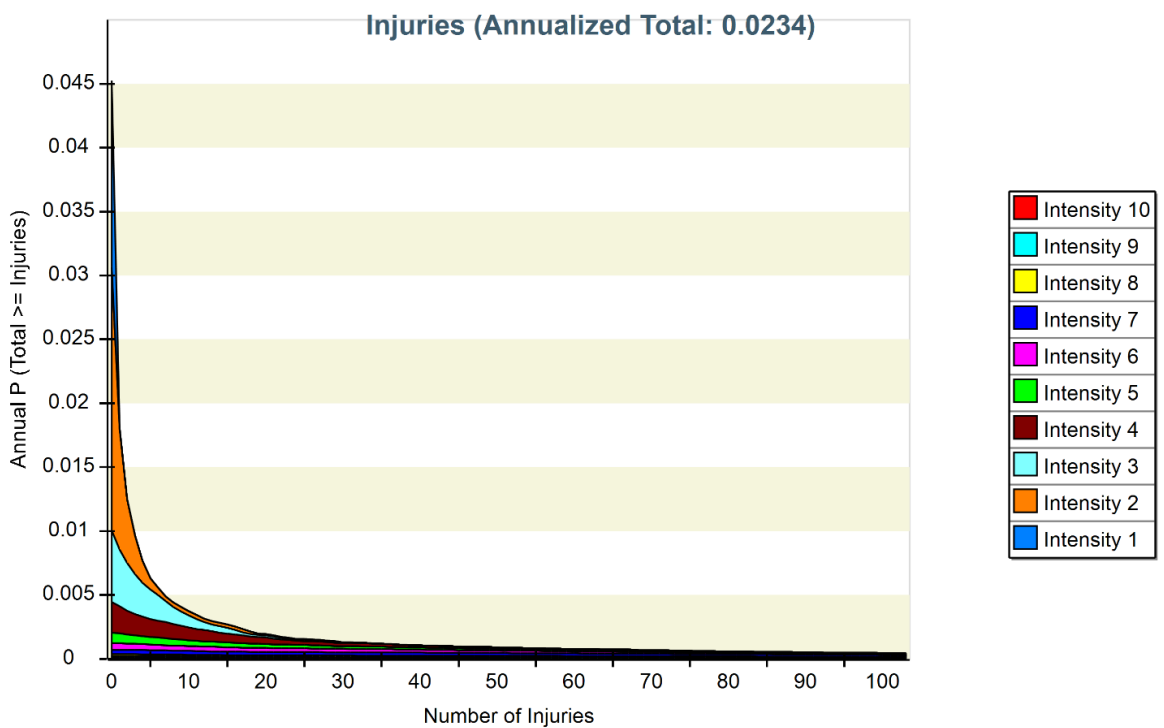


Figure 7.24: Annualized injuries rate for B4 model

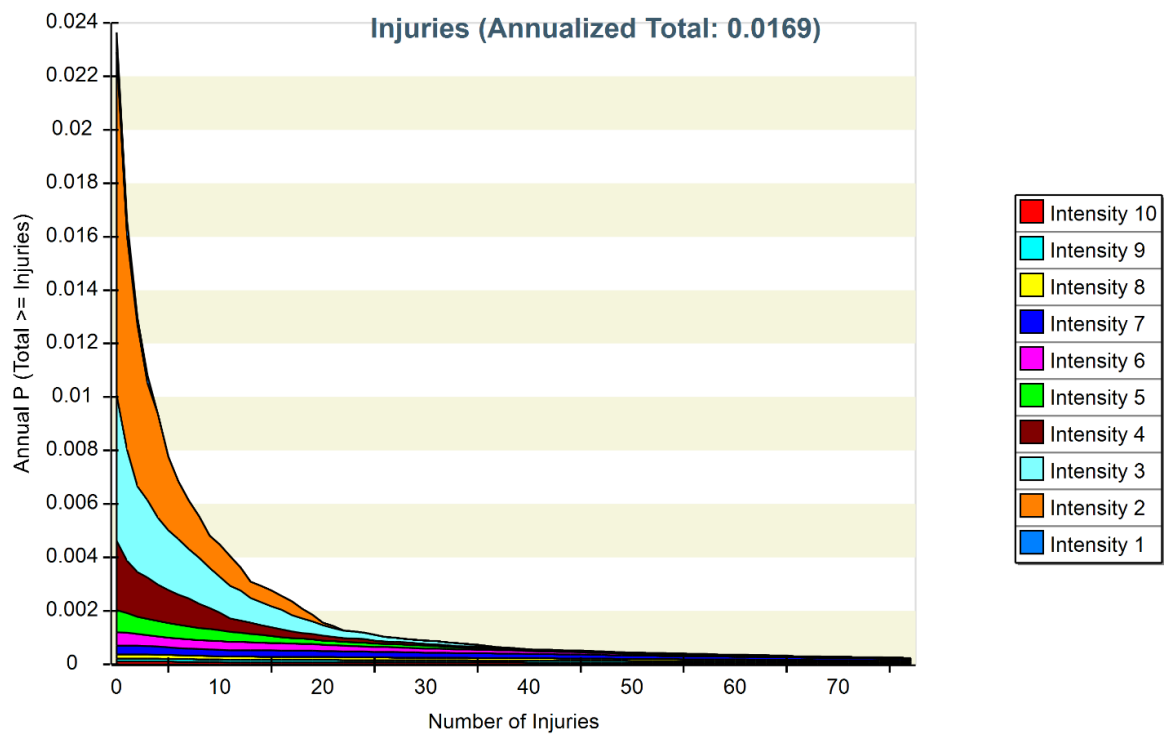


Figure 7.25: Annualized injuries rate for B5 model

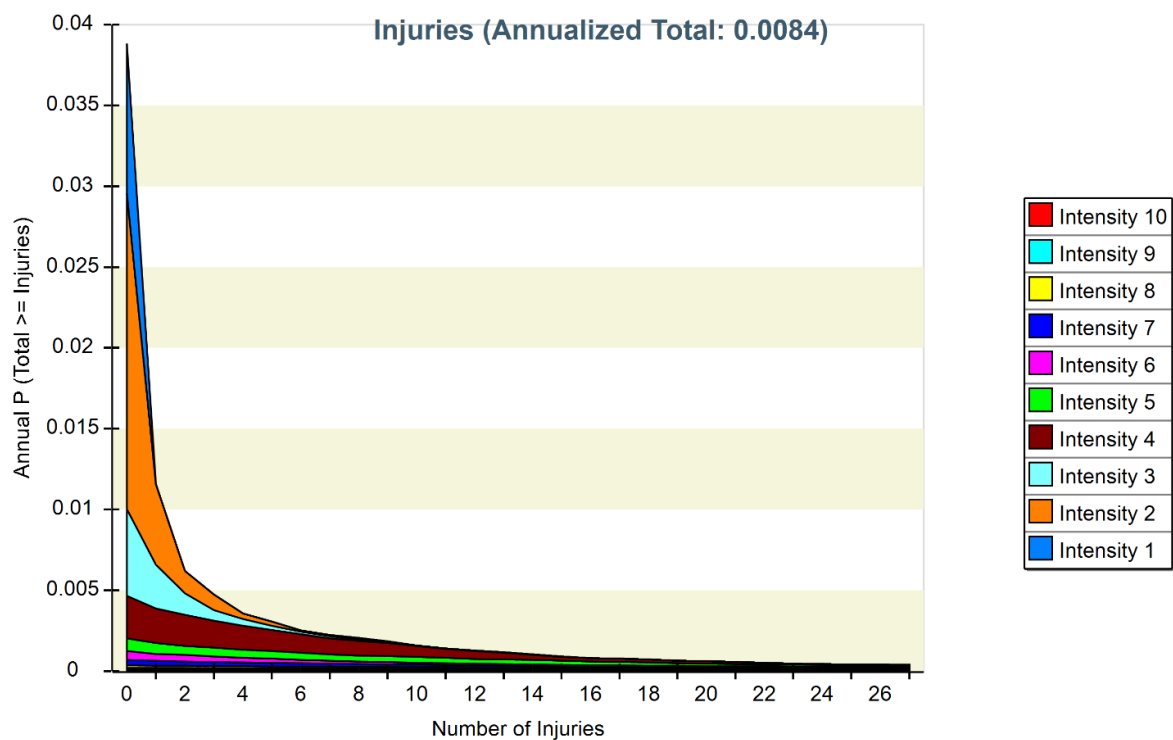


Figure 7.26: Annualized injuries rate for BI model

### 7.2.3 Unsafe Placard

Unsafe placarding is a performance measure with indirect cost consequences. This status shows that the building is not safe for post-earthquake use or occupancy determined by safety investigations after earthquake. Unsafe placarding incurred either when the building is deemed as irreparable or damage states with unsafe placarding potential has occurred at least in a certain percentage of components within the performance group. For example, the benchmark buildings are considered as unsafe if 20% of the total concrete joints are severely damaged. Each damage state with potential unsafe placarding has a median and dispersion for this performance measure which defines the extent of damage likely to result in posting an unsafe placarding.

Table 7.4 gives the annualized probability of unsafe placarding which varies from 0.0133 for B1 to 0.00254 for B5 as the highest and lowest records among all models. BI models has a greater probability of unsafe placarding than B5 model. The reliability index against unsafe placarding is also provided in the table which varies between 2.2 to 2.8 for B1 and B5, respectively. BI is slightly less reliable than B5 with a reliability index of 2.7.

Table 7.4: Annualized probability of unsafe placarding and reliability indices

<b>Model</b>	<b>Unsafe Placarding annualized probability</b>	<b>Reliability against unsafe placarding</b>
<b>B1</b>	0.01330	2.2
<b>B2</b>	0.00967	2.3
<b>B3</b>	0.00804	2.4
<b>B4</b>	0.00562	2.5
<b>B5</b>	0.00254	2.8
<b>BI</b>	0.00330	2.7

#### 7.2.4 Collapse

PACT tool was unable to successfully perform ample realizations to predict accurate collapse probabilities particularly for B5 and BI model. For this reason, a separate Monte Carlo simulation was performed to estimate the annual and 50-year collapse probabilities. A Macro code was developed in Excel to perform the simulations. Each benchmark buildings require 10 different simulations performed at each shaking intensity. Simulations for high shaking intensities were performed until at least 100 collapse has occurred. For low shaking intensities, only 10 collapses were considered as it requires up to millions of simulations to reach this number of collapse. By integrating over all intensities annual probabilities of collapse and total annualized collapse probability is calculated. The collapse probability over the useful life of the building (50 years) is a good indicator of the collapse risk for a long period of time.

Table 7.5 shows the collapse probability along with the reliability index for 1 year (annual) and 50 year periods. The annual reliability of the buildings against collapse is estimated as 3.9 for B1 and increases to its maximum value, 5.4, for B5. BI model is also very reliable with 5.1 reliability index. This number simply implies 1 one out 5 million of buildings built with similar designs may collapse within 1 year period.

The 50-year probability of collapse changes from 2.9 for B1 model to its maximum value, 4.7, estimated for B5. BI model with a 4.3 reliability index is the second best system which performs way superior to conventionally designed fixed-based models, B1, B2, and B3.

Table 7.5: Annualized and 50-year probability of collapse and reliability indices

<b>Model</b>	<b>Collapse annualized prob.</b>	<b>Annual reliability against vollapse</b>	<b>50-year collapse prob.</b>	<b>50-year reliability against collapse</b>
<b>B1</b>	3.98E-05	3.9	1.99E-3	2.9
<b>B2</b>	2.06E-05	4.1	1.03E-3	3.1
<b>B3</b>	1.51E-05	4.2	7.55E-4	3.2
<b>B4</b>	5.76E-6	4.4	2.88E-4	3.4
<b>B5</b>	3.05E-08	5.4	1.53E-6	4.7
<b>BI</b>	2.01E-07	5.1	1.01E-5	4.3

### 7.3 Decision Making

Time-based assessment gives very useful results by combining various performance measures into an equivalent cost or risk factor which makes comparisons between design alternatives possible. With the new performance assessment methodology, alternative designs can be compared against an equivalent performance measure such as costs. Cost-benefit analysis determines whether investments toward increasing safety or lowering seismic risks is justifiable. Time-based assessment provided mean values of annualized performance measure including initial costs, repair costs and time which can be used to make equivalent cost comparisons. The useful life of isolator devices is considered to be 25 years. The replacement cost of these devices was added to initial costs considering the effective interest rate which will be explained in this section.

Repair costs are not the only loss imposed after earthquake, repair time poses partial or complete loss of use or downtime in the building occupancy and subsequently causes loss of revenue. The business interruption during downtime may also lead to some long term losses as the business may not be able satisfy its current clients and damage its repute. Low performance designs like B1 requires considerably longer repair times relative to B5 or BI models.

In addition to repair time, downtime also include the time needed to conduct building inspections, damaged assessment, and preparation of repair plans/schemes by professional engineers, and bidding process by contractors. During downtime a temporary place with the same area footage of the original damaged building is leased. The lease amount is certainly dependent on the office location. An average rent of \$ 24.9 Sf/year for the city of Los Angeles was estimated using quotes by websites (Loopnet.com) as a temporary replacement for benchmark buildings.

Repair time cost consequences does not include the business interruption and restoration period, period of time required to restore the business to its normal operability. The period of restoration begins after the date of earthquake occurrence and ends at the date when the business is resumed at its new location. When the building is posted with unsafe placard, the amount of damage is to the point at which the building must be evacuated for inspections by professionals. In addition, design for retrofitting of the damaged building and starting the repair actions takes considerably long period of time. Therefore, we assumed that in the cases of unsafe placarding, relocation to another place is the measure most likely taken. A minimum restoration period of one month for resuming the business at its full functionality is also assumed based on current business property insurance policy limits. The business revenue sustained during the period of restoration is the loss due to business interruption. Revenue per employee is a good index to estimate the total revenue of the business during the restoration period. Table 5.20 represents the average revenues per employee for several industries obtained in 2007 (Money.cnn.com).

Table 7.6: Average revenues per employee (money.cnn, 2007)

<b>Industry</b>	<b>Revenues per employee (\$ millions)</b>
Insurance: P & C (stock)	1.0
Commercial Banks	0.4
Household and Personal Products	0.3
Computers, Office Equipment	0.3
Medical Products & Equipment	0.3
Industrial & Farm Equipment	0.3
Electronics, Electrical Equipment	0.2
Engineering, Construction	0.2
Publishing, Printing	0.2
Information Technology Services	0.2

Engineering construction industry is nearly at the lower bound of productivity defined by revenues per employee. Assuming a total number of 154 employee (0.004 employees per square foot) present in the building and an average revenue of \$200,000 each, total expected revenues for this office is estimated as \$30.8M a year. Table 7.7 provides the annual business revenue loss during the assumed 30-day restoration period considering annual probability of unsafe placarding occurrence.

Table 7.7: Annual loss estimation during restoration period

<b>Model</b>	<b>Restoration period (days)</b>	<b>expected revenue in restoration (millions)</b>	<b>Annual probability of unsafe placarding</b>	<b>Annual loss during restoration time</b>
<b>B1</b>	30	2.57	0.01330	\$34,181
<b>B2</b>	30	2.57	0.00967	\$24,852
<b>B3</b>	30	2.57	0.00804	\$20,663
<b>B4</b>	30	2.57	0.00562	\$14,443
<b>B5</b>	30	2.57	0.00254	\$6,528
<b>BI</b>	30	2.57	0.00330	\$8,481

Fatalities and injuries as another indirect costs represent the costs associated with the human loss or medical expenses for injured people after earthquake. The National Safety Council (NSC) has investigated the average costs of unintentional fatal and non-fatal injuries including wage losses, medical and administrative expenses. Based on the comprehensive cost concept, they suggest these costs should be used for any cost-benefit analysis whenever unintentional human death or injuries involved. Table 7.8 shows the average costs for 2011 estimated for work injuries both with and without the employer costs. Fatal and nonfatal costs for all benchmark designs is estimated using the values provided in this table.

Table 7.8: Average economic costs for unintentional human death and injuries

(NSC, 2011)

<b>Work Injuries</b>	<b>Average economic costs</b>	
	Death	Disabling injury
<b>Without employer costs</b>	\$1,370,000	\$49,000
<b>With employer costs</b>	1,390,000	\$54,000

The net present value of all costs is used for cost-benefit analysis. An equivalent present value of all direct or indirect costs is calculated assuming an effective interest rate (annual rate of return of investment). Annualized return is based on S&P500 (2013) over different date ranges given in Table 7.9. All date ranges end with year 2013 as the most recent available data.

Table 7.9: Average annual rate of return

Date range	2003-2013	1993-2013	1983-2013	1973-2013	1963-2013
<b>Annualized Return</b>	9.19%	11.15%	12.67%	12.62	11.45%

Investors in the U.S. stock should expect a return of 6% to 7%, Warren Buffet says. For the date range from 1950 to 2013, stock market annual rate of return also points to 7% rate of return when adjusted for inflation. Figures 7.27 to 7.30 show the net present value of all designs for 3%, 5%, 7%, and 9% effective annual rate of return, respectively. Initial construction costs, repair costs, repair time, business interruption costs, fatalities, and injuries together with total net present value are given in the tables.

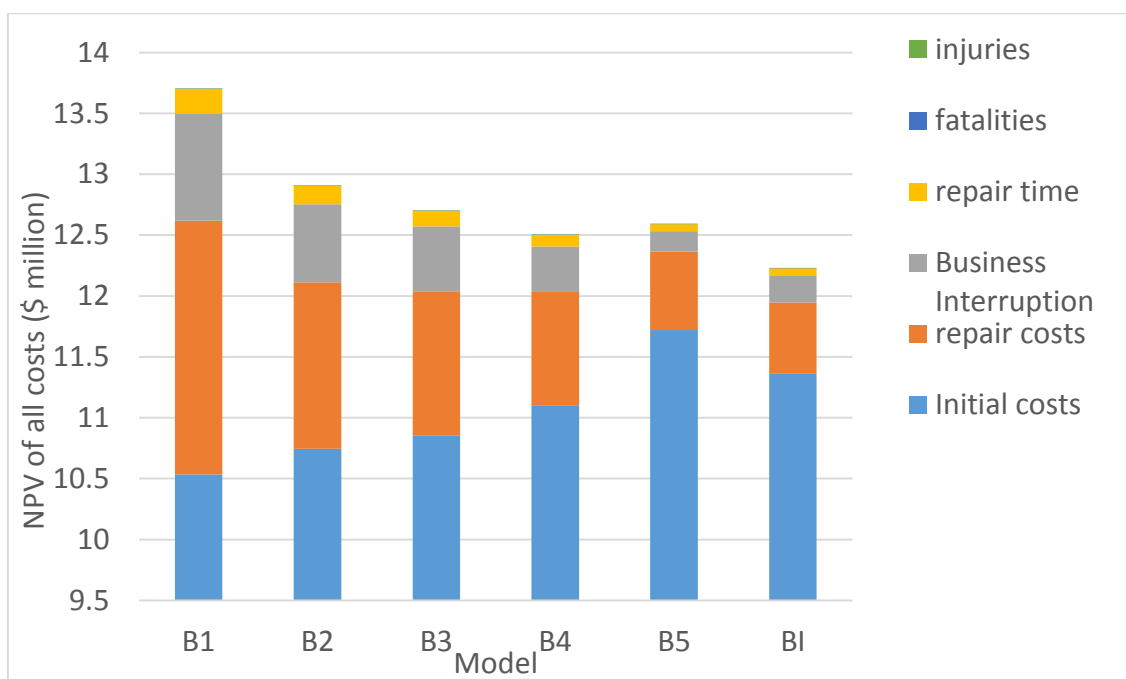


Figure 7.27: Total net present value (NPV) of benchmark buildings, 3% annual rate of return

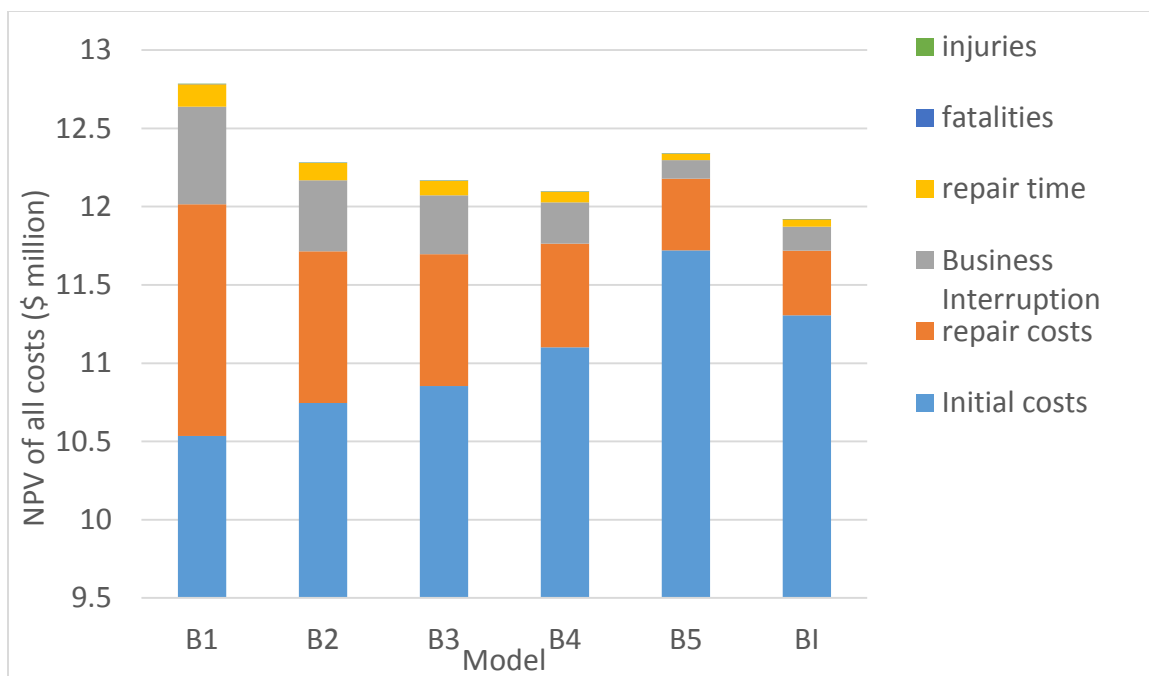


Figure 7.28: Total net present value (NPV) of benchmark buildings, 5% annual rate of return

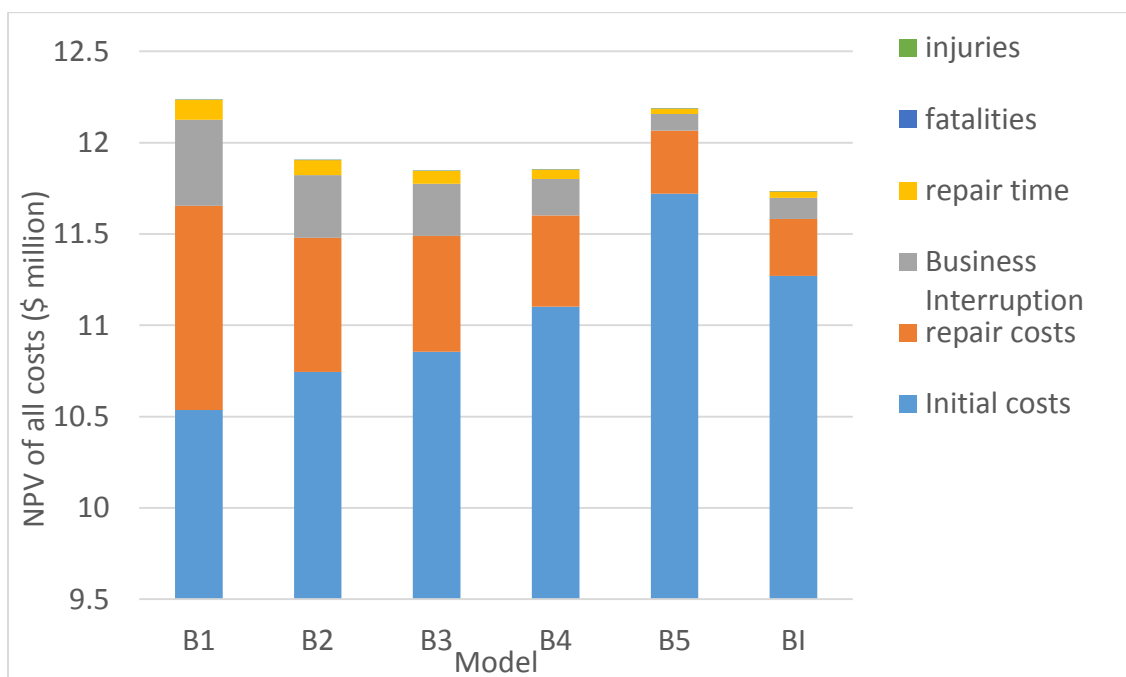


Figure 7.29: Total net present value (NPV) of benchmark buildings, 7% annual rate of return

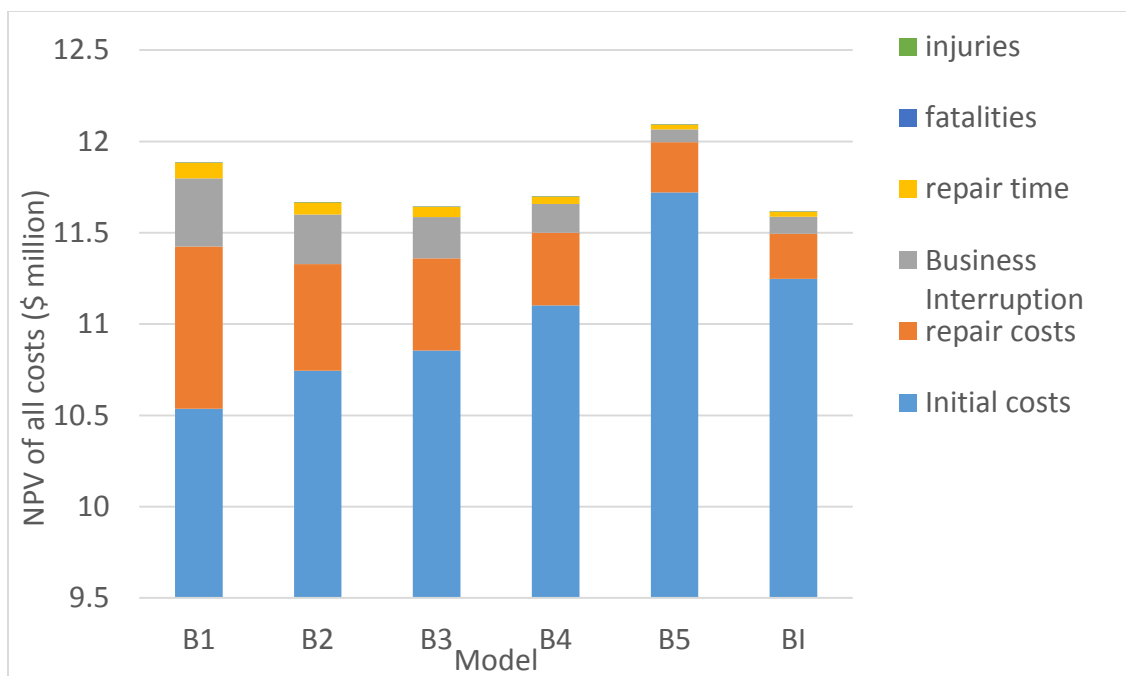


Figure 7.30: Total net present value (NPV) of benchmark buildings, 9% annual rate of return

Total cost increase/decrease percentage of all benchmark buildings with respect to design B1 is represented in Figure 7.31 for all interest rates. B1 is the most expensive design alternative at 7% interest rate which is the recommended value based on the U.S stock market data in the last 60 years. Lower repair costs, time, and substantially shorter business restoration periods for high performance models has resulted in lower long term costs for these designs. B2, B3, and B4 designs have all performed superior to basic model, B1, with cost decrease percentages equal to 2.7%, 3.2% and 3.1%, respectively. Even the model with the biggest initial costs, B5, ends up more economical than the basic model, B1. Base-isolated models is the best alternative with 4.1% total cost decrease with respect to B1 which is huge considering that its initial costs is 6.4% higher. Increasing interest rate results in less NPV of costs in all designs, but the cost decrease is

substantially greater for B1. Thus, the difference between design alternatives total costs is reduced in favor of B1. For a 9% interest rate, B2, B3, and B4 are still less costly than B1 model. B5 is the most expensive design with 1.7% cost increase over B1. BI is still the best alternative offering 2.6% cost decrease over B1.

Lower interest rates like 3% and 5% is often used for cost-benefit analysis known as discount rates which takes into account the uncertainty in future returns. Total costs decrease for all models with respect to B1 as the present generation and future generations are not much different in these rates. A cost decrease of 12% and 7.5% relative the basic model, B1, is obtained for design BI as the superior model at 3% and 5% interest rates.

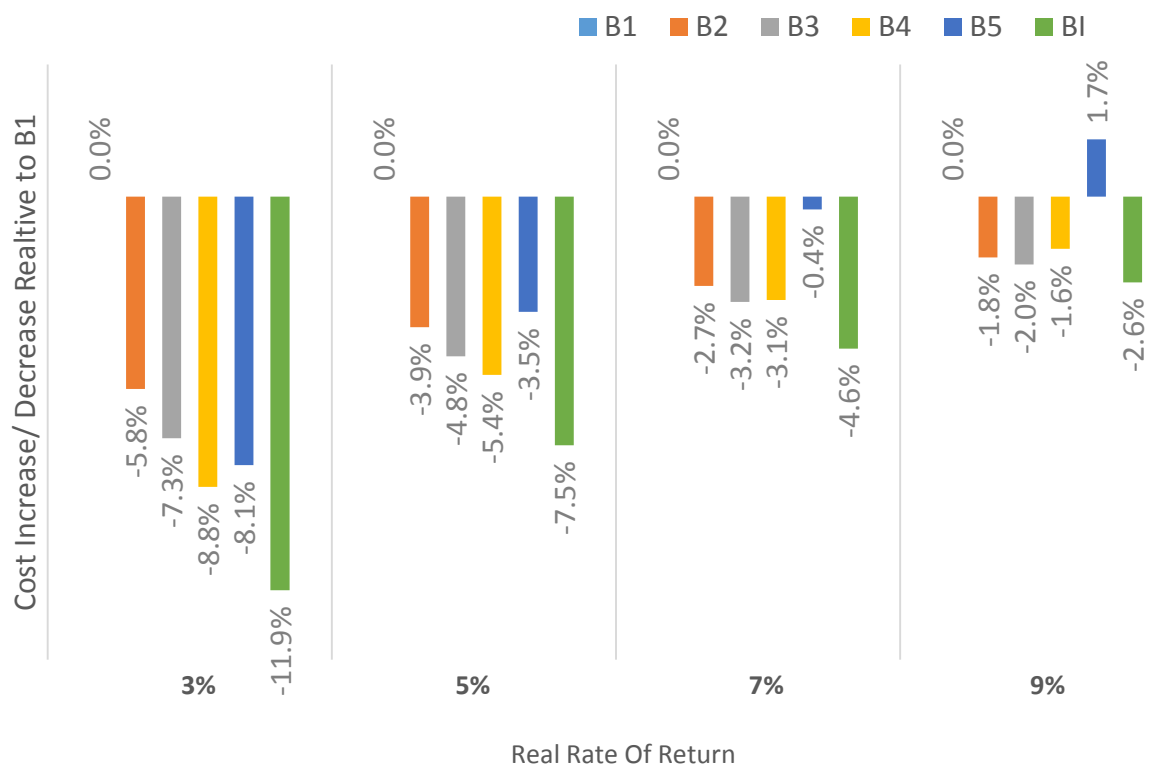


Figure 7.31: NPV of benchmark buildings to NPV of B1 design

## Chapter 8 : Conclusion

Cost-benefit analysis of buildings considering seismic loads is rather complicated due to many uncertain factors involved. The uncertain nature of earthquakes is not only limited to their maximum intensity often represented by PGA, but also the duration and frequency content. The analytical tools used to estimate the structural demands under seismic include many simplifying assumptions. In addition, the response of components to demand values are completely uncertain due some factors including construction quality. In this study, the most recent performance assessment methodology, developed by PEER and Applied Technology Council, is used to assess the long term costs of several fixed-base and base-isolated benchmark buildings. This methodology, though not mature yet, is so helpful for estimating the probable consequences of an earthquake including repair cost, time, fatalities and injuries.

Six benchmark buildings were selected including five fixed-base and one base-isolated model. Fixed-base buildings are designed for different seismic loads varies from one to three times the minimum recommended by IBC 2012 for an office building. Cost estimations are conducted using RS Means (2012) and ATC-58 normative quantity tools. Initial costs increased by 2%, 3%, 5.2%, and 11.2% for B2, B3, B4, and B5 buildings with respect to basic model, B1. These buildings are designed for seismic loads 25%, 50%, 100%, and 200% greater than the minimum recommended values used for B1.

Isolation increased initial costs by 6.4%. B2 and B3 models, designed according to minimum requirement of buildings with seismic risk category III and IV, primarily appear to be better options than BI for their lower initial costs. This is the main reason for

which owners and designers are not willing to adapt the isolation technology. This direction will not change unless the long term costs of these systems have been solidly investigated and reported by engineering communities and researchers.

The buildings are evaluated using Time-Based Assessment which considers all probable losses in the useful life span of the building (50 years). The losses include repair costs, repair time, business interruption costs, fatalities, injuries. The results of Time-Based Assessment shows that the lower long term costs of high performance buildings has the potential to justify their additional initial costs. B2, B3, and even B4 models perform superior to B1 in all assumed interest rates. B5 model costs is also comparable to B1 especially when assuming low interest rates. Extremely low future losses of B5 offsets the extra initial costs. Base-Isolated model unquestionably offers the best performance. The net present value of base-isolated building is 4.6% lower than B1 at an assumed interest rate of 7%. At the upper limit of interest rates, 11%, this model along with B2 and B3 still have the lowest NPV offering 1.2% cost decrease from B1.

Base Isolation cost performance has unfortunately been judged by its higher initial construction costs. The results of this study shows these extra costs can be offset by low future losses. We think that the performance of base-isolated building can even exceed those presented in this study due to following reasons:

- 1- Base-isolated building cost can be reduced by installing them on the first floor columns providing a useful basement or parking space. This eliminates the need for and extra beam-slab system which further reduces the costs.

- 2- There are several components for which the fragility functions have not yet been developed. The cost difference between base-isolated and fixed-base models is expected to further increase in favor of base-isolated one when more components are involved in the performance assessment.
- 3- With more widespread use of isolation systems, lower production costs of devices are likely. As a major source of costs, this can reduce the overall costs of this system.
- 4- In this study, the base isolation model was intentionally designed to perform at its lower bound of effectiveness to produce conservative results. Considerably higher target period of isolation is obtainable using friction pendulum bearings which can lead to a better performance.
- 5- We believe that the lifecycle analysis of buildings can be misleading when estimated without the deadly effects of earthquakes or any other disaster. Base-isolated building can be a competitive alternative when it comes to lifecycle costs. Keeping a building operational after an earthquake or reducing recovery time is important when it comes to the resiliency concept in sustainability. Environmentally, carbon emissions and energy consumption associated with repair and reconstruction efforts can be considerably lower for these buildings which are the integral part of a green building design concept. These factors further support the use of resilient base-isolated designs over the traditional system.

With the introduction of LRFD method, reliability has always been the subject of research. The components reliability as oppose to system reliability has mostly been focus of studies. A very interesting part of results of this study is the estimation of the structural system reliability index. For base-isolated model, the reliability against collapse in a 50-year period is 4.3. It is considerably safer than B1, B2, B3, and B4 models with reliability indices of 2.9, 3.1, 3.2, and 3.4, respectively.

The main limitation on this study is that the benchmark buildings are located in a high seismic prone area. Lower consequences is expected at regions where seismic demands are less. So, net present value of costs is predicted to increase for base-isolated system relative to fixed-base one. Future researchers may be interested to conduct a similar investigation for difference seismic zones. The occupancy type of the building is another potential area of research. The performance assessment of office buildings differ from residential ones, for example, as business interruption costs is irrelevant for such buildings which may reduce costs in favor of a fixed-based design.

## References

- ACI Committee 318. (2011). *Building Code Requirements for Structural Concrete*. ACI 318-11, American Concrete Institute, Farmington Hills.
- ACI-ASCE Committee 352. (2002). *Recommendations for Design of Beam-Column Connections in Monolithic Reinforced Concrete Structures*. American Concrete Institute, ACI 352-R02, Farmington Hills, MI.
- Altoontash, A. (2004). *Models For Performance Assessment Of Reinforced Concrete Beam-Column Joints Simulation And Damage*. Stanford University, A Dissertation For The Degree Of Doctor Of Philosophy.
- American Society of Civil Engineers (ASCE). (2010). *Minimum design loads for buildings and other structures (ASCE/SEI 7-10)*. American Society of Civil Engineers, ASCE 7, Reston, VA.
- ATC. (1996). *Seismic Evaluation and Retrofit of Concrete Buildings*. ATC-40, Applied Technology Council, Redwood City, California.
- ATC. (2012). *Seismic Performance Assessment of Buildings*. ATC-58, Applied Technology Council, Redwood City, California 94065.
- Chopra, A. K. (2007). *Dynamics of structures: Theory and applications to earthquake engineering, 3rd Ed*. Prentice-Hall, Upper Saddle River, N.J.
- Computeres and Structures Inc. (2012). *Structural Analysis Program Advanced 15.2.1*. Berkeley.
- Fardis, M. N., & Biskinis, D. E. (2003). Deformation Capacity of RC Members, as Controlled by Flexure or Shear. *Otani Symposium*, (pp. 511-530).

- Federal Emergency Management Agency. (2000). *Prestandard and Commentary for the Seismic Rehabilitation of Buildings*. FEMA-356, Washington, D.C.
- Haselton, C. B., Goulet, C. A., Mitrani-Reiser, J., Beck, J. L., Deierlein, G. G., Porter, K. A., . . . Taciroglu, E. (2008). *An Assessment to Benchmark the Seismic Performance of a Code-Conforming Reinforced Concrete Moment-Frame Building*. University of California, Pacific Engineering Research Center, PEER 2007/12, Berkeley, California.
- Haselton, C., Liel, A., Taylor Lange, S., & Deierlein, G. (2006/2007). *Beam-Column Element Model Calibrated for Predicting Flexural Response Leading to Global Collapse of RC Frame Buildings*. University of California, Pacific Engineering Research Center, PEER 2006/7, Berkeley, California.
- Ibarra, L., Medina, R., & Krawinkler, H. (2005). Hysteretic Models that Incorporate Strength and Stiffness Deterioration. *Earthquake Engineering and Structural Dynamics*, 34(12), 1489-1511.
- International Code Council (ICC). (2012). *International building code 2012*. Falls Church, Va.
- Kelly, J. M. (1999). The role of damping in seismic isolation. *Earthquake Engineering and Structural Dynamics*, 28, 3-20.
- Kikuchi, M., & Black, C. J. (2008). On the response of yielding seismically isolated structures. *Earthquake Eng. Struct. Dyn.*, 37(5), 659-679.
- Komodromos, P. (2000). *Seismic Isolation for Earthquake-Resistant Structures*. Southampton, UK: WIT Press.

- Krawinkler, H., & Miranda, a. (2004). Performance-based earthquake engineering. In *Earthquake engineering: from engineering seismology to performance-based engineering*. CRC Press.
- Lee, T. H., & Mosalam, K. M. (2006). *Probabilistic Seismic Evaluation of Reinforced Concrete Structural Components and Systems*. University of California, PEER Report 2006/4. California.
- Lowes, L. N., Mitra, N., & Altoontash, A. (2003). *A Beam-Column Joint Model for Simulating the Earthquake Response of Reinforced Concrete Frames*. University of California, Pacific Engineering Research Center, PEER 2003/10, Berkeley, California.
- Mander, J., Priestley, M., & Park, R. (1988). Theoretical stress-strain model for confined concrete. *Journal of the Structural Division, ASCE, 114*(8), 1804-1826.
- Mayes, R. L. (1990). Impediments to the implementation of seismic isolation. *Earthquake Spectra, 6*(2), 283-296.
- Meinheit, D. F., & Jirsa, J. O. (1981). Shear Strength of R/C Beam-Column Connections. *Journal of the Structural Division, 107*(No. ST11), 2227-2244.
- Mitra, N., & Lowes, L. N. (2004). Modeling the Response of RC Beam-Column Joints. *13th World Conference on Earthquake Engineering*, (pp. 1001-1011). Vancouver, Canada.
- National Safety Council (NSC). (2011). *nsc.org*.
- Nowak, A., & Szerszen, M. M. (2003). Calibration of Design Code for Buildings (ACI 318) Part 1: Statistical Models for Resistance. *ACI Structural Journal, 100*(3), 377-382.

- Office Property Asking Rent - Lease Trends. (2014). *Loopnet*. Retrieved from [http://www.loopnet.com/LOS-ANGELES\\_California\\_Market-Trends](http://www.loopnet.com/LOS-ANGELES_California_Market-Trends)
- OpenSees. (2002). *Open System for Earthquake Engineering Simulation*. University of California at Berkeley , Pacific Earthquake Engineering Research Center, Berkeley, California .
- PACT. (2012). *Performance Assesment Calculation Tool*. Applied Tachnology Council, Redwood City, California.
- Panagiotakos, T. B., & Fardis, M. N. (2001). Deformations of Reinforced Concrete at Yielding and Ultimate. *ACI Structural Journal*, 98(2), 135-147.
- Popovics, S. (1973). A numerical approach to the complete stress strain curve for concrete. *Cement and concrete research*, 3(5), 583-599.
- Porter, K. A., Shaikhutdinov, R. V., & Beck, J. L. (2002). *Investigation of Sensitivity of Building Loss Estimates to Major Uncertain Variables for the Van Nuys Testbed*. University of California, Pacific Engineering Research Center, PEER 2002/03, Berkeley.
- RS Means Co. (2013). *Building constructio cost data*.
- Ryan, K. L., & Chopra, A. K. (2004). Estimation of seismic demands on isolators based on nonlinear analysis. *Journal of Structural Engineering*, 130(3), 392–402.
- Ryan, K. L., Morgan, T. A., & and Sayani, P. (2006). Consistent performance comparison of seismic-isolated and fixed-base buildings. *8th National Conference on Earthquake Engineering*. San Francisco, CA: Earthquake Engineering Research Institute.

- Sayani, P. J., & Ryan, K. L. (2009). Comparative evaluation of base-isolated and fixed-base buildings using a comprehensive response index. *Journal of Structural Engineering*, 135(6), 698-707.
- SEAOC. (1995). *Vision 2000 - A Framework for Performance Based Earthquake Engineering*. Structural Engineers Association of California, Sacramento, California.
- Sezen, H. (2002). *Seismic behavior and modeling of reinforced concrete building columns*. Department of Civil and Environmental Engineering, University of California, Berkeley, Ph.D. Thesis.
- Shima, H., Chou, L.-L., & Okamura, H. (1987). Bond characteristics in post-yield range of deformed bars. *Concrete Library of JSCE, No 10, Japan*, 113-124.
- Shima, H., Chou, L.-L., & Okamura, H. (1987a). Bond-slip-strain relationship of deformed bars embedded in massive concrete”,. *Concrete Library of JSCE, No 10, Japan*, 79-94.
- Sritharan, S., Ingham, J. M., Priestley, M. J., & Seible, F. (1998). Bond Slip of Bridge Column Reinforcement. *ACI Special Volume on Bond and Development of Reinforcement – A Tribute to Dr. Peter Gergely, ACI SP-180*, 319-345.
- Taghavi, S., & Miranda, E. (2003). *Response assessment of nonstructural building elements*. Pacific Earthquake Engineering Research Center, PEER Report No. 2003-05. Berkeley, California: University of California.
- Taucer, F., & Spacone, E. (1991). *A Fiber Beam-Column Element for Seismic Response Analysis of Reinforced Concrete Structures*. UCB/EERC-91/17, Earthquake Engineering, Berkeley, CA.

- Top industries: Most Bang For The Buck: Revenues P. (2007). *money.cnn*. Retrieved from [http://money.cnn.com/magazines/fortune/fortune500/2007/performers/industries/revenues\\_per\\_employee/](http://money.cnn.com/magazines/fortune/fortune500/2007/performers/industries/revenues_per_employee/)
- Umemura, H., & Aoyama, H. (1969). Evaluation of Inelastic Seismic Deflection of RC Frames Based on Tests of Members. *Proc. 4th WCEE*. Chile.
- USGS. (2007). *Probabilistic Seismic Hazard Analysis*. U.S. Geological Survey Earthquake Hazard Maps.
- Wang, P., Shah, S., Naaman, P., & Antoine, E. (1978, November). High-Strength Concrete in Ultimate Strength Design. *Journal of the Structural Division*, 1761-1773.
- Zareian, F. (2006). *Simplified Performance-Based Earthquake Engineering*. Stanford University, Ph.D Dissertation, Stanford, California.